AN EFFICIENT ENERGY STORAGE & RETURN PROSTHESIS

Abu Zeeshan Bari

Ph.D. Thesis **2013**

AN EFFICIENT ENERGY STORAGE & RETURN PROSTHESIS

Abu Zeeshan Bari

Centre for Health Sciences Research
University of Salford, Salford, UK

Submitted in Partial Fulfilment of the Requirements of the Degree of Doctor of Philosophy, March 2013

Dedicated to my late parents, who taught me how to read and write.

TABLE OF CONTENTS

LIST OF FIGURES

LIST OF TABLES

NOMENCLATURE

ΔE	Total energy stored over one gait cycle
B	Bulk modulus of oil
$C1$	Coefficient of the 4th order term of the quartic equation
$C2$	Coefficient of the 3rd order term of the quartic equation
$C3$	Coefficient of the 2nd order term of the quartic equation
$C4$	Coefficient of the 1st order term of the quartic equation
$C5$	Coefficient of the zero order term of the quartic equation
Cs	Slip coefficient
D_{act} or D	Actuator's instantaneous volumetric displacement
d	Slider position
dA	Differential changes in ankle angle
dA_{vda}	Differential changes in gearbox output shaft rotation
dA_{gb}	Differential changes in gearbox input shaft rotation
$d\beta_{vda}$	Differential changes in VDA shaft angle
Dia	Cylinder bore
d_l	Differential changes in cylinder stroke
D_{max}	Actuator's maximum volumetric displacement
dV_{vda}^{ideal}	Differential changes in oil volume of VDA for ideal conditions
dV_{vda}^{real}	Differential changes in oil volume of VDA for real conditions
dV_{cyl}	Differential changes in oil volume of cylinder
dV_F^{ideal}	Differential changes in oil volume of accumulator for ideal case
dV_F^{real}	Differential changes in oil volume of accumulator for real case
$d\beta$	Differential changes in the shaft angle

F_1	Piston force due to accumulator pressure
F_2:	Component of the force F (acting perpendicular to F_1)
k	Specific heat ratio
K_m	Machine type coefficient
l	Cylinder length
M_{act}	Actuator Moment
M_{ank}	Ankle moment
N	Gear ratio
n, a, b	Coefficients for the flow loss model
P or P_{acc}	Instantaneous accumulator pressure
P_{atm}	Atmospheric Pressure
P_h	Higher working pressure
P_l	Lower working pressure
P_{max}	Maximum rated pressure
P_{min}	Minimum rated pressure
P_{pr}	Pre-charge pressure
q	Instantaneous flow rate
q_{vda}^{ideal}	Ideal actuator flow rate
$q_{compressibility}$	Flow loss due to compressibility
q_{ideal}	Ideal flow rate
$q_{leakage}$	Leakage flow
q_{real}	Flow rate obtained with real conditions
q_{vda}^{real}	Real actuator flow rate
T or T_{vda}	Instantaneous actuator torque
T_{fr}	Gearbox friction torque

T_{ideal}	Torque output for ideal conditions
T_N	Nominal torque
T_{real}	Torque output for real conditions
V_A	Accumulator capacity/size
V_F	Instantaneous accumulator oil volume
V_G	Gas volume
V_h	Higher working oil volume
V_{hg}	Higher working gas volume
V_l	Lower working oil volume
V_{lg}	Lower working gas volume
V_{max}	Maximum oil volume
V_{min}	Minimum oil volume
V_{oil}	Useable oil volume
V_{pr}	Maximum gas volume (also equal to VA)
V_r	Volume ratio
X	Actuator's instantaneous stroke
X_{max}	Actuator's maximum stroke
x,y	Actuator Position
X_{max}	Actuator's maximum stroke
α	Ankle Angle
β	Actuator shaft angle
μ	Absolute viscosity of oil
ω	Ankle's angular velocity
ω_{gb}	Gearbox input shaft angular velocity
ω_{vda}	VDA angular velocity

ω_{max}	Maximum VDA shaft angular velocity

ACKNOWLEDGEMENTS

I am deeply indebted to my trio of supervisors, Professor David Howard and Drs Laurence Kenney and Martin Twiste, who as a team, kept this thesis on track through to completion with their endless support, intellectual guidance, and enduring patience. Indeed, without their extraordinary guidance, this thesis would not be possible. I would like to thank Dr. Richard Jones for his help on certain aspects of this work. I offer my sincere gratitude to Rachel Shuttleworth for all her support and to my office colleagues for the stimulating discussions.

I am highly grateful to my teachers at the NED University of Engineering & Technology, Pakistan, especially Prof. Dr. Muzaffar Mahmood and Prof. Neelofur Master, for being excellent educators, a constant source of inspiration, and for instilling in me a love of creative pursuits in science. I feel extremely privileged to have been their student. I extend my gratitude to the NED University of Engineering & Technology, for the grant of fellowship and study leave to pursue this work.

I am deeply thankful to my siblings for their support and prayers when they were most needed. This last word of acknowledgment I have saved for my dear wife Saira, who has happily shared all my burdens without a complaint, and my son Ali, who has been a constant source of motivation for this work.

DECLARATION

I declare that this thesis has been composed by myself and embodies the results of my own course of study and research whilst attending the University of Salford from January 2009 to March 2013. All sources and material have been acknowledged.

ABSTRACT

Amputee gait is characterised by a higher metabolic cost of walking compared with anatomically intact subjects. Anatomically intact gait kinetics reveals that tendons crossing the ankle joint store and return strain energy during the stance phase of walking to provide forward propulsion. One of the main reasons for the high-energy cost of amputee gait is that passive prosthetic feet store little energy compared with the equivalent human structure and hence cannot provide the required energy at push-off. In addition, passive prosthetic feet are uncontrolled in the storage and release of strain energy, and do not provide natural levels of resistance and propulsion. Therefore, designing a passive prosthesis to efficiently store and transfer energy between joints, with continuous control over ankle torque, remains a research challenge.

With the aim of developing an energy efficient passive prosthesis capable of mimicking the controlled energy recycling behaviour seen in an anatomically intact limb, a hydraulics-based design was investigated in this work. A first design concept, based on a hydraulic accumulator, a variable displacement hydraulic actuator (VDA), a gearbox, and a low-pressure oil tank, was developed. The accumulator served as energy storage medium, where VDA served as the only actuator to provide ankle torque. Simulation showed that the design outperformed commercial passive prostheses as well as a recent novel design based on a spring-clutch mechanism. For level walking, it provided 86% and 69% of the peak power required by the anatomical ankle whilst providing near normal ankle torques. The system was able to store all of the available energy during gait and provide correctly timed release of energy. However, a feasibility study showed problems with size and weight of a potential prototype.

To address this problem a second design was developed with the aim of reducing the size and weight of VDA in design I. The second design comprised of a spring to provide ankle torque and to reduce the torque load on the VDA. The spring is connected to the ankle via a lever arrangement, and the VDA is used to vary the lever arm to continuously control ankle torque. Simulation results showed that design II outperformed design I; it delivered higher values of peak power, and a feasibility study showed that, using bespoke component designs, it might be possible to incorporate it into a lower limb prosthesis.

1. INTRODUCTION

During the stance phase of gait, the ankle contributes 60% of the positive mechanical work performed collectively by the ankle, knee and hip joint and majority of this work is provided by a release of strain energy (stored earlier in gait) through tendons crossing the ankle joint (Sawicki et al., 2009). Therefore, utilizing the spring-like behaviour of the tendons by using a compliant prosthetic foot might restore near to the anatomically intact ankle work.

In order to provide similar ankle mechanical work, a prosthetic foot must satisfy three requirements: a) resist both plantarflexion and dorsiflexion in load acceptance and mid-stance; b) assist plantarflexion and resist dorsiflexion in late stance; and c) assist dorsiflexion in swing without consuming unnecessary amount of energy (Winter, 2004a). A summary of these requirements is that the prosthetic foot should provide natural levels of resistance and propulsion. In other words, the compliant elements of the prosthesis must store and release energy (whilst providing near to the anatomically intact ankle torques) at the right instant during the gait cycle.

Commercially available energy storage and return (ESR) prostheses do not meet these requirements pertaining to the uncontrolled energy storage/release by their compliant elements. For instance, an anatomically intact ankle resists the initial plantarflexion and subsequent dorsiflexion during load acceptance and mid-stance respectively, due to eccentric contraction of the relevant muscles and tendons, resulting in a build-up of strain energy in relevant tendons. In turn, in a passive ESR prosthesis, the strain energy stored in the rear foot during load acceptance is released during mid-stance (when an anatomically intact foot is storing energy while resisting dorsiflexion), thus failing to satisfy requirement (a) set out above.

In late stance, by the time when an anatomically intact limb releases its stored energy to assist plantarflexion, the ESR prosthesis, having dissipated all the stored energy earlier, does not assist the late stance plantarflexion (and so, do not assist in forward propulsion of the limb). Furthermore, at push-off, as the load increases, the prosthetic foot dorsiflexes at a point in time when an anatomically intact foot would be plantarflexing.

Designing a passive prosthesis that could utilize the passive energy storage and return behaviour observed in an anatomically intact ankle remains a research challenge. Therefore, the aim of the work described here was to develop a design concept that is able to mimic the energy recycling behaviour as seen in anatomically intact gait. Hydraulics based design concepts were investigated as hydraulics allowed for continuous control, and high-density energy storage/transfer between joints.

This thesis addresses three objectives:

1- Identify efficient means of energy storage and return mechanism as observed in an anatomically intact gait.

2- Based on the understanding of energy flows at a joint level, develop a passive prosthesis (with controlled energy storage and return mechanisms) through modelling, while considering feasibility for developing a prototype.

3- Virtual testing of the prosthesis using published gait data for level, declined, and inclined walking.

The novel contributions of this work were the development of two concept designs utilizing hydraulics technology that were shown to be capable of efficiently storing and returning energy with continuous control of ankle torque. In addition, this was the first study to show that a conceptual prosthetic design based on hydraulics is practically feasible and could equal the performance of an actively powered prosthesis over level ground and decline walking.

The remainder of this thesis is separated into four chapters. Chapter 2 provides a basis for studying gait efficiency in anatomically intact and amputee gait, including the role of the ankle for an efficient gait, prosthesis design, and previous approaches to improve the energy efficiency in transtibial amputee gait. Chapter 3 describes the development of a new model for an energy efficient prosthesis, with definition/description of the components used, including the development of mathematical equations for the components used in the model, their sizing, and selection, and then testing of the model using gait data. Based on the results obtained from the first design, Chapter 4 presents another approach to further improve the first design in terms of size and weight, working principle, modelling, and simulation and testing of the model. This is followed by Chapter 5, which provides an overall discussion on the aims and objectives, findings of the work, novel contributions, limitations, and future work.

2. LITERATURE REVIEW

2.1 Healthy Gait

Human gait is a complex biomechanical phenomenon involving forward progression of the body in a controlled manner. The term “gait cycle” refers to the time elapsed between two identical gait events, typically the instant of one of the feet making ground contact (Whittle, 2003). With this definition, the gait cycle is divided into two major phases; stance and swing. Stance phase, during which the foot remains in contact with the ground, typically makes up 60% of the gait cycle. Swing phase involves the forward progression of the limb, during which the foot leaves the ground, and typically makes up the remaining 40% of the gait cycle. When both feet are in contact with the ground, the period is called double support (Rose & Gamble, 2006). An overview of the gait cycle is shown in Figure 2.1.

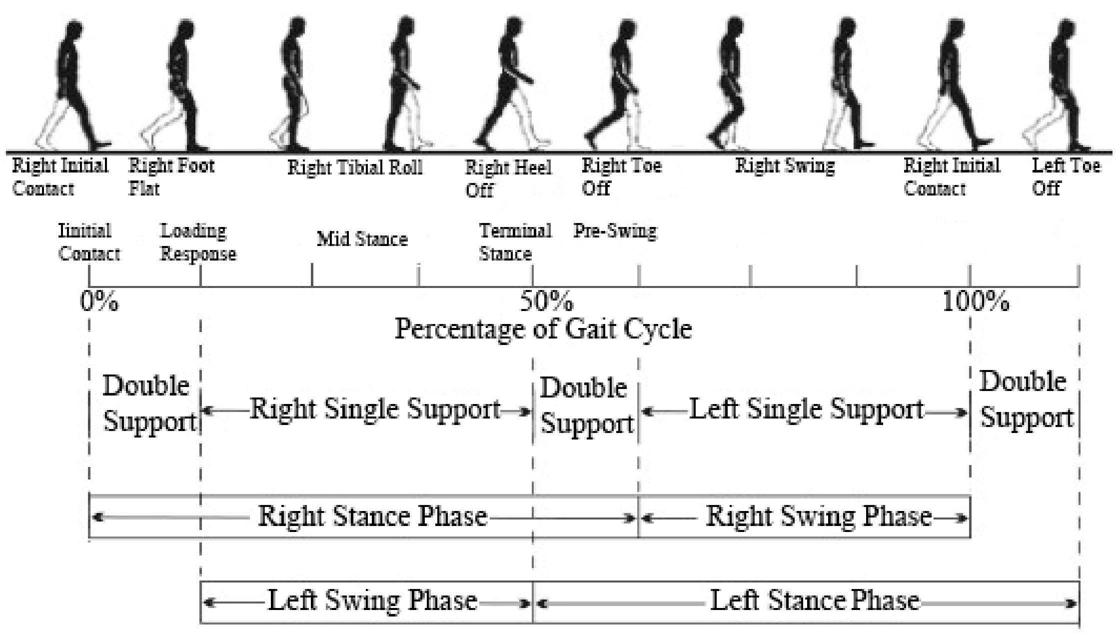

Figure 2.1: A normal gait cycle. Figure adapted from Racic et al., 2009.

2.1.1 METABOLIC COST OF WALKING

Taking into account that aerobic metabolism requires burning up of carbohydrates, fats and proteins in the presence of oxygen, metabolic energy expenditure can be indirectly calculated by measuring the volume of oxygen intake (VO_2) (Kirtley, 2006). As metabolic energy expenditure increases with body mass to allow for comparison between subjects, energy expenditure values are typically presented as normalized by body mass. Energy expenditure can be represented either as a time rate of oxygen (termed as "O_2 Rate" with typical units of ml/(kg.min)), or as oxygen consumed per unit distance (termed as "O_2 Cost" with typical units of ml/(kg.m)). Using an energy equivalent of 21.1 J for one ml of O_2 as defined by Brockway, 1987, the O_2 cost can be represented as energy cost with units of J/(kg.m).

In the absence of external factors, such as the environment that could affect someone's task performance, individuals usually adopt a way of performing a task that requires minimal effort. Energy cost of walking has been extensively studied (for example, Ralston, 1958; Waters & Mulroy, 1999; Mccann & Adams, 2002; Malatesta et al., 2003 and Farris & Sawicki, 2012). A common consensus from these studies is that the energy cost is unsurprisingly dependent on walking speed, following a U-shaped curve, which varies with age. Typically self-selected "comfortable walking speed" (1.1 to 1.3 m/s) corresponds to the minimal value of the energy cost. In addition to the walking speed, age also affects the energy cost of walking, and it has been shown that the energy cost for older adults is higher than for younger ones, for both comfortable as well as fast walking speeds (Malatesta et al., 2003). Figure 2.2 presents the energy cost as a function of walking speed in healthy adults.

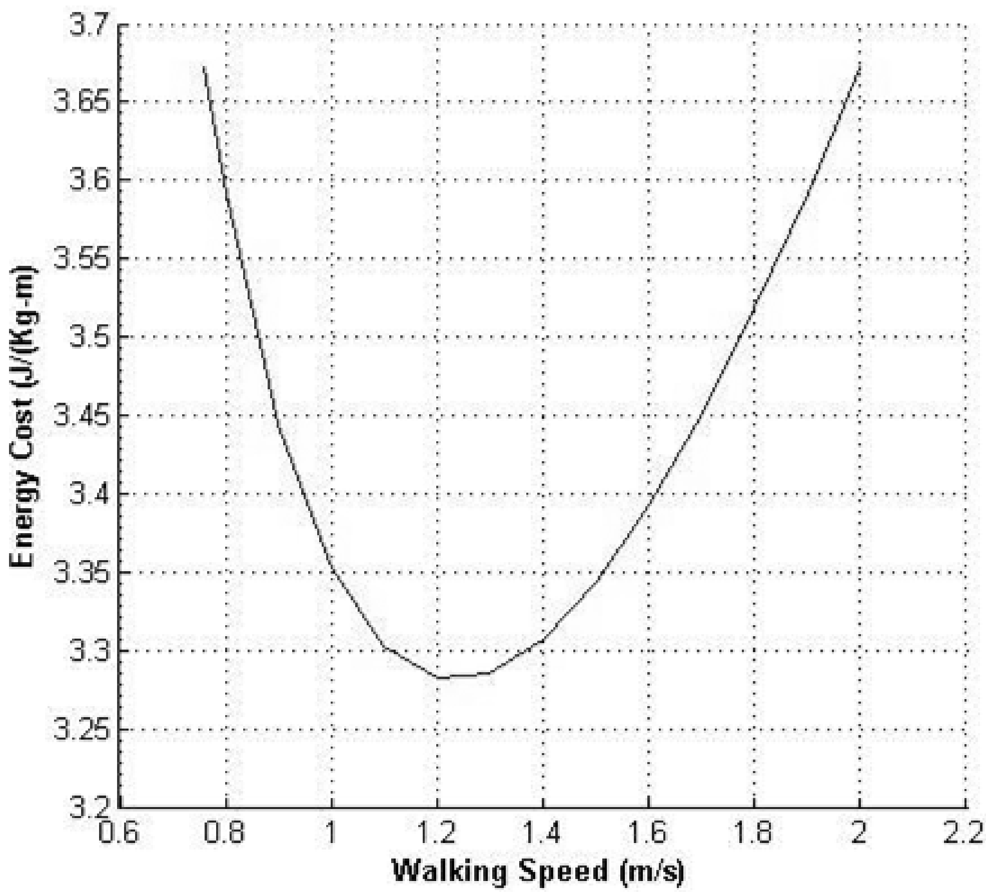

Figure 2.2: Energy cost of walking as a function of speed. Figure adapted from Ralston, 1958.

The slope of the walking surface also affects the energy cost of walking. While uphill walking requires more energy than level walking due to an increased work to perform, it is natural to consider downhill walking to be a less exhaustive task than level and/or uphill walking. However, it has been shown that, for downhill walking, a minimum energy cost closely corresponds to a downhill slope of approximately -6° (or -10% gradient) for all speeds ranging from 1.08 to 1.86 m/s. Steeper than a -6° downhill slope would cause the energy cost to increase again, irrespective of the most economic/optimum walking speed at those slopes (Saibene & Minetti, 2003). Figure 2.3 represents the energy cost of walking as a function of slope and speed.

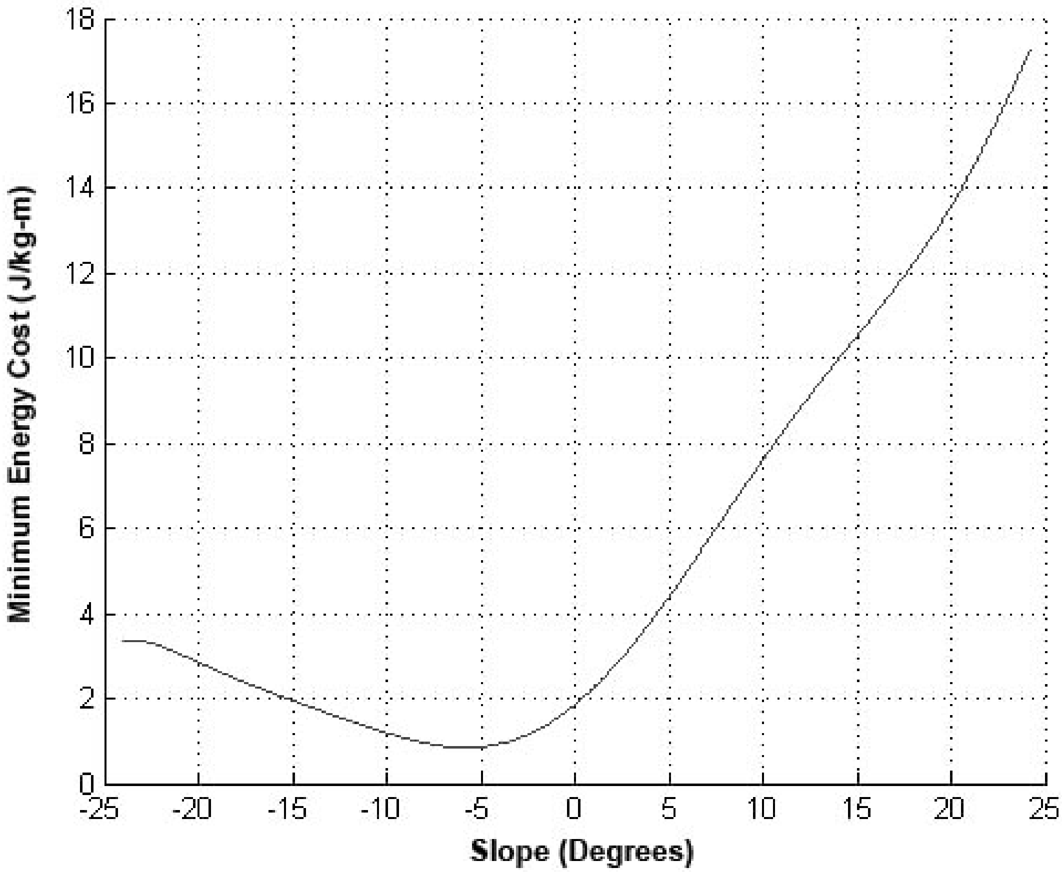

Figure 2.3: Minimum energy cost of walking as a function of slope. Figure adapted from Minetti et al., 2002. *(Note: While there is a consensus about the minimum energy cost to be around 3 J/(kg.m) during level walking (Ralston, 1958; Waters & Mulroy, 1999; Mccann & Adams, 2002; Malatesta et al., 2003 and Farris & Sawicki, 2012), Figure 2.3 indicates the energy cost of level walking to be slightly less than 2 J/(kg.m). This might be because the subjects used in that study were elite runners, who are more efficient than the average population for walking/running tasks; however, further investigation is needed to test this hypothesis. As the reasons for the discrepancy remain unknown, and because of the unavailability of any other study about the effect of slopes on the energy cost to compare with these results, the results are presented as published.)*

Walking is an energy efficient task compared to other activities. Waters & Mulroy, 1999, have reported O_2 rates (in ml/(kg.min)) for resting and for comfortable walking speeds. From this data, and using a factor of 21.1 J/ml O_2, it can be observed that, while resting, a healthy male adult of mass 80 kg would consume approximately 284 kJ of metabolic energy every hour. Surprisingly, the same individual would cover a distance of 1 km while walking at a comfortable speed of 80 m/min and would consume approximately 255 kJ of metabolic energy. In terms of food intake, a small apple, having an energy content of 333 kJ, is enough to power this walk.

2.1.2 MECHANICAL ANALYSIS OF HUMAN ENERGETICS

In order to understand the efficiency of gait (work input/work output), it is essential to describe how mechanical work during human gait may be estimated. Mechanical energy is defined as the ability to do work. Mechanical work can be divided into internal and external work. Total internal work is the change in the kinetic energy of body segments and represents the work done in accelerating body segments with respect to the body centre of mass (COM); external work during steady gait may be estimated by change in the total energy (kinetic and potential energy) of the COM (Winter, 2004a).

Energy flow between adjoining body segments provides the measure of the internal mechanical work done at the joint and is central to this thesis *(Note: The estimate of mechanical work at a segmental level can only be based on the observed dynamics and hence does not account for factors such as co-contraction, which are not directly measurable).* Using measures of gait kinematics and kinetics, it is possible to use an inverse dynamics model to calculate joint moments, angular velocities and hence power. Integrating power with respect to time gives work (Equation 1.1 – net internal work between times *t1* and *t2* done by muscles acting on a joint).

$$Muscle's\ internal\ work = \int_{t1}^{t2} (M\omega)dt \ldots\ldots\ldots Eq.(1.1)$$

As seen in Eq. (1.1), when muscle moment and joint angular velocity act in the same direction, their product will result in a positive power, which, when integrated with respect to time, would result in a net positive mechanical work done by the muscles representing energy flow to the limbs. The negative work is done during the eccentric activity (typically when decelerating the limbs) when lengthening of the muscle under a load takes place. This happens when the muscle moment and the joint angular velocity act in opposite directions, hence their product will result in negative power, and when integrated over time, negative work represents energy flow from the limbs to the muscles.

2.1.3 Gait Efficiency

Economy and/or efficiency are the terms often used for measuring the energetic performance of an individual during walking. Economy represents the metabolic cost of walking, and efficiency is related to the mechanical efficiency, which is described in mechanical systems as the work output per work input. In the case of human gait, it is impossible to measure directly, either metabolic or mechanical work at an individual muscle level. Therefore, work is calculated at each joint and then summed across the joints to give the whole body mechanical work. Metabolic work associated with gait is calculated as the difference between resting metabolic cost and the cost measured during gait. This leads to:

$$Mechanical\ Efficiency = \frac{Muscle's\ mechanical\ work\ (internal + external)}{Metabolic\ cost\ for\ gait - Resting\ metabolic\ cost}$$

2.2 Gait Models

Simple mechanical models of gait provide insight into the basic mechanics of anatomically intact gait and attempt to explain why anatomically intact gait is an energy efficient task. Two types of mechanical model have been proposed to provide insight into human walking. The six determinants of gait model, defined by Saunders et al., 1953, propose that the vertical and lateral movement of the body's COM is energetically costly.

The model further suggests that certain joints (e.g. pelvis and knee) coordinate their movements in order to smooth out these COM displacements and hence minimize energy expenditure. However, experimental studies have contradicted at least three of the six determinants (Gard & Childress, 1997; Gard & Childress, 1999 and Kerrigan et al., 2001). For example, by adopting a gait in which an individual actively reduces the vertical COM displacements, the metabolic cost is significantly increased (Gordon et al., 2009), in some cases by as much as 100% when compared with normal gait (Ortega & Farley, 2005). This "model" is now considered invalid (Baker, 2012).

In contrast to the six determinants, the inverted pendulum model by Cavagna et al., 1963 and Cavagna & Margaria, 1966, recognises that the COM undergoes vertical sinusoidal trajectories, while rotating over each stance leg similar to the trajectories observed in an energetically conservative pendulum motion. This is illustrated in Figure 2.4.

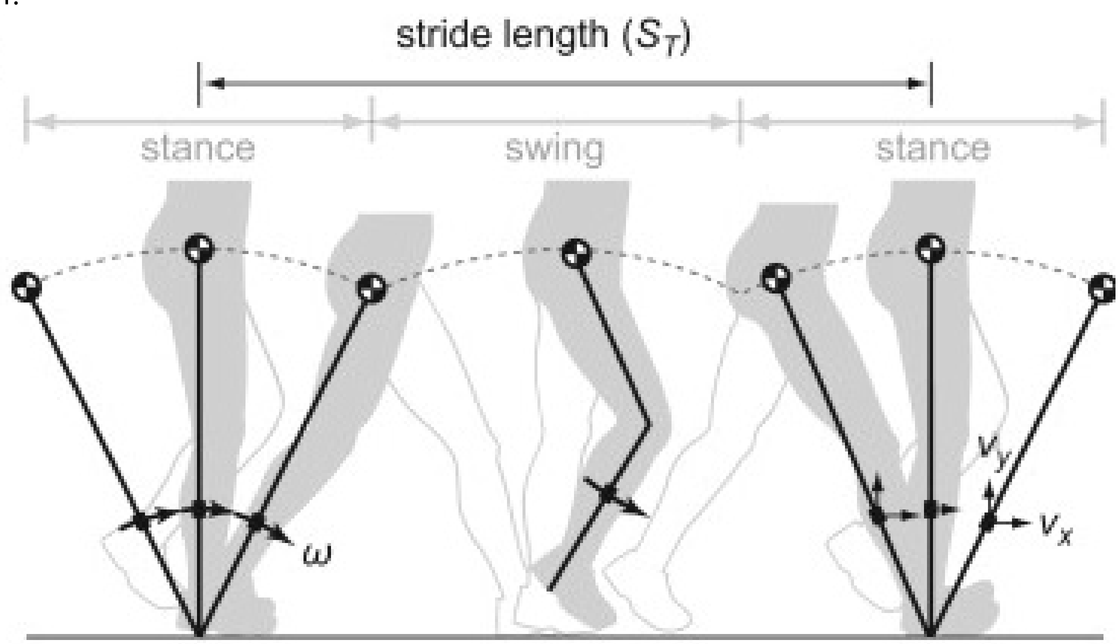

Figure 2.4: Illustration of COM trajectories by the inverted pendulum model. Figure adapted from (Li et al., 2010).

With the sinusoidal trajectories of the COM, after foot flat during double support, the COM is at its lowest point and hence has maximum kinetic energy and minimum potential energy. As the progression continues, the COM travels upwards and reaches the highest point at mid-stance during single support, and hence kinetic energy is at its minimum and potential energy at its maximum, i.e. an interchange of kinetic and potential energy takes place during each step. The efficiency of this interchange of energy is thought to be central to the observed high energy efficiency of gait (Massaad et al., 2007). Mochon & Mcmahon, 1980a and Mochon & Mcmahon, 1980b, have shown that the swing leg acts like a non-inverted pendulum. Therefore, during a gait cycle, energy is constantly flowing between the coupled inverted pendulum motion of the stance leg and the pendulum motion of the swing leg.

Although the pendulum motion, and more specifically every pendulum arc (stance or swing), is energetically conservative, however, walking does involve metabolic work. This could be because the energy requirement for the period during which one pendulum arc completes and the next one starts is not yet accounted for. The transition between consecutive pendulum arcs (or steps) is the double support period, and is termed as step-to-step transition. While progressing forward, the COM's velocity has a downward direction at the end of one arc, and this velocity needs to be re-directed upward (to prescribe the next pendulum arc) in order to continue forward progression. This re-direction of the COM's velocity during step-to-step transitions requires muscle work, and explains why metabolic energy is required for level walking (Kuo et al., 2005), a concept also supported by Grabowski et al., 2005. Figure 2.5 illustrates the step-to-step transitions and that the leading leg performs negative work on the COM at heel strike, whereby this negative work needs to be replenished by positive work done on the COM by the trailing leg.

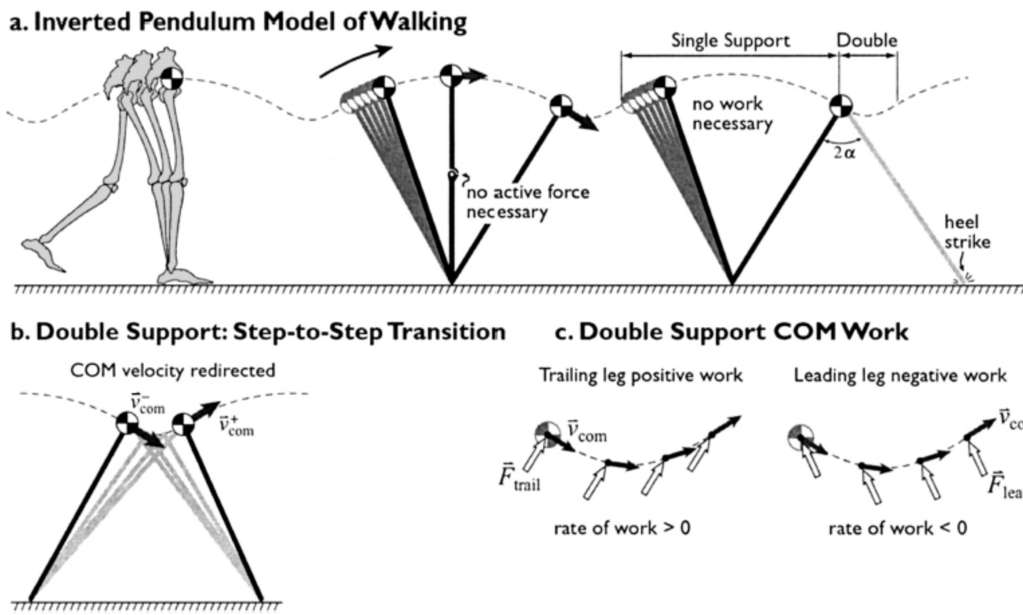

Figure 2.5: Inverted pendulum model.(a). Inverted pendulum model showing the single and double supports.(b). Work required to redirect COM velocity during step-to-step transitions. (c). Leading and trailing leg work to redirect COM velocity. Figure adapted from Kuo et al., 2005.

The most energy efficient way to replenish the negative work undertaken by the leading leg is considered a power burst from the trailing leg just before the heel strike of the leading leg (Houdijk et al., 2009). This can be achieved either by an exclusively active actuation or supplemented by an appropriately timed release of energy that could be stored in elastic elements (typically tendons) during the earlier foot-ground collisions. Storing energy in elastic elements occurs at a number of lower limb joints, whereby Eng & Winter, 1995 and Kuo et al., 2005, have shown that during push-off, the ankle joint contributes more power than the hip or knee.

The relative contribution of the ankle muscle's positive work or Achilles tendon's passive return of the stored energy to this push off power has been studied using ultrasound techniques (Fukunaga et al., 2001; Ishikawa et al., 2005 and Lichtwark & Wilson, 2006). These studies have shown that the ankle muscles contribute little positive work, whereby the majority of the push-off power comes from the strain energy stored in the Achilles tendon. Specifically, during push-off, the Achilles tendon releases its stored strain energy and the ankle plantarflexor muscles contract approximately isometrically. This mechanism is thought to be a major factor in reducing the metabolic cost during gait (Sawicki et al., 2009).

As the ankle joint is believed to play a major role in determining the overall energy efficiency of gait, it is beneficial to look in more detail at its role during gait, as described in the following section.

2.3 Role of Ankle in Anatomically Intact Gait

The data presented in this section describes the sagittal plane kinematics and kinetics at the ankle joint. The only publically available full numerical data set (including ankle angle, moment, and angular velocity) of level walking found during a literature search is in Appendix A of Winter, 2004a. However, these sets of data are based on only one subject; a female weighing 56.7 kg. Due to the low body mass and the fact that only one subject's data is available, it was decided to use data previously gathered (by Jones R – personal communication) in the same department where the work for this thesis was undertaken. Details on the protocol used to collect the data are provided in Appendix- A.

The data corresponding to comfortable walking speed was chosen for the current study and averaged across individuals of similar weight. Figure 2.6 represents the averaged data for the ankle joint of seven participants in the study by Jones R – personal communication.

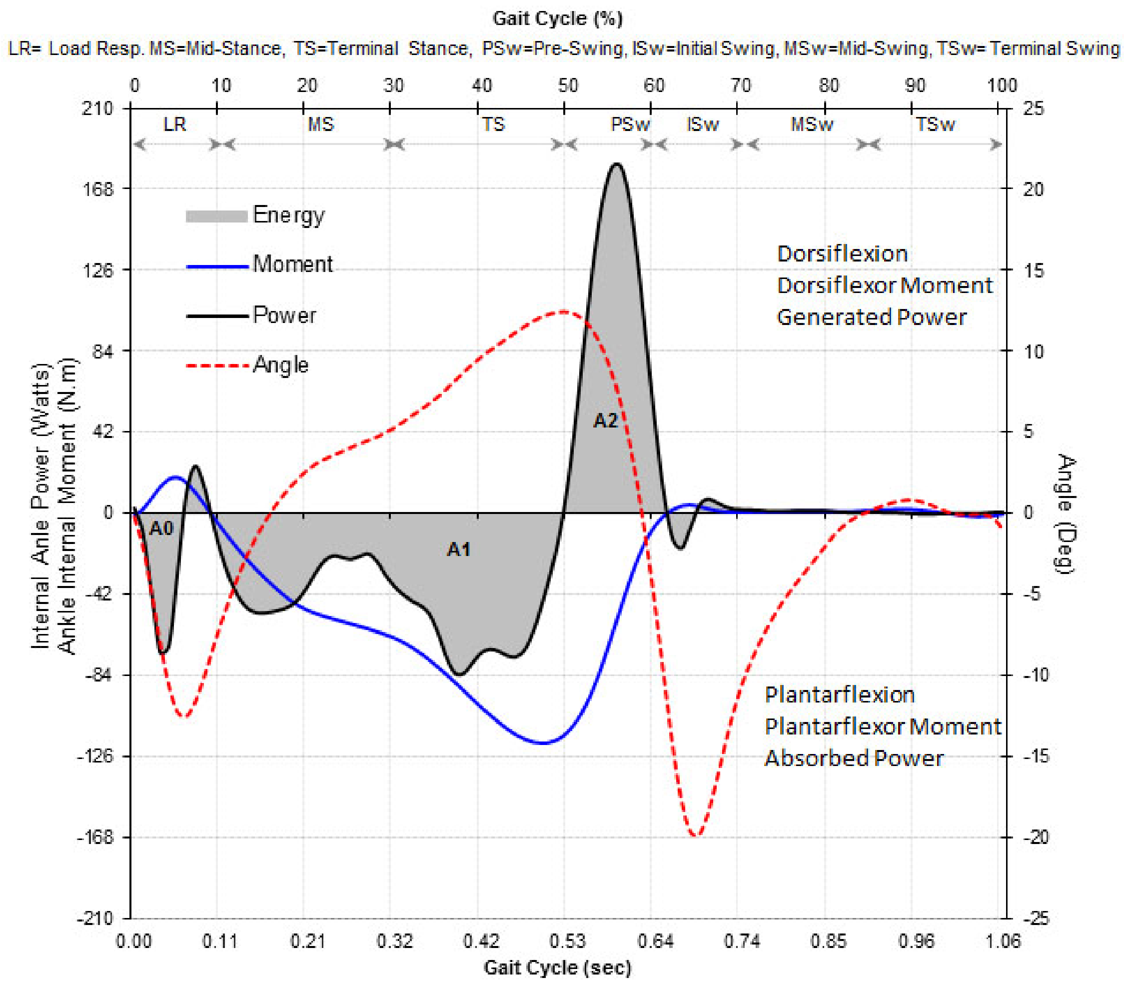

Figure 2.6: Ankle angle, internal moment, and power data for healthy individuals.

Referring to the Figure 2.6, at the start of the gait cycle, the ankle is close to a neutral position or slightly plantarflexed. Just after initial contact, the ankle rapidly plantarflexes under the action of eccentric contraction of the tibialis anterior (during 0-7% of gait cycle) and reaches foot flat at the end of this plantarflexion peak (at 7% of gait cycle). It then reverses its direction and starts dorsiflexing by the eccentric contraction of the triceps surae, during which the foot remains flat on the ground while the tibia rotates forward over it. The dorsiflexion continues until the end of terminal-stance period (approximately 43% of gait cycle, when opposite foot makes contact with the ground). It then rapidly plantarflexes due to concentric contraction of the triceps surae, until toe off begins (at 62% of gait cycle). This is followed by a dorsiflexion phase under the action of tibialis anterior until mid-swing to gain a neutral position in preparation for the next cycle (Perry, 1992; Whittle, 2003).

2.3.1 ANKLE KINETICS

The same nomenclature for negative and positive work phases (which refers to the build-up and release of strain energy, respectively, in the relevant muscles and tendons) established by Winter & Sienko, 1988, is adopted here for the description of ankle kinetics.

Referring to Figure 2.6, following heel strike, the rapid but controlled plantarflexion of the foot to achieve a smooth touchdown and an earlier foot-flat position (for stabilisation) is achieved by a small eccentric dorsiflexion moment. The resulting energy absorption phase is labelled as A0 (additional phase), which corresponds to a small energy absorption phase during the foot-ground collision as proposed with the simple pendulum model. After foot-flat is achieved, ankle dorsiflexion (while the foot remains on the ground) due to tibial rotation over the foot, is again resisted by an eccentric plantarflexion moment to provide stability during this single support phase. This is a major energy absorption phase, which occurs from early through to late stance, and is labelled as A1. This phase corresponds to the slow stretching period of the Achilles tendon as observed by Fukunaga et al., 2001; Ishikawa et al., 2005 and Lichtwark & Wilson, 2006, and during which the triceps surae muscles remain approximately isometric (Figure 2.7 with specific focus on the gastrocnemius muscle). During push-off, rapid plantarflexion of the ankle takes place due to an active concentric plantarflexion moment labelled as A2. This is the major energy generation phase, similar to the rapid recoil by the Achilles tendon (Ishikawa et al., 2005), and is the most important contributor to assisting push-off and acceleration of the leg into swing phase (Winter, 1983).

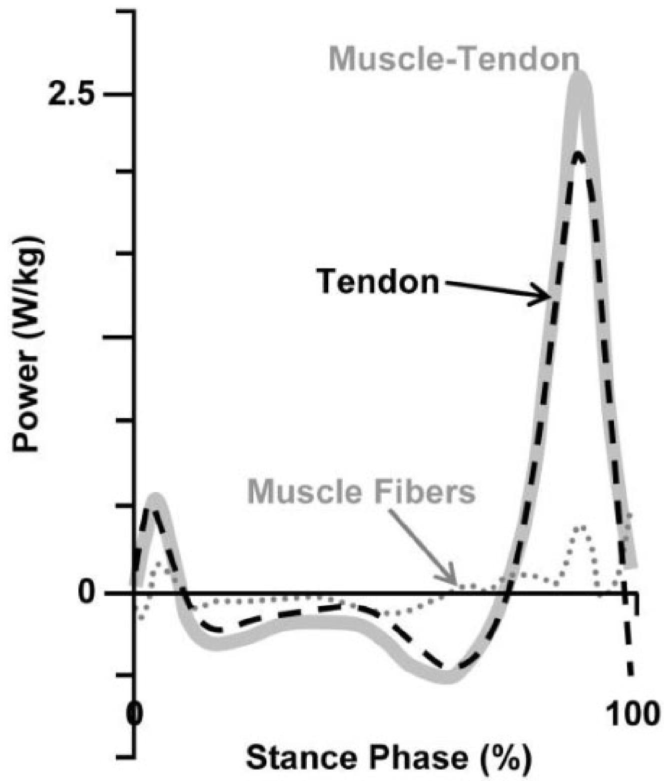

Figure 2.7: Ultrasound imaging data from human walking showing the instantaneous power for gastrocnemius muscle fibres and Achilles tendon. Figure adapted from Sawicki et al., 2009.

Taking purely stance phase into consideration, the ankle joint's contribution to the total positive work done by the ankle, knee and hip is approximately 60% (Sawicki et al., 2009). The majority of this positive work comes from energy storage and return of the Achilles tendon alone; reaching approximately, 0.41 J/kg compared to the muscle's contribution of only 0.02J/kg (see Figure 2.7). This difference highlights the importance of the ankle's energy storage and return mechanisms in powering push-off during gait.

2.4 Amputee Gait

Amputee gait is characterised by consistent deviations from anatomically intact gait in terms of temporospatial, kinematic, kinetic, and metabolic gait parameters. Skinner & Effeney, 1985, have reported obvious deviations from anatomically intact gait in both the transfemoral and transtibial amputee gait. For instance, both these amputee groups walk asymmetrically and have a slower than the self-selected walking speed for anatomically intact individuals (Waters et al., 1976; Winter & Sienko, 1988; Torburn et al., 1990; Gitter et al., 1991 and Winter, 2004b) because they rely more on the intact limb to compensate for the prosthetic side during single support phase. These compensations require more effort (increasing the metabolic cost and decreasing the walking economy) by the amputee, as will be discussed below, to cover the same distance and/or walk at the same speed as a non-amputee (Waters & Mulroy, 1999 and Genin et al., 2008a).

2.4.1 Energy Efficiency of Amputee Gait

Several studies have reported the metabolic cost among a range of transtibial amputees for self-selected walking speeds during level walking (Ganguli et al., 1974; Gailey et al., 1994; Casillas et al., 1995; Torburn et al., 1995; Waters & Mulroy, 1999; Schmalz et al., 2002 and Paysant et al., 2006). Figure 2.8 shows the energy cost and comfortable walking speed from these studies compared with the energy cost of anatomically intact adults as reported in Ralston, 1958.

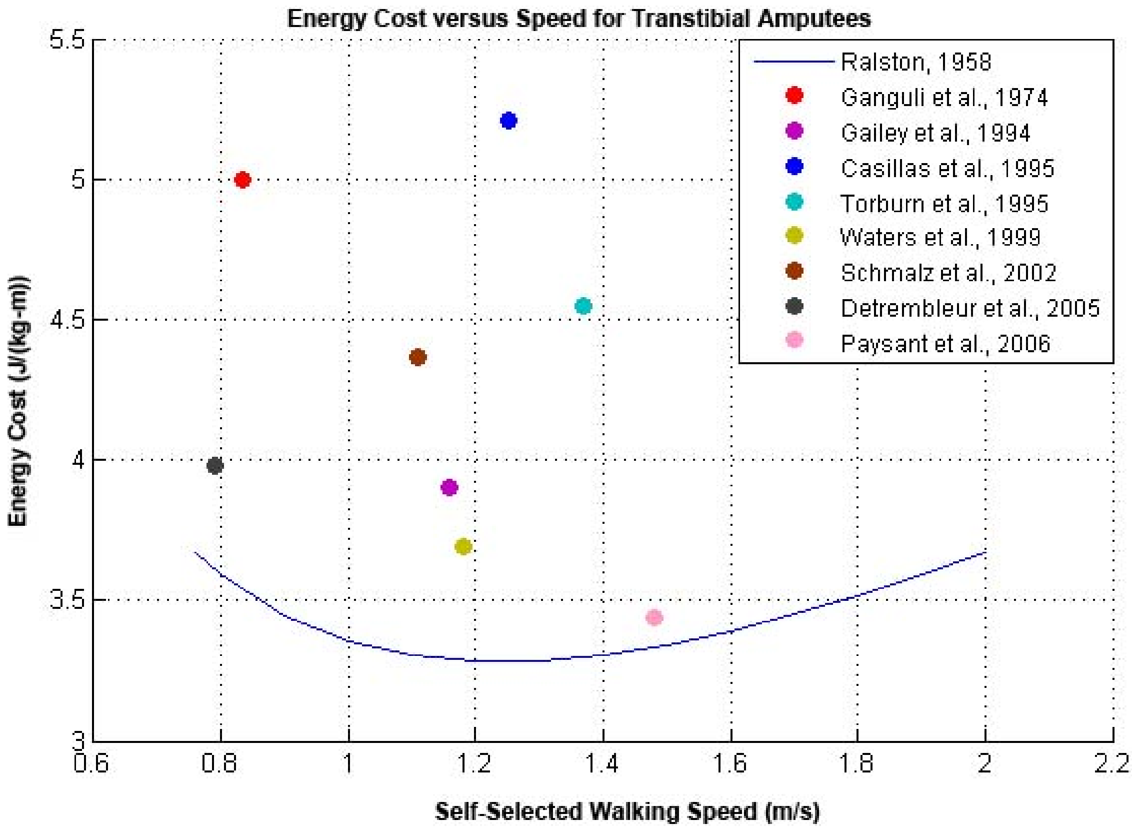

Figure 2.8: Reported energy cost for transtibial amputees (scattered plot) at self-selected walking speeds. The solid blue line represents the energy cost of anatomically intact adults as a function of walking speed.

Figure 2.9 shows the energy cost, obtained from Buckley et al., 1997; Waters & Mulroy, 1999; Schmalz et al., 2002; Orendurff et al., 2006; Genin et al., 2008b and Starholm et al., 2010, for a range of transfemoral amputees at self-selected walking speeds, and these are compared with the energy cost of normal adults as reported in Ralston, 1958.

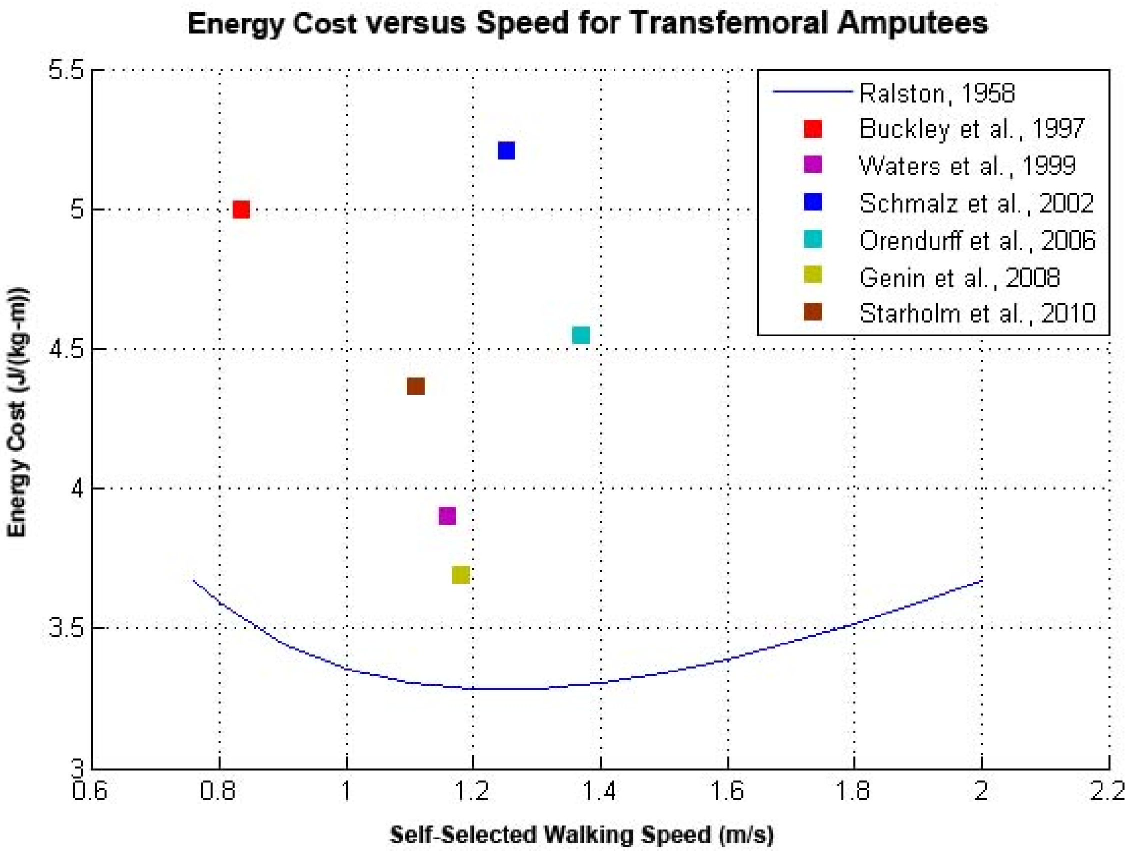

Figure 2.9: Reported energy cost for transfemoral amputees (scattered plot) at self-selected walking speeds. The solid blue line represents the energy cost of anatomically intact adults as a function of walking speed.

Figure 2.8 and Figure 2.9 show that amputee gait is metabolically more expensive and hence less efficient than anatomically intact gait.

2.5 Current Prosthetic Feet

2.5.1 Conventional & Energy Storing/Return Prosthetic Feet

As the efficiency of amputee walking is generally poor, there have been many studies aimed at designing improved prosthetic components, notably feet.

The Solid Ankle Cushioned Heel (SACH) foot was introduced in the 1950's and comprises of a wooden keel, which is embedded in an elastic material and provides mid-stance stability with little lateral movement. Its heel is composed of a compressible polyurethane material to absorb shock at heel strike by compression, and thus provides limited (pseudo) plantarflexion.

Articulated feet are categorised based on movements offered at their axes of rotations. A single axis foot has an ankle joint allowing motion only in the sagittal plane with a rigid keel. Two rubber bumpers limit the range of motion and allow for different stiffness characteristics during walking. A multi axis foot is similar to a single axis foot, but allows additional motion in the frontal plane and often also in the transverse plane (Versluys et al., 2009).

Energy storage and return (ESR) prosthetic feet have been designed with the aim of storing energy during early and mid-stance and returning a portion of this stored energy to the amputee later in stance. The Seattle Foot (Seattle Limb Systems, Poulsbo, WA, USA) and Flex-Foot (Ossur Americas Holdings Inc, CA, U.S) are examples of this type of foot. However, as is discussed in the following section, the results of clinical studies have yet to demonstrate a clear advantage in terms of energy efficiency of ESR feet compared with conventional prosthetic feet.

2.5.2 Review of Studies on Comparing Different Prosthetic Feet and Their Effect on Amputee Gait

The energy storage and return behaviour of ESR feet are aimed at simulating, to some extent, the functional behaviour of the anatomical intact shank and foot. Various subjective as well as evaluative studies have been carried out to compare these with the non-ESR feet. Despite some controversies found between subjective feedback (Nielsen et al., 1988 and Alaranta et al., 1994) and biomechanical measurements (Gitter et al., 1991 and Postema et al., 1997), amputees generally seem more inclined towards the use of

ESR feet, such as Seattle and Flex-Foot feet, possibly because they experienced greater comfort with less skin disorders, greater stability on uneven ground walking and achieved higher walking speeds during uphill walking with ESR feet compared to SACH feet (Nielsen et al., 1988 and Alaranta et al., 1994). However, many other biomechanical studies concluded that, despite certain advantages over conventional feet, ESR feet do not return a significant amount of energy to the amputee, and energy requirements of amputee gait remain higher in comparison with the anatomically intact gait (Waters et al., 1976; Nielsen et al., 1988; Torburn et al., 1990; Gitter et al., 1991; Barth et al., 1992; Colborne et al., 1992; Lehmann et al., 1993; Geil, 2000; Hafner et al., 2002; Versluys et al., 2008a and Grabowski & Herr, 2009). Barr et al., 1992, have reported an ESR prosthetic foot to deliver 7.5% of peak power required by an anatomically intact ankle, which is approximately double than the peak power delivered by a conventional prosthetic foot. Similarly, Segal et al., 2006, have reported an average of 24.7% of peak power required, to be delivered by two ESR prostheses. These results showed that ESR feet are unable to provide a significant amount of ankle work. Apart from the reduction in delivered power, peak power outputs do not necessarily occur at the same time during gait compared with the anatomically intact ankle, resulting in a badly timed energy return (Menard & Murray, 1989). A summary of a few other studies comparing the energy costs of different conventional as well as ESR feet is shown in Figure 2.10.

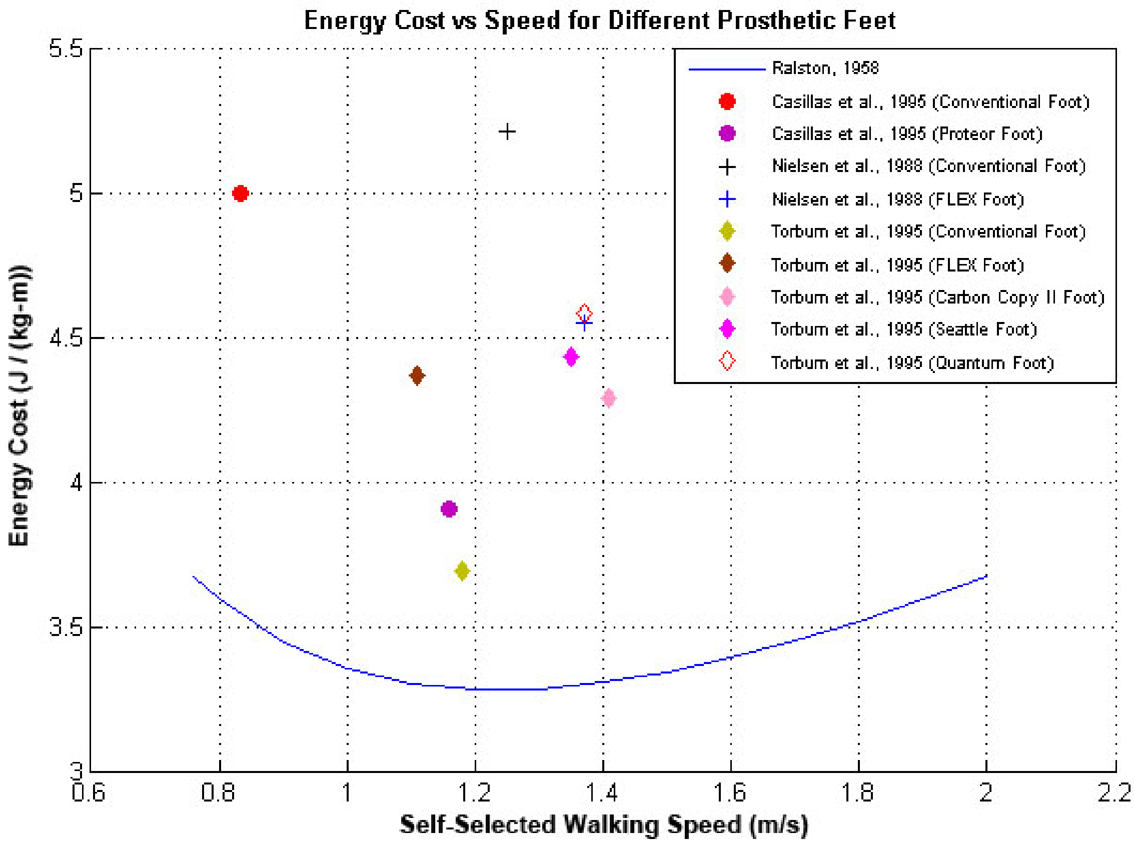

Figure 2.10: Energy cost for transtibial amputees (scattered plot) using different commercially available prosthetic feet at self-selected walking speeds.The solid blue line represents the energy cost of anatomically intact adults as a function of walking speed.

It is obvious that current commercially available ESR prosthetic feet provide no improvements over conventional feet in the joint moment/power level or in terms of improving the metabolic costs of amputees. The reason for poor performance of passive prosthetic feet, whether ESR or conventional, lies in the uncontrolled nature of their storage and release of energy. This will be discussed in the following section.

2.5.3 Gait Deviations at the Ankle in Amputees

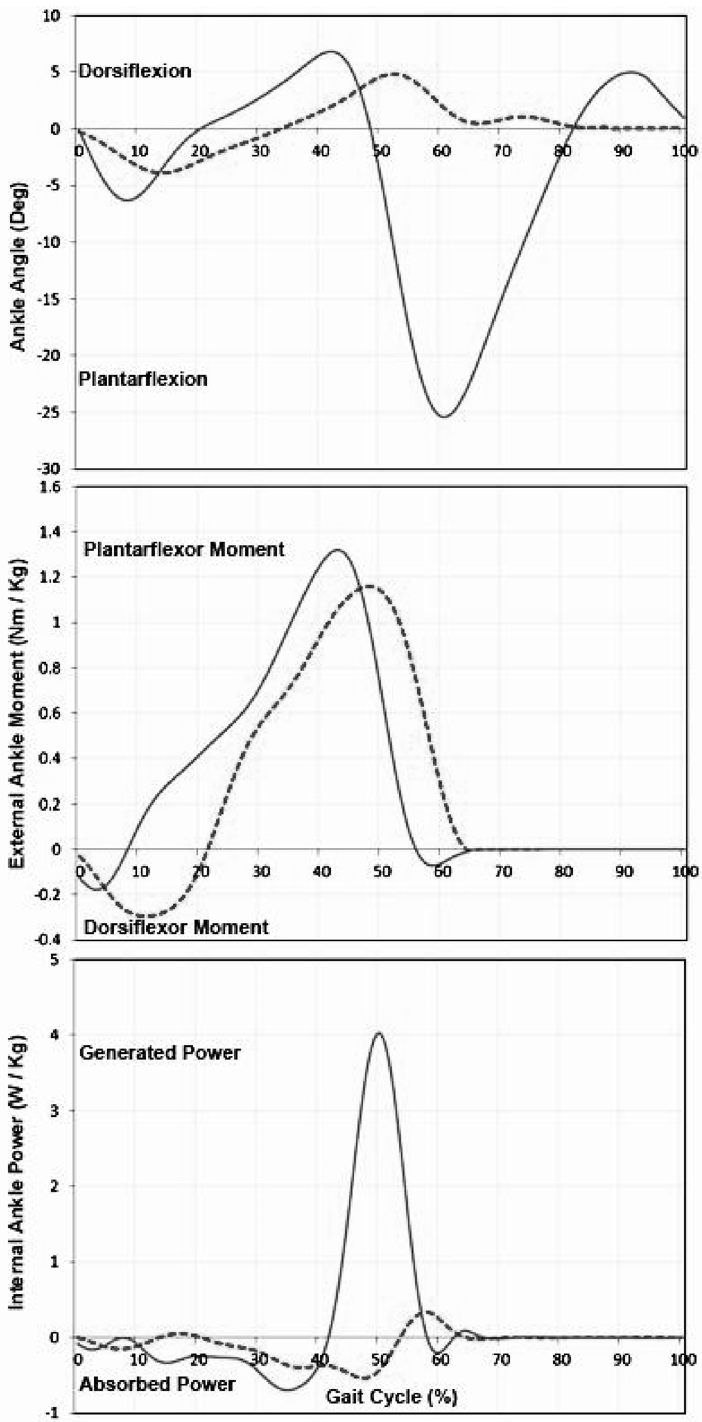

Figure 2.11: Comparison of gait parameters between a healthy individual and a transtibial amputee. Solid line represents the data for an anatomically intact subject, whereas the dashed line represents the data for a transtibial amputee with an SACH foot. Figure adapted from Whittle, 2003.

Figure 2.11 represents a comparison between gait parameters of the ankle joint for an anatomically intact individual and a unilateral transtibial amputee fitted with a SACH foot. The data of both individuals, taken from Whittle, 2003, are presented on the same graphs to allow easy comparison. In anatomically intact gait, rapid plantarflexion early in stance leads to early foot-flat. In contrast, plantarflexion of the prosthesis during early stance is rather prolonged, resulting in delayed foot-flat and probably relatively poor stability (Winter & Sienko, 1988).

Mid to late stance dorsiflexion in anatomically intact gait begins at approximately 10% of the gait cycle and increases steadily to approximately 40% of the gait cycle. In the example presented here in Figure 2.11, the amputee shows slower and delayed dorsiflexion with a lower peak moment, possibly because the solid keel of the SACH foot has deformed minimally, (and thus restricted motion) and the resulting compression of the foot material likely dissipates significant strain energy (Winter & Sienko, 1988). Unlike the data on the anatomically intact ankle, the most prominent feature of the prosthesis data is the absence of rapid and sustained plantarflexion at push off. More specifically, the prosthetic ankle never goes beyond neutral plantar-dorsiflexion after being dorsiflexed during mid to late stance. This lack of push off occurs because the energy absorbed during stance is dissipated by the prosthetic foot, and this dissipation is reflected in the power curve, in contrast to the energy released at the anatomically intact ankle.

These deviations from an anatomically intact gait will require the amputee to compensate for with other joints (Winter & Sienko, 1988; Gitter et al., 1991; Zmitrewicz et al., 2007 and Silverman & Neptune, 2012), as will be discussed in the following section.

2.5.4 PROPOSED REASONS FOR LOW ENERGY EFFICIENCIES

As discussed in Section 2.2, energy optimisation of anatomically intact gait involves pendulum-like exchanges of kinetic and potential energy during step-to-step transitions. The ankle plantarflexors are considered as the most important contributors for energy transfer between the leg and trunk segments. Neptune et al., 2001, have shown that the plantarflexor group increases and decreases energy of the trunk before mid-stance and afterwards respectively, and damage to, or loss of, this muscle group due to amputation would certainly affect the walking performance and would require compensations from other muscle groups.

Recently, Silverman & Neptune, 2012, have carried out a 3D model-based simulation of amputee and anatomically intact gait. Data from various anatomically intact individuals and transtibial amputees, using a combination of ESR and conventional feet, were collected. The model was optimised to provide a best match with the experimental data in order to explain the synergistic contributions of both the prosthesis and the individual muscles' work to provide body support, forward propulsion, leg-swing initiation, and medio-lateral balance during amputee walking. The optimised simulation results proved to be statistically indifferent from experimental data, and the role of different muscle groups was reported for the residual limb, the amputee intact limb and for the anatomically intact limb. The authors concluded that the prosthesis partially replaced the ankle plantarflexors' function in providing forward propulsion by absorbing energy from the residual limb throughout the stance phase and returning parts of the stored energy to the trunk. However, the amount of absorbed energy by the prosthesis was much greater than the delivered energy, resulting in reduced push-off because the total energy was negative. Therefore, the prosthesis failed to return substantial positive energy that the ankle plantarflexors in anatomically intact subjects deliver to the trunk during the same phase and hence failed to functionally replace the ankle plantarflexors' role (Silverman & Neptune, 2012).

2.6 Previous Attempts to Address the Problems of Energy Efficiency in Transtibial Amputee Gait

To address the limitations with passive ESR feet, a number of controlled and actuated prosthetic ankle devices have been developed. These designs are reviewed below.

2.6.1 ACTIVE PROSTHESES

Active prostheses attempt to replicate the total human ankle behaviour by actively providing the push off power and control to the user. These prostheses can be classified based on their actuation principles.

2.6.1.1 Pneumatically Actuated Devices

Various attempts have been made in developing pneumatically actuated devices. Klute et al., 2000 and Klute et al., 2002, have described the development of a pneumatic actuator that replicates the functional behaviour of the triceps surae muscles and the Achilles tendon. The actuator comprises of a McKibben muscle connected in parallel with a damper with two fixed orifices, forming the artificial muscle's triceps surae part of the actuator. The mechanical counterpart for the Achilles tendon is a linear spring connected in series with the pneumatic muscle and serves as an artificial tendon, as shown in Figure 2.12.

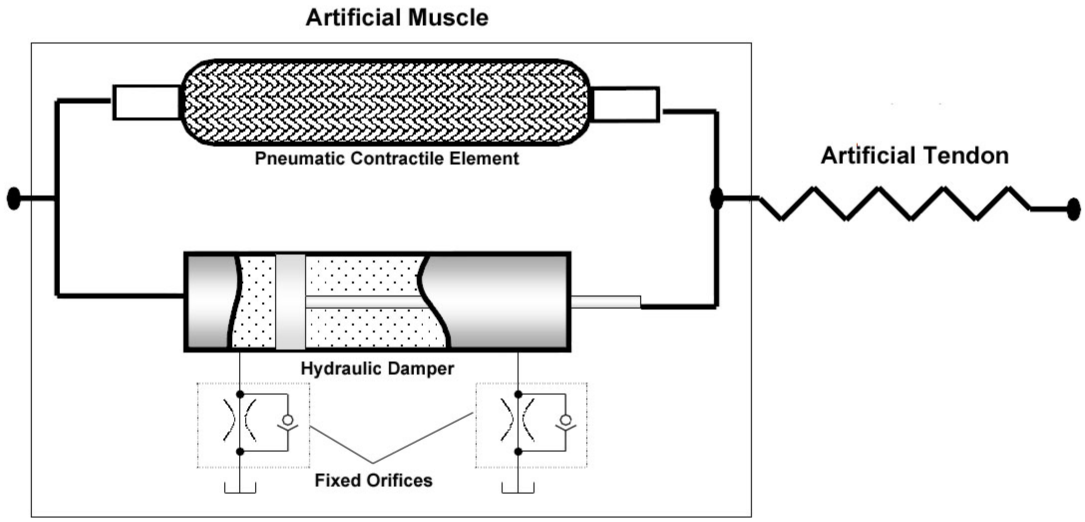

Figure 2.12: Schematic diagram of the pneumatic actuator. Figure adapted from Klute et al., 2002.

The authors have claimed that experiments with the actuator have shown its capabilities in providing high torque and near-normal ankle range of motion. However, no published article was found on the experiments with the actuator except for a photograph given on the authors' website.

Versluys et al., 2008b and Versluys et al., 2009, have developed a powered prosthesis based on pleated pneumatic artificial muscles (PPAMS) (the design details and characteristics of PPAMS are beyond the scope of this thesis and can be found in Daerden & Lefeber, 2001). Their prosthesis comprises of three PPAMS, which are connected in parallel to achieve the required ankle torque. The purpose of their study was similar to the previous study one, i.e. to mimic the human musculature and its force generation properties. Three servo valves were used with a pressure source to supply constant pressure of 7 bar to the PPAMS.

Sup et al., 2007, have used compressed nitrogen to develop a transfemoral prototype prosthesis. Rather than using muscle-like actuators, they have utilised double acting pneumatic cylinders, which are controlled by four-way servo valves at an operating pressure of 20 bar. Tests were conducted on an anatomically intact subject with a flexed-knee adapter to show that the prototype produced the required torques and powers with a near anatomically intact gait pattern. All of the above-mentioned studies have utilised compressed gas to power the actuators, and their focus was to produce human-like ankle characteristics.

However, one issue using pneumatics is that the energy cost of producing human-like ankle work is not taken into account by any of these studies. For instance, a small commercially available aluminium air compressor requires 1.1 kW of electrical power and weighs about 23 kg to provide a maximum pressure of 8 bar (http://www.ingersollrandproducts.com (accessed 18/02/2013)). Comparing the required input power to the compressor with a typical peak power of around 200 W, required at the ankle would yield an overall efficiency of approximately 18 % for the whole system.

Another issue with pneumatics is the autonomy of the system. For instance, the tank that was used to maintain a constant pressure supply (maximum pressure of 5 bar only) in the study by Klute et al., 2002, is 4,000 times bigger than the actuator in terms of volume. Similarly, the compressors require a petrol/diesel engine or an alternating current (AC) supply, and are large and heavy, even with an aluminium construction. The design by Sup et al., 2007, requires even higher pressure (20 bar), which would add to the compressor size and weight. In addition, the losses related to compressed air production, storage and transmission also add to the already degraded efficiency of the system. Furthermore, use of dampers to mimic the muscles' eccentric behaviour (Klute et al., 2002) is simply a waste of energy (into e.g. heat and noise). An efficient way would be to utilise regenerative braking for the energy conversion, rather than wasting the energy by dissipation. Also, all these designs are equipped with servo valves (which are essentially orifices), in which the energy losses remain high due to the inevitable pressure drop, further adding to the overall efficiency degradation.

2.6.1.2 Electrically Actuated Devices

Sup et al., 2009, have developed a self-contained transfemoral prosthesis that utilises the same slider-crank mechanism as described in Sup et al., 2008, but with the pneumatic actuation being replaced by electrically (motor driven) actuation at both the knee and ankle joints. The complete prosthesis weighs approximately 4.2 kg, and their initial experiments with a unilateral transfemoral amputee for ten consecutive trials at self-selected speed of level-ground walking showed that the prosthesis enabled the user to attain a walking speed of 1.41 m/s compared to 1.13 m/s with a passive prosthesis. The knee and ankle angle, moment and power data with the prosthesis were similar to data on anatomically intact gait, as described in Winter, 1991. As the average power consumption of the battery (at self-selected speed) is 66 W and the battery has an energy capacity of 118 W.h, the user would have to recharge the battery after every 1.8 hours of walking (at self-selected speed). This charging cycle is on the optimistic side as daily activities of a user are not limited to steady state walking at self-selected speed. In fact, everyday tasks, such as shopping or moving around house, require the user to frequently brake and accelerate, and both of these simple tasks require more energy compared to walking continuously at a steady rate.

The development of series elastic actuator (SEA) by Pratt & Williamson, 1995, has provided efficient means to develop electrically powered robotic, prosthetic and orthotic devices with small sized motors. An SEA comprises of a spring connected in series with a mechanical transmission and a direct current (DC) motor. The spring compliance between the motor and load reduces impedance (increases back-driveability) with noise-free force outputs. The reduced impedance of the actuator allows for the use of a smaller and lightweight motor, and consequently the power input to the motor could be reduced.

With these benefits of SEAs, different research groups have utilised these actuators to develop electrically actuated prostheses. For instance, a prosthesis developed by Au et al., 2007, utilises an additional spring connected in parallel with an SEA. This spring shares the load requirement with the SEA, thus reduces the SEA's load in terms of peak torque requirement, thereby reducing the overall size and weight of the motor. The reduced size of the motor would reduce the energy input and consequently the current and copper losses, and hence would lead to a reduction in weight, thus it would altogether improve the overall efficiency of the system. In addition, the advantage of SEAs is also of significance as it minimizes the transmission damage due to shock loads during the gait cycle, e.g. at heel strike.

The experiment with a bilateral transtibial amputee showed improvement in the metabolic economy compared to using a passive elastic prosthesis (Au et al., 2008). A prototype prosthesis with an SEA was subsequently successfully commercialised as PowerFoot Biom (iWalk, Cambridge, MA). The final product is, according to Herr & Grabowski, 2012, capable of allowing for near normal metabolic costs, walking speeds and late stance kinetics and kinematics. These authors have reported a metabolic cost of transport (COT) of 0.051 for amputees using the PowerFoot Biom prosthesis, whereby the given figure is a dimensionless parameter obtained from dividing the metabolic energy required (J) by the product of body weight (N) and distance travelled (m). An equivalent COT of the motor was also calculated by assuming that the muscles' mechanical work can be completely replaced by the motor. Therefore, with 23.86 J of net positive work performed by the motor, and on the basis that muscles have an efficiency of 25% to perform positive work, the equivalent metabolic energy required by the motor is 95.44 J. Using the amputees' mean mass of 99.5 kg and mean walking speed of 1.75 m/s, the COT of the motor is calculated as 0.056. This means that a reduction in metabolic cost for the amputees using bionic prosthesis is slightly less than the metabolic equivalent of the energy input from the electric motor. Without the motor, the bionic prosthesis would functionally behave as a standard ESR foot/prosthesis. This shows that the energy storage and return characteristics of this design is not much different from commercially available ESR feet in terms of inefficient storage, as it solely relies on the power source rather than utilising the potential energy storage opportunities available during the A2 phase of the anatomically intact ankle power profile (Figure 2.6).

Another notable attempt has been made by the researchers at the Arizona State University where investigators have utilised a robotic tendon, first introduced by Hollander et al., 2006, similar to an SEA to develop a transtibial prosthesis under the name of SPARKy (Spring Ankle with Regenerative Kinetics projects). The robotic tendon is actuated by a motor to provide power when required during gait while relying on the stored energy in the spring as a major contributor to push off power (Hitt et al., 2007). The third generation of this device (SPARKy 3) incorporates active control in both the sagittal and coronal planes, weighs 2.1 kg (Bellman et al., 2008 and Hitt et al., 2008), and is claimed to be capable of providing amputees with enough power to sprint and jump. However, no published literature was found on the testing of the prototype.

2.6.1.3 Quasi-Passive Devices

Collins & Kuo, 2010, have developed a microprocessor-controlled foot capable of storing some energy at heel strike using a spring that is locked by a clutch mechanism throughout stance phase. The locked spring is released by another clutch, thereby releasing energy at push-off. The storage mechanism is completely passive, and the only active components are the microcontroller and two small motors, which are used for releasing the energy-storing spring and for resetting the mechanism for the swing phase (Figure 2.13). The mechanism is capable of automatically adapting to different walking surface slopes.

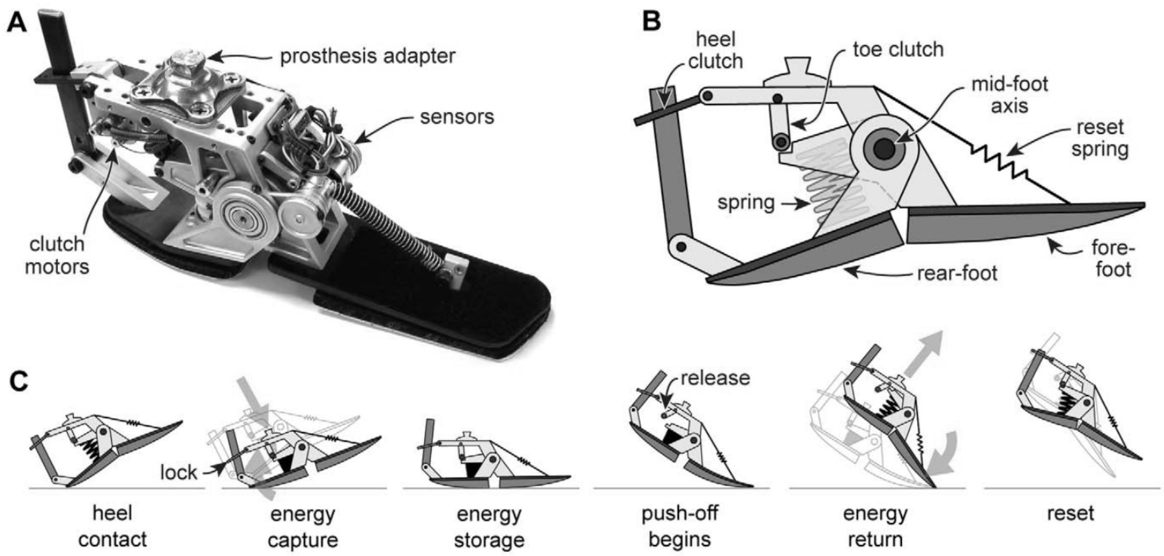

Figure 2.13: A) Prototype device. (B) Schematic design. (C) Working sequence. Figure adapted from Collins & Kuo, 2010.

The power profile for the energy recycling foot is presented in Figure 2.15.

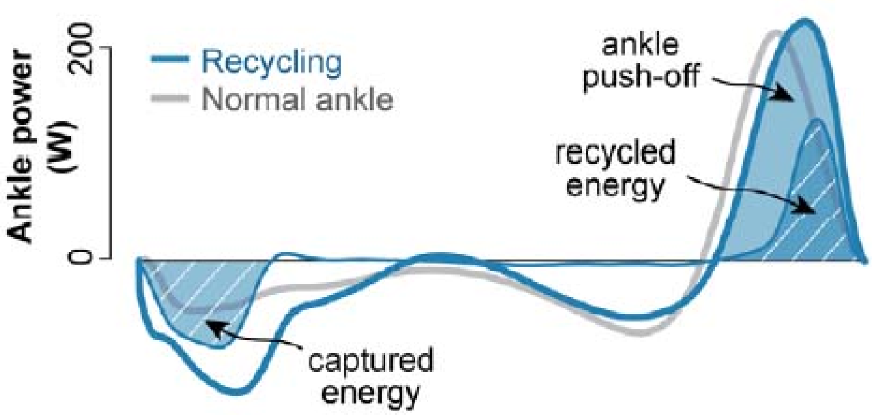

Figure 2.14: Hatched area corresponding to the stored and released energy by the energy recycling foot. Figure adapted from Collins & Kuo, 2010.

The hatched area in Figure 2.14, as described by Collins & Kuo, 2010, corresponds to the storage and release of energy by the energy recycling foot. On close inspection, this power profile appears to be questionable in two respects. For anatomically intact gait, the load acceptance work (A0 phase in Figure 2.6) is very small compared to the mid-stance work (A1 Phase in Figure 2.6). In fact, the majority of publications (Perry, 1992; Whittle, 2003; Winter, 2004a and Kirtley, 2006) have considered the mid-stance work as the major energy-storing phase. In this context, the anatomically intact gait data presented by Collins & Kuo, 2010, as shown in Figure 2.14, contradicts the consensus described above. The second reason is that the load-acceptance work stored by the energy recycling foot (Figure 2.14) is greater than previously published values from studies of anatomically intact walking. This could only be achieved by a greater than normal resistance to initial plantarflexion (to achieve foot flat), resulting in an abnormal gait pattern, as well as requiring the user to consume more metabolic energy.

In summary, it is clear from the design that the energy recycling foot does not store the mid-stance work, which is the large majority of the eccentric ankle work during stance. This may explain the limited metabolic cost reduction with the energy recycling foot (which remained above 7% to what is seen in an anatomically intact gait) as reported by Segal et al., 2012. Nevertheless, the concept of the design to utilize a hybrid form of passive ESR and active prosthetic foot (controlled storage and release of passive work), could offer a cost effective and reliable solution in improving amputee gait biomechanics.

2.6.1.4 Summary of Active Prostheses

In the previous sections, the limitations with pneumatic and electric actuation and the quasi-passive design were discussed. As mentioned before, pneumatically actuated devices, although serving as a proof of concept, are highly inefficient, with autonomy as the biggest challenge. Electrically actuated devices incorporating an SEA are improvements, but even the state-of-art bionic foot relies purely on the battery power and does not utilise the ample energy recycling opportunities available at the ankle during gait. Further, the commercialised version, the Bionic Foot, costs more than £30,000 (http://massacademy.wordpress.com/2011/02/24/powerfoot-seeks-to-redefine-human-prosthetics-2/ (accessed 18/02/2013)).

The right approach to develop a highly efficient and cost effective solution lies in a design that could harness the energy saving opportunities available at the joints, similar to the quasi-passive design by Collins & Kuo, 2010. However, theirs only stores energy during the load acceptance phase (A0 phase of the ankle power profile, Figure 2.6), but does not utilise the ample energy storage opportunities during the A1 phase. However, the design shows that using a passive yet controllable energy storage and return mechanism could be beneficial in improving amputee gait biomechanics.

2.7 Alternative Actuation Technologies

It is well possible that the solution to the problems described above lies in the selection of energy storage elements and the actuation mechanisms. Devices utilising passive storage elements with discrete control via spring/clutch mechanisms lead to an increase in size and weight of the prosthesis. Spring/clutch mechanisms may not be a very efficient way of capturing all the available energy during the eccentric power phases of gait. Therefore an alternative storage and actuation technique might be beneficial for the design of an efficient and cost effective solution that could harness all of the available energy to be stored and released at the right instant during gait.

Before exploring alternative solutions, it is necessary to first of all establish the key requirements for the energy storage mechanisms during gait. For instance, the storage mechanism must be robust with an ability to charge and discharge quickly in a single gait cycle (of approximately 1 sec). As a safe estimate, the mechanism should be able to store an estimated energy of approximately 100 J and release approximately 30 J (Herr & Grabowski, 2012) within the gait cycle. The mechanism must also be able to release the stored energy as a short power burst of 300 W for level walking (Winter, 2004a) and approximately 500 W for incline walking (Lay et al., 2006). The mechanism must be able to maintain these charging/discharging cycles for at least approximately 5,000 steps or the equivalent of walking 5 km at a comfortable walking speed of 75 m/min. This would enable the system to exceed the upper limit of the 3,063±1,893 steps per day typically walked by an active transtibial amputee (Stepien et al., 2007). The combined foot and shank segment's mass should not be more than 6.1% of total body mass for an anatomically intact individual (Winter, 2004a) with a height of approximately 18 cm from the ground to the pyramid attachment at the distal end of the socket (based on the nominal height of a conventional transtibial prosthesis (Au et al., 2009). It should also be free of complex controls and should be simple to install. In addition, energy density (W.h/kg (measure of the amount of energy that a device can hold)) and power density (W/kg (measure of the amount of power that a device can deliver)), which are two key characteristics of energy storage mechanisms, need to be high enough to provide long running times and power peaks, respectively.

Based on these requirements, typical energy storage mechanisms such as flywheels, batteries, super capacitors, and hydraulic accumulators were reviewed. A brief summary about the feasibility of these alternatives, compared with the design specifications/requirements, is presented below:

Flywheels

Flywheels require a complex set of multiple controls, which represent potential single points of hazardous failure. These have low energy density and require continuous rotation during normal operation, which is prone to efficiency loss (Hadjipaschalis et al., 2009). Simple calculations for a typical flywheel to store approximately 100 J of energy, indicates that its required diameter, mass and rotational speed would be 12 inches, 1 kg, and 900 rpm, respectively (http://www.calculatoredge.com/mech/flywheel.htm (accessed 05/06/2013)). The size and weight of the flywheel could be reduced by increasing its rotational speed. For instance, to store the same amount of energy (100 J), with halved weight and size, the rotational speed would reach approximately 2500 rpm. However, due to the size/weight and/or high rotational speeds, it would be very difficult to incorporate a flywheel storage mechanism into a prosthesis, because of the space and size constraints. In addition, due to the gyroscopic effects, a flywheel would pose difficulty for the user to make turns.

Hydraulic Accumulators

Hydraulic accumulators are a very mature technology and have very high energy and power density, which makes them very suitable for longer run times and peak power bursts. As hydraulic accumulators work at high pressures, the components can be designed small, with low flow rates making it possible to have a single small energy storage component to store and release power when needed during gait. Hydraulic accumulators could be charged and discharged during a single gait cycle with virtually no limit on the charging/discharging cycles. With advances in material technologies, very lightweight accumulators are already commercially available. For instance, CTG (CTG Ltd, UK) offers virtually any bespoke size of hydraulic accumulators with a range of standard sizes. The smallest one is of 100 cc capacity, with a maximum operating pressure of 220 bar, a length of 104 mm, a diameter of 68 mm, and a weight of 180 grams (http://www.ctgltd.co.uk/page/hydraulicaccumulators/47 (accessed 18/02/2013)).

Batteries

There are several types of batteries based on Lead, Nickel and Lithium. Current battery technologies have decent discharge power but these cannot be charged fast enough (within a gait cycle) and have strong memory effect (limited life cycles) (Dahlen, 2003), rendering them as unfeasible for a regenerative-braking based system.

Super capacitors

The main advantages of super capacitors are their ability to charge quickly over shorter periods of time and to provide peak power bursts due to high power density. However, they have low energy density and higher self-discharge rates compared to batteries (Willer, 2003), and may not store enough energy within the gait cycle for later release. In addition, complexity is involved in making a safe and reliable super capacitor storage system.

Using a system utilizing electrical energy storage would require an actuator that could work as a generator during negative work phases of gait to charge batteries/super capacitors. The same actuator would then draw the power from the storage system to provide power during positive work phases of gait. Therefore, the storage system would need to be rapidly charged (during negative work phases of the gait cycle) to compensate for both the self-discharge as well as for the discharge of power for positive work phases. Rapid charging techniques are still in the research phase, and achieving a rapid recharge within a second is still a research challenge. Therefore, an electrical energy storage system might not be feasible in designing a sustainable standalone energy efficient prosthesis system.

	Specific Energy (Wh/kg)	**Specific Power (W/kg)**	**Charge/Discharge Cycles Over Life**
Requirements	***30-50***	***300-500***	***At least 2500 cycles/day***
Ni-Cd Battery	45 to 80	150 to 300	1500
NiMH Battery	60 to 120		300 to 500
Lead-Acid Battery	30 to 50	75 to 300	200 to 300
Li-ion Battery	110 to 160	200 to 315	300 to 500
Reusable Alkaline Battery	80		50
Super Capacitor	2 to 10	800-10000	1,000,000
Flywheel	100	11900	~10,000,000
Hydraulic Accumulator	10-100	5000	~11,000,000

Table 2.1: Comparison of energy storage technologies.Figures taken from Mackay, 2008; Hadjipaschalis et al., 2009; Rydberg, 2009 and from http://www.machinerylubrication.com/Read/2305/hydraulic-accumulators (accessed 30/7/2013).

Table 2.1 indicates that battery technology is very inadequate in terms of charge/discharge cycles over life and only super capacitors, flywheel, or hydraulic accumulator system can provide sufficient charge/discharge cycles. However, the energy storage capacity of super capacitors (specific energy) is too low when compared against the requirements. Therefore, the choice of an energy storage system remains with flywheel or hydraulic accumulators. As discussed earlier, a flywheel system is difficult to incorporate into a prosthesis due to its mass, high rotational speeds and gyroscopic effects, another difficulty with flywheels is safety issue. In case of flywheel failure, the shattered metal fragments are projected outwards with very high speeds. Therefore, the choice left is hydraulic accumulators and comparing with the requirements, these have high specific energies, specific power, and potentially unlimited life cycles.

2.8 Conclusions

Amputee gait is characterised by consistent deviations from anatomically intact gait in terms of temporospatial, kinematic, kinetic, and metabolic gait parameters. Currently available passive prostheses are uncontrolled in the storage/release of strain energy, and do not provide natural levels of resistance and propulsion. Designing a passive prosthesis to efficiently store and transfer energy between joints remains a research challenge.

To replicate the efficient energy recycling mechanisms seen in anatomically intact gait for the design of a prosthesis, selection of efficient energy storage and actuation mechanisms is critical. This is so because efficient design would require storing the negative work performed during gait and to use the stored energy for positive work phases. This is similar to regenerative braking principles adopted in vehicles, where electric regenerative braking (using batteries to store energy) is shown to capture 50% of the braking energy (Mackay, 2008). On the contrary, flywheels and hydraulic accumulators have been shown to salvage 70% of the braking energy (Mackay, 2008). However, the need for rapid recharging, memory effects, limited specific power and life cycles associated with batteries/super capacitors restrict their use in developing a sustainable energy recycling prosthesis design. Therefore, using mechanical energy storage systems (flywheels or hydraulic accumulators) seem to be a better choice to recycle energy for the design.

Where size/weight, complex controls, gyroscopic effects and safety hazards associated with the flywheels limit their use in a prosthetic system, hydraulic accumulators are advantageous in terms of being robust, with rapid cycling time and high energy/power density. Therefore, a hydraulic accumulator is chosen as an energy storage system to incorporate it in a novel conceptual design of an energy efficient prosthesis, which is described in the next chapter.

3. CONCEPT DESIGN I

Considering the efficacy and potential benefits of using a hydraulic accumulator as energy storage medium as outlined in previous sections, this chapter presents a unique design concept, utilizing a hydraulic accumulator as the energy storage medium. With a hydraulic accumulator as the energy-storing component, selection of a hydraulic actuation mechanism to provide torque is the next step in the design process. Using a fixed-displacement rotary actuator, acting as both motor and pump, to perform positive and negative work respectively is one option. However, in order to provide continuous control over the torque, the pressure drop across the actuator would need to be modulated using servo-valves. The issue with using servo-valves to control pressure is that they form an orifice in the line. The relationship between flow and pressure drop in an orifice is quadratic. i.e. if flow is doubled, then the pressure drop will increase four times, and this pressure drop is entirely dissipative (Cundiff, 2010). Therefore, considering the situation when the accumulator is fully charged and is required to release energy during the push-off phase, part of the stored energy would be lost through the valve in the form of heat, reducing the energy flow for the positive work. This would be an undesirable as well as unavoidable waste of energy stored in the accumulator. The losses associated with the pump, rotary actuator and valves would add up and may lead to an inefficient design. Therefore, a basic solution that could avoid the valves altogether would be to use a hydraulic accumulator with a variable displacement actuator (VDA). The loss of energy through valves would be completely avoided, leading to a simple yet efficient system.

With the decision of utilizing a hydraulic accumulator and a VDA, an overview of the design concept and its working principles is presented in Section 3.1. Section 3.2 briefly describes the system components. Sections 3.3 to 3.5 describe the theory and mathematical modelling of the system components. Section 3.6 presents the system simulation and calculation process of the hydraulic model of the design. Section 3.7 explains the sizing procedure of the actuator/actuator-gearbox using simulation. Section 3.8 describes a pseudo control of the design with gait data previously collected at the University of Salford, and this is followed by testing of the design with published gait data from Lay et al., 2006, and finished with a discussion.

3.1 Overview

The design concept is based on the hydraulic accumulator, a pressure relief valve, a VDA, a gearbox, and a low-pressure oil tank. The accumulator is used to store and release energy, the relief valve would ensure that the maximum accumulator pressure would not exceed the safe limits; the VDA would act as actuator to provide ankle torque; and the oil tank would be used to provide oil to the respective components. The design concept would be first studied using ideal conditions for the VDA-gearbox, with a gear ratio of one (to eliminate the gearbox), and then with real conditions (including losses) using relevant gear ratios. Based on the results, coupling of the gearbox with the VDA with real conditions would be compared with the ideal conditions and the design trade-off to be explored is whether the addition of a gearbox, and hence a reduction in the VDA size and associated weight, would result in an overall system weight that was lower than the VDA-only mode. Referring to Figure 2.6 for the anatomically intact ankle power curves, during the eccentric work phases of gait (predominantly from early through to late stance), the VDA would work as a pump, pumping oil from the low-pressure oil tank to the high-pressure accumulator, thereby storing energy in it, either in the form of a compressed spring or compressed gas. The stored energy in the accumulator would then be released during the concentric work phases of gait (predominantly during push-off), by the release of oil back into the low-pressure tank through the VDA, making it work as a motor, and hence providing the required ankle torque (at the VDA shaft in VDA-only mode, or at the gearbox shaft in VDA-gearbox mode). This concept is different from the commercially available ESR prostheses and from the Energy Recycling foot developed by Collins & Kuo, 2010, (refer to Section 2.6.1.3). The difference being controlled release of energy and the ability to harness all the available energy during eccentric phases of gait, making it more efficient. Given that the Energy Recycling Foot has a discreet control, which does not allow a continuous control of ankle torque and introduce noise impulses, the proposed design in this work would allow a continuous control of ankle torque offering smooth operation. In addition, the Energy Recycling Foot is based on a mechanical spring, making it difficult to take advantage of the substantial knee eccentric work during level walking (Winter, 2004a), and hence is limited for transtibial amputees only. Whereas, the concept of using a VDA with a hydraulic accumulator described here, would have an added benefit of using accumulator as a central energy storage component (where eccentric work from other joints e.g. knee could be stored), providing potential to develop it into a transfemoral prosthesis. Figure 3.1 shows the circuit diagram of the concept in its simplest form.

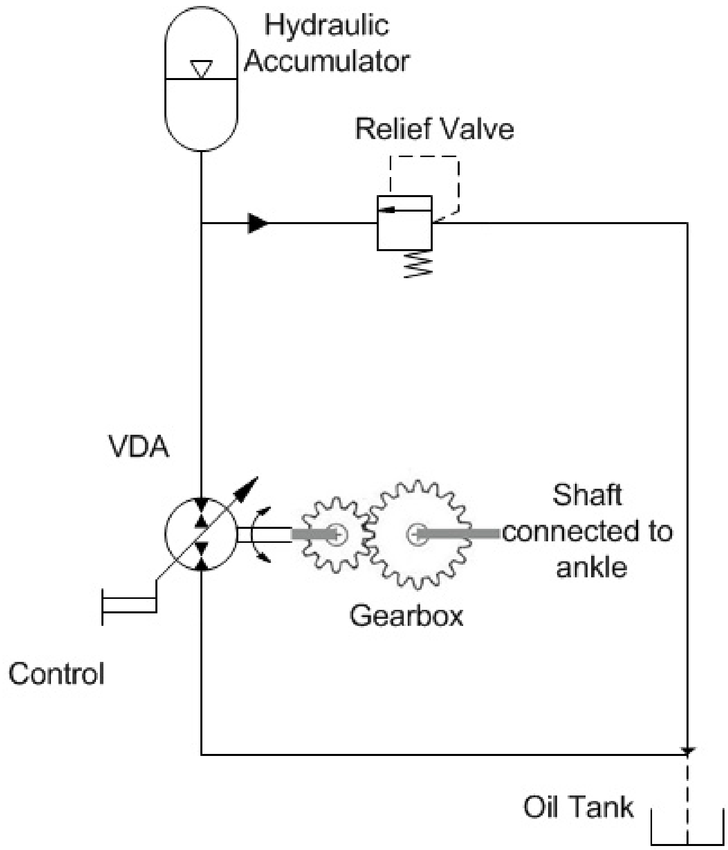

Figure 3.1: Schematic diagram of the concept design.

Referring to the Figure 3.1, the VDA is connected to the ankle joint through a gearbox. Therefore, the ankle joint rotation would cause the VDA shaft to rotate at a rate determined by the gear ratio. As a starting point for both cases, data on ankle angle and torque previously collected at the University of Salford were used as inputs with which to run the simulation. The ankle angle was converted into a signal to drive the VDA/gearbox shaft, and the ankle's torque was used as a signal to control the VDA's displacement (assuming perfect control). In a real system, the control system would modulate the VDA's displacement (and hence volume of oil pumped per unit rotation) to control ankle torque (a perfect control is always assumed in this work), and the ankle rotation would be determined by the dynamics of the system as a whole, including the amputee.

As mentioned earlier, during the eccentric phases of gait, the VDA would work as a pump, pumping oil from the tank to the accumulator, and during the concentric phases, the oil would be released by the accumulator to the tank, driving the VDA as a motor to provide torque at the ankle. To implement such a system, there would be a primary need to monitor gait phases in real time as a means of controlling the behaviour of the actuator as a pump or motor. There are a number of well-established approaches to gait phase detection, including the use of foot switch-(es) or pressure sensitive insoles, although the detailed design of the gait monitoring system and control design is left for future work. However, to estimate how the control system would modulate, a pseudo control was implemented, and the results are presented. The following section provides a discussion on the design components.

3.2 System Components

This section presents a description of the proposed design components.

3.2.1 Variable Displacement Actuator

A variable displacement pump/motor is chosen as the actuator for this design for two reasons. The first reason is that it could work as both a motor and pump, and therefore, the requirement of two separate actuators to account for the positive and negative work during gait is eliminated. The second reason is its capability of providing the variable oil displacement, which is necessary to provide a variable mechanical advantage during gait and thus continuous control of ankle torque. These VDAs are widely used for industrial purposes, and are available in a wide variety of sizes, weights, and types (axial piston or vane). So far, no attempt is known regarding their use in prosthetic/orthotic applications and as this work presents a conceptual design, therefore a commonly used axial piston pump/motor unit would be used to describe its working principles. Figure 3.2 shows a schematic diagram of a general axial piston VDA.

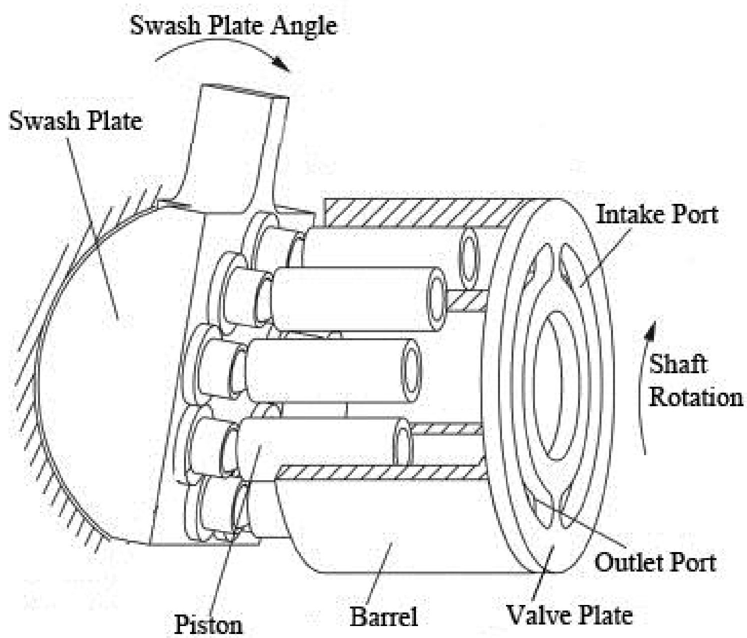

Figure 3.2: Schematic diagram of a variable displacement pump/motor. Figure adapted from Kemmetmüller et al., 2010.

A typical VDA comprises a number of piston-cylinders, arranged in parallel to form a circular barrel, which could rotate around a central shaft. The piston side of the barrel is attached to a swash plate, whose angle can be varied, whereas the cylinder head side is connected to a valve plate, which alternately connects the cylinders to the intake and outlet supply.

The rotation of the barrel against the tilted swash plate will cause the pistons to reciprocate with different strokes in their respective cylinders, causing variable amount of oil flow to and from cylinders. Therefore, by adjusting the angular position of the swash plate, the amount of the pump displacement can be changed. If it is perpendicular to the pistons, no oil will flow, as the pistons will not reciprocate. For the VDA to work, both as a pump and motor, the swash plate is allowed to move in both directions from the perpendicular position, to allow the oil to flow in both directions without reversing the direction of rotation of the drive shaft. The varying angle of the swash plate to vary flow is a smooth operation as flow is directly proportional to displacement.

At maximum swash plate angle, there would be more displacement and hence maximum torque generated as torque is directly proportional to displacement at a given pressure. This is important from the control point of view, as during the A2 power phase (Figure 2.6), the maximum power peak would require a maximum torque at a certain angular velocity. That is why monitoring the gait phases in real time by the control system is necessary, in order to provide continuous adjustments to the swash plate angle (and hence displacement) as per the torque requirements at the ankle.

3.2.2 HYDRAULIC ACCUMULATOR

Hydraulic accumulators are used to store mechanical energy, either in the form of potential energy (weight-loaded accumulators) or strain energy (spring-loaded or gas-charged accumulators). Weight-loaded accumulators cannot be used in the current design, because of their massive size, and hence are not relevant for this study. Below, spring-loaded and gas-charged accumulators are discussed.

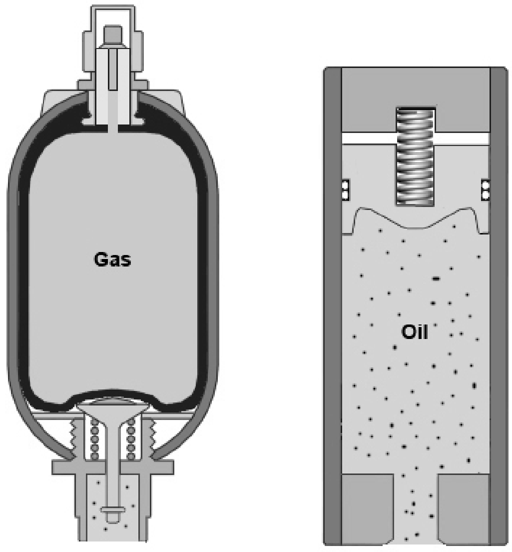

Figure 3.3: Gas-charged accumulator (left) and Spring-loaded accumulator (right).

3.2.3 SPRING-LOADED ACCUMULATOR

In the spring-loaded accumulator, when the oil is pumped into the oil chamber, the spring compresses, thereby storing energy. The compressed spring acts against the piston to push the oil back into the system during energy storing periods. In this type of accumulators, during the oil discharging periods, the output pressure drops with the reduction in spring force during extension. Being simpler to represent than the gas-charged accumulators (described below), the design is first modelled with a spring-loaded accumulator and then with a gas-charged accumulator.

3.2.4 GAS-CHARGED ACCUMULATORS

These are the most commonly used type of accumulators, as they are available in a variety of sizes and are particularly advantageous in terms of high flow rates, high/low temperature tolerance, high compression ratios, long life and good serviceability. These accumulators consist of a shell containing two separate chambers, one for the oil, and one for the compressed gas, usually nitrogen, which serves as the energy storage medium. The gas and oil chambers are completely separated with a physical barrier, which can be a piston or a bladder. Bladder type accumulators comprise a non-pleated, flexible rubber bladder as the physical barrier between the gas and the oil. Compared to their piston type counterparts, these are the most commonly used accumulators, being not prone to friction losses (between the piston seals and cylinder walls as in piston type) and have a faster response (due to the absence of any static friction to overcome and low inertia of the bladder).

As mentioned earlier, both the spring-loaded and gas-charged accumulators are used for the simulation. However, the selection of a specific type of accumulator will depend on the availability of the specific type in relation to the working pressure, size, and weight of the accumulator shell, which is beyond the scope of this study.

3.2.5 PRESSURE RELIEF VALVE

The pressure in the accumulator needs to be monitored with a pressure relief valve, which releases oil to the tank if the accumulator pressure reaches its maximum limit. A relief valve is normally a closed valve with a spring, and only opens when the pressure at its inlet exceeds the spring force, allowing the pressure to remain within the safe limits. For the concept design, during uphill walking, the accumulator pressure would not exceed the maximum limits (as will be explained later), however, it may reach its maximum limits during level or downhill walking, during which the relief valve will operate to maintain the accumulator pressure within its allowable limits.

3.3 Modelling and Sizing of Hydraulic Accumulator

Referring back to design specification in Section 2.7, both the actuator and the accumulator need to be compact and lightweight to be used in a prosthesis. There are trade-offs between operating pressure and oil (and hence accumulator) volume and pump capacity. For a given amount of energy storage, the higher the pressure, the thicker the walls of the accumulator, but the smaller the volume of oil required and hence the smaller the volume of the accumulator and pump capacity. The trade-off is also constrained by detailed design limitations on pump and actuator design, which will be partially reflected in the range of commercially available components. With almost all commercially available hydraulic accumulators designed to work at 200 bar or more, finding a commercially available accumulator to work at 100 bar or below is extremely difficult, but keeping in view of the bespoke designs, a maximum rated pressure of 100 bar is used for accumulator sizing to compare the results with the higher-pressure accumulator.

The following sections presents a definition of different accumulator parameters, followed by accumulator sizing calculations, with the objective of finding a most suitable size (small, lightweight) for the design concept.

3.3.1 DEFINITIONS OF ACCUMULATOR PARAMETERS

There is a wide variety of literature available for the design's specific components. While there is a universal understanding related to the VDA and relief valve parameters, this is not the case with accumulators. A careful examination in the literature reveals that there is a mix of definitions for different key parameters of accumulators. For instance, many manufacturers treat the maximum and minimum accumulator pressures as a working pressure range; however, for this study, the working pressure range was kept between the maximum and minimum allowable pressure limits to allow for losses and safety. Another reason for specifically defining the parameters of accumulators is that the sizing of accumulators is a rather more complex task than the sizing of the VDA for this work and later sections explains the sizing procedure for the accumulators used in the design. However, the sizing of the VDA would not require a separate mathematical procedure and the simulation itself would be used for selecting the appropriate size of the VDA. Therefore, before proceeding to the selection and sizing of the accumulator for the design, it is necessary to provide a clear understanding of different accumulator parameters. In addition, it should be taken into consideration that these parameters are defined specifically for the design used in this study and might differ slightly from the available literature.

a) Pre-charge Pressure

The Pre-charge pressure (P_{pr}) is defined as the gas pressure (in the case of gas-charged accumulators) or the pre-compressed spring force divided by piston area (in the case of spring-loaded accumulators) inside the accumulator when the accumulator is completely empty (without any oil). The manufacturer recommends the correct pre-charge pressure for specific accumulator types and applications for which the particular accumulator will be used. Normally, accumulators are pre-charged to 90% of minimum rated pressure.

After pre-charging, oil is pumped into the accumulator against the pre-charged gas/spring, which results in an increase in pressure. During discharging, this increased gas pressure/spring force pushes the oil out of the accumulator into the circuit, until the minimum rated pressure is reached. At this minimum rated pressure (P_{min}), a small volume of oil (V_{min}) is retained in the accumulator (minimum rated pressure is always kept slightly higher than the pre-charge pressure) to avoid a sudden oil pressure drop in the circuit; which could cause the whole circuit to collapse under vacuum.

b) Maximum Rated Pressure

Maximum rated pressure (P_{max}) is the maximum pressure the accumulator is designed to hold. At this pressure, maximum volume of oil (V_{max}) would be stored in the accumulator. Additionally, in the case of gas-charged accumulators, there would be a minimum volume of gas inside the accumulator at this pressure.

c) Minimum Rated Pressure

The Minimum rated pressure (P_{min}) is the pressure the accumulator reaches in its completely discharged state. At this pressure, a minimum volume of oil (V_{min}) would be retained in the accumulator. Additionally, in the case of gas-charged accumulators, there would be a maximum volume of gas inside the accumulator at this pressure.

The difference between the maximum and minimum rated pressures (P_{max}- P_{min}) specifies a rated pressure range for the accumulator to work within. However, any working pressure ranges (depending on the specific application requirements) with a higher working pressure (P_h) and lower working pressure (P_l) may be selected for the accumulator to work, but this working pressure range must lie within the rated pressure range.

d) Compression Ratio

The Compression ratio (P_{max}/P_{min}) is the ratio of maximum rated pressure to minimum rated pressure and determines the total amount of useable oil in the accumulator. As explained earlier, some oil is retained in the accumulator when the minimum rated pressure is reached, but this oil cannot be used for work, hence is not counted as useable. Generally, these are pre-specified by the manufacturer with typical ratios of 2:1 for bladder type gas-charged accumulators and higher for other types (e.g. piston type). For spring-loaded accumulators, a typical ratio could not be found and therefore, as a conservative estimate, a compression ratio of 2:1 is used for sizing of both the spring-loaded and gas-charged accumulators.

e) Accumulator Capacity

The Accumulator capacity/size (V_A) is the total capacity of the accumulator. For gas-charged accumulators, it can be considered as the total volume of gas at pre-charge pressure. However, for a spring-loaded accumulator, it refers to the maximum oil volume that can be delivered to/from the accumulator while working between the pre-charge and maximum rated pressure range. See Figure 3.3 where the labels “Gas” and “Oil” refer to the total gas and oil volumes for the gas-charged and spring-loaded accumulators; representing the respective accumulator capacities.

f) Instantaneous Oil Volume

The Instantaneous Oil Volume (V_F) is defined as the volume of oil delivered to/from the accumulator at instantaneous pressure (P) in the working pressure range, $P_l<P<P_h$, where P_l and P_h are the lower and higher working pressures, respectively.

With the key parameters defined, the next section provides the sizing procedure for the hydraulic accumulators.

3.3.2 Energy Stored Over a Gait Cycle

To proceed with the sizing of the accumulators for the concept design, it is necessary to first establish the amount of negative work (and hence amount of energy to be stored in the accumulator) for an anatomically intact subject during level walking for one gait cycle. Once this is established, the accumulators would then be sized accordingly to store that amount of energy. Referring to Section 2.3, the net joint power (P) is calculated for each time instance by taking the product of net joint moment (M) and the joint angular velocity (ω) for the data collected. Using the trapezoidal rule of numerical integration, the net joint power is cumulatively integrated to yield the total energy stored over the gait cycle. The plot of the energy stored during one gait cycle is presented in Figure 3.4.

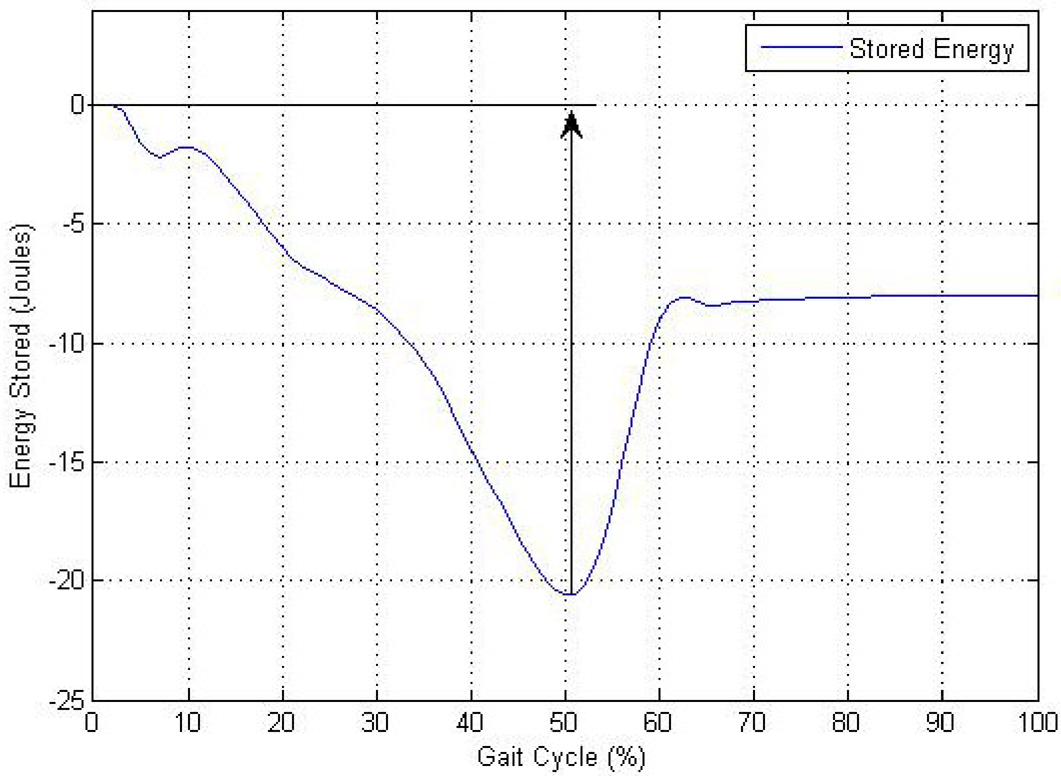

Figure 3.4: Energy stored over a gait cycle.

From the data, the stored energy (ΔE) was found to be 20.61 J. With this requirement of energy storage, the following sections will cover the derivation of equations for the energy storage and sizing for both the spring-loaded and gas-charged accumulators.

3.3.3 DEVELOPING EQUATIONS FOR SIZING A SPRING-LOADED ACCUMULATOR

a) General Case

Assuming an arbitrary curve representing the pressure-volume relationship of an accumulator in Figure 3.5, the x-axis represents the oil volume stored in the accumulator, and the y-axis represents the pressure inside the accumulator.

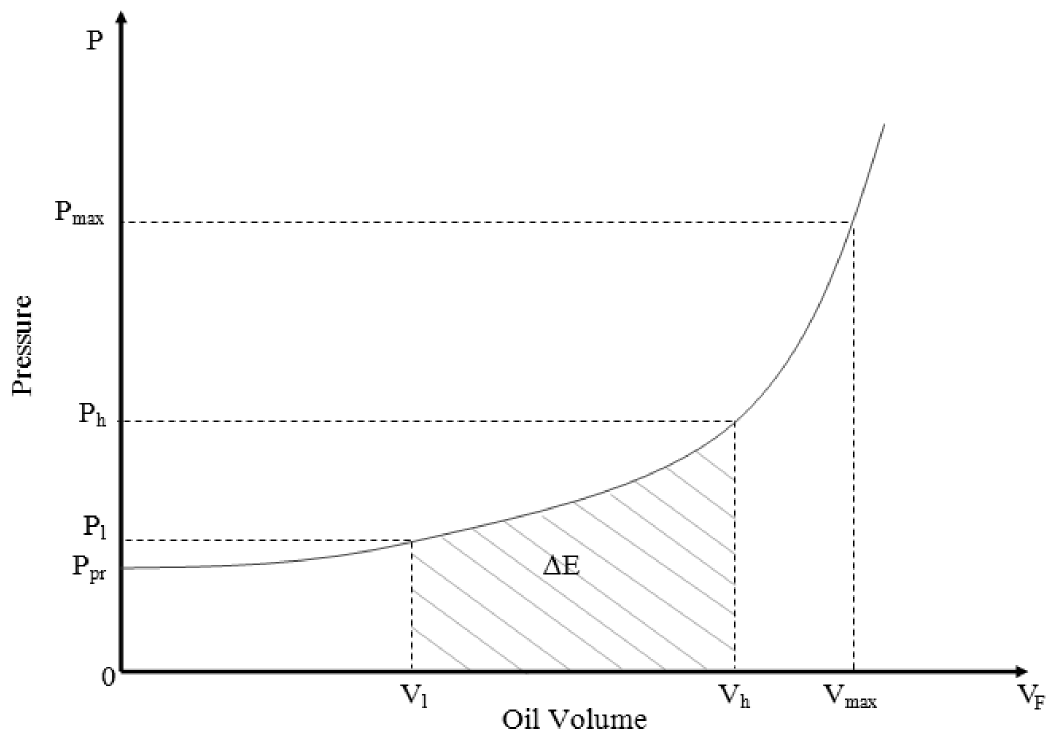

Figure 3.5: An arbitrary pressure profile of an accumulator.

The plot shows that at the pre-charge pressure, the oil volume in the accumulator is zero. As soon as oil starts to fill inside the accumulator, the pressure starts to rise. When a maximum rated pressure (P_{max}) is reached, the corresponding oil volume is represented as V_{max}. An arbitrary working pressure range is selected, with a high-pressure limit of P_h and a low-pressure limit of P_l. The corresponding upper and lower limits of working oil volumes are represented as V_h and V_l, respectively.

Here ΔE represents the energy stored (shaded area) during the working pressure range (P_l to P_h) and can be found by evaluating the area under the curve between these points. Mathematically,

$$\Delta E = \int_{V_l}^{V_h} P dV_F \dots\dots\dots\dots Eq. (3.1)$$

This equation can be used for specific types of accumulator with the only difference being the pressure profiles. Once the pressure profile and amount of stored energy is known, the equation can be evaluated and subsequently solved to find the volume (or size) of the accumulator that is capable of storing the required energy.

b) Spring-loaded Accumulator

For a spring-loaded accumulator, the pressure-volume relationship is linear (http://www.servoconalpha.com/product/prod-descript/accumulators/spring.htm(accessed 02/06/2013)), as shown in Figure 3.6 below.

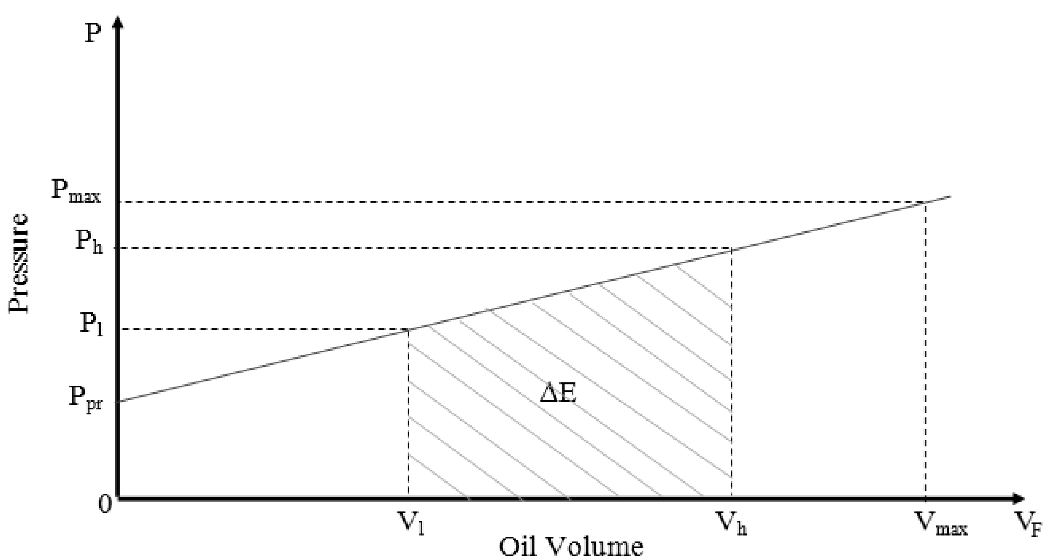

Figure 3.6: Pressure profile of a spring-loaded accumulator.

In Figure 3.5 and Figure 3.6,

V_{max} Maximum oil volume. In this case it is also the accumulator capacity (V_A)

V_h Upper limit of working oil volume, at high working pressure (P_h)

V_l Lower limit of working oil volume, at low working pressure (P_l)

V_F x-axis (oil volume)

P y-axis (gauge pressure)

P_{pr} Pre-charge pressure (gauge)

P_l Lower limit of working pressure (gauge)

P_h Upper limit of working pressure (gauge)

P_{max} Maximum rated pressure (gauge)

ΔE Energy stored while working between P_l to P_h

Comparing the pressure profile of a spring-loaded accumulator (Figure 3.6) with the arbitrary pressure profile (Figure 3.5) described earlier, the only difference is the nature of the pressure-volume relationship. Being linear, it is straightforward to derive the equation for the stored energy. Once the equation is derived, and the value of stored energy in one gait cycle is known, the correct size of the spring-loaded accumulator to be used in the design can be calculated.

As the pressure profile for a spring-loaded accumulator is linear (Figure 3.6) (http://www.servoconalpha.com/product/prod-descript/accumulators/spring.htm(accessed 02/06/2013)), the slope-intercept form of a straight line is used as a starting point and the followed derivation for determining accumulator capacity (Eq. (3.16)) is the original work described in this section. Based on the slope-intercept form of a straight line, the pressure profile for the spring-loaded accumulator (Figure 3.6) can be represented as:

$$P = KV_F + P_{pr} \dots\dots\dots\dots Eq. (3.2)$$

Where K is the slope of the straight line, V_F is the volume of oil and P_{pr} is the pre-charge pressure. Mathematically, K is represented as:

$$K = \frac{(P_{max} - P_{pr})}{V_{max}} \dots\dots\dots\dots Eq. (3.3)$$

Since pre-charge is typically set to 90% of minimum rated pressure, as described in section 3.3., we get:

$$P_{pr} = 0.9P_{min} \dots\dots\dots\dots Eq. (3.4)$$

In addition, from the definition of compression ratio (P_{max}/P_{min}) of 2:1 in section 3.3., we get:

$$\left(\frac{P_{max}}{P_{min}}\right) = 2 \Rightarrow P_{min} = \frac{P_{max}}{2} \dots\dots\dots\dots Eq. (3.5)$$

Substituting in Eq. 3.4:

$$P_{pr} = 0.9\left(\frac{P_{max}}{2}\right) \Rightarrow P_{pr} = 0.45P_{max} \dots\dots\dots\dots Eq. (3.6)$$

Substituting in Eq. (3.3):

$$K = P_{max}\frac{(1 - 0.45)}{V_{max}} \Rightarrow K = \frac{0.55P_{max}}{V_{max}} \dots\dots\dots\dots Eq. (3.7)$$

Now, substituting the value P from Eq. (3.2) in Eq. (3.1), we get:

$$\Delta E = \int_{V_l}^{V_h} (KV_F + P_{pr})dV_F \dots\dots\dots\dots Eq. (3.8)$$

Substituting the value of P_{pr} from Eq. 3.6):

$$\Delta E = \int_{V_l}^{V_h} (KV_F + 0.45P_{max})dV_F$$

$$\Delta E = \left[\frac{KV_F{}^2}{2} + 0.45P_{max}V_F\right]_{V_l}^{V_h}$$

$$\Delta E = \frac{K}{2}(V_h^2 - V_l^2) + 0.45P_{max}(V_h - V_l) \dots \dots \dots \dots Eq.(3.9)$$

Calculating limits:

Substituting Eq. (3.6) and Eq. (3.7) in Eq. (3.2) and re-arranging:

$$V_F = \frac{(P - 0.45P_{max})}{0.55P_{max}} V_{max} \dots \dots \dots \dots Eq.(3.10)$$

As mentioned earlier, the working pressure range can be selected at designer's discretion; and P_h is defined as a higher working pressure. It can be assumed that P_h corresponds to a certain fraction of maximum rated pressure (P_{max}), and hence it can be represented mathematically as:

$$P_h = bP_{max} \quad \forall\ a < b < 1 \dots \dots \dots \dots Eq.(3.11)$$

Similarly:

$$P_l = aP_{max} \quad \forall\ 0 < a < b, \qquad P_l > P_{pr} \dots \dots \dots \dots Eq.(3.12)$$

Replacing V_F and P with V_h and P_h respectively in Eq. 3.10 and by substituting the value of P_h from Eq. 3.11, it can be deduced that:

$$V_h = \frac{(bP_{max} - 0.45P_{max})}{0.55P_{max}} V_{max}$$

$$V_h = \left[\frac{(b-0.45)}{0.55}\right] V_{max} = BV_{max} \qquad \forall\, B = \frac{(b-0.45)}{0.55} \dots\dots\dots\dots Eq. (3.13)$$

Similarly:

$$V_l = \left[\frac{(a-0.45)}{0.55}\right] V_{max} = AV_{max} \qquad \forall\, A = \frac{(a-0.45)}{0.55} \dots\dots\dots\dots Eq. (3.14)$$

Eq. (3.13) and Eq. (3.14) provide the limits for Eq. (3.9). Therefore substituting these into Eq. (3.9) yields:

$$\Delta E = \frac{K}{2}[(BV_{max})^2 - (AV_{max})^2] + 0.45P_{max}(BV_{max} - AV_{max})$$

$$\Delta E = \frac{K{V_{max}}^2}{2}(B^2 - A^2) + 0.45P_{max}V_{max}(B - A) \dots\dots\dots\dots Eq. (3.15)$$

Substituting the values of *K*, *B* and *A* (after simplification from Eq. (3.7), Eq. (3.13), and Eq. (3.14) respectively in the above equation and re-arranging:

$$V_{max} = \frac{1.1\ \Delta E}{P_{max}(b^2 - a^2)}$$

Or

$$V_A = \frac{1.1\ \Delta E}{P_{max}(b^2 - a^2)} \dots\dots\dots Eq. (3.16)$$

With the stored energy known from the gait cycle, and with a choice of maximum rated pressure and defined working pressure range, this equation can be used to find the spring-loaded accumulator's capacity.

As $P_l = aP_{max}$ and $P_h = bP_{max}$, a value of maximum rated pressure can be selected, from which a higher working pressure value (P_h) can be calculated by keeping it slightly lower than P_{max} to allow for safety. For example, for a selected value of P_{max}=200 bar, and P_h=95%P_{max}:

$$P_h = bP_{max} = 0.95P_{max} \quad \Rightarrow b = 0.95 \dots\dots\dots Eq.(3.17)$$

Similarly, the lower working pressure (P_l) would be set slighter higher than P_{min} and will be expressed in terms of P_{max} as:

$$P_l = 110\%\, P_{min} \quad and \quad P_{min} = \frac{P_{max}}{2} \ (from\ Eq.(2.5))$$

$$\therefore P_l = \frac{1.1P_{max}}{2} \quad = 0.55P_{max} = \ aP_{max} \Rightarrow \quad a = 0.55 \ \dots\dots\dots\dots Eq.(3.18)$$

With these values of a and b, ΔE, and P_{max} are known, the accumulator capacity can be calculated for this set of values.

The same process is repeated, with fixed ΔE, P_{max} and P_h (or b) values. However, progressively narrowing down the working pressure range (by increasing the lower working pressure, and hence increasing the value of coefficient "a"), different values of accumulator capacities are obtained. From those results, a decision on the accumulator selection based on the size and working pressure range can be made.

3.3.4 SPRING-LOADED ACCUMULATOR-SIZING AND SELECTION

With ΔE=20.61 J and for the selected ranges of high and low working pressures and maximum rated pressure, Eq. (3.16) can be used to have different accumulator sizes capable of storing the required energy. The S.I. system of units is used to define the parameters and carry out the sizing procedure. However, the results for all the calculations are presented in units that are easier to visualize than the S.I. system. For instance, it is rather easier to visualize a comparison of an accumulator volume of 200 cc with a commercially available water bottle of 250 cc capacity, rather than comparing the same accumulator volume expressed in S.I. units (i.e. $2e^{-4}m^3$) to the same water bottle. The same is the case with pressure because a unit of bar can easily be visualized by comparing it to the atmospheric pressure of 1 bar rather than using the S.I. equivalent of $1e^5$ Pa. The following two cases explain the procedure for sizing a spring-loaded accumulator for a maximum rated pressure of 100 and 200 bar (which correspond to the typical maximum pressures used in hydraulic systems), respectively:

a) Case 1:

P_{max} =100 bar (selected as a design variable)

P_{pr} =0.45 Pmax (referring to Eq. (3.6))

P_{pr} =0.45*100 bar = 45 bar

P_h =0.95Pmax = 95 bar and b=0.95 (from Eq. (3.17))

P_l =0.55Pmax = 55 bar and a=0.55 (from Eq. (3.18))

i.e. a maximum rated pressure of 100 bar (as a design variable) is selected, for which the pre-charge and low/high working pressure of 45, 55, and 95 bar (respectively) were calculated. By adjusting the value of low working pressure while keeping fixed the high working pressure, a number of design scenarios can be explored. The reason for not decreasing the high working pressure (P_h) (to lower the operating pressure range) is that working at a higher working pressure may potentially decrease the overall size and hence increase the portability of the system. Secondly, it would be pointless to use an accumulator at lower pressures although it is designed to withstand higher pressures.

b) Case 2:

For case 2, P_{max} is set to 200 bar (selected as a design variable) for which the subsequent values of the pre-charge and low/high working pressures are 90, 110 and 190 bar following the same formulae/procedures as in case 1.

Following the same procedure as in case 1, accumulator capacities are obtained for the above-mentioned values using Eq. (3.16) and capacities for both cases are presented in the table below for comparison.

Maximum Pressure=100 bar			**Maximum Pressure=200 bar**		
Working Pressure Range (bar)	ΔP (P_h-P_l) (bar)	Accumulator Capacities (cc)	Working Pressure Range (bar)	ΔP (P_h-P_l) (bar)	Accumulator Capacities (cc)
55 to 95	40	3.8	110 to 190	80	1.9
60 to 95	35	4.2	120 to 190	70	2.1
65 to 95	30	4.7	130 to 190	60	2.4
70 to 95	25	5.5	140 to 190	50	2.7
75 to 95	20	6.7	150 to 190	40	3.3
80 to 95	15	8.6	160 to 190	30	4.3
85 to 95	10	12.6	170 to 190	20	6.3
90 to 95	5	24.5	180 to 190	10	12.3
91 to 95	4	30.5	182 to 190	8	15.2
92 to 95	3	40.4	184 to 190	6	20.2
93 to 95	2	60.3	186 to 190	4	30.1
94 to 95	1	120	188 to 190	2	60

Table 3.1: Spring-loaded accumulator capacities obtained for different working pressure ranges for maximum rated pressures of 100 and 200 bar.

Referring to Table 3.1, smaller capacity accumulators have a larger operating pressure range whereas the larger capacity accumulators have a lower pressure range. This is because, for a given volume of oil, a smaller accumulator will charge/discharge over a larger working pressure range than a larger accumulator will. In addition, it is also obvious that doubling the working pressure would reduce the accumulator size by half.

It is obviously advantageous to use an accumulator that works over a larger pressure range, as the accumulator capacity would be reduced resulting in a smaller and lightweight accumulator. From Table 3.1, the largest capacity accumulator for a maximum pressure of 100 bar is just 120 cc, which is very small in relation to the size of a transtibial prosthesis. This means that accumulator size is not a design constraint and any of these sizes (Table 3.1) can be used for simulation work. However, for developing a prototype, selection of a specific accumulator size would mainly depend on the cost associated with a specific size.

During a search for commercially available spring-loaded accumulators, it became clear that most accumulators of this type are designed to operate at and above 200 bar. Referring to Table 3.1, while a 60 cc accumulator capacity is easily small enough to be incorporated into a prosthesis, it nevertheless results in a very small working pressure range and therefore was selected for simulation work.

3.3.5 DEVELOPING EQUATIONS FOR SIZING A GAS-CHARGED ACCUMULATOR

Before deriving the expression of energy storage in terms of accumulator capacity and pressures for the gas charged accumulators, it is useful to refer back to the general case of energy storage in accumulators, as explained earlier using Figure 3.5. For convenience, the same figure is repeated below.

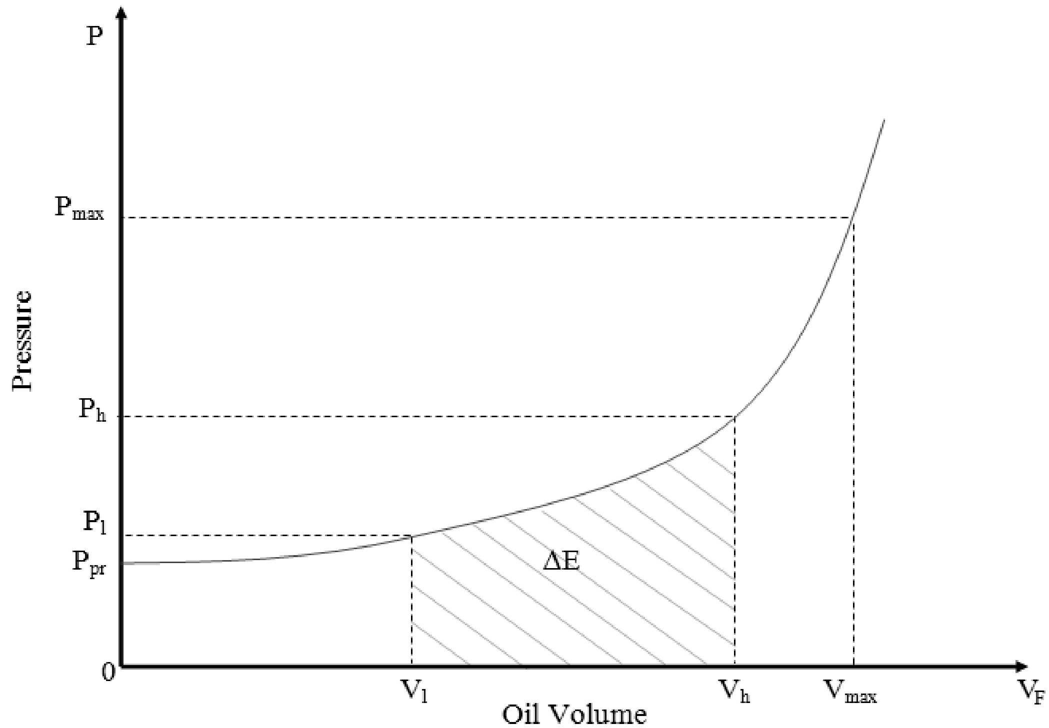

Figure 3.5: An arbitrary pressure profile of an accumulator

In Figure 3.5, ΔE represents the energy stored (shaded area) over the working pressure range (P_l to P_h) and can be found by evaluating the area under the curve between these points. Mathematically:

$$\Delta E = \int_{V_l}^{V_h} P dV_F \dots\dots\dots\dots Eq. (3.1)$$

The pressure-volume relation for an ideal gas (Kenneth Jr, 1995) is used here as a starting point and the followed derivation for determining gas-charged accumulator capacity (Eq. (3.26)) is the original work described in this section. The working principle of gas-charged accumulators is explained in Section 3.2.4. Referring back to this, and using the ideal gas relation (Kenneth Jr, 1995), the gas compression process for a gas charged accumulator is represented by the equation:

$$P.V_G^k = constant \dots\dots\dots\dots Eq.(3.19)$$

Where P is the absolute pressure of the gas and V_G is the gas volume. For an isothermal process (where the compression process is so slow that the temperature of the gas remains constant), k is taken as 1. For an adiabatic process (where the process is so rapid that there is no heat transferred to/from the gas), k is taken as 1.4. The pressure-volume relationship for a gas-charged accumulator is presented in Figure 3.7 below:

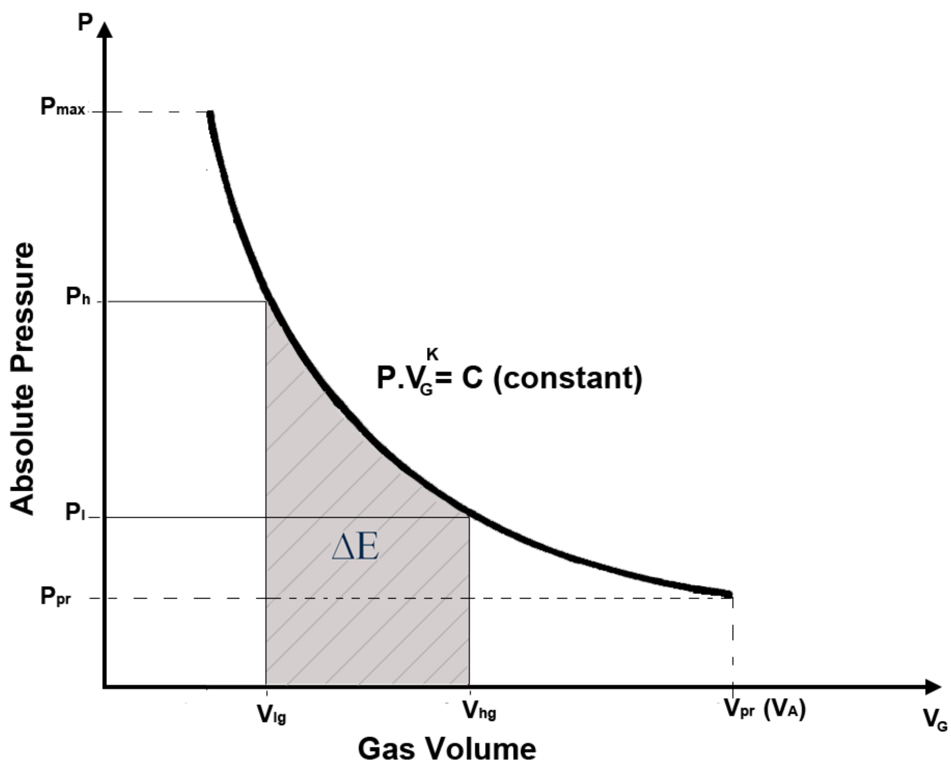

Figure 3.7: Pressure-volume relationship for a gas-charged accumulator.

In Figure 3.7,

V_{pr} Gas volume at pre-charge pressure and is equal to the accumulator capacity V_A

V_{hg} Upper limit of working gas volume at lower working pressure (P_l)

V_{lg} Lower limit of working gas volume at higher working pressure (P_h)

V_G x-axis (Gas-Volume)

P y-axis (Absolute Pressure)

P_{pr} Pre-charge pressure (absolute)

P_h Upper limit of working pressure (absolute)

P_l Lower limit of working pressure (absolute)

P_{max} Maximum rated pressure (absolute)

Comparing Figure 3.5 with Figure 3.7, the major difference between the two is the volume of the fluid used. Figure 3.5 relates the pressures to the oil volume, whereas Figure 3.7 relates the absolute pressures to the gas volume. In gas-charged accumulators, it is simpler to derive the equation for the energy storage and accumulator capacity using the gas volumes, rather than converting the relationship into oil volumes, whereas in the general case as well as in spring-loaded accumulators, it is more straightforward to use the pressure-oil volume relationship. It is also important to use absolute pressures (sum of atmospheric and gauge pressures), while working with the gas-charged accumulator as the ideal gas relationship is used.

In addition, for the general and spring-loaded accumulator cases, an increase in the oil volume would mean an increase in the energy storage as governed by Eq. 3.1. However, in the case of gas-charged accumulators, the gas compresses (decrease in gas volume), with the increase in pressure (increase in stored energy). Therefore, the equation for energy storage (shaded areas in Figure 3.7), while working between pressures P_l and P_h, with the respective oil volumes (V_{hg} and V_{lg}) can be represented as:

$$\Delta E = -\int_{V_{hg}}^{V_{lg}} P dV_G \ldots\ldots\ldots\ldots Eq. (3.20)$$

The negative sign indicates the inverse relationship between the stored energy and gas volumes. The limits, V_{lg} and V_{hg} represents the lower and higher working gas volumes at higher and lower working pressures (P_h and P_l), respectively.

Here,

$$PV_G{}^k = C, \qquad \qquad where\ C\ is\ a\ constant$$

$$PV_G{}^k = P_{pr}V_{pr}{}^k$$

$$P = \frac{P_{pr}V_{pr}{}^k}{V_G{}^k}$$

Substituting in Eq. (3.20):

$$\Delta E = -P_{pr}V_{pr}{}^k \int_{V_{hg}}^{V_{lg}} \frac{dV_G}{V_G^k}$$

$$\Delta E = \frac{P_{pr}V_{pr}{}^k}{k-1} \left. V_G{}^{1-k} \right]_{V_{hg}}^{V_{lg}}$$

$$\Delta E = \frac{P_{pr}V_{pr}{}^k}{k-1} \left[V_{lg}{}^{1-k} - V_{hg}{}^{1-k} \right] \ldots\ldots\ldots\ldots Eq. (3.21)$$

Evaluating terms in parenthesis:

$$\because PV_G{}^k = C,$$

$$\therefore P_l V_{hg}{}^k = C \Rightarrow V_{hg} = \left(\frac{C}{P_l}\right)^{\frac{1}{k}}$$

$$V_{hg}{}^{(1-k)} = \left(\frac{C}{P_l}\right)^{\left(\frac{1-k}{k}\right)} \dots\dots\dots\dots Eq. (3.22)$$

Similarly,

$$V_{lg}{}^{(1-k)} = \left(\frac{C}{P_h}\right)^{\left(\frac{1-k}{k}\right)} \dots\dots\dots\dots Eq. (3.23)$$

Substituting values from Eq. (3.23) and Eq. (3.22) in Eq. (3.21)

$$\Delta E = \frac{P_{pr}V_{pr}{}^{k}}{k-1}\left[\left(\frac{C}{P_h}\right)^{\left(\frac{1-k}{k}\right)} - \left(\frac{C}{P_l}\right)^{\left(\frac{1-k}{k}\right)}\right]$$

$$\Delta E = \frac{P_{pr}V_{pr}{}^{k}\, C^{\left(\frac{1-k}{k}\right)}}{k-1}\left[\frac{1}{P_h{}^{\left(\frac{1-k}{k}\right)}} - \frac{1}{P_l{}^{\left(\frac{1-k}{k}\right)}}\right]$$

$$\Delta E = \frac{P_{pr}V_{pr}{}^{k}\, C^{\left(\frac{1-k}{k}\right)}}{k-1}\left[P_h{}^{\left(\frac{k-1}{k}\right)} - P_l{}^{\left(\frac{k-1}{k}\right)}\right] \dots\dots\dots\dots Eq. (3.24)$$

$$\because\ PV_G{}^{k} = C \text{ and } V_{pr} = V_A$$

$$\therefore\ P_{pr}V_{pr}{}^{k} = C \quad or \quad P_{pr}V_A{}^{k} = C \quad or \quad C^{\left(\frac{1-k}{k}\right)} = V_A{}^{1-k}P_{pr}{}^{\left(\frac{1-k}{k}\right)} \dots\dots\dots Eq. (3.25)$$

Substituting the value of *C* from Eq. (3.25) and replacing V_{pr} with V_A in Eq. (3.24)

$$\Delta E = \frac{P_{pr}{}^{1+\left(\frac{1-k}{k}\right)}\, V_A^{k+(1-k)}}{(k-1)}\left[P_h{}^{\left(\frac{k-1}{k}\right)} - P_l{}^{\left(\frac{k-1}{k}\right)}\right]$$

$$\Delta E = \frac{P_{pr}{}^{\frac{1}{k}}\, V_A}{(k-1)}\left[P_h{}^{\left(\frac{k-1}{k}\right)} - P_l{}^{\left(\frac{k-1}{k}\right)}\right]$$

$$V_A = \frac{\Delta E(k-1)}{P_{pr}^{\frac{1}{k}}\left[(bP_{max})^{\left(\frac{k-1}{k}\right)} - (aP_{max})^{\left(\frac{k-1}{k}\right)}\right]} \qquad as\ P_h = bP_{max}\ \&\ P_l = aP_{max}$$

$$V_A = \frac{\Delta E(k-1)}{P_{pr}^{\frac{1}{k}} P_{max}^{\left(\frac{k-1}{k}\right)}\left[b^{\left(\frac{k-1}{k}\right)} - a^{\left(\frac{k-1}{k}\right)}\right]} \ldots\ldots\ldots\ldots Eq.(3.26)$$

With the stored energy known from the gait cycle, and with a choice of maximum rated pressure and defined working pressure range, Eq. (3.26) can be used to size a gas-charged accumulator. However, as mentioned earlier, to find out the size of a gas-charged accumulator, the pressures used must be absolute pressures, whereas for the spring-loaded accumulator, gauge pressures are used.

The following section presents the selection and sizing of a gas-charged accumulator.

3.3.6 GAS-CHARGED ACCUMULATOR-SELECTION AND SIZING

The same procedure of defining a maximum rated pressure and coefficients *a* and *b* is used here as explained previously, and the same procedure of narrowing down the working pressure range is repeated to obtain a set of accumulator capacities. From those results, a decision on the accumulator selection based on the size, pressure profile and commercial availability can be made.

The following two cases explain the procedure for sizing the gas-charged accumulator for maximum rated pressures of 100 and 200 bar (absolute), respectively.

a) Case 1:

P_{max} =100 bar (selected as a design variable)

P_{pr} =0.45 Pmax

P_{pr} =0.45*100 = 45 bar

P_h $=0.95P_{max} = 95$ bar and $b = 0.95$

P_l $=0.55P_{max} = 55$ bar and $a = 0.55$

i.e. for a maximum rated pressure of 100 bar, the pre-charge and high/low working pressure are 45, 55 and 95 bar, respectively. By adjusting the value of low working pressure while keeping fixed the value of high working pressure, a number of design scenarios can be explored.

b) Case 2:

For case 2, P_{max} is set to 200 bar (selected as a design variable) for which the subsequent values of the pre-charge and high/low working pressures were 90, 110 and 190 bar following the same formulae as in case 1.

Following the same procedure as in case 1, accumulator capacities are obtained for the above-mentioned values. The accumulator capacities obtained for both cases are presented in Table 3.2 for comparison.

Maximum Pressure=100 bar			Maximum Pressure=200 bar		
Working Pressure Range (bar)	ΔP (P_h-P_l) (bar)	Accumulator Capacities (cc)	Working Pressure Range (bar)	ΔP (P_h-P_l) (bar)	Accumulator Capacities (cc)
55 to 95	40	10	110 to 190	80	5
60 to 95	35	12	120 to 190	70	6
65 to 95	30	14	130 to 190	60	7
70 to 95	25	18	140 to 190	50	9
75 to 95	20	23	150 to 190	40	11
80 to 95	15	31	160 to 190	30	15
85 to 95	10	47	170 to 190	20	24
90 to 95	5	97	180 to 190	10	48
91 to 95	4	121	182 to 190	8	61
92 to 95	3	162	184 to 190	6	81
93 to 95	2	244	186 to 190	4	122
94 to 95	1	490	188 to 190	2	245

Table 3.2: Sizing results (rounded values) for gas-charged accumulators.

From Table 3.2, it can be observed that smaller capacity gas-charged accumulators have a larger operating pressure range, whereas the larger capacity gas-charged accumulators have a lower operating pressure range, as with spring-loaded accumulators (Table 3.1). Obviously, this is because for the same amount of energy to be stored, larger capacity accumulators would not fill and discharge completely (and hence have a smaller operating pressure range). Therefore, smaller capacity accumulators could be used for the prototype depending on the cost and availability.

Following the search for the components in terms of commercial availability, the specifications of a bespoke design was obtained for a 16 cc accumulator manufactured by CTG (CTG Ltd, Oxfordshire, UK) for motor sports. Despite their small size, these accumulators are also designed to work at pressures of 200 bar or greater. However, considering that the accumulator capacity is not a constraint for the design, a gas-charged accumulator of 245 cc for a maximum pressure of 200 bar was selected for simulation for two reasons. One reason is that selecting the largest capacity accumulator (245 cc) from the sizes obtained would serve a conservative estimate of the final design size/weight, and the second is that this size is very small in relation to prosthesis size, and it would probably be more cost effective than to have very small accumulators manufactured.

Until this point, the sizing and selection of hydraulic accumulators to be used in the concept design is complete. However, although the sizing of the VDA would be concluded from the simulation, the mathematical model of the VDA needs to be described before proceeding with the modelling of the actual concept design. Therefore, the following section describes the mathematical modelling of the VDA.

3.4 Modelling of Variable Displacement Pump/Motor

As mentioned earlier, the sizing procedure of the VDA is not complex and simulation will be used for this purpose, however, compared to hydraulic accumulators, VDA are prone to different losses, which affect their efficiency. The modelling and simulation of the concept design is therefore first carried out using an ideal model of the VDA (which neglects all losses and assumes the VDA to be 100% efficient), and then a loss model of the VDA is used, which takes the losses into consideration. This comparison would provide insights into how efficient the design is in restoring normal ankle functions to the user.

The displacement of a VDA is defined by the following equation:

$$D = \frac{D_{max}.X}{X_{max}} \dots \dots \dots Eq. (3.27)$$

Here, D is the instantaneous displacement, i.e. amount of oil delivered in/out of the VDA as the shaft rotates. The S.I. units of displacement are m^3/rad. D_{max} is the maximum displacement that the VDA can deliver and it determines the size of the VDA, X and X_{max} are the instantaneous and maximum stroke of the pistons, where X is normalised (by setting $X_{max}=1$), so that X varies between 0 (zero displacement) and 1 (maximum displacement).

3.4.1 IDEAL VDA MODEL

In ideal conditions, (without any flow losses), the flow rate, and torque of a VDA are expressed using the following equations:

$$q_{ideal} = D_{max}.X.\omega \ldots \ldots \ldots Eq.(3.28)$$

$$T_{ideal} = D_{max}.X.P_{acc} \ldots \ldots \ldots Eq.(3.29)$$

Combining these equations yields:

$$q_{ideal} = \frac{T_{ideal}.\omega}{P_{acc}} \ldots \ldots \ldots Eq.(3.29A)$$

Here, P_{acc} is the instantaneous pressure, and ω is the angular velocity of the shaft. The S.I. unit of pressure is Pa, and angular velocity is rad/sec.

3.4.2 VDA LOSS MODEL

Flow losses in a VDA are divided into leakage and compressibility losses (Mccandlish & Dorey, 1984). When subjected to pressure, oil is forced to leak through small clearances between the moving parts of a VDA contributing to the leakage losses. Although liquids are assumed as incompressible, however, when subjected to high pressure, a slight compressibility could be observed, which contributes to the flow losses due to compressibility effects.

Mccandlish & Dorey, 1984, have described linear and non-linear mathematical models to model these flow losses. These models have been found to be a good representation of experimental data for certain commercially available variable displacement pumps. However, the coefficients described in these models need to be evaluated from the experimental data for the actual VDAs, and such experimental data are not available for the VDA that has been assumed in this work. Therefore, model coefficients, as evaluated in Grandall, 2010, have been used in this work to provide an idea of the extent of the losses of the VDA in real conditions. Different models used in the latter study were tested, but the *"GM2"* model, as described in Grandall, 2010, was chosen for the simulation, because the coefficients described in this model produced comparatively less noisy results than with the other models in the same study or with the models and coefficients described in Al-Kharusi, 2004.

The flow losses would always result in drainage of oil from the accumulator to the tank, resulting in an increased work input and decreased work output as compared to the ideal case. In other words, during accumulator charging, the leakage losses would require the VDA to produce more work, and during accumulator discharging less work would be produced by the VDA. Therefore, for both the negative and positive work phases, the flow losses would always increase the oil requirement from the accumulator than the ideal situation. Therefore, the equation for the real flow could be written as:

$$q_{real} = q_{ideal} - K_m\left(q_{leakage} + q_{compressibility}\right) \dots\dots\dots Eq. (3.30)$$

The coefficient K_m in the above equation is introduced only to avoid having two separate equations for the pump and motor mode of VDA. K_m would be 1 for pump mode (losses would decrease the oil flow to the accumulator), and -1 for the motor mode (more oil would be drained from the accumulator). Whereas, the pump and motor mode of the VDA can easily be determined using the direction of torque and angular velocity. When the torque and angular velocity act in opposite directions (i.e. one clockwise and other anti-clockwise and vice versa), the VDA will do negative work (pump mode). Whereas, when the torque and angular velocity act in the same directions (i.e. both clockwise or both anticlockwise), the VDA will work in motor mode.

The leakage and compressibility models are taken from Grandall, 2010, along with the coefficients, and are described by the following equations:

$$q_{leakage} = C_s \left(\frac{P}{P_{atm}}\right)^n \left(a + b\left(\frac{\omega}{\omega_{max}}\right)\right)\frac{PD_{max}}{\mu} \dots\dots\dots Eq. (3.31)$$

$$q_{compressibility} = \frac{P\omega D_{max}}{B}\left(V_r + \frac{1+X}{2}\right) \dots\dots\dots Eq\ (3.32)$$

Here, the coefficients *Cs, a, b* and *n* should be experimentally determined for the particular VDA adopted, but as explained earlier, the values of these coefficients were taken from Grandall, 2010, because no experimental data were available. Similarly, V_r, which defines the ratio of the piston's clearance volume to the swept volume, and *B*, which is the bulk modulus of oil, are also taken from Grandall, 2010.

Therefore, the flow rate equation including losses (Eq. 3.30) can be re-written by substituting in it the Eq. (3.29A, 3.31 and 3.32) and is as follows:

$$q_{real} = K_m \frac{|T_{ideal}|.|\omega|}{P_{acc}} - K_m \left[C_s \left(\frac{P}{P_{atm}}\right)^n \left(a + b\left(\frac{\omega}{\omega_{max}}\right)\right)\frac{PD_{max}}{\mu} + \frac{P\omega D_{max}}{B}\left(V_r + \frac{1+X}{2}\right)\right] \dots\dots\dots Eq. (3.33)$$

Eq. (3.33) can therefore be used to model the flow accounting for the leakage and compressibility losses in both the pump and motor mode with the same definition of coefficient K_m as described above.

3.5 Modelling of Gearbox

As a starting point, simulation of the design concept was carried out first without considering any losses and with a gear ratio of one, essentially eliminating the effect of the gearbox altogether. This would make the VDA as a sole component that is providing the required ankle torque, and the simulation results with these (ideal) conditions (no losses, no gearbox) would provide a baseline with which to compare simulation results obtained later by taking into account the flow losses in the VDA as well as the effects of the gearbox (with a gear ratio other than one). The design trade-off to be explored by this comparison is whether the addition of a gearbox, and hence a reduction in the VDA size and associated weight, would result in an overall system weight that was lower than the ideal conditions (i.e. VDA only, no losses).

With a potential advantage of having a reduced size/weight of the actuator-gearbox system, friction torque losses in a gearbox is a potential disadvantage. These losses are mainly due to friction, and modelling the individual frictional losses due to specific factors (sliding friction, rolling friction, oil churning etc.) is a complex process and beyond the scope of this study. However, all these individual losses have been accounted for as a lumped frictional loss, which could be modelled using a linear fit on the data published by gear manufacturers. For instance, a gearbox having an efficiency of 95% and nominal torque output of 100 Nm would be 5% inefficient. In other words, the actual torque loss (T_{fr}) due to combined frictional losses would be equal to 5 N.m. Therefore, to develop a simple loss model, a search was carried out for published data on the efficiency of a specific gearbox as a function of gear ratio and nominal torque, which is presented in the table below:

Gear Ratio N	Nominal Torque Tn Nm	Efficiency η
3	85	98
4	115	98
5	110	98
7	65	97
8	50	97
9	130	97
10	38	96
12	120	97
15	110	96
16	120	96
20	120	96
25	110	95
32	120	95
40	110	94
60	110	92
64	50	89
80	120	91
100	120	90
120	110	89
160	120	88
200	110	85
256	120	84
320	110	80
512	50	57

Table 3.3: Gearbox efficiency data obtained for a commercial gearbox(Neugart model PLE-80).

From this data, % inefficiency (*1-η/100*) was calculated corresponding to the gear ratios and nominal torque. A linear curve fit was performed on the inefficiency values obtained against the gear ratio (*N*), which resulted in the following linear equation:

$$\%\ Inefficiency = 6.913e^{-4}N + 2.557e^{-2} \ldots\ldots\ldots Eq.(3.34)$$

To calculate friction torque, Eq. (3.34) is multiplied by a constant value of nominal input torque (this would correspond to the maximum value of the in-vivo ankle torque data used). Therefore, the final equation for the gearbox losses used in the model is:

$$T_{fr} = (6.913e^{-4}N + 2.557e^{-2})T_N \ldots\ldots\ldots Eq.(3.35)$$

Where, T_N is nominal torque, which would correspond to a peak value (constant and absolute) of the in-vivo ankle torque. In addition, the following two additional equations are also used to describe the gearbox.

$$\omega_{vda} = \omega_{gb} \times N \ldots\ldots\ldots Eq.(3.36)$$

Where ω_{vda} represents the VDA shaft's angular velocity, whereas ω_{gb} represents the gearbox shaft's angular velocity (which being connected to the ankle) would be equal to the ankle angular velocity.

$$T_{vda} = \frac{M_{ank}}{|M_{ank}|.N}\left[|M_{ank}| - K_m T_{fr}\right] \ldots\ldots\ldots Eq.(3.37)$$

Where K_m is the same coefficient as described above and introduced for sign convention, as explained in Section 3.4.2.

For simulation, the ankle moment and angle data would serve as input to the gearbox. The product of the ankle's angular velocity and gear ratio would provide the angular velocity of the VDA shaft (Eq. 3.36). Similarly, the ankle torque data serves as input to the gearbox, where, Eq. 3.37 would provide the torque input (T_{vda}) to the VDA.

3.6 System Simulation

This section describes the model used to simulate the ideal as well as real conditions, the description of relevant blocks and equations used. The modelling was carried out using MATLAB's Simulink Software (Mathworks, Cambridge, UK), which is a software package for modelling, simulating, and analysing dynamical systems. It allows modelling of both the linear and non-linear systems with discreet or continuous sample times. It makes modelling very convenient as it offers a graphical user interface (GUI) to build models as block diagrams by simple click-and-drag operations. The blocks required for building a model can be selected from a built-in blocks library or can be custom made by the user. The blocks are essentially mathematical models of different physical components and designing a custom block for a specific model is easy as the user is only required to provide mathematical equations representing the behaviour of the particular component along with the inputs and outputs. The inputs of the block can be provided as constant values or as time dependent signals.

A model can be quickly built by using different blocks (custom or built-in) which can be interconnected by a line for the propagation of input/output signals. After defining a model, with specified inputs, simulation can be run using a choice of built-in solvers. This is another convenience the Simulink offers, as the user do not have to write code for separate solvers as in the case of other programming languages for instance C. The simulation outputs can be observed using blocks such as scopes while the simulation is being run. The outputs can also be exported to MATLAB workspace for further operations. (www.mathworks.com/help/simulink/gs/product-overview.html (accessed 26/07/2013)).

Figure 3.8 represents the Simulink model circuit. The inputs to the model are ankle angle and moment data obtained for anatomically intact individuals. The model outputs are VDA displacement (X), accumulator pressure (P_{acc}), and accumulator oil volume (V_F). From these parameters, torque delivered by VDA/gearbox, flow rate, and accumulator hydraulic power is calculated. In this context, it should be emphasised that human movement control (i.e. by the brain and central nervous system) is not included in this model. It is for this reason that measured ankle angle and ankle moment data are used as inputs to the simulation model.

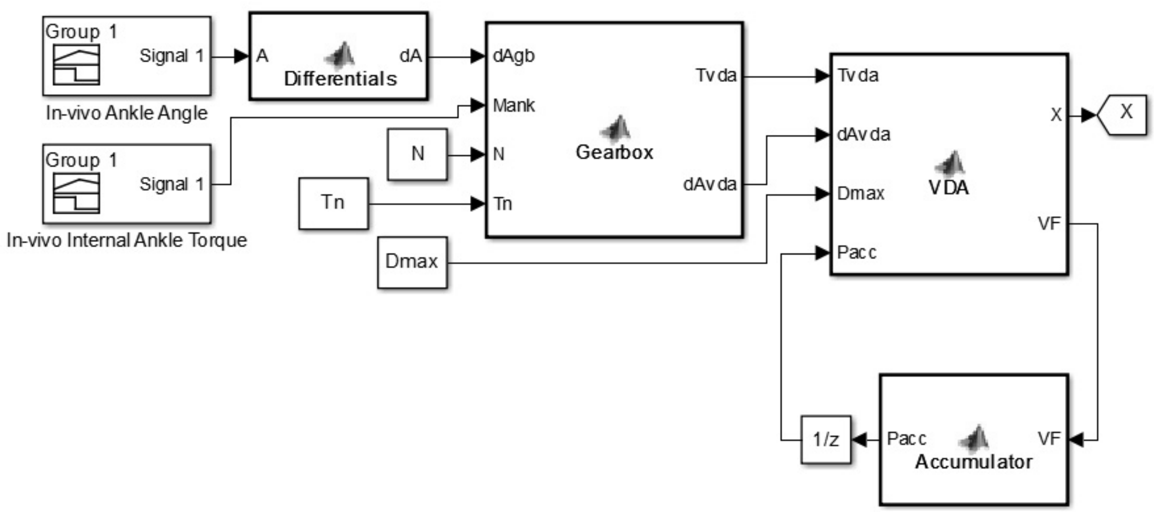

Figure 3.8: Simulink circuit for concept design I.

Figure 3.9 represents a simplified flow chart of the calculation process, which is followed by a description of the blocks used.

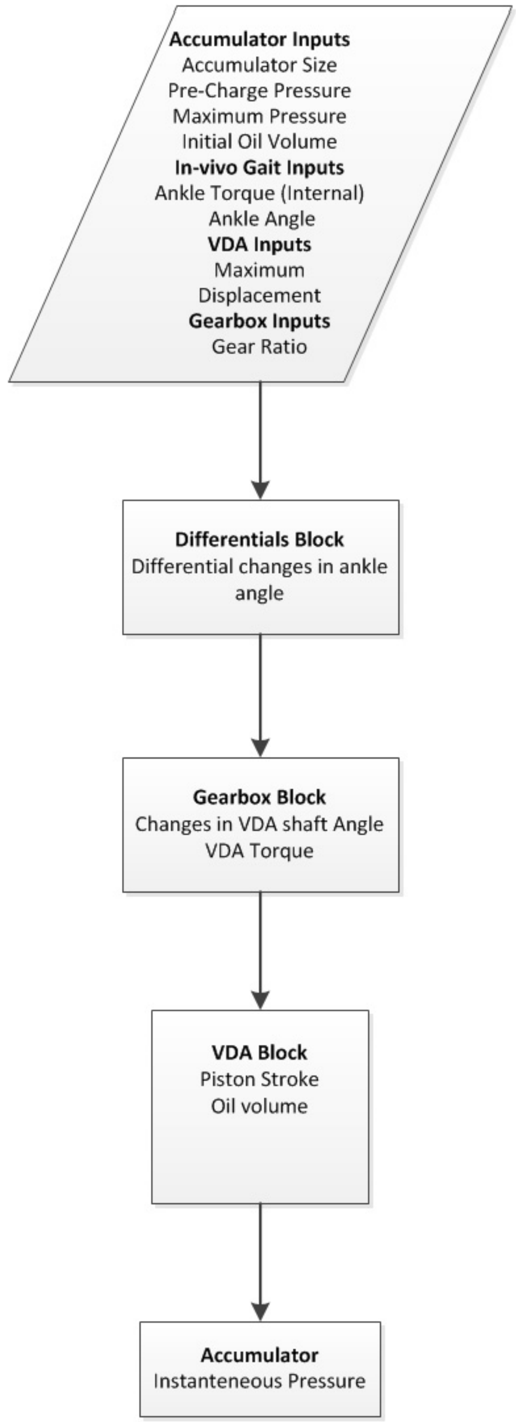

Figure 3.9: Simulation process flow.

3.6.1 DIFFERENTIALS AND GEARBOX BLOCKS

Eq. (3.36) described previously in the gearbox model, converts the angular velocity of the gearbox input shaft (which, being connected to the ankle, is essentially the same as the ankle angular velocity), and by multiplying it with the gear ratio it is converted into the angular velocity of the VDA shaft (output shaft of the gearbox is connected to the VDA, (Figure 3.1)). However, as the angular velocity is a time rate of change of angle, therefore, Eq. (3.36) (which is repeated below for convenience) can be re-written in terms of time derivatives of relevant angles as shown in Eq. (3.38):

$$\omega_{vda} = \omega_{gb} \times N \dots\dots\dots Eq. (3.36)$$

$$\frac{dA_{vda}}{dt} = \frac{dA_{gb}}{dt} \times N \dots\dots\dots Eq. (3.38)$$

For simulation work, a fixed time step was used, therefore, with *dt* cancelled out, Eq. (3.38) becomes:

$$dA_{vda} = dA_{gb} \times N \dots\dots\dots Eq. (3.39)$$

Where, dA_{vda} and dA_{gb} represent infinitesimal changes in the gearbox output shaft and input shaft rotation, respectively. The significance of this modification is that potential numerical errors due to derivatives could be reduced, and that the ankle angle (rather than angular velocity) is used as an input signal.

Therefore, for simulation, the differentials block is specified with Eq. (3.39), and with the in-vivo ankle angle signal as input it calculated the differential changes in ankle angle (*dA*) with units of radians (rad). This is essentially equal to the differential changes in gearbox input shaft (dA_{gb}), being connected to ankle. The dA_{gb} is then fed to the gearbox to drive the VDA shaft (determined by the gear ratio used).

In addition to Eq. (3.39), the gearbox block is specified by the equations derived earlier in section 3.5, which are repeated here for convenience.

$$T_{fr} = (6.913e^{-4}N + 2.557e^{-2})T_N \dots\dots\dots Eq. (3.35)$$

$$T_{vda} = \frac{M_{ank}}{|M_{ank}|.N}\left[|M_{ank}| - K_m T_{fr}\right] \dots\dots\dots Eq. (3.37)$$

The differential ankle angle changes (*dA*) from the differentials block are fed into this block, which serves as differential changes in gearbox input shaft rotation (dA_{gb}). With gear ratio (*N*) as an independent input, differential changes in VDA shaft rotation (dA_{vda}) are calculated using (Eq. (3.39). A nominal torque (T_N) (corresponding to a constant absolute value of the peak in-vivo ankle torque) and in-vivo ankle moment (M_{ank}), also serve as input to this block. These inputs are used to calculate the torque loss due to friction (T_{fr}). As explained earlier, when both the M_{ank} and dA_{vda} would be acting clockwise or anti-clock wise, the VDA would work as a motor (and $K_m = -1$) would be used. Whereas, when the M_{ank} and dA_{vda} would act in different directions (one clockwise, other anti-clockwise and vice versa), VDA would work a pump (and $K_m=1$).

Conditional statements in the code (Appendix-B) were used to determine the positive and negative VDA work phases, and using Eq. (3.35), the VDA torque (T_{vda}) was calculated using Eq. (3.37). The calculated dA_{vda} and T_{vda} are fed to the VDA block.

To simulate ideal conditions, the gearbox transmits the changes in ankle angle and torque without any effect on the VDA as inputs. Since the gearbox makes no difference in ideal conditions (as the T_{fr} would be zero), therefore a gear ratio ($N=1$) was assumed to simulate a VDA only mode. For real conditions, however, relevant gear ratios (*N*), as well as T_N, were used to simulate the effect of gearbox and torque losses due to friction.

3.6.2 VDA BLOCK

This block takes in the VDA size (D_{max}) and accumulator instantaneous pressure (P_{acc}) in addition to the dA_{vda} and T_{vda} (calculated in previous block) and is specified by the following equations, which were previously derived in Section 3.4.

Eq. (3.29) was re-arranged (as shown below) to calculate the piston stroke (X).

$$X = \frac{T_{vda}}{D_{max} P_{acc}} \dots \dots \dots Eq. (3.40)$$

Where T_{vda} is calculated previously from the gearbox block, D_{max} is initially supplied as an arbitrary independent input (and then was sized properly based on the simulation results as explained in a later section), and P_{acc} is supplied as an initial accumulator pressure.

Taking into account that, instead of using angular velocity, differential changes in angles were used, therefore, instead of using flow rates (time derivatives of changes in oil volume), the flow rate equation, including losses (Eq. 3.33) (repeated below for convenience), can be re-written as Eq. 3.41:

$$q_{real} = K_m \frac{|T_{ideal}|.|\omega|}{P_{acc}} - K_m \left[C_s \left(\frac{P}{P_{atm}}\right)^n \left(a + b\left(\frac{\omega}{\omega_{max}}\right)\right) \frac{PD_{max}}{\mu} + \frac{P\omega D_{max}}{B}\left(V_r + \frac{1+X}{2}\right)\right] \dots Eq. (3.33)$$

$$dVF_{real} = K_m \frac{|T_{ideal}|.|dA_{vda}|}{P_{acc}} - dt.K_m \left[C_s \left(\frac{P}{P_{atm}}\right)^n \left(a + b\left(\frac{\omega}{\omega_{max}}\right)\right) \frac{PD_{max}}{\mu} + \frac{P\omega D_{max}}{B}\left(V_r + \frac{1+X}{2}\right)\right] \dots Eq. (3.41)$$

In Eq. (3.41), the first term on the left hand side represents the changes in oil volume, including losses. The first term on the right hand side, represent the changes in oil volume for ideal conditions whereas the second and third terms on the right represent the leakage and compressibility flow losses. For the losses, inevitably the angular velocity of the VDA shaft was used (to avoid any errors, as all the coefficients used in these terms were originally calculated using angular velocity). However, these combined flow losses were multiplied with the time step (*dt*) to make the equation dimensionally correct (with units of m^3).

For ideal conditions, the combined losses terms in Eq. (3.41) were set to zero and for real conditions, the coefficients were defined within the block to calculate the changes in oil volume including the losses.

The differential changes in oil volume, which were calculated based on the conditions for the VDA to work as a pump or motor, were then cumulatively added to provide oil volume for the accumulator. The oil volume was taken to be positive when the VDA pumped it to the accumulator and negative when the accumulator discharged oil during positive work phases (motor mode).

The oil volume is fed to the accumulator block, which used it to calculate the pressure for the next cycle using relevant equations for spring-loaded or gas-charged accumulators. This process continues until the simulation end time is reached.

3.6.3 ACCUMULATOR BLOCK

This block takes in the oil volume (V_F) calculated from the VDA block as input. Both the spring-loaded as well as gas-charged accumulators are used for simulation, and the equations relating the accumulator instantaneous pressure with oil volume can be derived as follows:

a) Spring-Loaded accumulator

Substituting the value of *K* from Eq. (3.3) in Eq. (3.2), and with $V_{max}= V_A$ (spring loaded accumulator capacity (V_A) is the maximum oil volume (V_{max})), we have:

$$P = \frac{(P_{max} - P_{pr})}{V_A} V_F + P_{pr} \dots \dots \dots Eq. (3.42)$$

To simulate the model with a spring-loaded accumulator, the block is specified with the above equation, where, P_{pr}, P_{max}, and V_A are already determined from the sizing section and are provided in the block. The V_F value calculated by the VDA block is used in this equation to solve for the instantaneous pressure, which is fed back to the VDA for the next simulation cycle.

It is important to note that the initial oil volume ($V_{F\ @t=o}$) would serve as an initial condition to start the simulation. To calculate this, the instantaneous pressure (P_{acc}) was taken to be equal to the minimum working pressure (P_l) for both accumulators. The reason for setting P_{acc}=P_l is that, form the in vivo data used, the gait cycle starts with the eccentric work first, meaning that at the start of the gait cycle, the eccentric work is minimum, and therefore the corresponding accumulator pressure should also be taken as minimum.

For simulation work and calculations, the S.I. system of units was used, and only the results were expresses in easy to visualise units (specified with the results).

b) Gas-Charged accumulator

Considering the ideal gas relationship, as mentioned in Eq. (3.19):

$$P.V_G^k = constant \dots \dots \dots \dots Eq. (3.19)$$

At a certain pressure P=P_{acc}, when there is some oil V_F in the accumulator, the gas volume in the accumulator would be equal to the difference between accumulator capacity (V_A) and the oil volume (V_F) at that pressure. Substituting these values in Eq. (3.19), we have:

$$P_{acc}(V_A - V_F)^k = constant \dots\dots\dots Eq. (3.43)$$

Similarly, at $P=P_{pr}$, the gas volume in the accumulator would be equal to the difference between the accumulator capacity (V_A) and minimum oil volume (V_{min}) that is retained in the accumulator (as explained in the definition of pre-charge pressure). Substituting these values in Eq. (3.19) and equating it with Eq. (3.43) we have:

$$P_{acc}(V_A - V_F)^k = P_{pr}(V_A - V_{min})^k$$

$$P_{acc} = P_{pr}\left(\frac{V_A - V_{min}}{V_A - V_F}\right)^k \dots\dots\dots Eq. (3.44)$$

To simulate the model with the gas-charged accumulator, the block is specified with the above equation, where, P_{pr}, k, and V_A are already determined from the sizing section along with a very small value of V_{min} provided in the block. The V_F value calculated by the VDA block is then used to calculate the instantaneous pressure, which is fed back to the VDA for the next simulation cycle.

With the Simulink model, explained along with the process flows for both the ideal and real conditions, the following section describes how the simulation was used to size the VDA for both the ideal and real conditions.

3.7 Design Simulations

This section describes how design simulations were used to find out the optimum design variables for both the ideal and real conditions for the Salford's gait data. The size of the accumulator was calculated earlier, which served as input for the design simulations, which were initially used to properly size the VDA for both the ideal and real conditions. Then the outputs obtained (with optimum sizes of the VDA) for real conditions were compared with those obtained from ideal conditions.

For ideal conditions, the gear ratio makes no difference to energy efficiency, as there are no friction losses and increasing the gear ratio by a factor of N simply decreases VDA displacement (size) by $1/N$. Therefore, a gear ratio of one was assumed in order to simulate a VDA only mode. The simulation was first run with an arbitrary assumed value of VDA size (D_{max}) for both the spring-loaded and gas-charged accumulator with ideal conditions (no losses).Then, from the results, an optimum size of the VDA was identified (details follow in next section). A final simulation was run with the correct D_{max}, and the resultant torque and power outputs were compared with the in-vivo gait data for a comparison.

The design simulation was then carried out for the loss model with the same type and sizes of the accumulators used for ideal conditions. In order to observe the effects of gearbox, a number of N values were selected, which were used in conjunction with a reduced D_{max} (corresponding to $|X_{peak}|=0.9$). Based on the results obtained by using different sets of D_{max} and N, a decision on selecting specific design variables set was made (the criteria and method is explained in later sections). A final design simulation was run with the optimum design variables and the resultant torque and power outputs were compared with those obtained with ideal conditions. The size and weight trade-off between VDA only and VDA-gearbox mode was then discussed by comparing the optimum sizes obtained from the ideal and real conditions.

The following sections describe the procedure used for VDA sizing for the ideal and real conditions, respectively.

3.7.1 VDA SIZING – IDEAL CONDITIONS

To simulate ideal conditions without the gearbox (VDA only mode), a gear ratio of one was used with all losses set to zero, and a first simulation run was started by providing an arbitrary D_{max} value (which represents the size of the VDA and needs to be properly sized). To find out the proper D_{max}, VDA piston stroke (X) served as the key output variable (Eq. (3.40)), which by definition, was defined earlier to vary between 0 (zero displacement) and 1 (maximum displacement). By this definition, a certain D_{max}, which resulted in an absolute maximum stroke ($|X_{peak}|$) of 1, would correspond to the optimum VDA size, as the VDA would be operating at the maximum limits (full load). However, to account for safety and/or variations in gait, a new range of 0 to 0.9 was used, where $|X_{peak}|=0.9$ would correspond to the maximum operating limits of the VDA, and the corresponding D_{max} would be taken as the optimum VDA size.

With this new range defined, if a particular value of D_{max} would result in $|X_{peak}|=0.9$, the same D_{max} would represent the correct size of the VDA. However, if a particular D_{max} would result in $|X_{peak}|$ of less than 0.9, this would mean that the VDA is operating at part-loads, because the size used is larger than required, and subsequently a lower D_{max} is required for the VDA to work at full capacity.

Therefore, the first simulation was run with an arbitrary value of 100 cc/rev. The resulting $|X_{peak}|$ was observed, and if it was found to be lower than 0.9, then the simulation was run again using a decreased value of D_{max} by 1cc/rev. The iterative process of progressively reducing the D_{max} by steps of 1cc/rev for each iteration was continued, until $|X_{peak}|$ of 0.9 was achieved.

The following example illustrates this procedure with a gas charged accumulator and only includes the results obtained for the arbitrary and for the optimized D_{max}. Although the model is defined with S.I. units, the example is shown with easy to visualise units, however, these values were accordingly converted into SI before running the simulation. The parameters for the first simulation were:

Actuator's arbitrary D_{max} for the first simulation run = 100 cc/rev

Gas-charged accumulator size (V_A = 245 cc)

Initial Oil volume (V_F = 101 cc)

From the results of the first simulation, the piston stroke of the actuator was obtained, as shown in Figure 3.10. The curve showed that using an arbitrary D_{max} of 100 cc/rev was too large for the VDA to operate at its full capacity for the above mentioned accumulator parameters, because the resulting peak absolute piston stroke was 0.394, whereas the iterative procedure of decreasing the D_{max} to get an $|X_{peak}|$ of 0.9001 resulted in a D_{max} of 43.8 cc/rev.

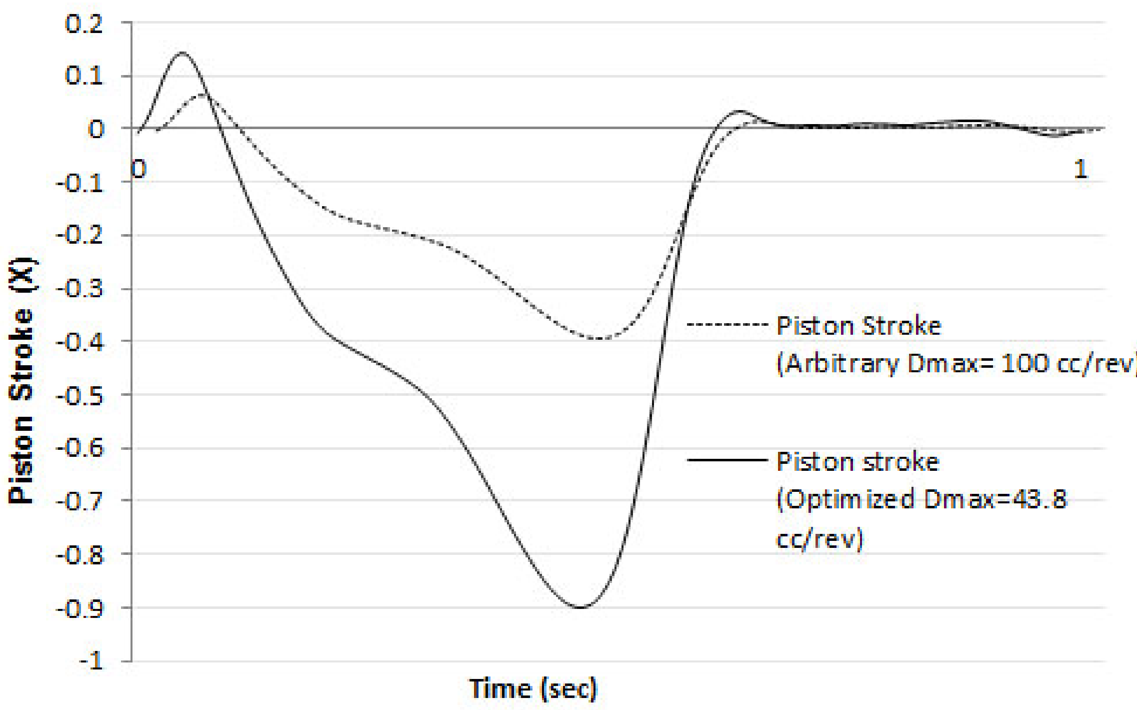

Figure 3.10: Piston Stroke (X) obtained from first simulation run with an arbitrary D_{max} and from an optimized D_{max} obtained as results of an iterative process.

The same process was repeated for the spring loaded accumulator of size 60 cc, and the results of the optimized D_{max} obtained for both the gas-charged and spring-loaded accumulators are presented in Table 3.4 below.

Spring-Loaded Accumulator			Gas-Charged Accumulator		
VA (cc)	Dmax (cc)	|Xpeak|	VA (cc)	Dmax (cc)	|Xpeak|
60	43.7	0.902	245	43.8	0.9

Table 3.4: Optimized size of the VDA obtained from simulation for both the spring-loaded and gas-charged accumulator type for ideal conditions.

With the correct D_{max} obtained for both types of accumulators, the simulation results indicated that the VDA produced the required ankle torque and power (as will be shown later). However, these results were obtained for an ideal case scenario where no losses were considered. Therefore, the following section describes how design simulations were used to size the VDA as well as the gearbox for the real conditions while keeping the flow losses and gearbox friction minimal with the constraint ($|X_{peak}|=0.9$) satisfied.

3.7.2 VDA/GEARBOX SIZING - REAL CONDITIONS

The simulation of an ideal case required only the correct sizing of the VDA, whereas the simulation of the model with real conditions required correct sizing of the VDA as well as the correct gear ratio while considering the losses.

The flow losses increase the oil leakage from the accumulator compared to the ideal model as governed by the loss models for the VDA and gearbox (Section 3.4 and 3.5). Therefore, in order to produce the required in-vivo data, more hydraulic power is required by the VDA than it would with the ideal model. Using a gearbox with the VDA would decrease the torque load at the VDA, and consequently its size would be reduced by increasing the gear ratio. While minimizing the VDA size is desirable (to decrease flow losses and weight), increasing the gear ratio increases gearbox friction losses.

The pressure profile of the accumulator would indicate the extent of flow losses. More losses cause less oil to be delivered to the accumulator and more oil to be drained to the tank. As a result, the accumulator pressure would drop more over the gait cycle. Therefore, in order to understand the effect of both the VDA size (D_{max}) and gear ratio (N) on the flow losses and consequently to find an optimum value of both of these design variables (to minimize losses), a final value of accumulator pressure would serve as a good indicator. In other words, the optimum set of D_{max} and N values would result in the *least* accumulator pressure drop at the end of the gait cycle, while satisfying the only constraint ($|X_{peak}| = 0.9$).

Therefore, to find the optimum set of design variables, a D_{max} of 44 cc was taken as an initial estimate, which was divided by gear ratios ranging from 2 to 20 with a step of 1. This resulted in 19 sets of design variables (with increasing gear ratios and decreasing D_{max} values). The simulation was then run with each set of these design variables and for each simulation, whereby only D_{max} was adjusted (with an accuracy of 0.1 cc/rev) to keep the constraint satisfied, i.e. for $|X_{peak}|$ to be equal to 0.9. The final accumulator pressure obtained with each set of the adjusted design variables (with the constraint satisfied) was plotted in Figure 3.11, in which the peak of the curve corresponded to the optimum set of D_{max} and N values (highest final accumulator pressure pertains to less oil drain to the tank attributing to minimum losses).

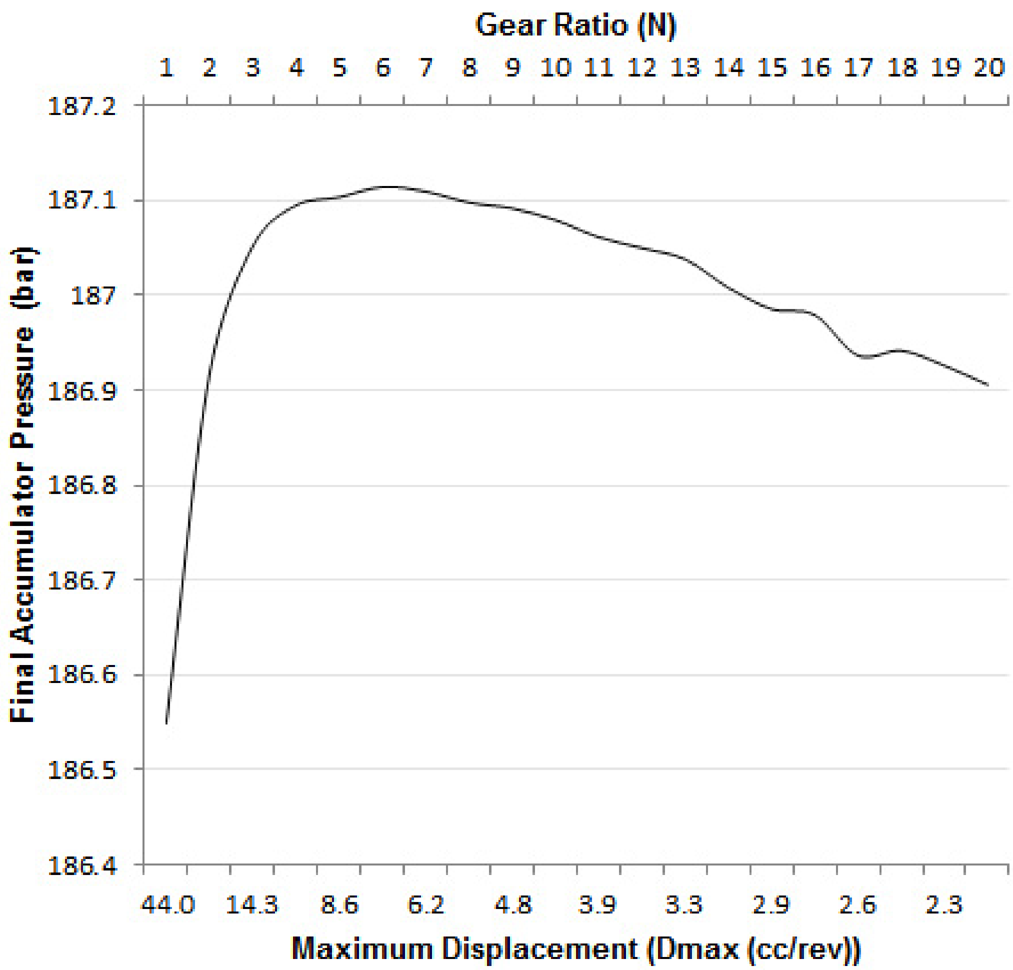

Figure 3.11: Final accumulator pressure for D_{max} and N.The peak value corresponds to the design variable set that produced minimal losses while keeping $|Xpeak|=0.9$.

The curve in Figure 3.11 is obtained using a gas-charged accumulator of 245 cc capacity with an initial pressure of 188 bar. Due to losses, the final pressure was lower more than the initial value for a range of design variable sets used. However, the peak of the final pressure curve indicates that the corresponding set of D_{max} and N produced minimal losses, while satisfying the constraint.

The same method was used to find the optimum design variables for the spring-loaded accumulator of 60 cc capacity with the same initial pressures. The resulting design variables for both the gas-charged and spring-loaded accumulators for both the ideal as well as real conditions are presented in the following table.

Accumulator Type	Accumulator Capacity (cc)	Iniital Pressure (bar)	Ideal Conditions			Real Conditions		
			Final Pressure (bar)	Dmax (cc/rev)	Gear Ratio	Final Pressure (bar)	Dmax (cc/rev)	Gear Ratio
Spring-Loaded	60	188	189.4	43.7	1	187.08	7.26	6
Gas-Charged	245	188	189.4	43.8	1	187.09	7.28	6

Table 3.5: VDA and gearbox sizes obtained for different accumulator sizes and types.

From Table 3.5, the effects of losses can be observed. For real conditions, as explained earlier, the flow losses increase the oil lost from the accumulator for both positive and negative work. This is evident from the final accumulator pressures obtained for the real conditions in comparison with ideal conditions. In ideal conditions, the end pressure for both accumulator types is higher than the initial pressure value (pertaining to the in-vivo data used where the net work performed was negative). This means that, without any losses, and for the particular in-vivo data used, the accumulator had some excess energy left after the VDA provided the required ankle power. The excess energy left over one gait cycle would require to be drained over the next few cycles through the relief valve. However, in the real case, due to the losses, and for the VDA to produce the required ankle power, the accumulator pressure profiles for both accumulators type indicate that the excess stored energy did not make up for the losses. The VDA produced the required ankle torque and, in order to do so, more oil is drained from the accumulator to compensate for the losses in order to produce similar in-vivo data. As a result, the pressure at the end of the cycle fell below the initial pressure. This would mean that, over the next few cycles, the accumulator would keep on draining until a point is reached when no more energy is stored and subsequently the system will simply stall.

3.8 Pseudo Control

As explained in the previous section, under real conditions the accumulator would gradually empty. In a physical system, this problem would be dealt with by the control system, which would ensure that the accumulator pressure remains periodic (i.e. the final pressure must not drop below the initial pressure value) by modulating the VDA oil flow rate at the expense of reduced push-off power. The control design is beyond the scope of this study and part of future work. However, as a proof of concept, following the working principle of the control system, and to account for the extent of push-off power loss as a result of maintaining a periodic accumulator pressure, this section presents a methodology that was carried out to impose a pseudo control on the results obtained and to observe the extent of reduced push-off power in real conditions.

The control system would ensure that the final accumulator pressure must not drop below the initial pressure value (i.e. pressure is cyclic). To illustrate this functioning, a sample ankle power data was taken, and its positive phases were scaled down. This resulted in a reduced ankle power profile, the eccentric phases of which remain unaffected while the concentric phases were reduced. The original data along with the reduced push-off represent the effect of the control system as a result of maintaining the accumulator pressure by compromising the push-off power, which is presented in Figure 3.12.

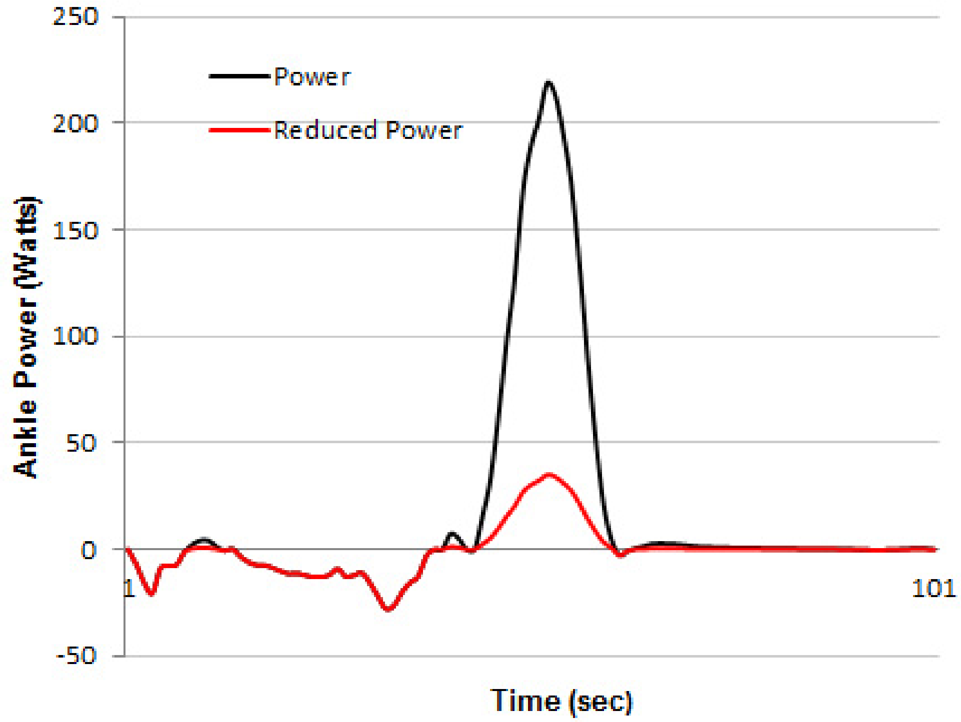

Figure 3.12: An ankle power profile sample compared with the effect of the control system.

In order to understand how this could be achieved with the design, the cumulative energy profiles (area under the power curves) corresponding to both the original and reduced power curves, shown in the previous figure is presented in Figure 3.13.

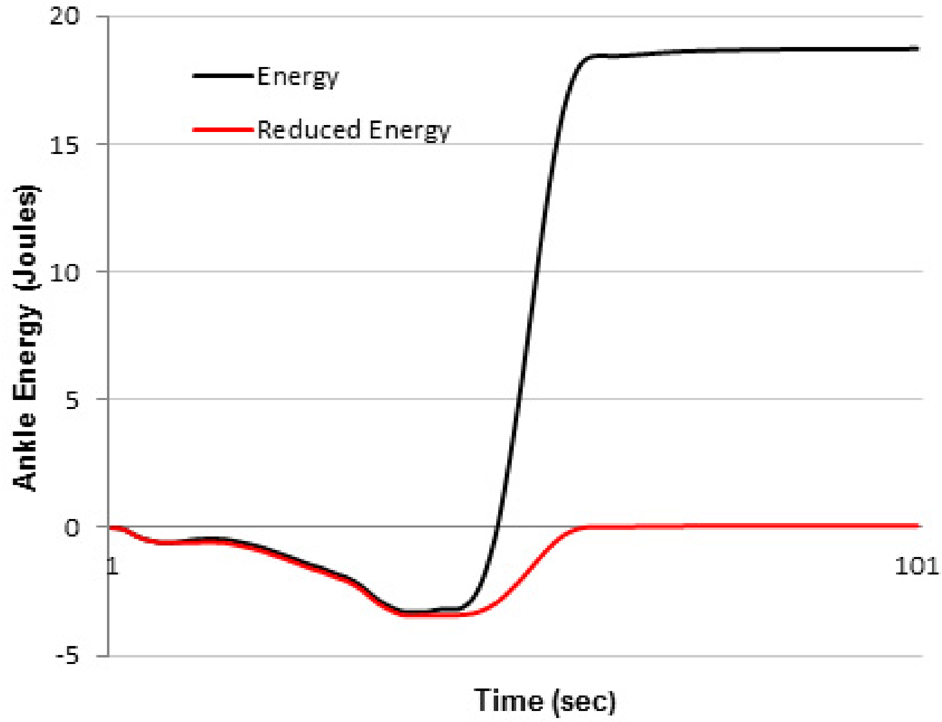

Figure 3.13: Energy profiles for the original ankle power data and for the reduced power data.

Figure 3.13 shows the energy profile obtained by integrating the sample ankle power and reduced power data plotted in Figure 3.12. Comparing the two energy profiles in Figure 3.13, the profile corresponding to the reduced power curve (in Figure 3.12) has equal initial and final values, which means that the released energy by the ankle was equal to what it stored earlier in gait. In turn, the other profile (obtained from the original ankle power data in Figure 3.12) illustrates that more energy was released than stored earlier.

With the accumulator as the energy storing component, its pressure profile is analogous to an inverted ankle energy profile (during eccentric work phases, cumulative ankle energy is negative, whereas accumulator pressure rises and vice versa). Therefore, the ankle power profile (rate of change of ankle energy) must also resemble the inverted profile of the rate of change of accumulator pressure (dP_{acc}/dt). The accumulator pressure profile, obtained from simulation with both the ideal and real conditions with the gas-charged accumulator of 245 cc, is shown in Figure 3.14.

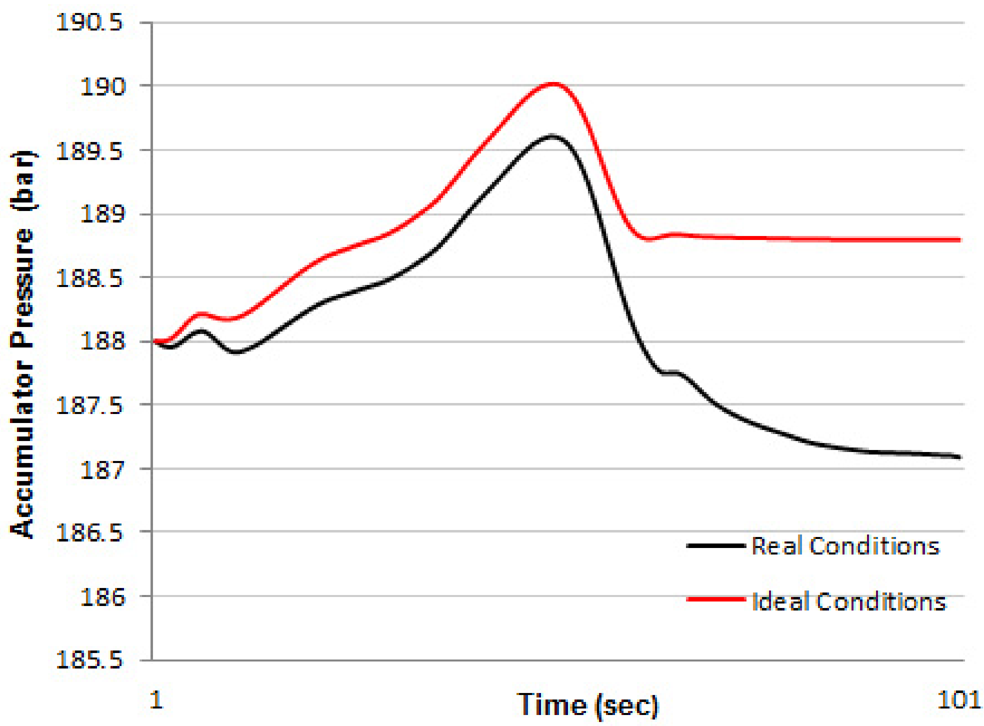

Figure 3.14: Accumulator pressures obtained with a gas-charged accumulator for ideal and real conditions.

In Figure 3.14, the final pressure for the profile obtained with the ideal model is higher than the initial pressure, whereas, with real conditions, the final pressure is lower than the initial pressure value. This behaviour is similar to the inverted ankle energy profile in Figure 3.13. Therefore, in order to bring the final pressure back to the initial pressure for real conditions, the time derivative of pressure (dP_{acc}/dt) curve for real conditions must be taken, and the negative phases of which should be scaled down (using factors ranging from 0 to 1). For each of these scaling iterations, the scaled dP_{acc}/dt curve, when integrated, would result in a scaled pressure profile. This process of scaling down the negative phases of dP_{acc}/dt, and subsequently integrating them would result in several scaled pressure profiles, and the one having equal initial and final values (cyclic pressure profile), would be the desired pressure profile. However, it should be noted that an actual control system would not scaled down the push off power, but would modulate the displacement in order to have equal initial and final accumulator pressures, and the assumption of a perfect displacement control is always assumed in this work. Therefore, the term "scaled" refers to those results where, the push off power has been scaled down and all the other cases (for instance, ideal or real), should not be interpreted as uncontrolled. A perfect control is always assumed for all the conditions.

Figure 3.15 represents the scaled accumulator pressure profile as a result of integrating the scaled-down negative phases of the dP_{acc}/dt curve (which was obtained from simulation with real conditions) for Salford's gait data. This Figure is plotted along with the ideal and real pressures.

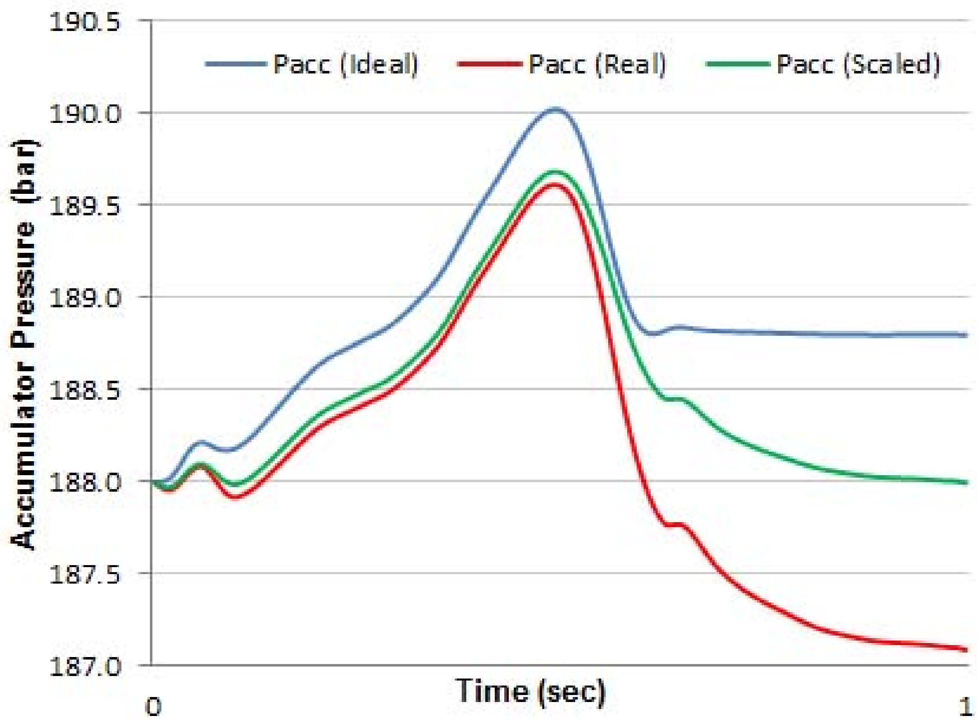

Figure 3.15: Accumulator pressures obtained with a gas-charged accumulator for ideal, real, and real scaled conditions using Salford's gait data.

To understand the extent of reduced push-off power as a result of reduced oil flow, the scaled pressure profile was used to calculate the oil volume using a re-arranged Eq. (3.44).

$$V_F = V_{min}\left(\frac{P_{pr}}{P_{acc}}\right)^{\frac{1}{k}} + V_A\left[1 - \left\{\frac{P_{pr}}{P_{acc}}\right\}^{\frac{1}{k}}\right] \dots\dots\dots Eq. (3.45)$$

Where, the real scaled pressure is used as P_{acc}, whereas the rest of the parameters remained unchanged (same values, which were used to calculate the accumulator size). This oil volume was numerically differentiated to get flow rate. The obtained flow rate, when multiplied by the scaled pressure, provided the scaled accumulator hydraulic power (Eq. (3.46).

$$Accumulator\ hydraulic\ power = \frac{dV_F.P}{dt} \dots\dots\dots Eq. (3.46)$$

Figure 3.16 and Figure 3.17 show the VDA torque and accumulator hydraulic power obtained using ideal conditions and real scaled conditions, for the Salford's gait data, and are compared with the original data.

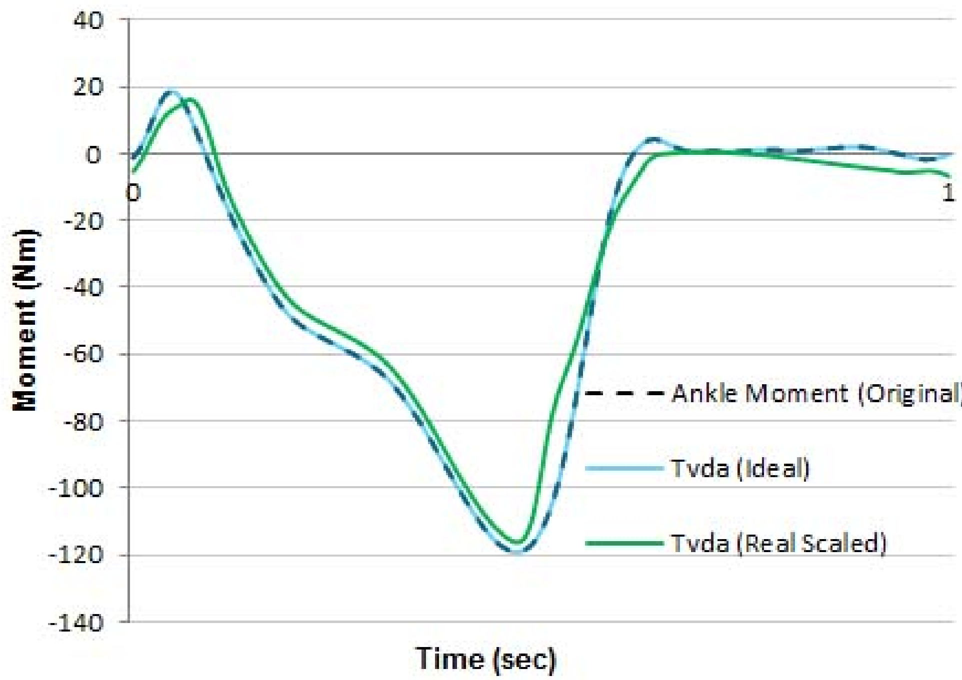

Figure 3.16: Torque profile for ideal and real scaled conditions using Salford's gait data.

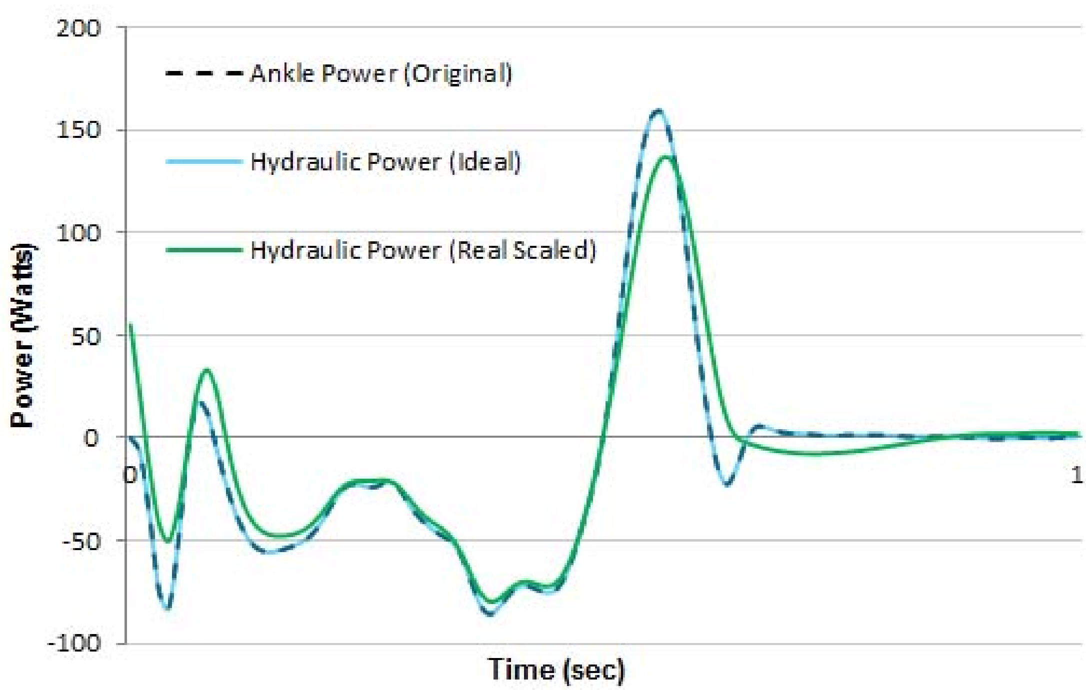

Figure 3.17: Power profile for ideal and real scaled conditions using Salford's gait data.

In Figure 3.17, the hydraulic power matches exactly with the in vivo ankle power for ideal conditions. With pseudo control implemented, the system was able to deliver a peak hydraulic power of 137 watts against 159 watts with ideal conditions. In other words, 13.8% of peak power was lost by reducing the push-off power to achieve a periodic accumulator pressure profile.

It should be noted that this comparison is between the two hydraulic powers, one is for the ideal case (which matches exactly with the in-vivo ankle power), and the other is for the real scaled conditions.

3.9 System Testing

To test the model's performance over level and slopes, data for level, incline and decline walking were taken from Lay et al., 2006, which is the mean of 66 trials for 5 male and 4 female subjects with a mean age and mass of 24 years and 73.36 kg, respectively, at a comfortable walking speed. The model was tested for the five walking conditions: self-selected walking on the level, 8.5° incline, 21° incline, 8.5° decline, and 21° decline. The simulation was run with the ankle angle and ankle moment data, and the accumulator pressures, VDA torque and hydraulic powers obtained with the ideal model were compared with the real model (using pseudo control to achieve a controlled accumulator pressure) in order to have an idea about the performance of a physical prototype. Before running the tests, individual data were used to find the optimum value of the maximum displacement and gear ratio as explained in Section 3.7.2, and the results are presented in Table 3.6 below.

Data Source	Terrain Type	Concept Design I			
		Ideal Conditions		Real Conditions	
		Dmax (cc/rev)	Gear Ratio	Dmax (cc/rev)	Gear Ratio
University of Salford	**Level**	43.8	1	7.26	6
Lay et al., 2006	**Level**	43.5	1	10.8	4
Lay et al., 2006	**8.5° Decline**	33.8	1	11.1	3
Lay et al., 2006	**21° Decline**	23.6	1	5.8	4
Lay et al., 2006	**8.5° Incline**	53.4	1	13.2	4
Lay et al., 2006	**21° Incline**	53.4	1	13.2	4

Table 3.6: Summary of optimum VDA and gearbox sizes for the test data.

Table 3.6 shows the optimum values of maximum displacement and gear ratio obtained for the gait data from the University of Salford and from Lay et al., 2006, for level and slope walking conditions. For ideal conditions, it is clear that using a stand-alone VDA to directly drive the ankle might not be a better option because the VDA size is large and would be prone to leakage losses in real conditions. Using a gearbox with the VDA would be beneficial in reducing the VDA size (and hence associated leakage losses), but the extent of torque loss due to friction in the gearbox must be considered.

The simulation was run with the optimum values of design variables listed in the table above for each condition, and the results for accumulator pressure (P_{acc}), VDA torque (T_{vda}) and hydraulic power are presented in the following section for the level, declined and inclined walking conditions.

3.9.1 LEVEL WALKING

a) Salford's Gait Data

Results for the level waking data from University of Salford, are already presented in Figure 3.15, Figure 3.16, and Figure 3.17.

a) Data from Lay et al, 2006

This section present the results obtained for the level walking data taken from Lay et al., 2006.

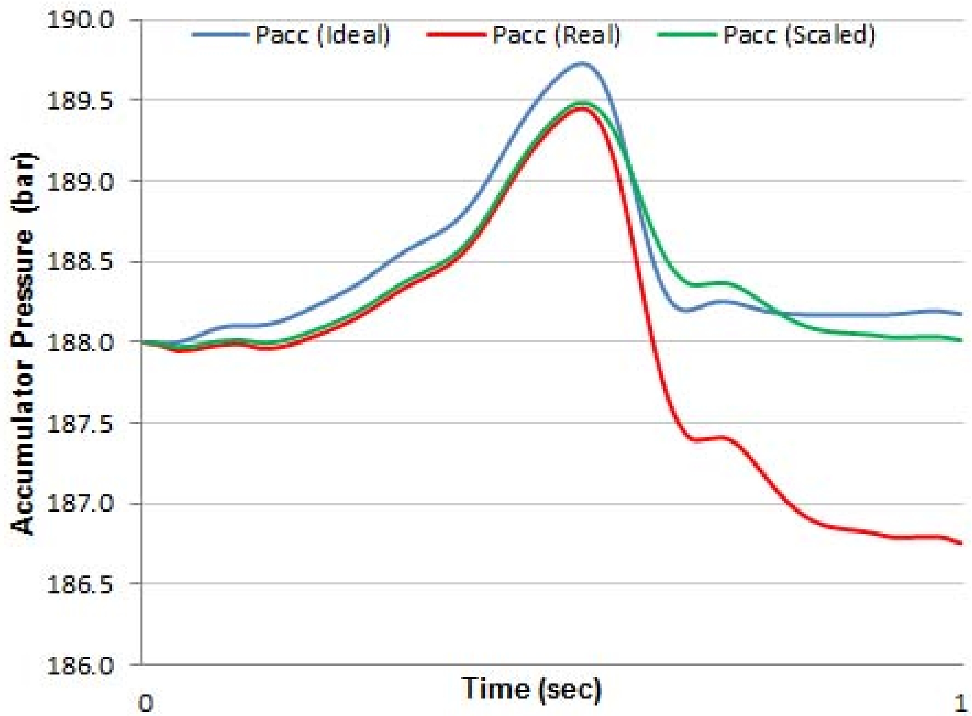

Figure 3.18: Pressure profile for ideal, real, and real scaled conditions using level walking data from Lay et al., 2006.

In Figure 3.18, the pressure profile for ideal conditions (solid blue curve) indicates that the final pressure is slightly higher than the initial pressure, indicating that there is more energy stored in the accumulator than released during the gait cycle.

However, the pressure profile for real conditions (solid red curve) indicates that the leakage losses caused the final accumulator pressure to drop lower than the initial value. i.e. more energy is released than stored in the accumulator. The pressure profile (solid green curve) represents the pressure profile obtained by implementing a pseudo control on the pressure obtained for real conditions.

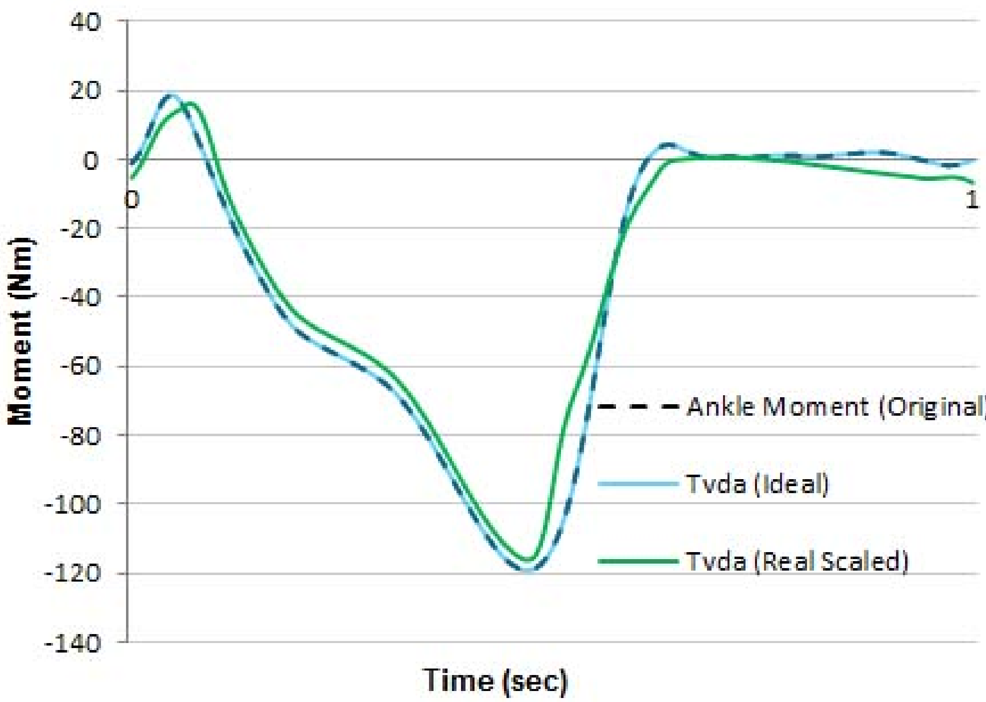

Figure 3.19: Torque profile for ideal and real scaled conditions using level walking data from Lay et al., 2006.

Figure 3.19 indicates that for the ideal conditions, the torque obtained from simulation matches exactly with the in-vivo data used. The torque obtained from a VDA by implementing pseudo control on accumulator pressure (solid green curve) is slightly lower than the ideal case, but it is still very close to normal ankle torque profile.

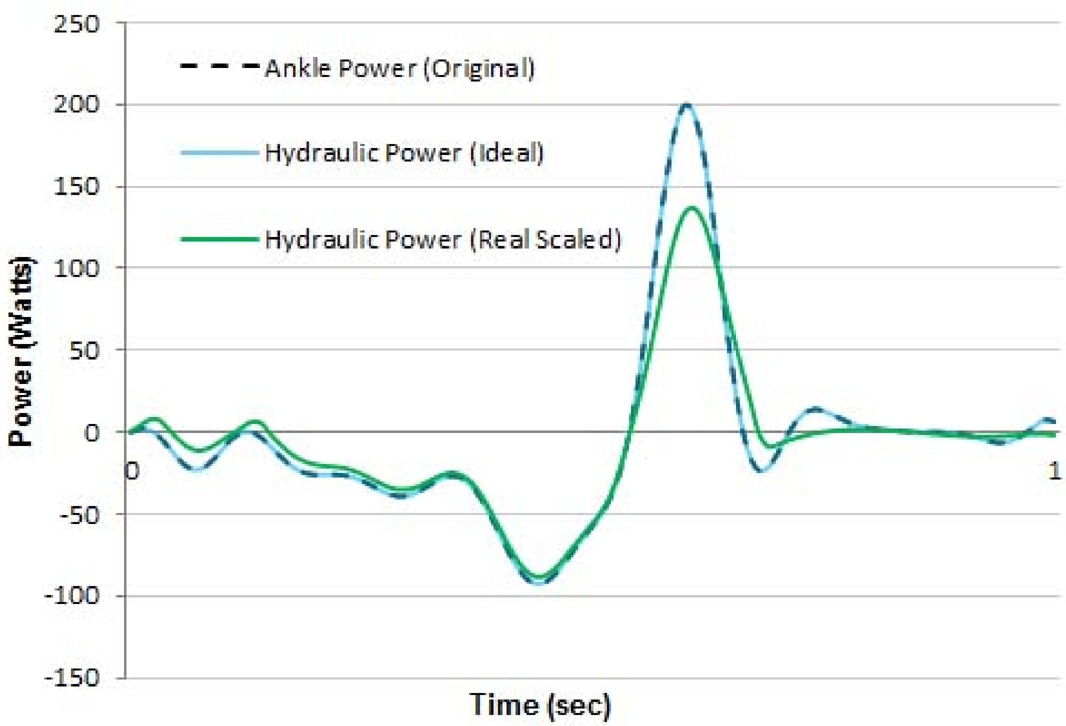

Figure 3.20: Power profile for ideal and real scaled conditions using level walking data from Lay et al., 2006.

Figure 3.20 shows the power profile for the intact ankle and accumulator hydraulic power obtained for the ideal and real scaled conditions. The intact ankle power and accumulator hydraulic power matches exactly. However, the power obtained (solid green curve) by implementing pseudo control indicates that the system was able to store all of the available negative work, but less peak power was delivered when losses were considered. In addition, the timings of the power delivery matches exactly with the ideal conditions.

3.9.2 DECLINE WALKING

The decline walking data from Lay et al., 2006, for the two degrees of decline: 8.5° and 21° is used here. The results are presented below:

b) 8.5° Decline

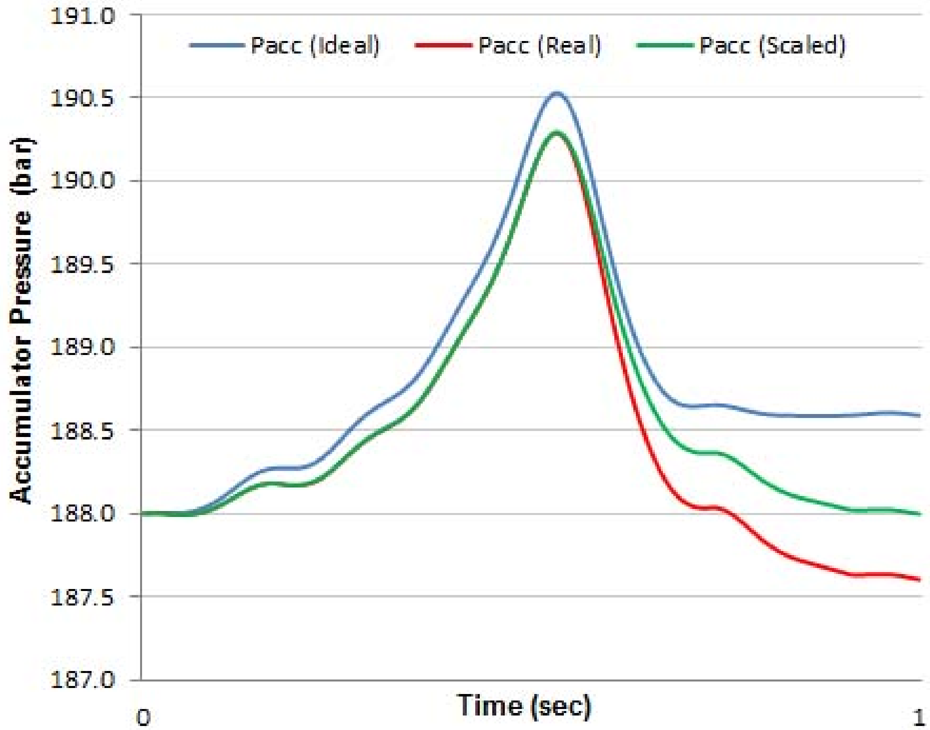

Figure 3.21: Pressure profile for ideal, real, and real scaled conditions using 8.5° decline walking data from Lay et al., 2006.

In Figure 3.21, the pressure profile for ideal conditions (solid blue curve) indicates that the final pressure is higher than the initial pressure, indicating that there is more energy available to store in the accumulator than released during the gait cycle. However, the pressure profile for real conditions (solid red curve) indicates that the leakage losses caused the final accumulator pressure to drop lower than the initial value (i.e. more energy is required than what is stored in the accumulator). The pressure profile (solid green curve) represents the pressure profile obtained by implementing a pseudo control on the pressure obtained for real conditions to obtain a cyclic pressure profile.

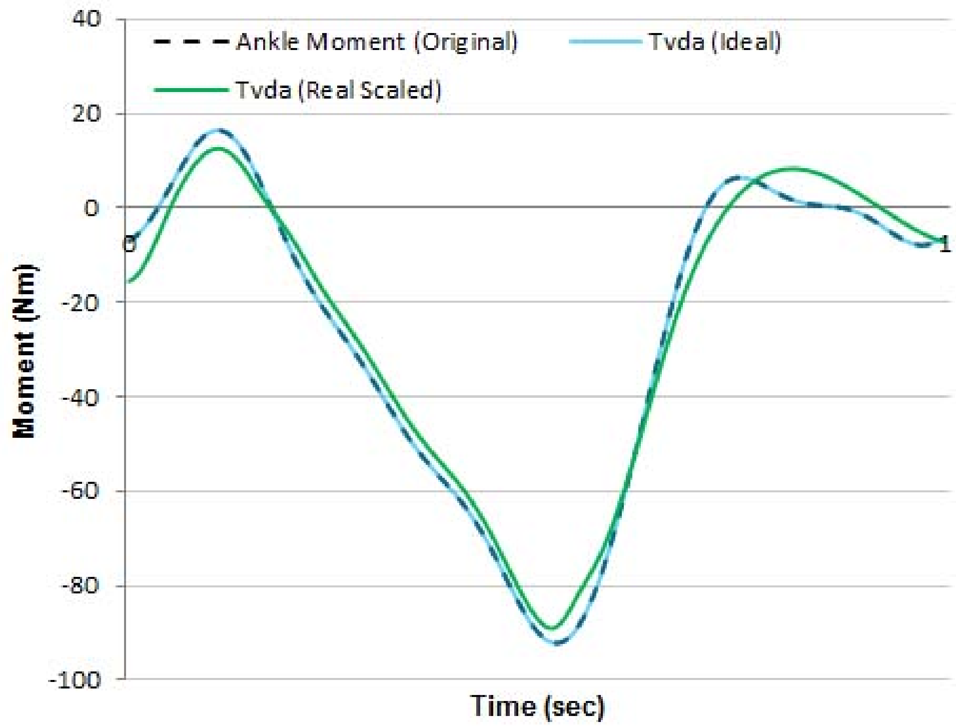

Figure 3.22: Torque profile for ideal and real scaled conditions using 8.5° decline walking data from Lay et al., 2006.

Figure 3.22 indicates that for the ideal conditions, the torque obtained from simulation matches exactly with the in-vivo data used. The torque obtained from a VDA by implementing pseudo control on accumulator pressure (solid green curve) is slightly lower than the ideal case, but it is very close to normal ankle torque profile.

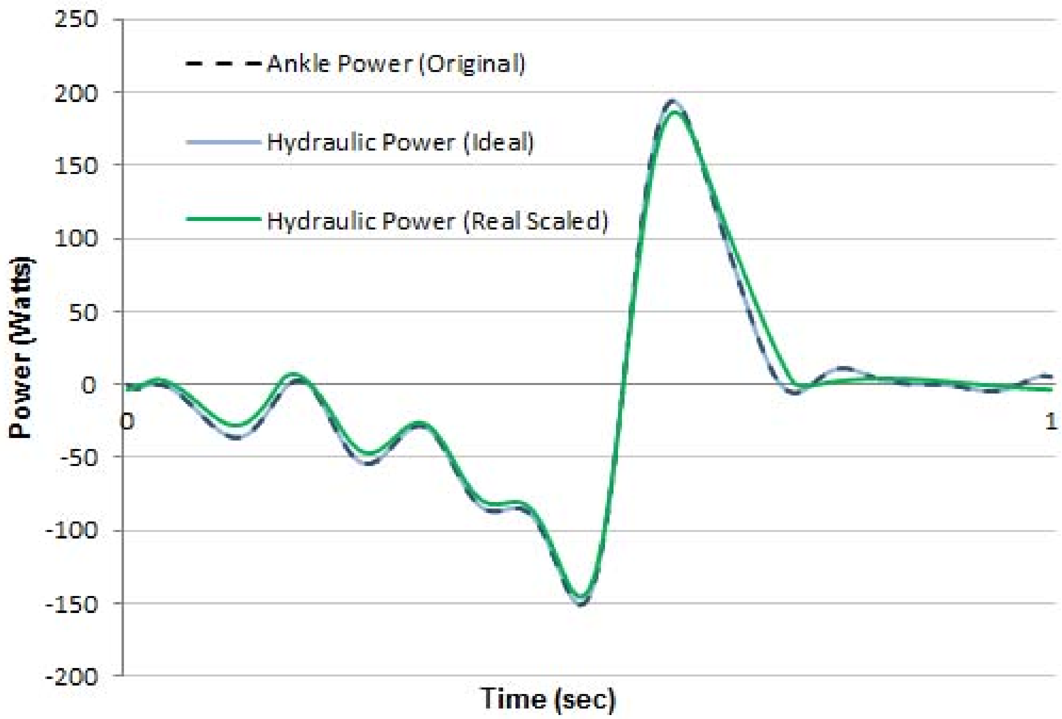

Figure 3.23: Power profile for ideal and real scaled conditions using 8.5° decline walking data from Lay et al., 2006.

Figure 3.23 shows the power profile for the intact ankle and accumulator hydraulic power obtained for the ideal and real scaled conditions. The intact ankle power and accumulator hydraulic power matches exactly. Even with losses, the scaled power obtained (to maintain a cyclic accumulator pressure) is very close to the required ankle power, because the additional energy available in the accumulator was utilized in compensating for the losses. Therefore, for decline walking, the system was able to deliver a close to normal ankle power profile.

c) 21° Decline

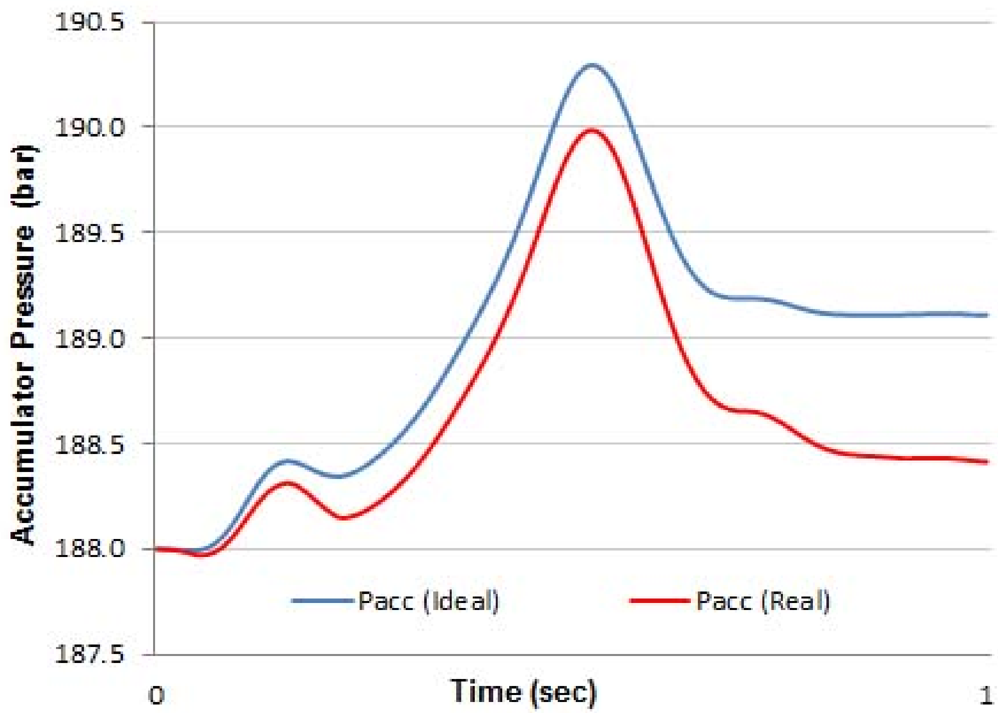

Figure 3.24: Pressure profile for ideal and real conditions using 21° decline walking data from Lay et al., 2006.

In Figure 3.24, the pressure profile for the ideal conditions (solid blue curve) indicates that the final pressure is higher than the initial pressure, indicating that there is more energy available to store in the accumulator than released during the gait cycle. This additional energy even after compensating for the leakage losses remained higher than released. Therefore, the final pressure for real conditions (solid red line), albeit dropped lower than the final pressure for the ideal conditions, it is still higher than the initial value. The excess energy would need to be drained through the pressure relief valve.

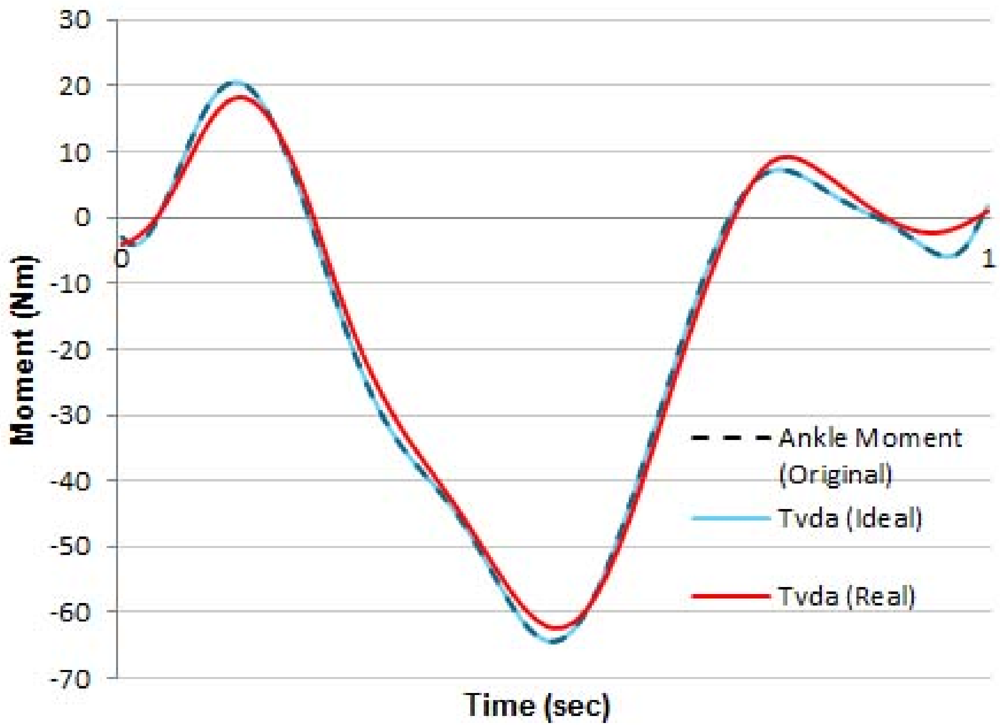

Figure 3.25: Torque profile for ideal and real conditions using 21° decline walking data from Lay et al., 2006.

Figure 3.25 indicates that for the ideal conditions, the torque obtained from simulation matches exactly with the in-vivo data used. The torque obtained from a VDA for real conditions (solid red curve) is also very similar to the torque profile for ideal conditions.

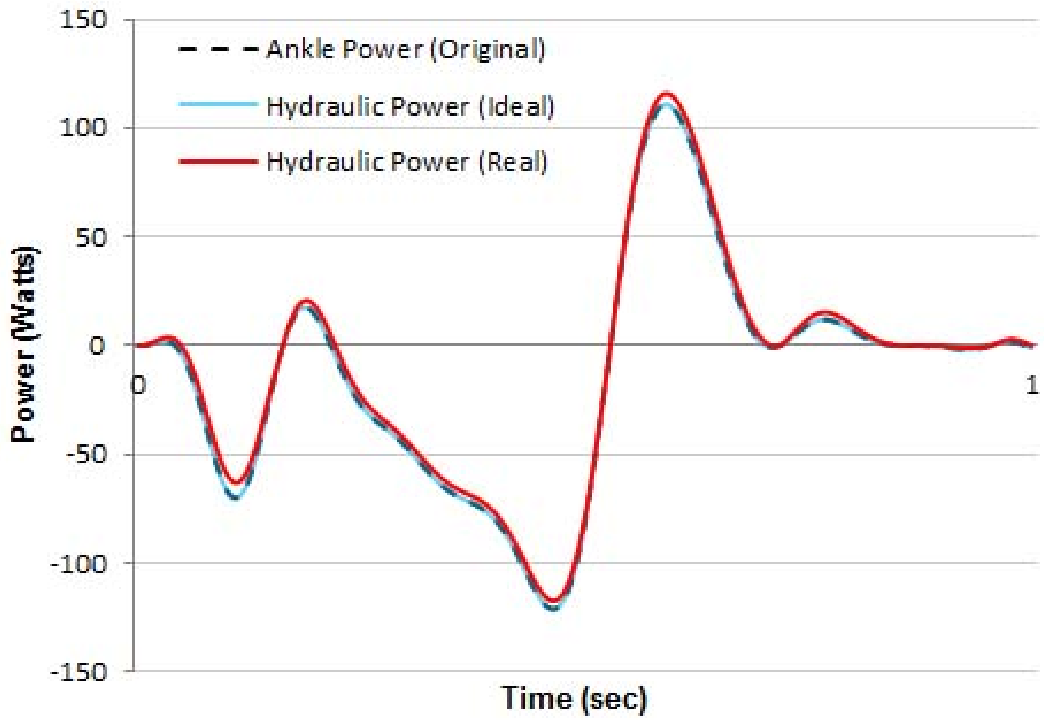

Figure 3.26: Power profile for ideal and real conditions using 21° decline walking data from Lay et al., 2006.

Figure 3.26 shows the power profile for the intact ankle and accumulator hydraulic power obtained for the ideal and real conditions. The intact ankle power and accumulator hydraulic power matches exactly. In addition, as there was more energy available in the accumulator even with losses, the delivered hydraulic power also matched almost exactly with the ideal power profile.

3.9.3 INCLINE WALKING

The incline walking data from Lay et al., 2006, for 21° and 8.5° is used for testing. The results are presented below:

a) 8.5° Incline

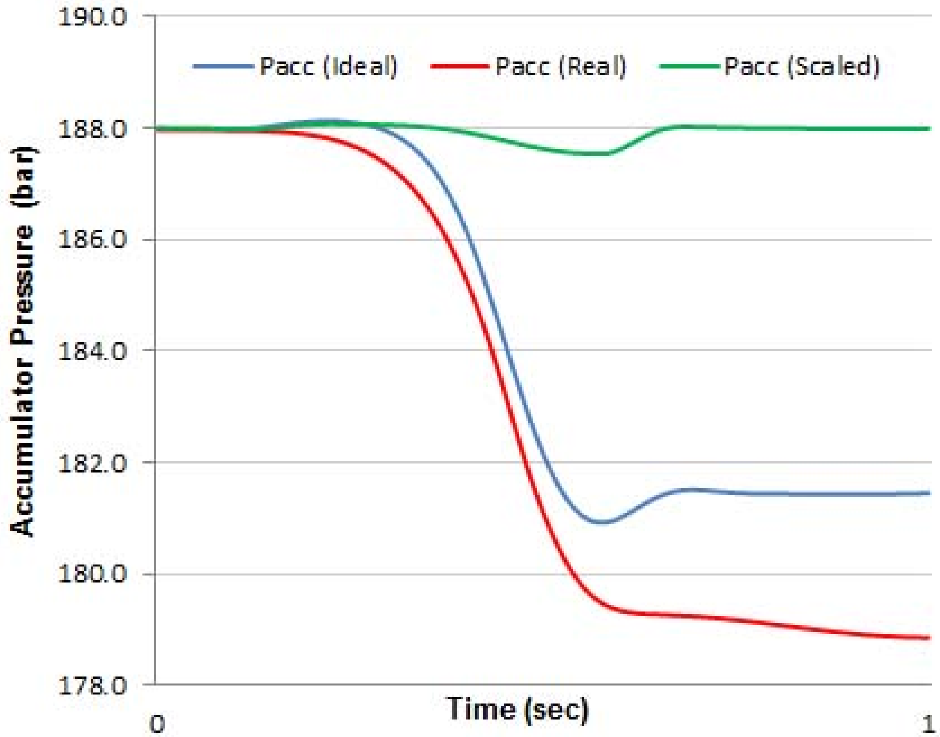

Figure 3.27: Pressure profile for ideal, real, and real scaled conditions using 8.5° incline walking data from Lay et al.,2006.

During incline walking, the active positive work contribution dominates the elastic energy storage and return work of tendons. Therefore being a passive system aimed to recycle the strain energy, there is very little energy to store and return. A perfect control was assumed in the simulation and therefore, in order to produce similar levels of musculo-tendon work, the accumulator had to be drained (final pressure dropped lower than the initial pressure), as shown in Figure 3.27. For real conditions, the situation was worse, as the pressure dropped more in order to compensate for the losses. However, scaling the pressure profile for real conditions (solid green curve) indicates that, in order to prevent the accumulator to be completely drained over few cycles, there would be very little energy to store and return.

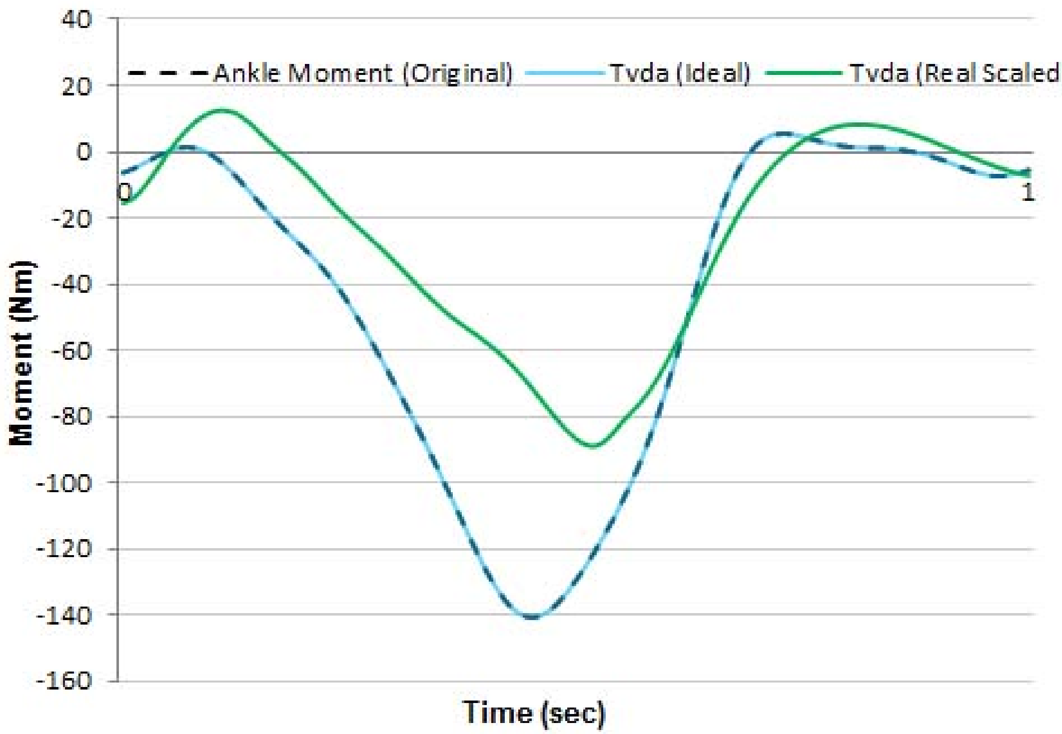

Figure 3.28: Torque profile for ideal and real scaled conditions using 8.5° incline walking data from Lay et al., 2006.

Figure 3.28 indicates that the torque obtained from simulation matches exactly with the in-vivo data used. However, this would cause the accumulator to be drained over few cycles, as discussed previously. The torque profile obtained by scaling the accumulator pressure (solid green curve) to prevent stalling the system represents a deviation from the normal ankle torque profile system for an 8.5° incline walking.

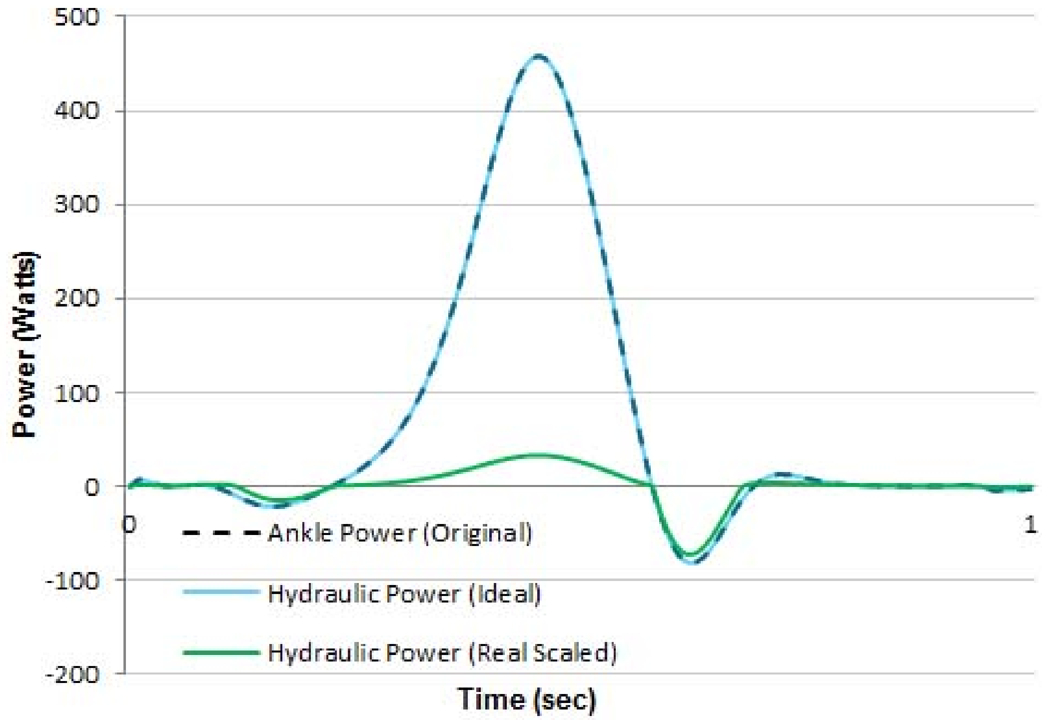

Figure 3.29: Power profile for ideal and real scaled conditions using 8.5° incline walking data from Lay et al., 2006.

Figure 3.29 indicates that, for incline walking, active positive work contribution dominates the elastic energy storage and return work of tendons. Therefore, being a passive system aimed to recycle the strain energy, there is very little energy to store and return, as indicated by the solid green curve.

b) 21° Incline

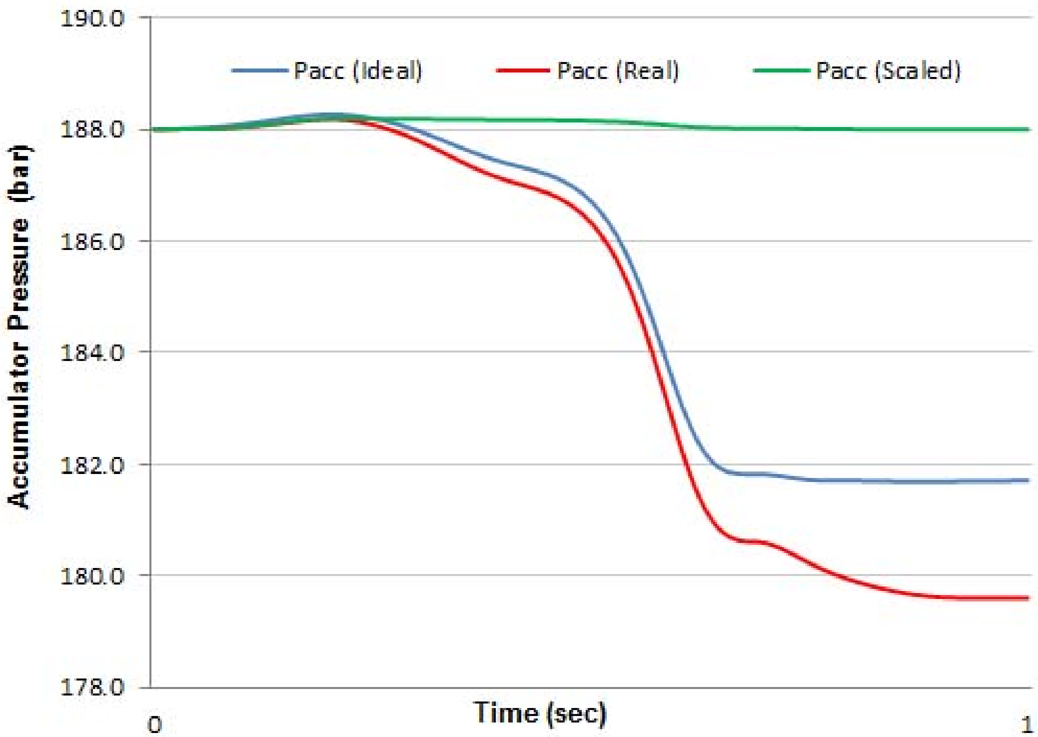

Figure 3.30: Pressure profile for ideal, real, and real scaled conditions using 21° incline walking data from Lay et al., 2006.

During incline walking, the active positive work contribution dominates the elastic energy storage and return work of tendons. Therefore, being a passive system aimed to recycle the strain energy, there is very little energy to store and return. A perfect control was assumed in the simulation and therefore, in order to produce similar levels of musculo-tendon work, the accumulator had to be drained (final pressure dropped lower than the initial pressure), as shown in Figure 3.30. For real conditions, the situation was worse, as the pressure dropped more in order to compensate for the losses. However, scaling the pressure profile for real conditions (solid green curve) indicates that, in order to prevent the accumulator to be completely drained over few cycles, there would be very little energy to store and return.

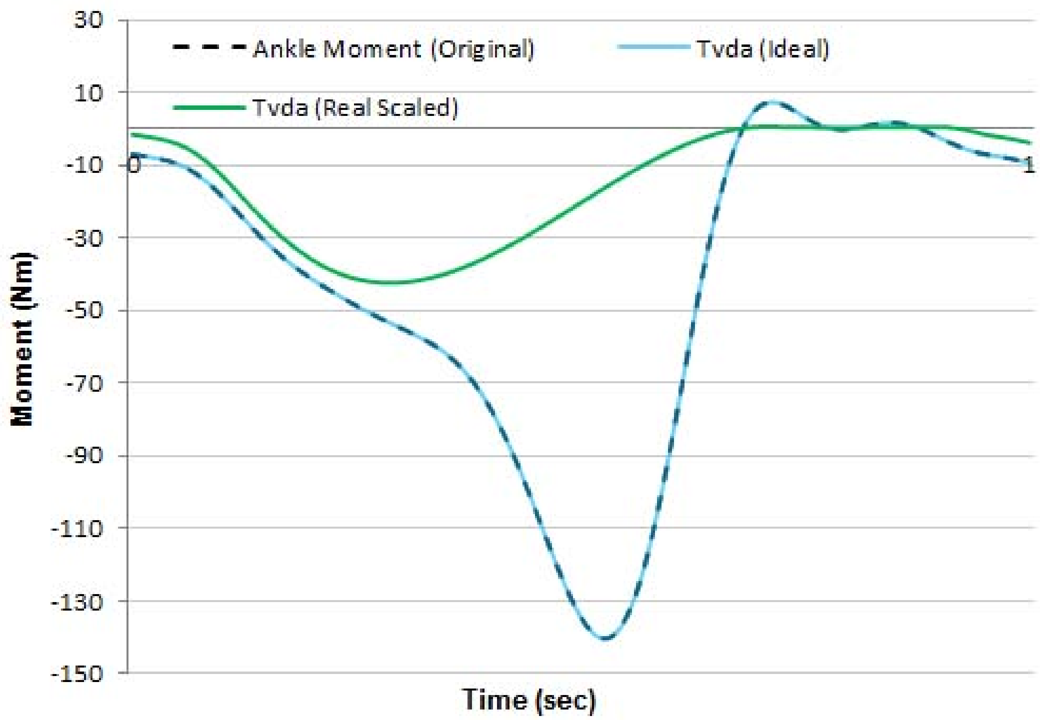

Figure 3.31: Torque profile for ideal and real scaled conditions using 21° incline walking data from Lay et al., 2006.

Figure 3.31 indicates that the torque obtained from simulation matches exactly with the in-vivo data used. However, this would cause the accumulator to be drained over few cycles, as discussed previously. The torque profile obtained by scaling the accumulator pressure (solid green curve) to prevent stalling the system represents a deviation from the normal ankle torque profile system for an 8.5° incline walking.

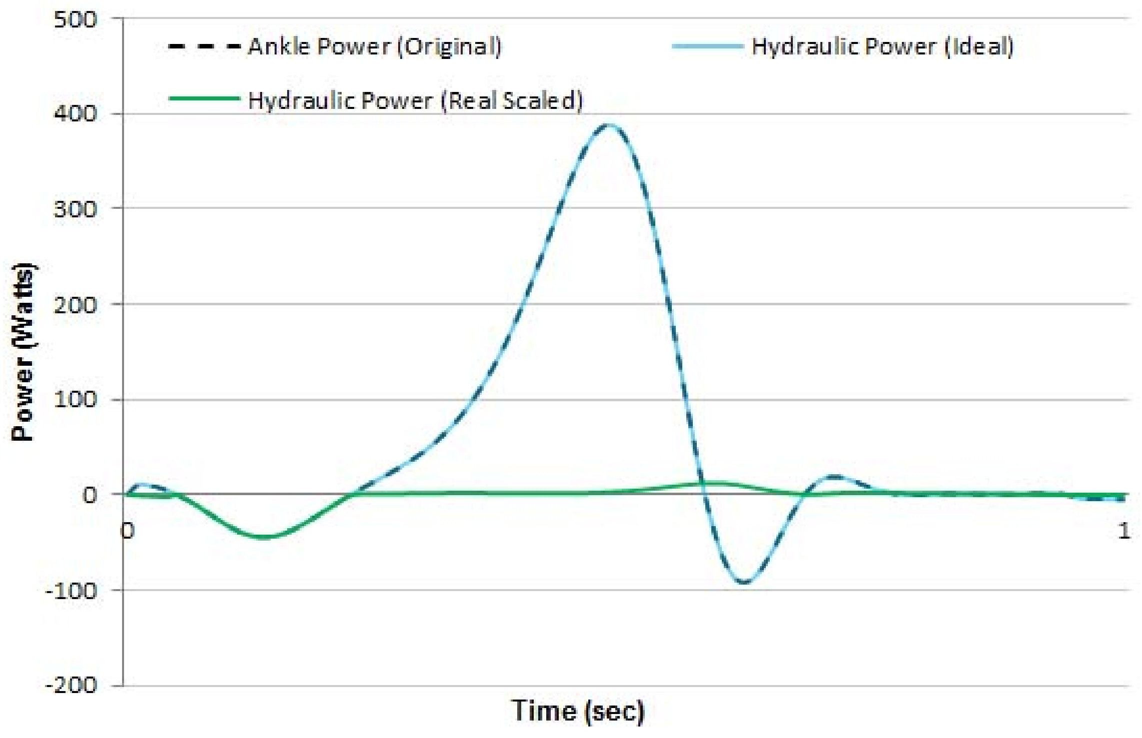

Figure 3.32: Power profile for ideal and real scaled conditions using 21° incline walking data from Lay et al., 2006.

Figure 3.32 indicates that for incline walking, active positive work contribution dominates the elastic energy storage and return work of tendons. Therefore, being a passive system aimed to recycle the strain energy, there is very little energy to store and return, as indicated by solid green curve.

3.9.4 SUMMARY

A summary of the peak power obtained from hydraulic power profiles for real scaled conditions versus ideal conditions (Figure 3.17, Figure 3.20, Figure 3.23, Figure 3.26, and Figure 3.29, and Figure 3.32), for the gait data tested is presented in Table 3.7 below.

Data Source	Population	Mean Age (years)	Mean Walking Speed (m/min)	Mean Subjects' Mass (Kg)	Walking Condition	Peak Power Required (Watts)	Peak Power Deliverd (Watts)	% Peak Power Delivered
University of Salford	7 Males	45.2	75	80	Level	159	136	86
Lay et al., 2006	5 Males, 4 Females	24	CWS	73.6	Level	200	137	69
	5 Males, 4 Females	24	CWS	73.6	8.5° Decline	194	186	96
	5 Males, 4 Females	24	CWS	73.6	21° Decline	111	116	105
	5 Males, 4 Females	24	CWS	73.6	8.5° Incline	457	33	7
	5 Males, 4 Females	24	CWS	73.6	21° Incline	387	12	3

Table 3.7: Summary of peak power delivered by the system against the required peak power for the gait data used.

3.10 Discussion

In this chapter a novel design concept was explored, the aim being to efficiently store energy available during the negative work phases of gait and timely release the stored energy to provide power when required. The design concept was not developed into a physical prototype and only simulation results were produced. Having identified the reasons for the poor energy efficiency of amputee gait and an incapability of the current interventions for any significant improvements in amputee gait biomechanics from Chapter 2, this chapter started with a simple design concept to investigate whether using hydraulics is viable option to develop a prostheses or not. As a starting point, a hydraulic accumulator as an energy-storing component, with a VDA as an actuator to directly drive the ankle to provide continuous torque control was considered. First, the mathematical models of two types of hydraulic accumulators were developed and then they were sized accordingly. Based on the sizing results, a 245 cc gas-charged accumulator was selected as a conservative estimate for the final design. In order to estimate the performance of the final design in real conditions, an ideal model with a VDA only mode was developed and modelled using Simulink, to provide a base line with which the results for a model with losses were to be compared. Then, a realistic loss model for a VDA with conservative assumptions was adopted from Grandall, 2010, and a simple yet realistic loss model of a gearbox was developed using manufacturer's gearbox efficiency data. The simulations were carried out for ideal conditions with VDA only mode, and then for real conditions (with losses) for a VDA-gearbox configuration. Then, a pseudo control methodology was described to approximate the performance of a physical prototype operating in real conditions governed by a control system.

For a discussion on the system performance, the results obtained for real and controlled conditions are presented along with those obtained for ideal conditions to approximately relate the performance of a physical prototype with the anatomical ankle.

In the following sub-sections, based on simulation results, the performance of the design for ideal conditions is compared with the performance for real conditions, to approximately relate the performance of a physical prototype with the anatomical ankle. In addition, a performance comparison is also carried out with commercially available as well as other novel prostheses to get an idea of what improvements could be achieved with a physical prototype.

3.10.1 System Performance

A conventional prosthetic foot delivers only 7.5% of the peak power required by an anatomical ankle (Barr et al., 1992). Better, but still poor performance is seen in studies of standard ESR prostheses. One study showed this type of prosthesis providing 24.7 % of required peak power seen in the anatomical control group (Segal et al., 2006). In addition to poor peak power delivery, conventional as well as ESR prostheses do not release the stored energy at the most appropriate time during gait (see Section 2.5.2). The prototype energy recycling prosthesis developed by Collins & Kuo, 2010, is claimed to produce better results than the commercially available prostheses. However, the peak push-off power of approximately 60.8% of values seen in anatomically intact gait studies, as seen from the power profile of their prosthesis (Figure 2.15), is questionable (see Section 2.6.1.3). Further, their design does not store the substantial mid-to-late stance negative work (as seen in anatomically intact gait studies), and it appears to delay the energy release during push-off.

The Bionic prosthesis by Herr & Grabowski, 2012, as discussed in Section 2.6.1.2, is actively powered (requiring a battery pack), Therefore, whilst widely publicised, their prosthesis is not a passive one and hence not directly comparable with the design developed in this work.

The simulation of the design presented in this chapter showed improved performance when compared to the commercially available prostheses, and the prototype prosthesis developed by Collins & Kuo, 2010, discussed above,. For level walking, it provided 86% and 69% of the peak power required by the anatomical ankle (Table 3.7), whilst providing near normal ankle torques (Figure 3.16 and Figure 3.19). The power profiles (Figure 3.17 and Figure 3.20) obtained for real and controlled conditions indicate that the system was able to store all of the available energy during gait, and provide correctly timed release of energy. This contrasts with the prototype energy recycling foot developed by Collins & Kuo, 2010, discussed above, which only stores the load acceptance work and shows delayed release of energy (Figure 2.15).

In 8.5° decline walking, there was more energy available than released for ideal conditions (Figure 3.21), however, when losses were modelled, simulation showed the system provided 96% of the peak push-off power required. The system performed even better for a 21° decline (Figure 3.24), as after compensating for the losses; there was still some excess energy left. Clearly, in a physical system, excess energy at the end of the gait cycle would be dissipated through a pressure relief valve. Therefore, even with losses modelled, the system provided 100% of the required peak power.

For incline walking, obviously, there is little energy available to store and more energy is being supplied actively by muscles. This is evident in the ankle power profiles (Figure 3.29 and Figure 3.32) for the original data, where the eccentric work is very small compared to the concentric work, i.e. over all work is positive. Therefore, as the system is completely passive it could only provide 7% (for an 8.5° incline) and 3% (for a 21° incline) of the required peak power at push-off (Table 3.7).

3.10.2 FEASIBILITY

Anthropometric measures of an anatomically intact human indicate that the combined foot and shank segment's mass can be approximated as 6.1% of total body mass (Winter, 2004a). Therefore, for a mean subject mass of 75 kg, the foot and shank would have a mass of approximately 4.5 kg. Therefore, if the new design is to be similar in mass to an anatomically intact limb, all the components, including the accumulator, tank, piping and VDA/VDA-gear box, should be accommodated in the prosthesis while satisfying the overall weight constraint of 4.5 kg.

Since the chosen design used a very small accumulator (245 cc), the volume and hence fluid mass was relatively small. The accumulator and tank could be made as an integral part of the shank, and therefore for these components, size is unlikely to be an issue.

As for the weights and size of the VDA/VDA-gearbox, a comparison of the optimum VDA and gear box sizes (optimum values obtained for the test data) with similar sized commercially available components is required. A search for similar-sized commercially available VDAs and gearboxes indicated that most commercial VDAs are very bulky and heavy, making them inappropriate to use as prosthetic components. Lightweight VDAs are used in the aerospace industry, but general design details (e.g. typical values for capacity, size, and weight) are difficult to obtain. However, Table 3.8 presents a weight comparison of the optimum VDA and gearbox sizes obtained for the test data (as mentioned in Table 3.6), with similar-sized commercially available VDAs (aluminium construction, for aerospace industry), and gearboxes (steel made for industrial applications). Both capable of operating at, or above 200 bar pressure, with an average maximum torque output of 100 Nm. The details of the models and manufacturers are provided in Appendix-D.

		IDEAL CONDITIONS				**REAL CONDITIONS**						
Data Source	**Terrain Type**	**Optimum VDA Sizes**		**Similar Commercially Available Sizes & Corresponding Weight**		**Optimum VDA sizes**	**Similar Commercially Available VDA Size**	**Commercially Available VDA Weight**	**Optimum Gearbox Sizes**	**Similar Commercially Available Gearbox Size**	**Commercially Available Gearbox Weight**	**Total Weight (Real Case)**
		VDA Size (cc/rev)	**Gear Ratio**	**VDA Size (cc/rev)**	**VDA Weight (kg)**	**VDA Size (cc/rev)**	**VDA Size (cc/rev)**	**VDA Weight (kg)**	**Gear Ratio**	**Gear Ratio**	**Gearbox Weight (kg)**	**VDA + Gearbox Weight (kg)**
Lay et al., 2006	**21° Incline**	53.4	1	49.16	***12.7***	13.2	12.29	4	4	4	1.5	***5.5***
Lay et al., 2006	**8.5° Incline**	53.4	1	49.16	***12.7***	13.2	12.29	4	4	4	1.5	***5.5***
Salford's Data	**Level**	43.8	1	39.33	***10.2***	7.26	7.21	3.2	6	5	1.9	***5.1***
Lay et al., 2006	**Level**	43.5	1	39.33	***10.2***	10.8	9.177	3.2	4	4	1.5	***4.7***
Lay et al., 2006	**8.5° Decline**	33.8	1	29.5	***9***	11.1	12.29	4	3	4	1.5	***5.5***
Lay et al., 2006	**21° Decline**	23.6	1	24.58	***6.8***	5.8	5.24	2.7	4	4	1.5	***4.2***

Table 3.8: A weight comparison of VDA and VDA/gearbox sizes obtained for ideal and real models for the test data with similar commercially available components.

From Table 3.8, it can be observed that, even for ideal conditions, the smallest VDA size of 23.6 cc/rev would correspond to a weight of 6.8 kg. This suggests the mass of the VDA is a major limiting factor with regard to the feasibility of the proposed design, and hence using a VDA as a stand-alone component is not feasible. The same can be observed for real conditions, where the smallest combined VDA-gearbox weight of

4.2 kg is still too heavy to be used in a prosthesis. Therefore the next chapter investigates an alternative approach that aims to reduce the torque required from the VDA/VDA-gearbox and, hence, reduce the weight of the system as a whole.

4. CONCEPT DESIGN II

The VDA in concept design I is the only provider of mechanical work. However, simulation of design I indicates that, while using the VDA without a gearbox can produce the required ankle torque, the size of the actuator is large, and the existing off-the-shelf components of similar capacity are too heavy (the weight range starts from 6.8 kg for the smallest VDA for ideal conditions, Table 3.8). Using a VDA-gearbox system reduces the size of the VDA, but then the gearbox poses similar weight and size problems. From a design point of view, as the VDA/VDA-gearbox is the only source that provides positive and negative work, the torque load on these components is hence a major factor that contributes to the size and weight problems of the system. Therefore, if the size and weight of the system are to be minimized, torque load on the VDA/VDA-gearbox must be reduced. Reducing the torque load on these components would also make the system more efficient as the VDA and gearbox losses would decrease with decreasing size of the actuator/gear-box system (see section 3.4.2 and section 3.5, respectively). Therefore, a second novel design concept is explored in this chapter, which is aimed at reducing the torque load on the VDA/VDA-gearbox and consequently reducing overall weight and size.

In order to reduce the torque load on the VDA/VDA-gearbox, one apparently simple solution is to use a compliant element, such as a spring, to produce all or some of the ankle torque. The spring would act directly to produce ankle torque, unlike concept design I where the VDA was used directly as a torque provider. However, in order to provide continuous control of ankle torque for adapting to different gait speeds and/or terrain, an actuator would still be required to change the mechanical advantage (provide a variable ratio) between the spring and ankle. Figure 4.1 presents a diagram of the alternative solution investigated in this chapter.

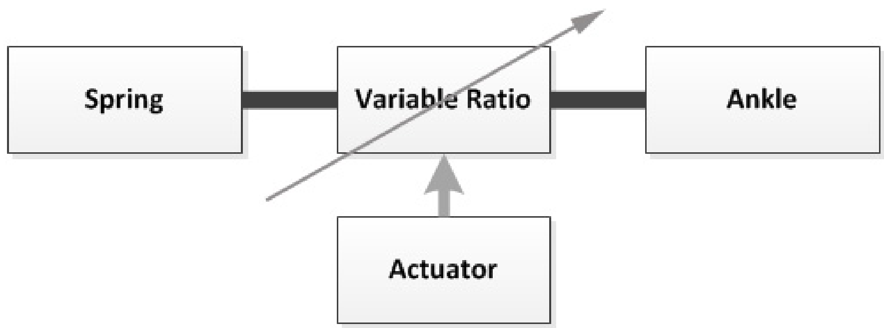

Figure 4.1: A simple block diagram of an alternative design approach.

This approach describe above would reduce the torque load on the actuator, and consequently its weight and size would be reduced. Using the actuator for only modulating the ratio gives the impression that very little work would be required by the actuator. However, given the fact that a spring is energetically conservative, the total work (negative and positive) done by the spring would be zero. Therefore, the actuator would be expected to do not all the work but at least the difference between negative and positive work. Nevertheless, the use of an energetically conservative spring would reduce the torque load on the actuator and might improve efficiency of the design.

To explore whether this general approach might provide improved performance an example implementation (design II) has been modelled as described in the following sections. The performance of design II is then compared with that of design I to see if the performance improvement justifies the increased design complexity.

4.1 Overview of example design

In this work, one particular mechanical implementation of the concept described by Figure 4.1 has been studied to demonstrate the principle. Referring to the conceptual sketch shown in Figure 4.2, a spring is connected to the ankle via a lever arrangement, where the actuator varies the lever arm to provide a variable ratio and hence control of ankle torque. As a hydraulic accumulator is being used to store energy, therefore, instead of a mechanical spring, a hydraulic cylinder (which, together with the accumulator resembles a gas spring) was considered for the design.

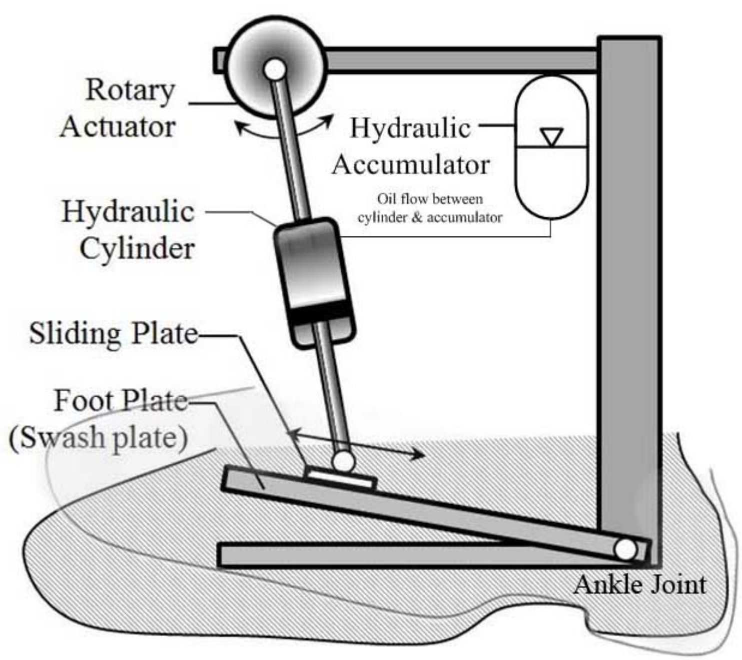

Figure 4.2: Conceptual sketch of design II showing only the slider-crank spring mechanism.

The rotary actuator controls the lever arm (mechanical advantage), by varying the distance between the point of contact on the footplate and the ankle joint. The design uses a double acting rotary actuator with its housing rigidly connected to the shank. The shaft of the rotary actuator would be rigidly connected to the head-side of the hydraulic cylinder (gas spring), and any rotation of the actuator shaft would cause the hydraulic cylinder to rotate (forming a crank mechanism). The piston rod of the hydraulic cylinder would be connected by a pin-joint to a small sliding plate. This sliding plate is made to slide on a footplate, which would be an integral part of the foot (no relative movement would occur between the foot body and the footplate), forming a linear sliding mechanism. The footplate itself would be connected to the shank via another pin-joint, forming an ankle joint with one degree of freedom in the sagittal plane.

With no relative movement between the footplate and the foot, the footplate will undergo the same angular motion as the ankle joint itself. As the foot rotates about the ankle, the piston moves inside the cylinder and oil is moved between the cylinder and the accumulator. The cylinder is assumed leakage free with no oil leaking to the rod side or transferred to/from the oil tank. Therefore, the hydraulic cylinder can be considered energetically conservative. The rotary actuator controls the cylinder rotation and hence the lever arm, providing control on the ankle torque. As the hydraulic cylinder is energetically conservative, the rotary actuator must provide at least the difference between positive and negative work.

Two small variants of the basic design described above are presented in the following sub-sections. The differences are only associated with the control of the rotary actuator.

4.1.1 ACTUATION CONCEPT I

As a first actuation concept, a fixed displacement double acting rotary actuator driven by a servo-valve was selected to reduce the weight and complexity. The potential drawback of the design at this point is the servo valve itself, as it dissipates energy inherently. However, it was hypothesized that any excess stored energy during anatomically intact gait could compensate for the energy losses at the servo valve, but this hypothesis could only be validated after developing the relevant equations for the model and subsequently carrying out the simulation of the design. Despite of the ambiguity about the extent of the energy loss at this stage and the design's effectiveness for transtibial amputees, the design might be feasible for transfemoral amputees where substantial amount of energy is eccentric and could be stored at the knee joint during level gait (Winter, 2004a). This, at the least, has a high probability of overcoming the energy losses at the servo valve.

Figure 4.3 presents a hydraulic circuit of for this actuation concept.

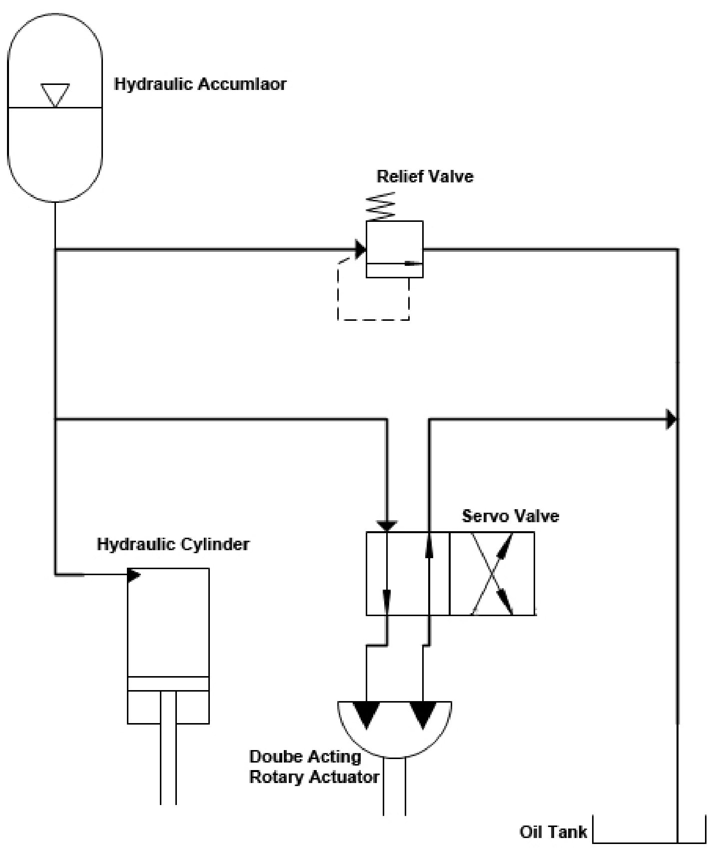

Figure 4.3: A simple hydraulic circuit with actuation concept I.

Referring to Figure 4.2 and Figure 4.3, the hydraulic port of the accumulator would be connected to the head side of the cylinder (creating a gas spring). The servo-valve is used to control the oil flow to the actuator, and the spool position of the servo valve during gait would determine the pressure across the actuator and hence the actuator's torque, which in turn would determine the control on ankle torque. It is therefore necessary to have a clear understanding of how the pressures across the actuator would be modulated by the servo-valve for the positive and negative work phases of the actuator. Figure 4.4 presents a very simple circuit diagram showing the pressures for positive work phases.

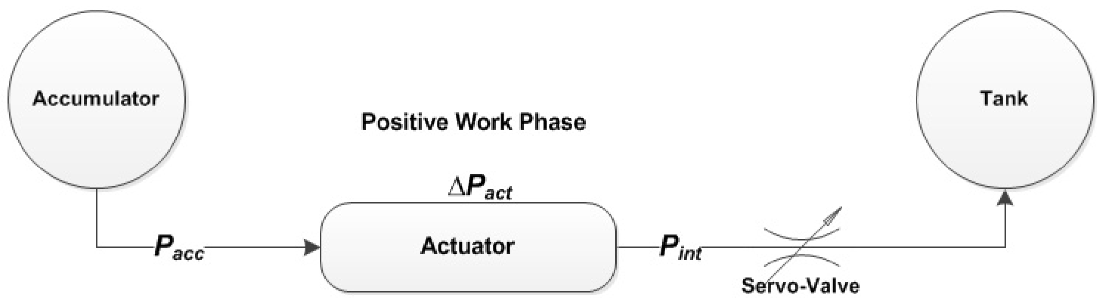

Figure 4.4: Pressures for positive work phases.

From Figure 4.4,

P_{acc} Accumulator Pressure

P_{int} Intermediate pressure between the servo-valve and actuator

ΔP_{act} Pressure drop across the actuator

Referring to Figure 4.4, when the actuator would be doing positive work, the accumulator pressure (P_{acc}) would be greater than the pressure drop across the actuator (ΔP_{act}) and the intermediate pressure (P_{int}) would be positive. These pressures are related by the following equation:

$$\Delta P_{act} = P_{acc} - P_{int} \dots \dots \dots Eq. (4.1)$$

The actuator torque (M_{act}) is related with the actuator pressure drop (ΔP_{act}) and actuator displacement (D) as:

$$\Delta P_{act} = \frac{M_{act}}{D} \dots \dots \dots Eq. (4.2)$$

Therefore, governed by Eq. (4.1), by modulating the oil flow through the servo valve (and consequently P_{int}), the pressure drop across the actuator and consequently actuator moment can be modulated (Eq. (4.2)). The negative work phase is shown in Figure 4.5 below:

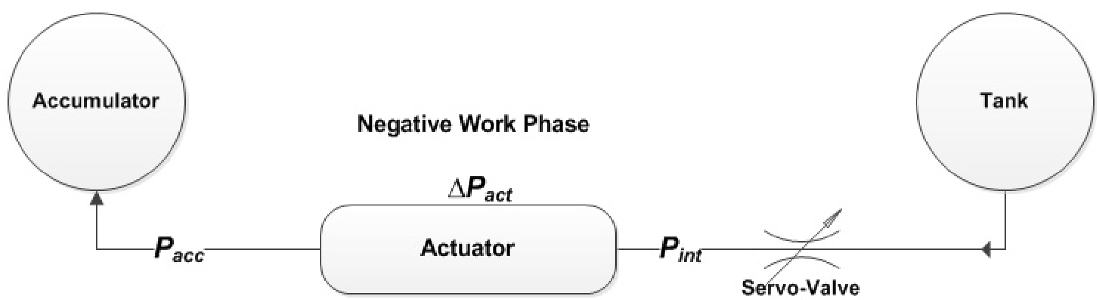

Figure 4.5: Pressures for negative work phases.

For negative work phases (Figure 4.5), the intermediate pressure (P_{int}) would be negative and the pressure rise across the actuator (ΔP_{act}) would always be greater than the accumulator pressure (P_{acc}). This would results in very high actuator torques that could not be less than ($D.\Delta P_{acc}$), resulting in no control over ankle torque.

In order to solve this control problem, an alternative is to use a two-way valve between the actuator and accumulator. For the positive work phases, the valve would not have any effect, however, for the negative work phases, instead of allowing the flow from the actuator to the accumulator; the valve will redirect it back to the tank. Figure 4.6 presents a simple diagram showing the pressures with this alternative.

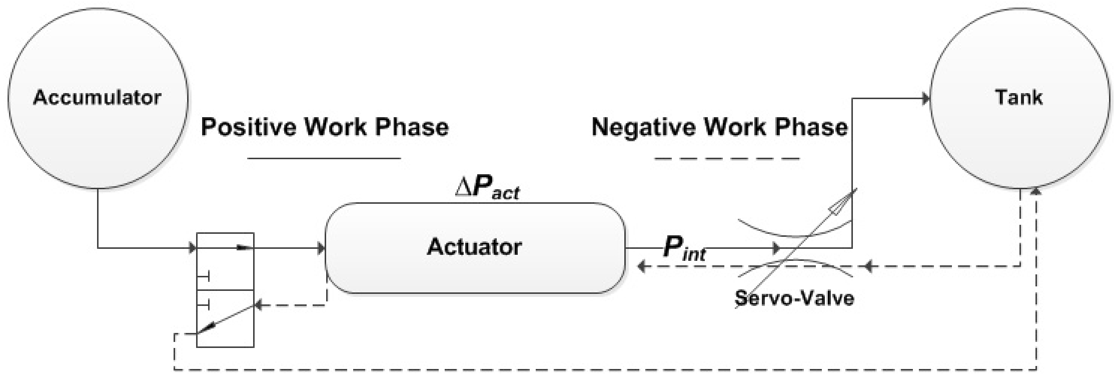

Figure 4.6: Alternate circuit to control actuator torque during negative work phases.

Referring to Figure 4.6, for positive work phases, P_{int} would remain positive, and actuator torque would be modulated. However, for negative work phases, a two-way valve between the accumulator and actuator would cause the oil to circulate between the tank and actuator, never reaching the accumulator. This will cause the ΔP_{act} to remain equal to P_{int} and hence controllable, resolving the uncontrolled actuator torque problem as discussed previously. However, after further reflection, it became apparent that there is a major flaw with this circuit, i.e. the cylinder does both positive and negative work on the accumulator, but over a gait cycle, the net-work is zero. However, the actuator would only (while performing positive work) drain the accumulator, and during negative work, oil would simply flow from tank to tank. Therefore, the accumulator simply will not charge during negative work as required, and once the accumulator is completely drained, the system would simply stall. Therefore, the first actuation concept, utilizing a fixed displacement rotary actuator with a servo-valve, was ruled out.

4.1.2 ACTUATION CONCEPT II

The hydraulic working principles of the design with the first actuation concept showed that if the accumulator was to be charged during the negative work phases, the actuator moment (and ultimately the ankle moment) could not be controlled. Modifying the hydraulic circuit to control ankle moment during negative phases did not help either, as in that case the accumulator could not be charged. This showed that the actuation of the design with a double acting rotary actuator with a servo-valve is not feasible and that an alternate actuation approach would be required to provide control of the ankle moment while allowing the accumulator to charge during negative work phases.

Therefore, as an alternative actuation, a VDA (as used in concept design I) was selected to replace the double acting rotary actuator and servo-valve. This would solve the issues with the first actuation technique (infeasible), with an additional benefit of eliminating the servo-valve (a source of energy loss). In addition, as discussed earlier, using a VDA with the slider-crank spring mechanism would reduce the workload on the actuator as the mechanism would share the workload with the spring (hydraulic cylinder) actuator and would reduce its size and weight, which was an issue with concept design I. Moreover, with a reduced VDA size, design II might prove to be more efficient than concept design I, as the smaller VDA would have lower flow losses than a larger VDA. The conceptual sketch of the design with the VDA would be the same as shown in Figure 4.2, but the rotary actuator would be replaced by the VDA.

Although using the VDA with the slider-crank spring mechanism would reduce its size, however, the addition of a gearbox with the VDA was also investigated. The design was first studied using the VDA for ideal conditions with a gear ratio of one, which essentially eliminates the gearbox, and then the losses as well as relevant gearing were used to compare the real results with ideal conditions. The design trade-off to be explored is whether the addition of a gearbox, and hence a reduction in the VDA size and associated weight, would result in an overall system weight that was lower than the VDA-only mode.

A new hydraulic circuit for concept design II with the VDA and gearbox is presented in Figure 4.7.

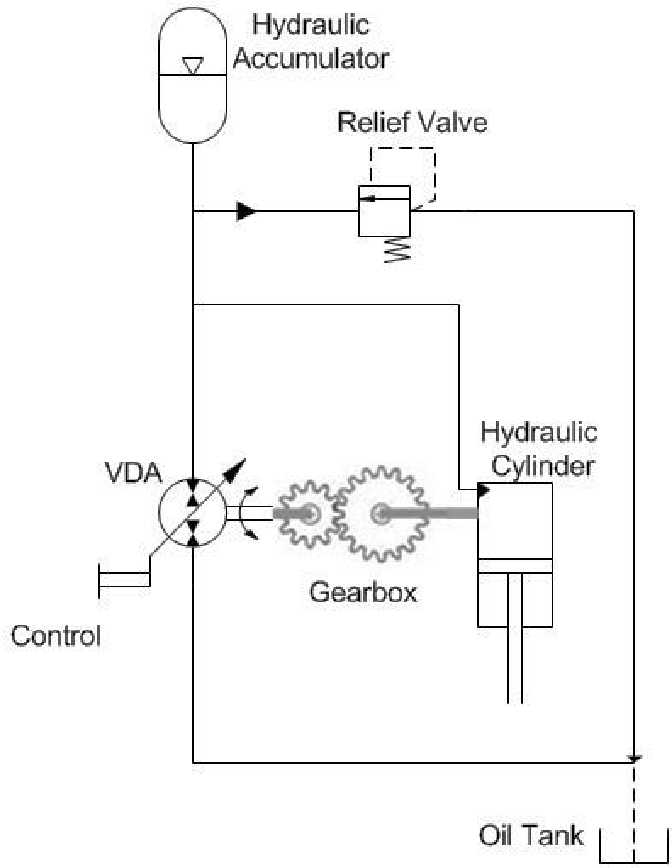

Figure 4.7: A simple hydraulic circuit for concept design II with VDA and gearbox.The VDA and gearbox act to rotate the hydraulic cylinder.

As far as the working of slider-crank spring mechanism is concerned, it will remain the same, as explained previously, and the VDA would be used instead of the rotary actuator. During negative actuator work phases, the VDA would work as a pump, pumping oil from the tank to the accumulator and storing energy in it whereas during positive actuator work phases, the oil discharged from the accumulator would drive the VDA to work as a motor. Being energetically conservative, the cylinder would have a net oil flow from the cylinder into the accumulator would be zero. Therefore, over the gait cycle, the cylinder must return to the same length (net work done by the cylinder is zero). The angular motion of the VDA-gearbox shaft (and hence cylinder), causes linear motion of the sliding plate, and thus alters the mechanical advantage between the spring (hydraulic cylinder) and the ankle joint.

Ideally, most of the ankle torque would be produced by the action of the cylinder, rather than the actuator. It is therefore necessary to understand which forces will act on the mechanism in order to solve the mechanics of the design. With the equations developed, the next stage would be to model the design using Simulink. Therefore, the following section presents the procedure to develop the equations that were used in the model.

4.2 Mechanics

Considering the conceptual sketch (Figure 4.2), repeated here for convenience, free body diagrams of the cylinder and footplate are presented in Figure 4.8.

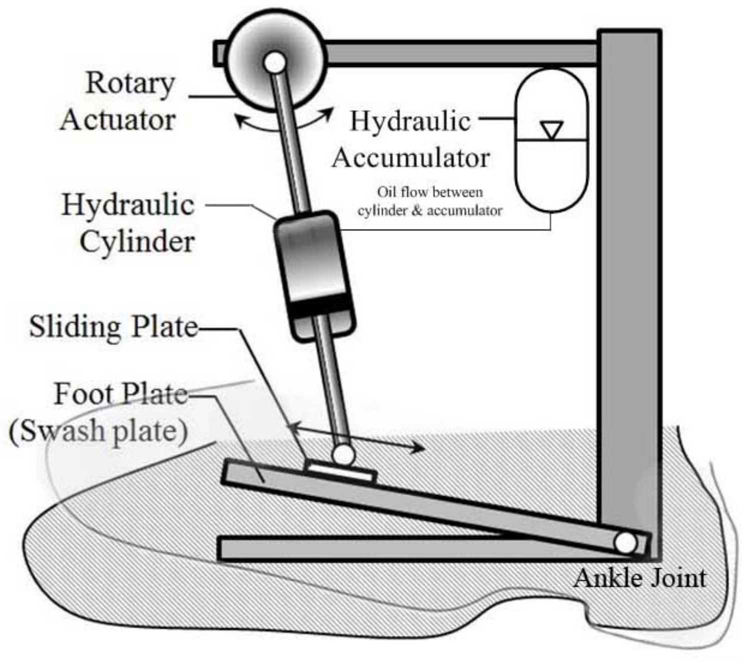

Figure 4.2: Conceptual sketch of design II.

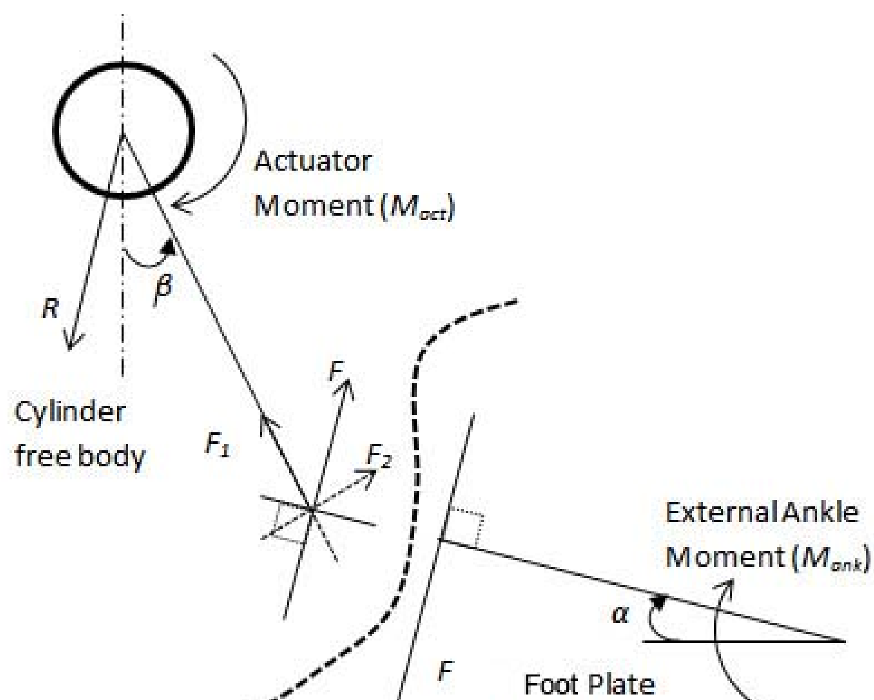

Figure 4.8: Free body diagrams showing forces acting on the cylinder and footplate.

From the free body diagram of the cylinder, at the point where the piston will be connected to the footplate, a force F would act on the point of contact of the piston (sliding plate) with the footplate and normal to the footplate. R is the reaction force that would be approximately equal to F assuming the system is in equilibrium and neglecting component weights. One rectangular component of this force (F_1) represents the cylinder force and would be determined by the accumulator pressure and cylinder area. The second rectangular component of the normal force is (F_2) would balance the torque at the actuator (M_{act}) assuming equilibrium and neglecting component weights. The angle α represents the ankle angle, and M_{ank} represents the external ankle moment known from gait data. Therefore, actuator shaft angle (β) and actuator moment (M_{act}) would be unknown and need to be found.

Therefore, Figure 4.9 below presents a sketch showing the geometry of the design concept (Figure 4.2) and the forces and moments (from Figure 4.8) in order to solve for β and M_{act}.

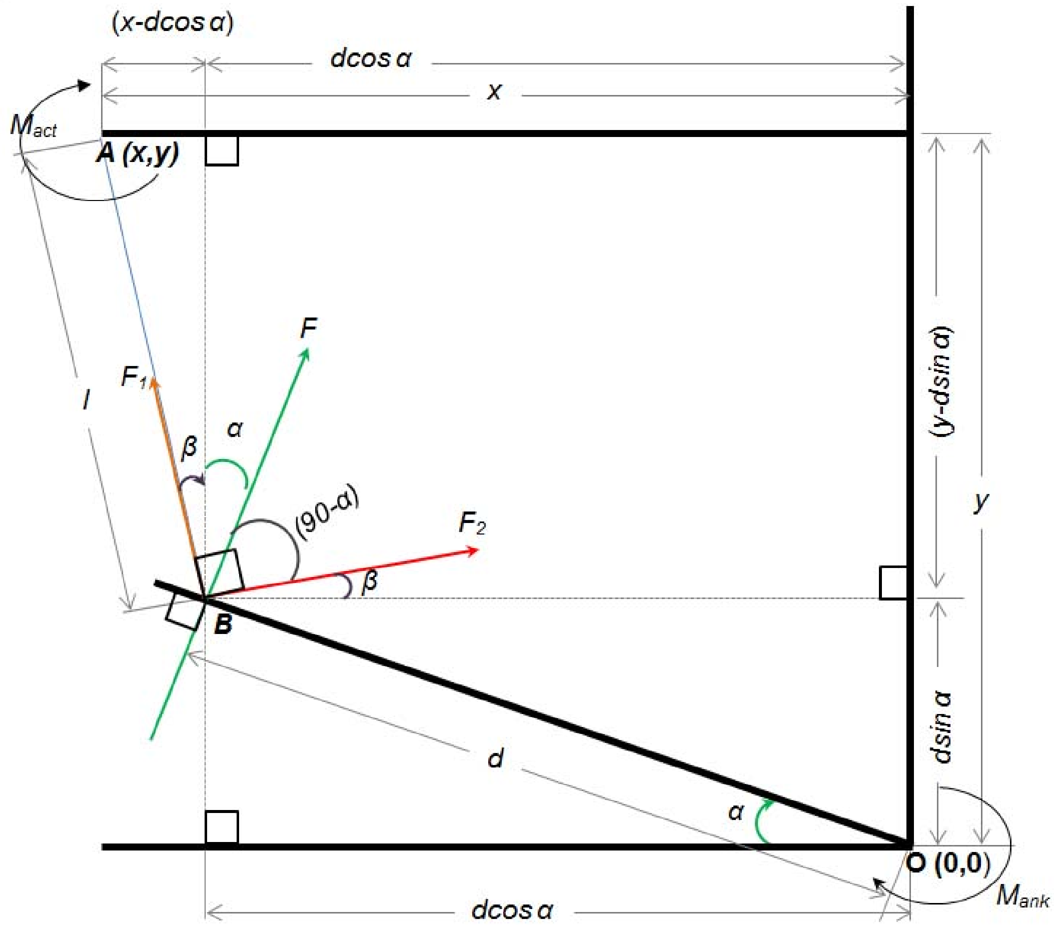

Figure 4.9: Geometry diagram with forces acting on the cylinder.

From this figure,

Point *A*: Position of the VDA

Point *B*: Position of the contact point of the sliding plate onto the footplate

Point *O*: Position of the ankle joint

d: Position of the slider from the ankle joint (distance from point *O* to point *B*)

F: Reaction force acting normal on the footplate

F_1: First rectangular component of the force *F*, acting through the hydraulic cylinder, representing the force due to accumulator pressure

F_2: Second rectangular component of the force F (acting perpendicular to F_1)

M_{ank}: External ankle moment

M_{act}: Actuator moment

(x,y): Position coordinates of the actuator (point A)

α: Ankle angle

β: Angle between the shank's axis (vertical axis) and hydraulic cylinder (i.e. shaft's angular motion)

l: Total length of cylinder

In order to solve for actuator moment (M_{act}), referring to geometry diagram

$$M_{act} = F.sin(\alpha + \beta).l \dots \dots \dots \dots Eq. (4.3)$$

Here α is known from the ankle angle, and β, l and F are unknowns. Referring to geometry diagram, F can be represented as:

$$F = \frac{F_1}{cos(\alpha + \beta)} \dots \dots \dots \dots Eq. (4.4)$$

Substituting in Eq. (4.3):

$$M_{act} = F_1.tan(\alpha + \beta).l \dots \dots \dots \dots Eq. (4.5)$$

F_1 would be determined from accumulator pressure using simulation, so the unknowns left are β and l, where l can be found using the following equation:

$$l = \sqrt{(x - d.cos\,\alpha)^2 + (y - d.sin\,\alpha)^2} \dots \dots \dots \dots Eq. (4.6)$$

Here, d is unknown and x,y serves as independent variables, which would be known, and α is known from the ankle angle, therefore d needs to be found in order to find l:

$$M_{ank} = F.d \dots \dots \dots \dots \dots Eq.(4.7)$$

Substituting F from Eq. (4.4) into the above equation and rearranging yields:

$$d = \frac{M_{ank}.cos(\alpha + \beta)}{F_1} \dots \dots \dots \dots Eq(4.8)$$

Alternatively:

$$d = c.cos(\alpha + \beta) \qquad \forall\ c = \frac{M_{Ank}}{F_1} \dots \dots \dots \dots Eq.(4.9)$$

M_{ank} would be the external ankle moment (known from gait data), so the unknown left is β. Once β is calculated, d can be found using Eq. (4.9), which can also be used to find l (Eq.4.6) and ultimately M_{act} (Eq. (4.5)). Therefore, the following procedure attempts to find β:

Again from geometry figure:

$$tan\,\beta = \frac{x - d.cos\,\alpha}{y - d.sin\,\alpha} \dots \dots \dots \dots Eq.(4.10)$$

Alternatively:

$$tan\,\beta = \frac{x - a.d}{y - b.d} \qquad \forall\ a = cos\,\alpha,\ \ b = sin\,\alpha \dots \dots \dots \dots Eq.(4.11)$$

$$y.tan\,\beta - b.d.tan\,\beta = x - a.d$$

$$y.tan\,\beta - x = (b.tan\,\beta - a)d \dots \dots \dots \dots Eq.(4.12)$$

Substituting the value of d from Eq. (4.9) in Eq. (4.12):

$$y.\tan\beta - x = (b.\tan\beta - a).[c.\cos(\alpha+\beta)] \ldots\ldots\ldots\ldots Eq.(4.13)$$

Applying the sum formula for cosine:

$$y.\tan\beta - x = (b.\tan\beta - a).[c.(\cos\alpha\,\cos\beta - \sin\alpha\,\sin\beta)]$$

$$y.\tan\beta - x = (b.c.\tan\beta - a.c).(\cos\alpha\,\cos\beta - \sin\alpha\,\sin\beta)$$

$$y.\tan\beta - x = (b.c.\tan\beta - a.c).(a.\cos\beta - b.\sin\beta) \quad \forall\ a = \cos\alpha,\ \ b = \sin\alpha$$

$$y.\tan\beta - x = (a.b.c.\tan\beta\cos\beta - b^2.c.\tan\beta\,\sin\beta - a^2.c.\cos\beta + a.b.c.\sin\beta) \ldots Eq.(4.14)$$

Multiplying both sides of Eq. (4.14) by *cosβ* and simplifying:

$$y.\sin\beta - x.\cos\beta - a.b.c.\sin\beta\cos\beta + b^2.c.\sin^2\beta + a^2.c.\cos^2\beta - a.b.c.\sin\beta\cos\beta = 0$$

$$y.\sin\beta - x.\cos\beta - 2.a.b.c.\sin\beta\cos\beta + b^2.c.\sin^2\beta + a^2.c.\cos^2\beta = 0 \ldots Eq.(4.15)$$

Let $t = \tan(\beta/2)$, then from half angle formulae:

$$\sin\beta = \frac{2t}{1+t^2} \ldots\ldots\ldots\ldots Eq.(4.16)$$

$$\cos\beta = \frac{1-t^2}{1+t^2} \ldots\ldots\ldots\ldots Eq.(4.17)$$

Substituting the values of *sin β* and *cos β* from Eq. (4.16) & Eq. (4.17) in Eq. (4.15):

$$y\left(\frac{2t}{1+t^2}\right) - x\left(\frac{1-t^2}{1+t^2}\right) - 2a.b.c\left(\frac{2t}{1+t^2}\right)\left(\frac{1-t^2}{1+t^2}\right) + b^2.c\left(\frac{2t}{1+t^2}\right)^2 + a^2.c\left(\frac{1-t^2}{1+t^2}\right)^2 = 0$$

$$2yt(1+t^2) - x(1-t^2)(1+t^2) - 4abct(1-t^2) + 4b^2ct^2 + a^2c(1-2t^2+t^4) = 0$$

$$2yt + 2yt^3 - x + xt^4 - 4abct + 4abct^3 + 4b^2ct^2 + a^2c - 2a^2ct^2 + a^2ct^4 = 0$$

$$(x+a^2c)t^4 + (2y+4abc)t^3 + (4b^2c-2a^2c)t^2 + (2y-4abc)t + (a^2c-x) = 0 \ldots Eq.(4.18)$$

This is a quartic equation with one unknown (t). It should be noted that the footplate can be fixed to the foot at a certain constant angle, and the angle (α) would be equal to the sum of that constant angle and the ankle angle. However, for convenience, α is considered to be equal to the ankle angle alone, which is a known variable from gait data, with $cos\alpha$ and $sin\alpha$ corresponding to "a" and "b", respectively. Sensibly assumed values of x and y will be used as an initial value to solve the equation for t. However, once the system of equations is solved, and after simulating the model, optimisation of the design would be required to establish the optimum position of the actuator (x, y) based on minimizing the actuator size and torque load.

In order to solve Eq. (4.18) for the true solutions, the most important parameter required is variable c, which is equal to M_{ank}/F_1. Although the ankle moment (M_{ank}) is known, the force F_1 is the force exerted by the hydraulic cylinder and would be evaluated using piston area and accumulator pressure. The pressure profile of the accumulator would be obtained from the simulation of the system, which is explained in the following section.

4.3 System Simulation

This section explains the modelling and simulation procedure for an ideal as well as a real condition, the description of relevant blocks used in the Simulink model and equations used in the blocks. Initially the modelling was carried out for ideal conditions i.e. all the components were considered to be 100% efficient and leakage free, which essentially eliminated the effects of the gearbox (used with a gear ratio of 1). After running the simulation for the ideal conditions, the modelling for the real conditions was carried out using the loss models described in previous chapter. The modelling was carried out using MATLAB's Simulink software and the code for both models is provided in Appendix-B. Figure 4.10 and Figure 4.11 present the Simulink model circuit and a simplified flow chart of the calculation process respectively, which is followed by the descriptions of the blocks used in the model.

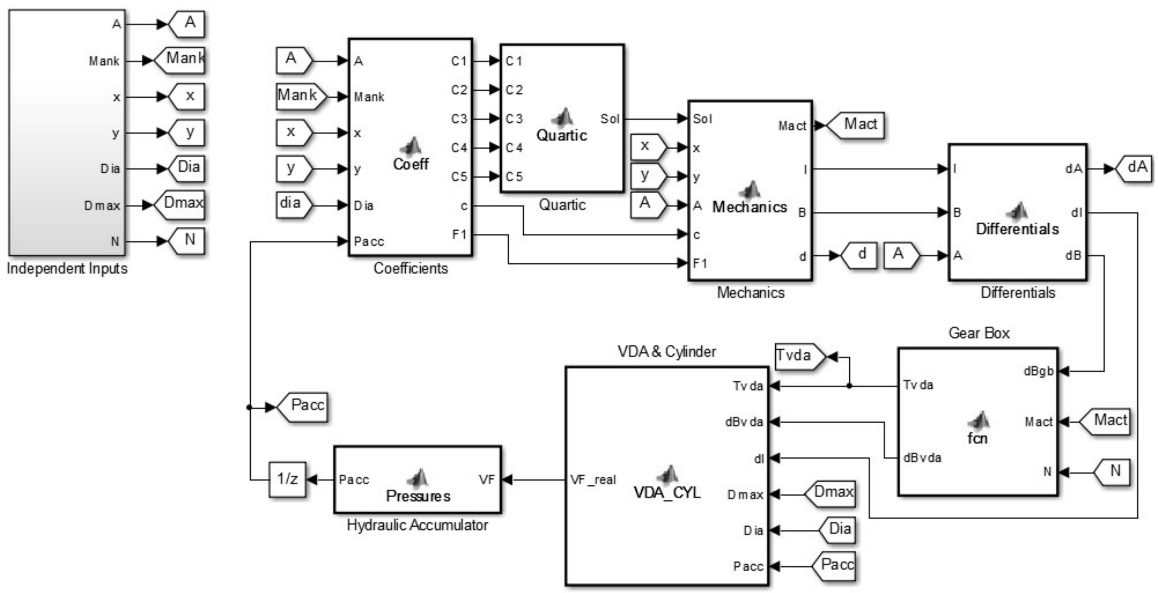

Figure 4.10: Simulink circuit for concept design II.

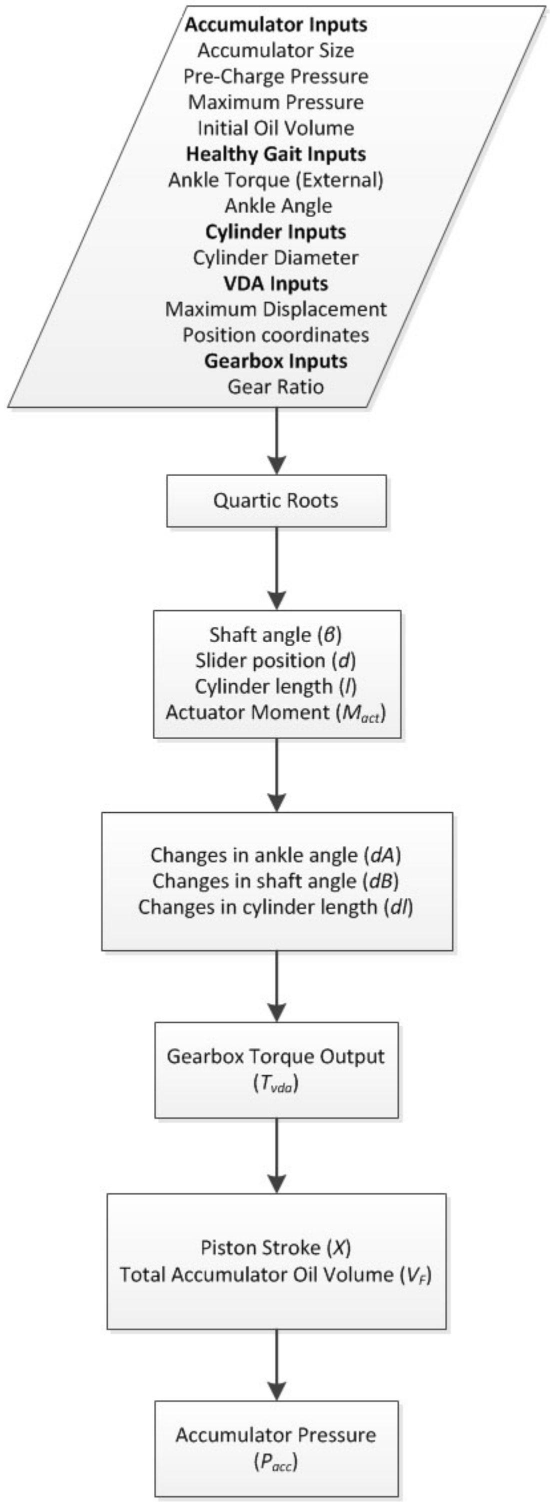

Figure 4.11: A simplified flow chart for the calculation process for concept design II.

The sizing of hydraulic accumulators is explained in previous chapter, where a 245 cc gas-charged accumulator was found to be the largest one to store the required energy of 20.61 Joules for the test gait data (Table 3.2). As the accumulator size is not a constraint for the design, therefore the 245 cc gas-charged accumulator was selected for simulation, because this size is small enough to be used in a transtibial prosthesis. A Spring-loaded accumulator was not used for simulation, as it was observed in concept design I that the accumulator type had no effect on simulation outputs. In addition, as the mathematical models of the VDA and gearbox are already explained in Sections 3.4 and 3.5 respectively, the equations used in the Simulink model blocks will be repeated for convenience. Referring to Simulink circuit (Figure 4.10), a description of the Simulink model block is as follows.

4.3.1 INDEPENDENT INPUTS BLOCK

This block contains the independent inputs for the simulation i.e. VDA position (x,y), VDA size (D_{max}), cylinder diameter (Dia), mean ankle angle (α) and external ankle moment (M_{ank}) from in-vivo gait data. The actuator position, size and cylinder diameter were chosen as design variables and multiple simulations were used to find the optimum values of these variables, as explained in later section.

In addition to these independent inputs, the accumulator pressure is provided as another input, calculated from the initial oil volume, and serves as initial condition. All these inputs except D_{max} are fed to the coefficients block.

4.3.2 COEFFICIENTS BLOCK

This block uses ankle angle and moment, position of VDA, accumulator pressure and cylinder diameter to calculate the coefficients of Eq. (4.18), as well as cylinder force

(F_1) and variable c. The equations specified in this block for these calculations are presented below.

$$a = cos\alpha$$

$$b = sin\alpha$$

$$F_1 = \left(\frac{\pi}{4} Dia^2\right) P_{acc}$$

$$c = \frac{M_{ank}}{F_1}$$

$$C1 = x + a^2c;\ C2 = 2y + 4abc;\ C3 = 4b^2c - 2a^2c;\ C4 = 2y - 4abc;\ C5 = a^2c - x$$

The coefficients C1 to C5 are then fed to the quartic block to solve Eq. (4.18).

4.3.3 QUARTIC BLOCK

This block takes in the coefficients calculated in the previous block, which are used to find the roots of Eq. (4.18). A standard MATLAB function *"roots"* was used to solve the equation. Being a quartic equation, the function provided four roots per time step (it was observed that for all simulations, two complex and two real roots were obtained). In order to avoid complex roots, the code was written so as to store only the real roots and discard the complex ones. However, selection of a real root to be used for further calculation was based on which root led to the expected geometry and associated variables (actuator moment M_{act}, cylinder length l, slider travel d, and shaft angle β). Therefore, each simulation was run twice, with each real root obtained, and all the variables mentioned above were checked in relation to the expected geometry (Figure 4.9), which indicates that a geometrically sensible shaft angle (β) would not allow the cylinder to go beyond the vertical position coordinate (y) of the actuator, i.e. the range of β should be $-90° < \beta < 90°$. In addition, a mechanically sensible mechanism would not allow both the cylinder and the footplate to beyond being parallel. i.e. the range of $-90° < (\alpha+\beta) < 90°$ must be satisfied. However, for every single simulation, one root always produced a β that would result in the cylinder going above (y) in Figure 4.9 with a range of $-180° < \beta < -90°$, as well as causing both the cylinder and the swash plate to go beyond being parallel with a range of $-180° < (\alpha+\beta) < -90°$. In addition, the same root (that distorted geometry) *always* produced very high actuator moment (M_{act}). Whereas, the second root always satisfied the expected geometry and *always* produced a ***minimum*** actuator moment (M_{act}). Nevertheless, the simulation was run twice each time to check the behaviour of each root, and the one root, which produced mechanically sensible results, was selected.

4.3.4 MECHANICS BLOCK

This block takes in the root (tested and selected for further calculations by previous block), actuator position (x, y), and ankle angle (α) from inputs block, variable c, and cylinder force (F_1) from coefficients block. With these inputs, the block first solves for the shaft angle (β) by using the following equation:

$$\beta = 2tan^{-1}t \quad (obtained\ by\ combining\ Eq.(4.16)\ and\ Eq.(4.17)$$

The other equations that are specified in this block are Eq. (4.9), Eq. (4.6), and Eq. (4.5), which is repeated here for convenience. With β calculated in the previous step, and with c and F_1 as inputs, these equations are sequentially solved for the variables d, l, and M_{act}.

$$d = c.cos(\alpha + \beta) \ldots\ldots\ldots\ldots Eq.(4.9)$$

$$l = \sqrt{(x - d.cos\,\alpha)^2 + (y - d.sin\,\alpha)^2} \ldots\ldots\ldots\ldots Eq.(4.6)$$

$M_{Act} = F_1.tan(\alpha + \beta).l \dots \dots \dots \dots Eq.(4.5)$

The variables l, β and α are fed to the differentials block.

4.3.5 DIFFERENTIALS BLOCK

It is useful at this point to re-cap the simulation process. Apart from the independent inputs, the initial condition to run the simulation is the accumulator pressure for the first time step. To calculate that initial pressure, we had used accumulator-sizing equations to find out the accumulator size and initial oil volume, which was done outside the MATLAB environment. For the next pressure values, the volume of oil in the accumulator is required, which could be determined from the oil flow rates through the actuator and the cylinder. The oil flow rates can be determined from the angular velocity of the actuator shaft and the linear velocity of the cylinder piston, by taking the time derivative of the shaft angle (β) and cylinder length (l), respectively. The actuator flow rate can be calculated by taking the product of its angular velocity (time derivative of β) by its displacement, and the cylinder flow rate can be calculated by multiplying its linear velocity (time derivative of l) by the cylinder area. The two flow rates can then be added to calculate the total flow rate of oil through the accumulator, which would then need to be integrated to get the accumulator oil volume, in order to solve for the next pressure value so that the simulation can carry on.

From this calculation sequence, it is obvious that the derivatives of the shaft angle and cylinder stroke are only required in order to be integrated later on. The differentiation in this case would be numerical, but this introduces noise and might affect the overall mechanics as well as accuracy of the simulation results. However, the differentiation in this case can be easily avoided by using infinitesimal changes (differentials) rather than the rate of changes (derivatives), and this block is specified to calculate the differentials of β and l.

The values of β and l, calculated from the previous block, are provided as input to this block, which calculates the infinitesimal changes in their values (termed as $d\beta$ and dl, respectively), and are fed into the VDA and cylinder block. This block also calculates the infinitesimal changes in ankle angle (termed as dA), for which the ankle angle is provided as an input from the inputs block and was used only to calculate the in-vivo ankle power to be compared with the power produced by the VDA. The variables $d\beta$ and dl are fed to the gearbox block.

4.3.6 GEARBOX BLOCK

This block is specified with Eq. (3.35), Eq. (3.37), and Eq. (3.39) with variables A replaced with β and M_{ank} replaced with M_{act}. The equations (with variables replaced) are repeated here for convenience.

$$T_{fr} = (6.913e^{-4}N + 2.557e^{-2})T_N \dots\dots\dots Eq. (3.35)$$

$$T_{vda} = \frac{M_{act}}{|M_{act}|.N}\left[|M_{act}| - K_m T_{fr}\right] \dots\dots\dots Eq. (3.37)$$

$$d\beta_{vda} = d\beta_{gb} \times N \dots\dots\dots Eq. (3.39)$$

The variable T_{fr} is the torque loss due to friction and is taken to be zero for ideal conditions (with a gear ratio N=1). However, for real conditions, relevant value of N is provided as input, after determining the optimum gear ratio (which is explained in latter sections). As opposed to concept design I, were the variable T_N corresponded to an absolute peak value of the in-vivo ankle torque, here it corresponds to an absolute peak value of actuator torque ($|M_{act}|$). Since the T_{fr} is calculated only for real conditions, therefore, for a specific in-vivo gait data, the M_{act} was recorded from simulation of ideal conditions from which the absolute peak value of (M_{act}) was provided in the model for running simulation with real conditions.

With T_{fr} calculated for real conditions, Eq. (3.37) is used to calculate the VDA torque output (T_{vda}), where the coefficient K_m (as used in previous sections) takes into account of the direction of friction torque, which would always oppose the direction of shaft rotation, i.e. when the shaft's angular velocity would be clock-wise, T_{fr} would be anti-clockwise and vice versa.

The differential shaft angle changes ($d\beta$) from the differentials block which is fed into this block, serves as differential changes in gearbox input shaft rotation ($d\beta_{gb}$). With gear ratio (N) as an independent input, differential changes in VDA shaft rotation ($d\beta_{vda}$) are calculated using (Eq. (3.39)). The dB_{vda} is fed to the VDA block, which uses it to calculate the leakage losses.

4.3.7 VDA AND CYLINDER BLOCK

This block takes in the values of T_{vda}, $d\beta_{vda}$, D_{max}, P_{acc}, dl, and Dia from the respective blocks and calculates the leakage and compressibility losses. It is specified with the following equations previously described and are repeated here for convenience:

$$X = \frac{T_{VDA}}{P_{acc}D_{max}} \dots\dots\dots Eq. (3.40)$$

Where T_{vda} is calculated previously from the gearbox block, D_{max} is initially supplied as an arbitrary independent input (and then was sized properly based on the simulation results as explained in later section) and P_{acc} is supplied as an initial accumulator pressure.

For ideal conditions, Eq. (3.28) and Eq. (3.29) were combined to provide ideal actuator flow as shown below:

$$q_{vda}^{ideal} = \frac{T_{vda}}{P_{acc}} . \omega_{vda} \dots \dots \dots Eq. (4.19)$$

For differential changes in oil volume, multiplying both sides by *dt:*

$$dV_{vda}^{ideal} = \frac{T_{vda}}{P_{acc}} . d\beta_{vda} \dots \dots \dots Eq. (4.20)$$

The block was specified with Eq. (4.21) shown below, in order to separately calculate the differential changes in oil volumes for the negative/positive work phases, by introducing K_m and absolute values of T_{vda} and $d\beta_{vda}$ in Eq. (4.20) to account for relevant (negative/positive) work phases.

$$dV_{vda}^{ideal} = K_m \frac{|T_{vda}||d\beta_{vda}|}{P_{acc}} \dots \dots \dots Eq. (4.21)$$

When the VDA torque and rotation act in the same direction (both clockwise or both anticlockwise), the VDA does positive work (motor mode, K_m= -1), and the oil comes out of the accumulator (negative flow). Whereas, when the VDA torque and its rotation is in opposite directions (one clockwise and the other anti-clockwise and vice versa), the VDA is doing negative (braking) work, pumping oil into the accumulator (pump mode, $K_m=1$).

Therefore, in order to differentiate between the negative work and positive working modes of the VDA (pump and motor modes, respectively), a careful consideration on the both the signs of the T_{vda} and its direction of rotation ($d\beta_{vda}$) are necessary. In this case, referring back to the Figure 4.8, β was defined <u>opposite</u> to the M_{act}

(clockwise M_{act} and anticlockwise β were positive). Therefore, when the VDA would be doing positive work (both acting clockwise), then their signs would be actually opposite to each other (contrary to concept design I, where both the T_{vda} and its direction had same signs when doing positive work). Therefore, the sign conventions for the VDA positive and negative work in both designs were explicitly specified in the code listed in Appendices B and C.

For changes in oil volume with losses, Eq. (3.41) was used with dVF_{real} replaced with dV_{vda}^{real}, and the first term on R.H.S. replaced with the R.H.S. of Eq. (4.21):

$$dV_{vda}^{real} = K_m \frac{|T_{vda}||d\beta_{vda}|}{P_{acc}} - dt.K_m \left[C_s \left(\frac{P}{P_{atm}} \right)^n \left(a + b \left(\frac{\omega}{\omega_{max}} \right) \right) \frac{PD_{max}}{\mu} + \frac{P\omega D_{max}}{B} \left(V_r + \frac{1+X}{2} \right) \right] \ldots Eq.(4.22)$$

Eq. (4.22) was specified in the block to calculate the changes in actuator oil volume for real conditions. The angular velocity of VDA shaft ($d\beta_{vda}/dt$) was used in the calculation for losses (to avoid any errors, as all the coefficients used in these terms were originally calculated using angular velocity). However, the combined flow losses were multiplied with the time step (dt) to make the equation dimensionally correct (with units of m^3).

Eq. (4.23) was specified in the block to calculate the oil changes in cylinder oil volume, following similar procedure of multiplying the flow rate by dt:

$$dV_{Cyl} = -\frac{\pi Dia^2}{4}\, dl \ldots\ldots\ldots Eq.(4.23)$$

To calculate the changes in oil volume for the accumulator, the block was specified by Eq. (4.24), which is simply a sum of differential changes in oil volume for the actuator and cylinder.

$$dV_F^{real} = dV_{Cyl} + dV_{vda}^{real} \ldots\ldots\ldots Eq. (4.24)$$

The changes in oil volume for the accumulator (Eq. (4.24)) were then cumulatively added to get oil volume (V_F), which was fed to the accumulator block.

4.3.8 ACCUMULATOR BLOCK

For Design II, a gas-charged accumulator with maximum capacity of 245 cc obtained from accumulator sizing section (Table 3.2) was used. This block takes in the oil volume previously calculated, and with all the other variables defined, the Eq. (3.34) (repeated below) was used to calculate the instantaneous pressure for the next time step, which is then used for the next simulation cycle.

$$P = P_{pr}\left(\frac{V_A - V_{pr}}{V_A - V_F}\right)^k \ldots\ldots\ldots Eq. (3.34)$$

The pressure calculated is then fed back to the coefficients block to solve for the next simulation cycle and the process is repeated until the simulation end time is reached.

4.4 Design Simulations

This section describes how design simulations were used to find out the optimum design variables for both the ideal and real conditions for the Salford's gait data. The design variables for concept design II are actuator position (*x,y*), cylinder diameter (*Dia*), VDA size (D_{max}) and gear ratio (*N*). Therefore, optimum values of these variables were required for testing the model. For ideal conditions, no losses were considered which effectively eliminated the effects of the gearbox (use *N=1*). Therefore, multiple simulations were used to find out the optimum values of *x, y,* and *Dia* to minimize M_{act}

for the ideal conditions. In other words, as *x,y* and *Dia* relate to the slider-crank spring mechanism, first, the optimum values of these were obtained. Then using these values, the optimum values of D_{max} and *N* for the actuator were obtained to minimize actuator losses. The following section describes the procedure to find the optimum values of the design variables for ideal conditions.

4.4.1 METHOD OF FINDING OPTIMUM VALUES OF DESIGN VARIABLES-IDEAL CONDITIONS

This section describes the procedure to find the optimum values of the design variables for ideal conditions.

Considering typical dimensions of a transtibial prosthesis, a range of -5 to +5 cm was selected for *x* (adjusted in 1 cm steps), and a range of 5 to 30 cm was selected for *y* (5, 10, 20 and 30 cm were tested). In addition to *x* and *y*, test values of 0.5 cm, 1cm, 2 cm, 3cm and 4 cm for cylinder diameter (Dia) was selected. All possible combinations were tested (i.e. the full factorial set of 220 combinations). Multiple simulations were run with these values and absolute maximum actuator moment ($|M_{act}|$) was recorded. The design variables that corresponded to a minimum $|M_{act}|$ were taken as optimum values. In addition, a constraint of absolute maximum VDA stroke ($|X_{max}|=0.9$) was also applied, in order to find the minimum D_{max} corresponding to minimum $|M_{act}|$.

The results of these full factorial set of tests are plotted in Figure 4.12, where the profiles of maximum $|M_{act}|$ follow U-shaped curves with its minimal value corresponding to *x=3cm, y=10cm, and Dia=1cm*. Therefore, this set of design variables was selected for further simulation and testing under real conditions (including VDA leakage losses and gearbox friction).

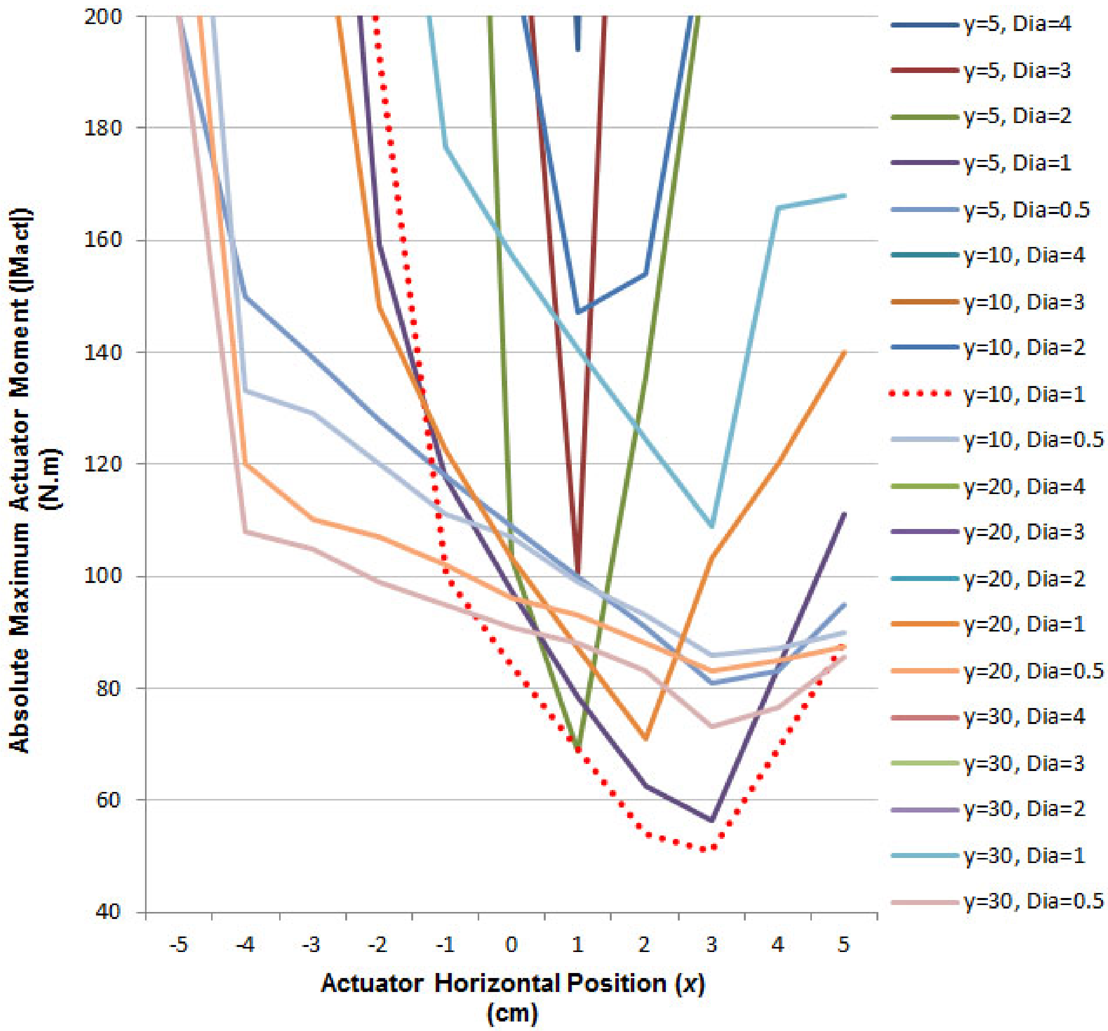

Figure 4.12: Optimum values of design variables for concept design II.

The simulation for the ideal conditions was carried out using the optimal variables and the results were recorded. The results were exactly the same as the in-vivo data used. As the ideal model provides a baseline, with which to compare the results of the model with losses, therefore the results obtained from the ideal model are presented in the later section, along with the outputs from the model with real conditions, to provide measure on the effectiveness of the design in real conditions. However, before testing the model for real conditions, correct sizing of the D_{max} and gear ratio (N) is required to minimise losses, which is explained in the next section.

4.4.2 VDA/Gearbox Sizing- Real Conditions

The same optimized values for actuator position (x,y) and cylinder diameter (Dia) (which were obtained previously for ideal model), were used for the real conditions. However, with the introduction of the VDA and gearbox losses, finding an optimized D_{max} and N was necessary. For this purpose, the same technique was used as described in Section 3.7.2 and the final accumulator pressure obtained for each set of the adjusted design variables (with the $|X_{peak}=0.9|$ constraint satisfied). The results are plotted in Figure 4.13, in which the peak of the curve corresponds to the optimum set of D_{max}-N values.

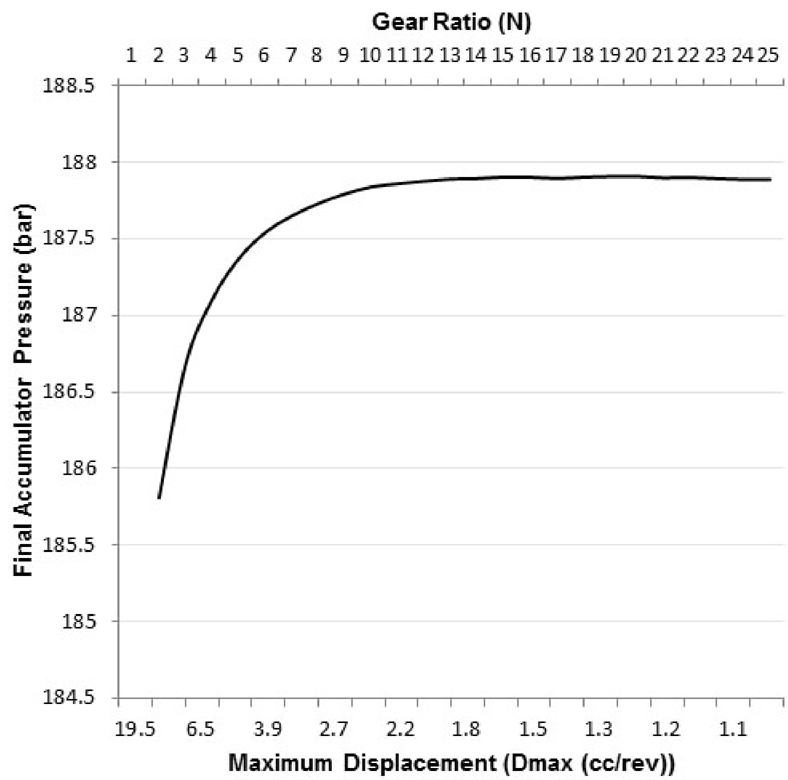

Figure 4.13: Final accumulator pressure for D_{max} and N.The peak value corresponds to the design variable set that produced minimal losses while keeping $|Xpeak|=0.9$.

Table 4.1 presents the design variables for the real model as well as the ideal model.

Design Variables	Optimized Results Ideal Conditions VDA only Mode	Optimized Results Real Conditions VDA/Gearbox System
x (cm)	3	3
y (cm)	10	10
Dia (cm)	1	1
Dmax (cc/rev)	19	1.95 to 0.79
N	1	10 to 25

Table 4.1: Design Variables used for ideal and real model.The D_{max} and N values corresponds to the Salford's level walking data.

Using the same x, y, and Dia values listed in the above table, optimum values of the D_{max} and N were calculated for design II, using the same method as explained in Section 3.7.2 for each of the test data. The optimum values of D_{max} and N obtained for design II (for the test data) are presented in Table 4.2 below, along with those obtained for design I (from Table 3.6) for a comparison.

Data Source	Terrain Type	Concept Design I				Concept Design II			
		Ideal Conditions		Real Conditions		Ideal Conditions		Real Conditions	
		Dmax (cc/rev)	Gear Ratio	Dmax (cc/rev)	Gear Ratio	Dmax (cc/rev)	Gear Ratio	Dmax (cc/rev)	Gear Ratio
University of Salford	**Level**	43.8	1	7.26	6	19	1	0.98	20
Lay et al., 2006	**Level**	43.5	1	10.8	4	19.7	1	1.1	18
Lay et al., 2006	**8.5° Decline**	33.8	1	11.1	3	18.9	1	0.9	20
Lay et al., 2006	**21° Decline**	23.6	1	5.8	4	16.3	1	0.93	18
Lay et al., 2006	**8.5° Incline**	53.4	1	13.2	4	42.5	1	2.8	21
Lay et al., 2006	**21° Incline**	53.4	1	13.2	4	42.5	1	2.3	20

Table 4.2: Comparison of VDA/VDA-gearbox sizes obtained for design II and compared with those obtained for design I.

The details on a pseudo control implementation is described in Section 3.8, and therefore, with the optimised values of the design variables obtained, the next section presents the results for both the ideal conditions as well as with controlled real conditions.

4.5 System Testing

This section presents the simulation results obtained by applying pseudo control (which is explained in Section 3.8) with the gait data previously used for concept design I. The results are plotted for ideal conditions and with pseudo control applied for real conditions. These results show plots for M_{ank}, accumulator pressure and hydraulic power. For design II, since M_{act} does not correspond to M_{ank}, the following calculation was used to obtain M_{ank}.

$$M_{act} = F_1.tan(\alpha+\beta).l \dots\dots\dots\dots Eq.(4.5)$$

$$F_1 = \frac{M_{ank}.cos(\alpha+\beta)}{d} \dots\dots\dots\dots Eq(4.8)(rearranged)$$

By substituting F_1 from the re-arranged Eq. (4.8) in Eq. (4.5), M_{act} or (T_{vda}) can be expressed as M_{ank} as shown below

$$M_{ank} = \frac{M_{act}.d}{l.sin(\alpha+\beta)} \dots\dots\dots\dots Eq(4.25)$$

The results of ideal, real, and real scaled accumulator pressure, ideal and real scaled torque as well ideal and real scaled power for the gait data is presented below.

4.5.1 LEVEL WALKING

b) Salford's Gait Data

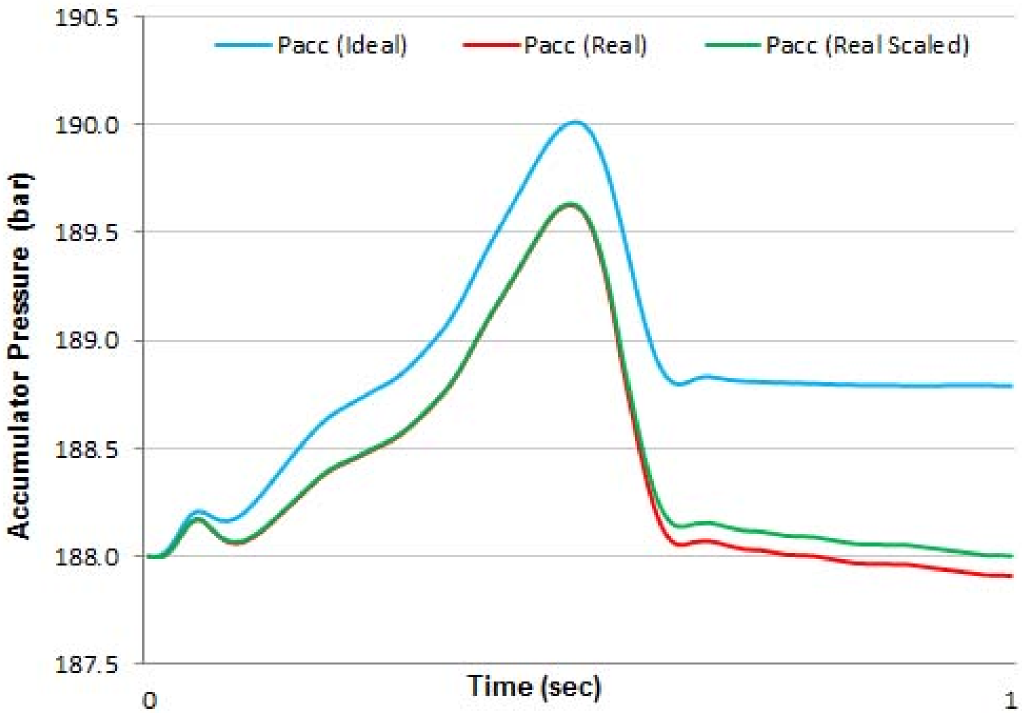

Figure 4.14: Pressure profile obtained for ideal, real, and real scaled conditions for Salford's gait data.

In Figure 4.14, the pressure profile for ideal conditions (solid blue curve) indicates that the final pressure is slightly higher than the initial pressure, indicating that there is more energy stored in the accumulator than released during the gait cycle. However, the pressure profile for real conditions (solid red curve) indicates that the leakage losses caused the final accumulator pressure to drop lower than the initial value. i.e. more energy is released than stored in the accumulator. The pressure profile (solid green curve) represents the pressure profile obtained by implementing a pseudo control on the pressure obtained for real conditions.

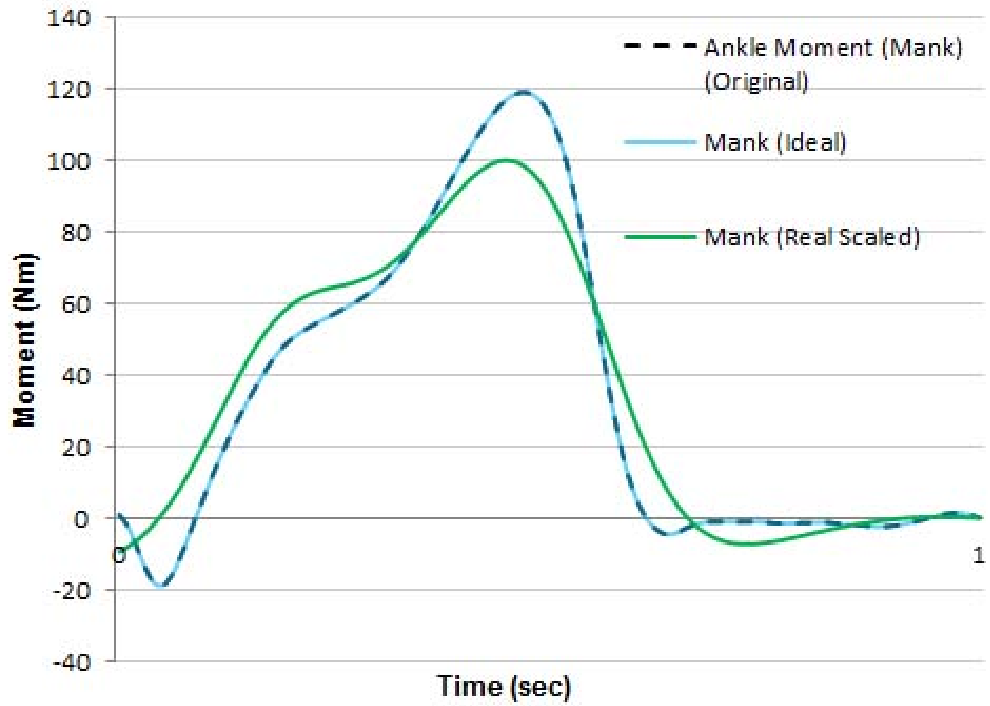

Figure 4.15: Torque profile obtained for ideal and real scaled conditions for Salford's gait data.

Figure 4.15 indicates that for the ideal conditions, the torque obtained from simulation matches exactly with the in-vivo data used. The torque obtained from a VDA by implementing pseudo control on accumulator pressure (solid green curve) is slightly lower than the ideal case, but it is still close to normal ankle torque profile.

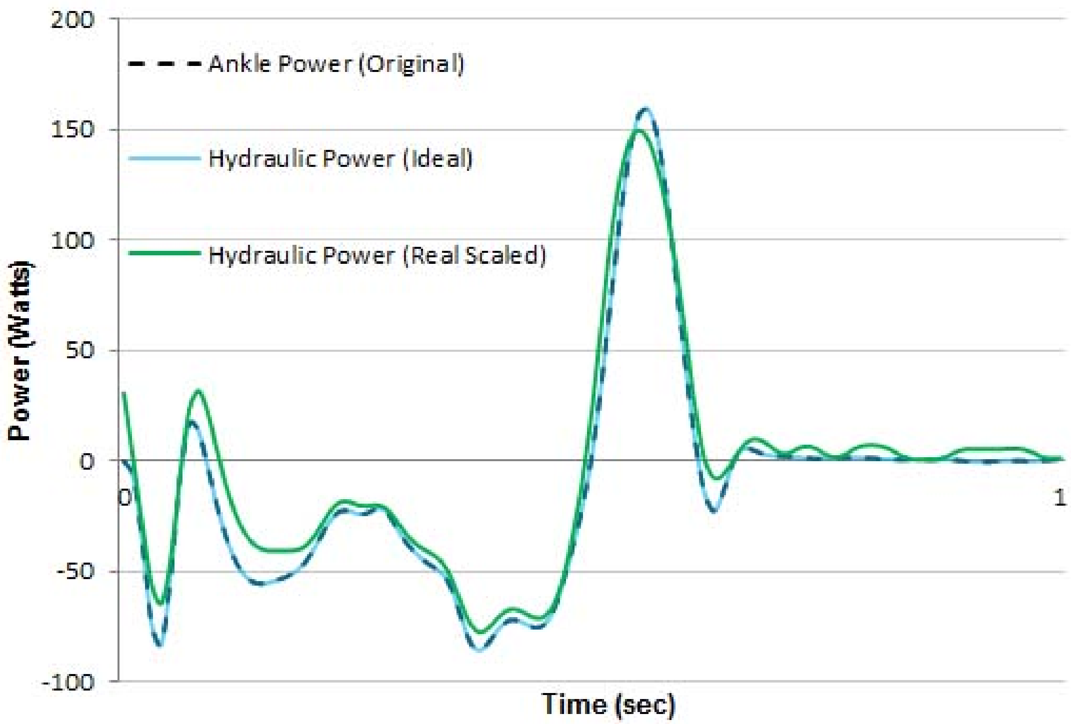

Figure 4.16: Power profile obtained for ideal and real scaled conditions for Salford's gait data.

Figure 4.16 shows the power profile for the intact ankle and accumulator hydraulic power obtained for the ideal and real scaled conditions. The intact ankle power and accumulator hydraulic power matches exactly. However, the power obtained (solid green curve) by implementing pseudo control indicates that the system was able to store all of the available negative work, but slightly less peak power was delivered when losses were considered. In addition, the timings of the power delivery matches exactly with the ideal conditions.

c) Data from Lay et al, 2006

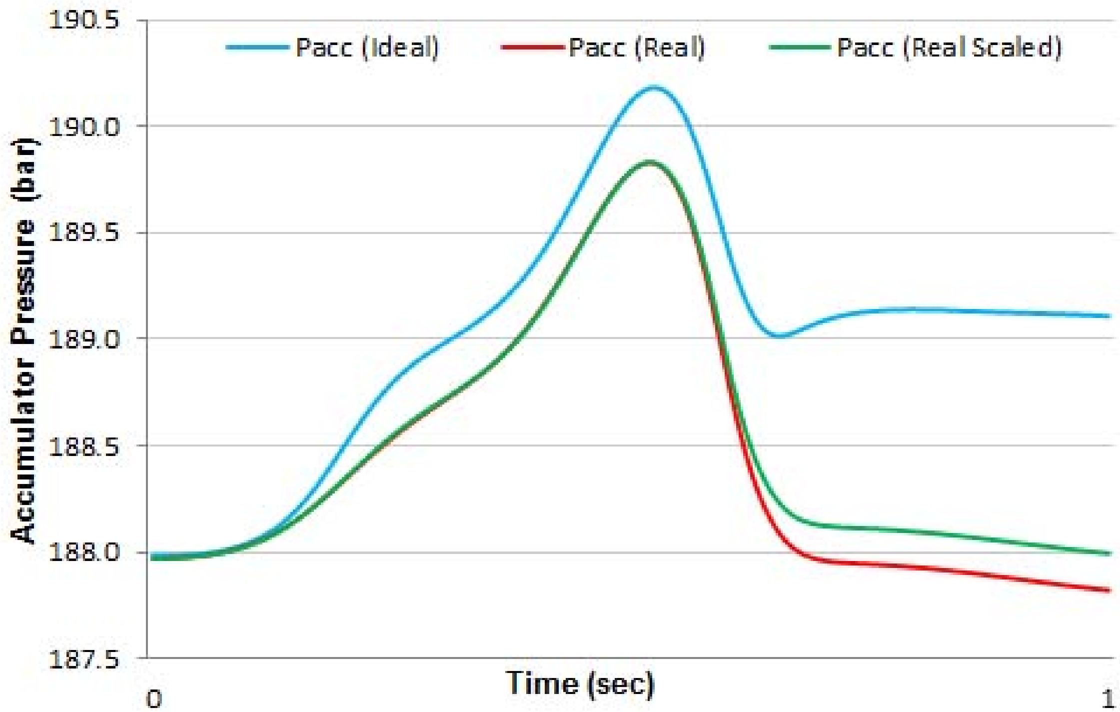

Figure 4.17: Pressure profile obtained for ideal, real, and real scaled conditions for level walking data from Lay et al., 2006.

In Figure 4.17 the pressure profile for ideal conditions (solid blue curve) indicates that the final pressure is slightly higher than the initial pressure, indicating that there is more energy stored in the accumulator than released during the gait cycle. However, the pressure profile for real conditions (solid red curve) indicates that the leakage losses caused the final accumulator pressure to drop lower than the initial value. i.e. more energy is released than stored in the accumulator. The pressure profile (solid green curve) represents the pressure profile obtained by implementing a pseudo control on the pressure obtained for real conditions.

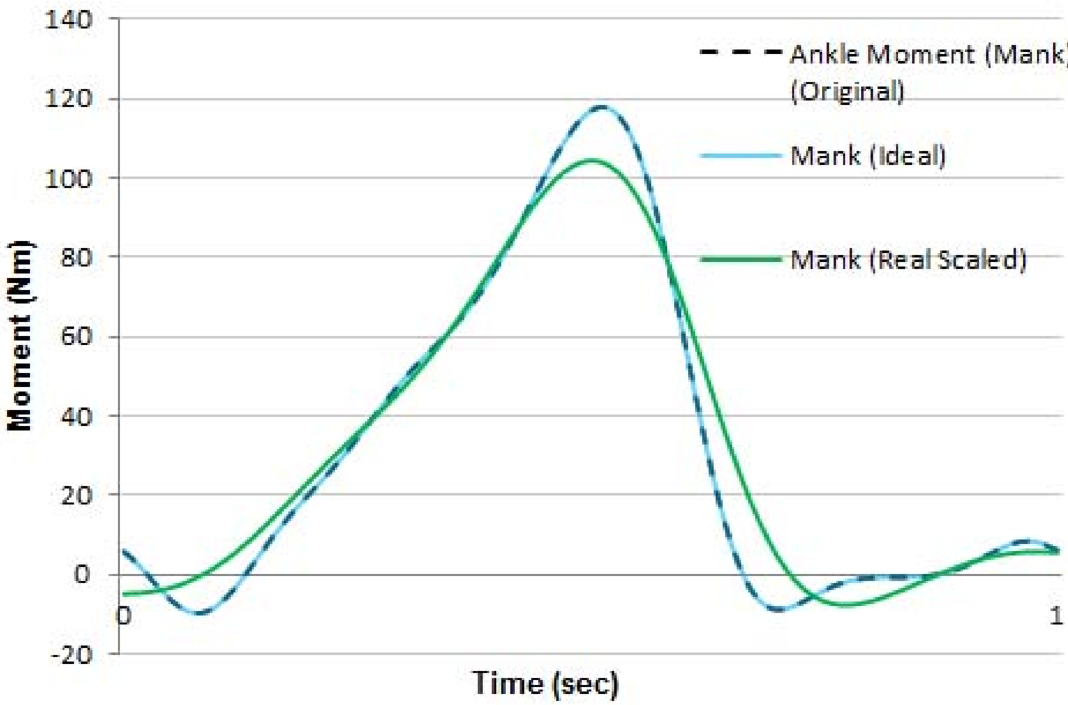

Figure 4.18: Torque profile obtained for ideal and real scaled conditions for level walking data from Lay et al., 2006.

Figure 4.18 indicates that for the ideal conditions, the torque obtained from simulation matches exactly with the in-vivo data used. The torque obtained from a VDA by implementing pseudo control on accumulator pressure (solid green curve) is slightly lower than the ideal case, but it is very close to normal ankle torque profile.

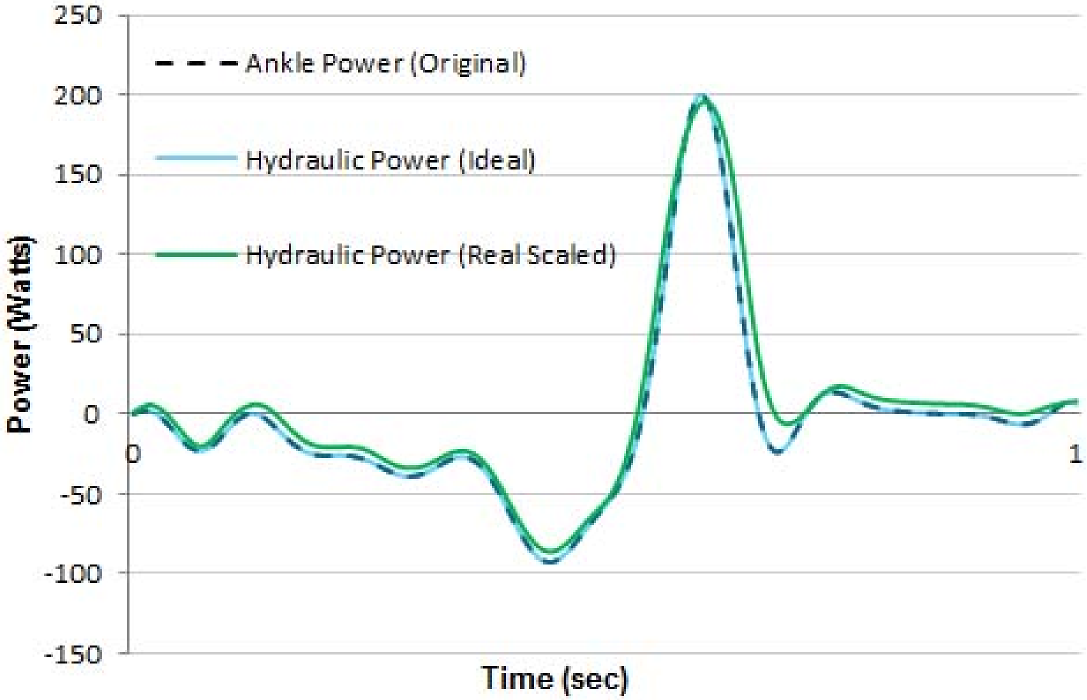

Figure 4.19: Power profile obtained for ideal and real scaled conditions for level walking data from Lay et al., 2006.

Figure 4.19 shows the power profile for the intact ankle and accumulator hydraulic power obtained for the ideal and real scaled conditions. The intact ankle power and accumulator hydraulic power matches exactly. However, the power obtained (solid green curve) by implementing pseudo control indicates that the system was able to store all of the available negative work, and almost same peak power was delivered when losses were considered. In addition, the timings of the power delivery matches exactly with the ideal conditions.

4.5.2 Decline Walking

The data for decline and incline walking was taken from Lay et. al, 2006.

a) 8.5° Decline

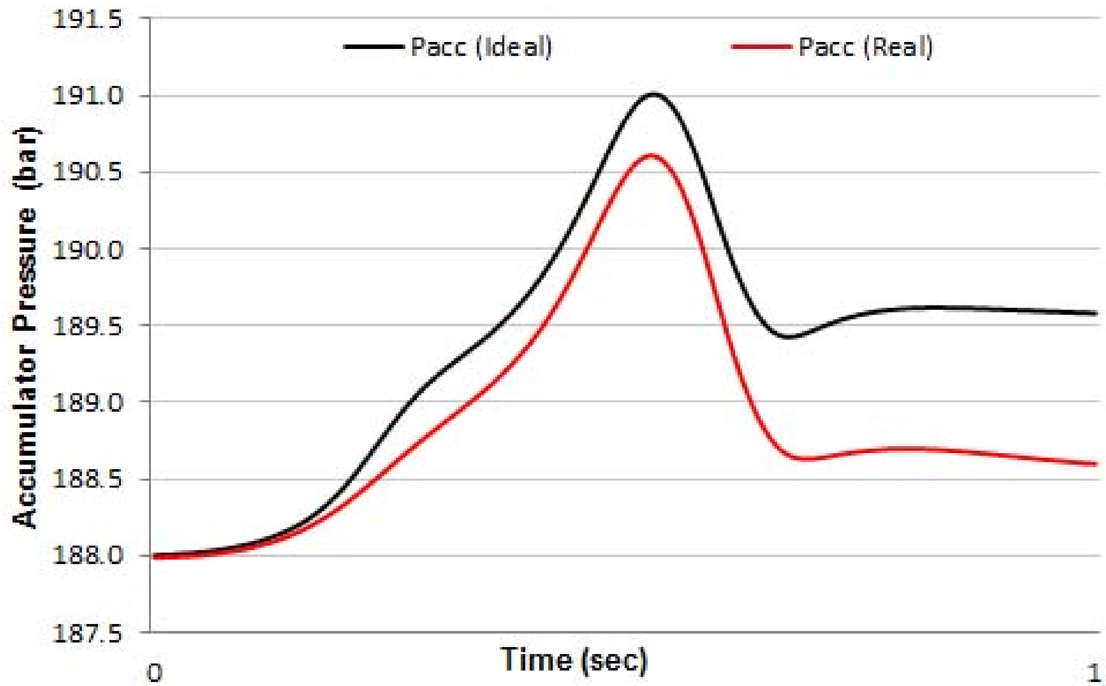

Figure 4.20: Pressure profile obtained for ideal and real conditions for 8.5° decline data from Lay et al., 2006.

In Figure 4.20, the pressure profile for ideal conditions (solid black curve) indicates that the final pressure is higher than the initial pressure, indicating that there is more energy available to store in the accumulator than released during the gait cycle. The same is observed for real conditions (solid red curve), that more energy is available to store even after compensating for the losses.

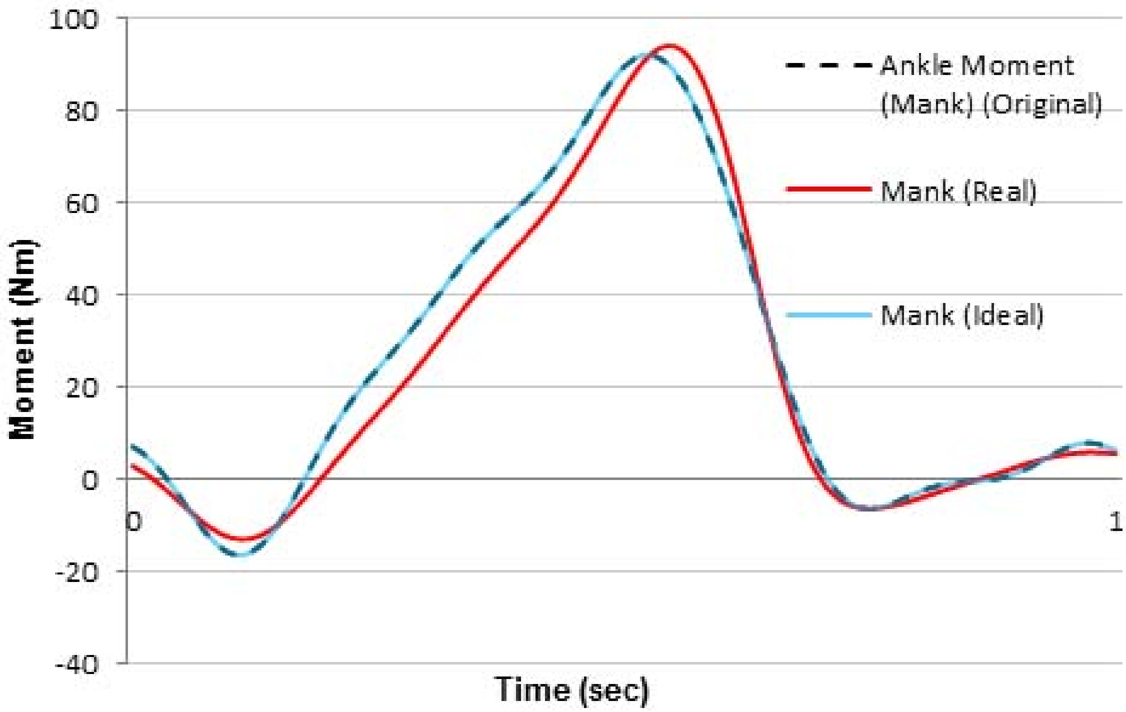

Figure 4.21: Torque profile obtained for ideal and real conditions for 8.5° decline data from Lay et al., 2006.

Figure 4.21 indicates that for the ideal conditions (solid blue curve), the torque obtained from simulation matches exactly with the in-vivo data (dashed curve) used. The torque obtained from a VDA for real conditions (solid red curve) is very close to normal ankle torque profile.

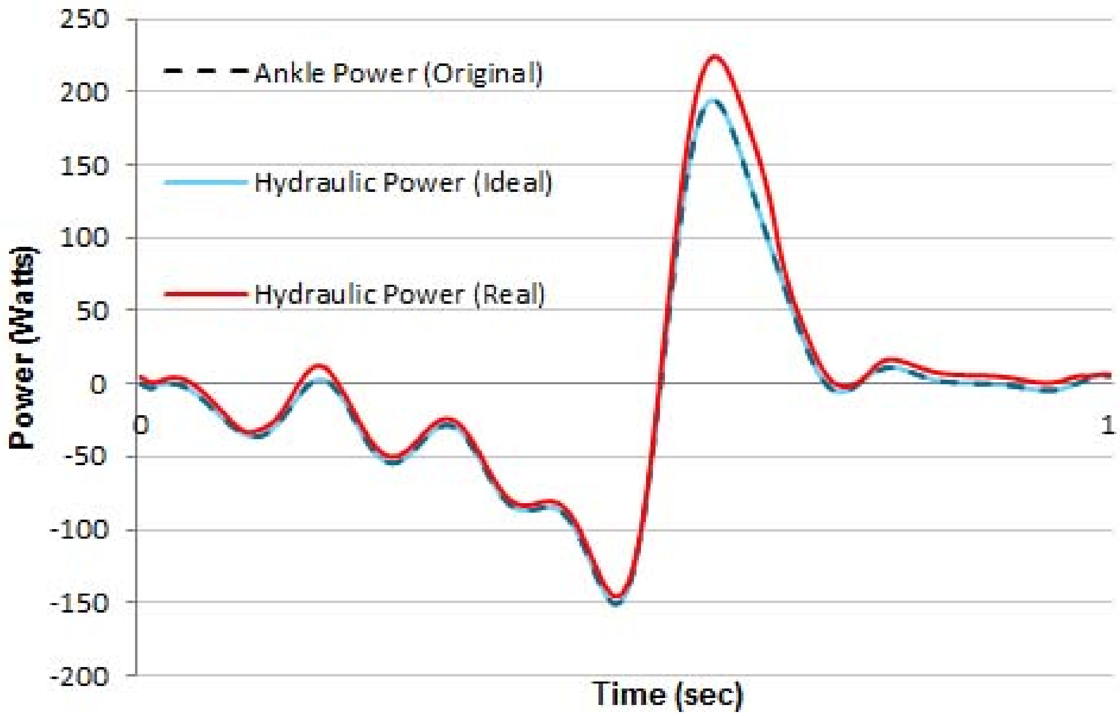

Figure 4.22: Power profile obtained for ideal and real conditions for 8.5° decline data from Lay et al., 2006.

Figure 4.22 shows the power profile for the intact ankle (dashed curve) and accumulator hydraulic power obtained for the ideal (solid blue curve) and real conditions (solid red curve). The intact ankle power and accumulator hydraulic power matches exactly. Even with losses, the real power obtained is very close to the required ankle power, because the additional energy available in the accumulator was utilized in compensating for the losses. Therefore, for decline walking, the system was able to deliver a close to normal ankle power profile.

b) 21° Decline

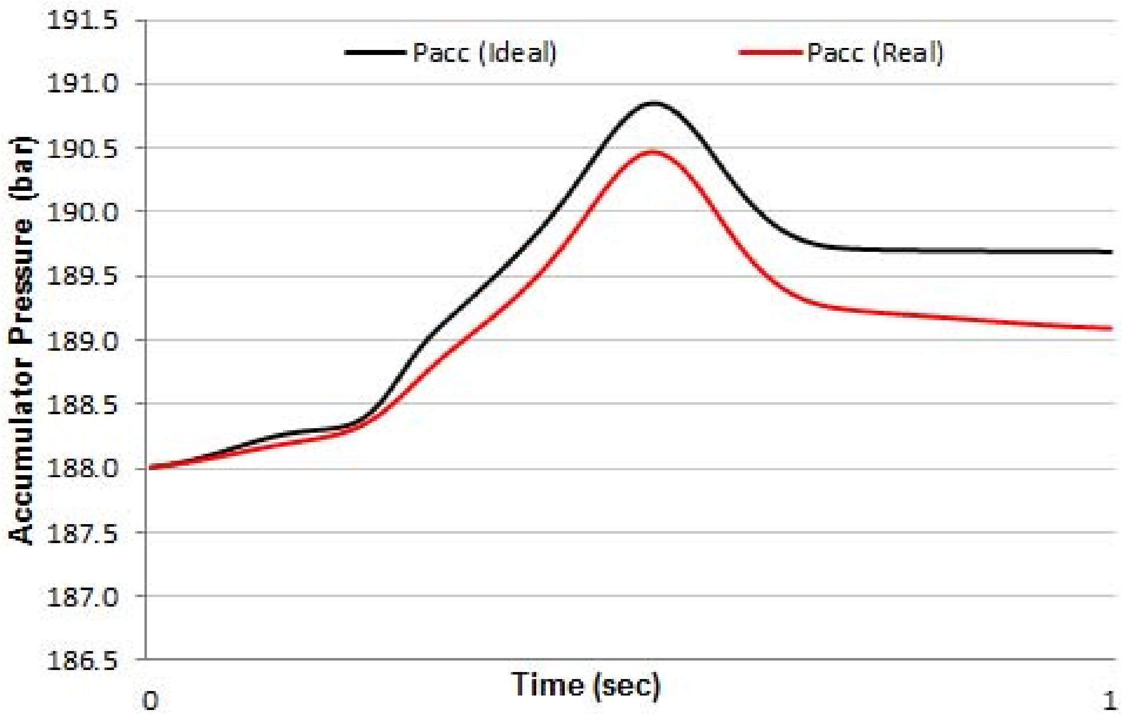

Figure 4.23: Pressure profile obtained for ideal and real conditions for 21° decline data from Lay et al., 2006.

In Figure 4.23, the pressure profile for ideal conditions (solid black curve) indicates that the final pressure is higher than the initial pressure, indicating that there is more energy available to store in the accumulator than released during the gait cycle. The same is observed for real conditions (solid red curve), that more energy is available to store even after compensating for the losses.

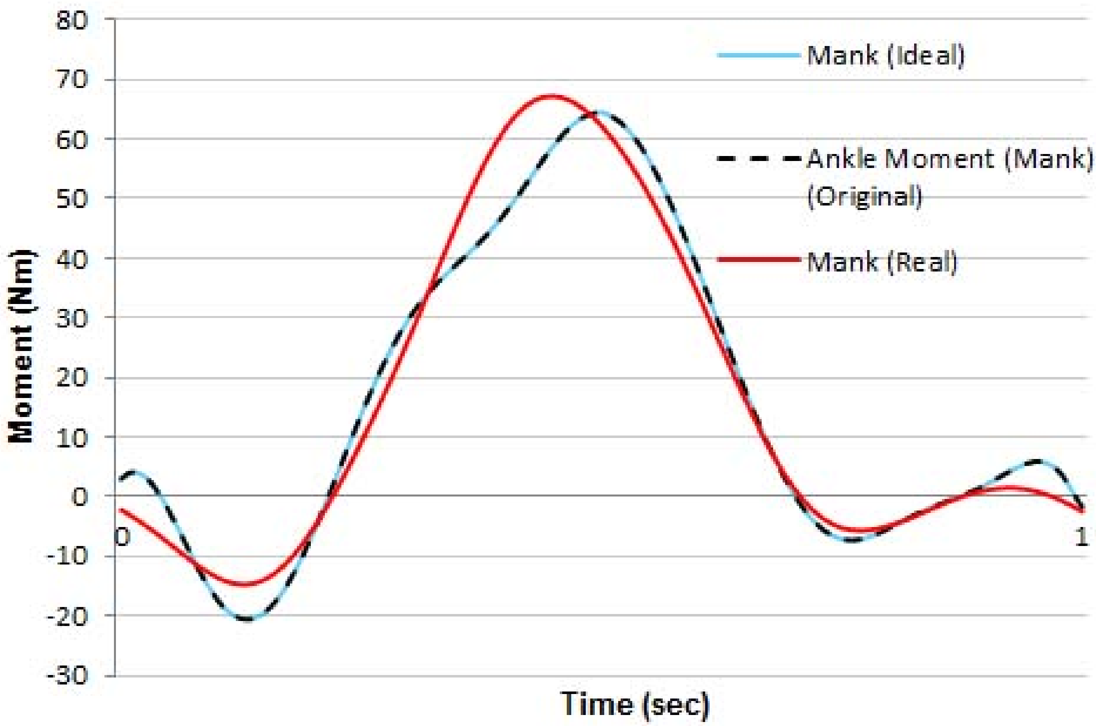

Figure 4.24: Torque profile obtained for ideal and real conditions for 21° decline data from Lay et al., 2006.

Figure 4.24 indicates that for the ideal conditions (solid blue curve), the torque obtained from simulation matches exactly with the in-vivo data (dashed curve) used. The torque obtained from a VDA for real conditions (solid red curve) is very close to normal ankle torque profile.

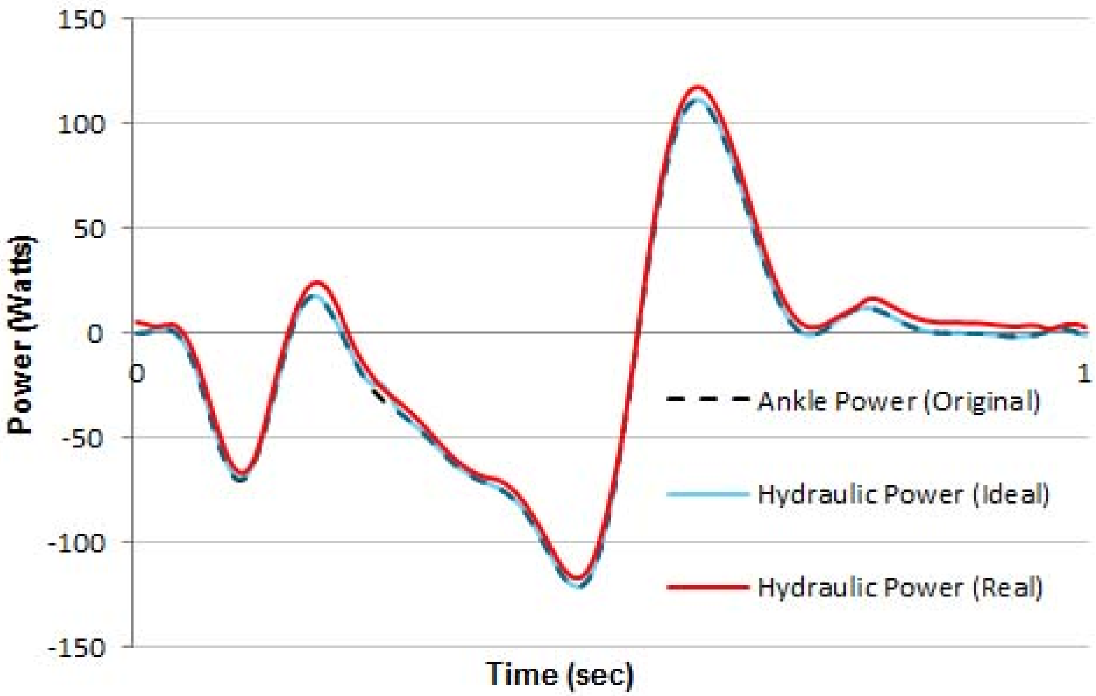

Figure 4.25: Power profile obtained for ideal and real conditions for 21° decline data from Lay et al., 2006.

Figure 4.25 shows the power profile for the intact ankle (dashed curve) and accumulator hydraulic power obtained for the ideal (solid blue curve) and real conditions (solid red curve). The intact ankle power and accumulator hydraulic power matches exactly. Even with losses, the real power obtained is very close to the required ankle power, because the additional energy available in the accumulator was utilized in compensating for the losses. Therefore, for decline walking, the system was able to deliver a close to normal ankle power profile.

4.5.3 INCLINE WALKING

a) 8.5° Incline

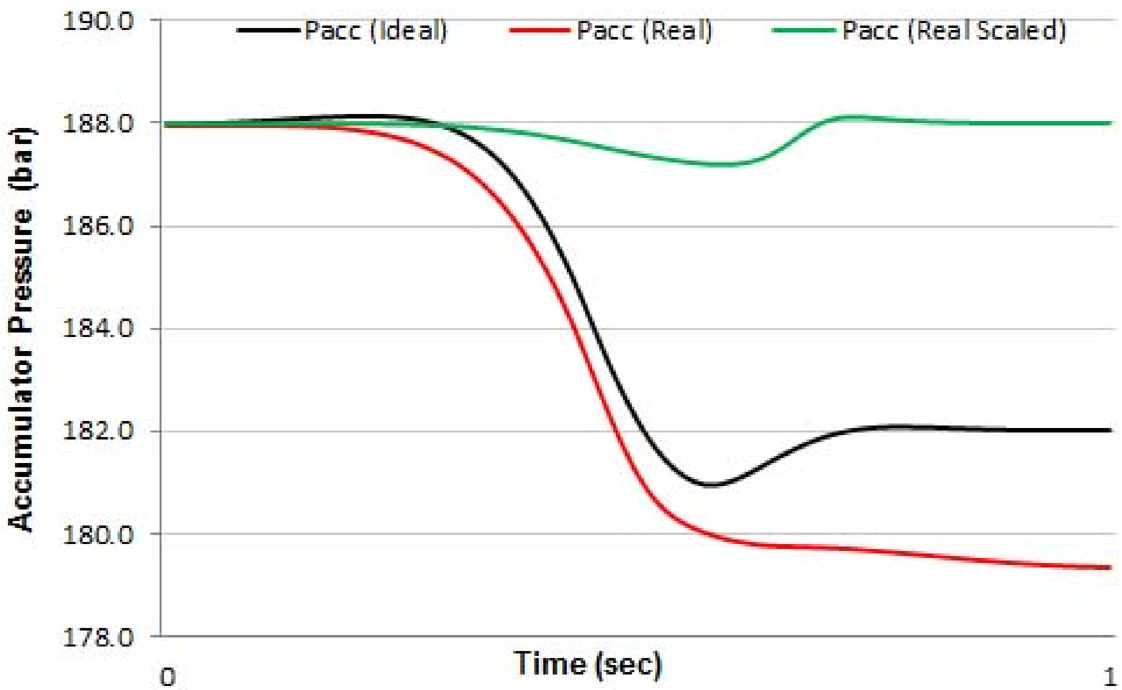

Figure 4.26: Pressure profile obtained for ideal and real conditions for 8.5° incline data from Lay et al., 2006.

During incline walking, the active positive work contribution dominates the elastic energy storage and return work of tendons. Therefore being a passive system aimed to recycle the strain energy, there is very little energy to store and return. A perfect control was assumed in the simulation and therefore, in order to produce similar levels of musculo-tendon work, the accumulator had to be drained (final pressure dropped lower than the initial pressure), as shown in Figure 4.26. For real conditions (solid red curve), the situation was worse, as the pressure dropped more in order to compensate for the losses. However, scaling the pressure profile for real conditions (solid green curve) indicates that, in order to prevent the accumulator to be completely drained over few cycles, there would be very little energy to store and return.

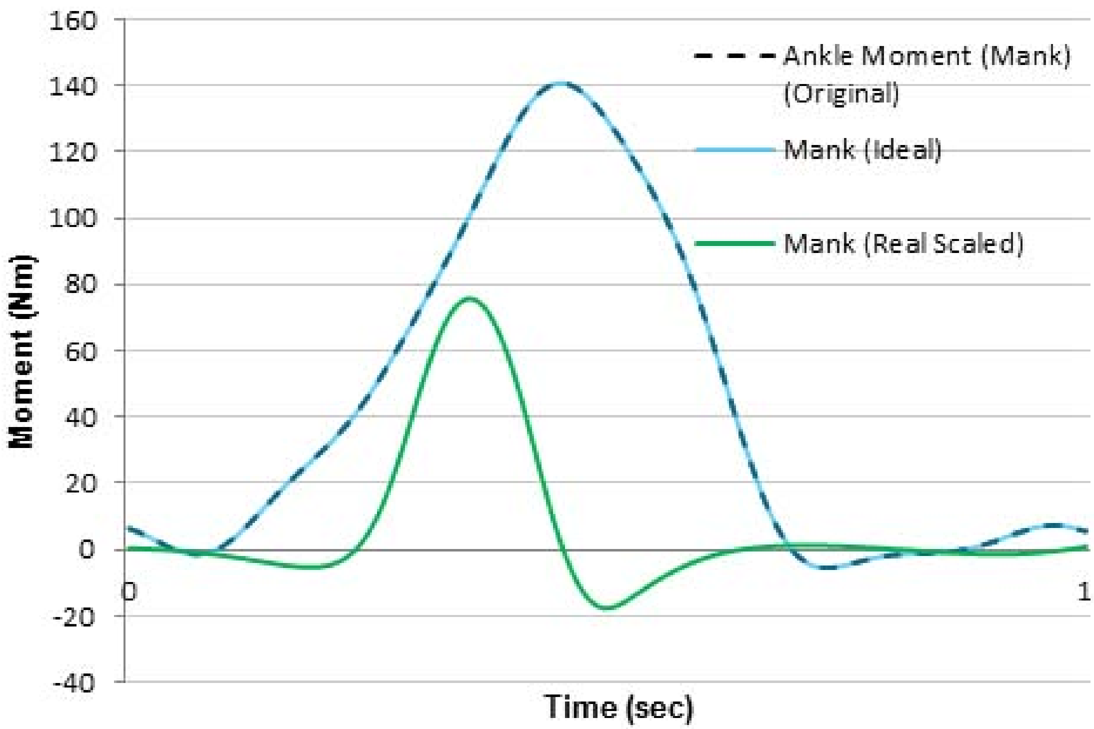

Figure 4.27: Torque profile obtained for ideal and real conditions for 8.5° incline data from Lay et al., 2006.

Figure 4.27 indicates that the torque obtained from simulation matches exactly with the in-vivo data used. However, this would cause the accumulator to be drained over few cycles, as discussed previously. The torque profile obtained by scaling the accumulator pressure (solid green curve) to prevent stalling the system represents a deviation from the normal ankle torque profile system for an 8.5° incline walking.

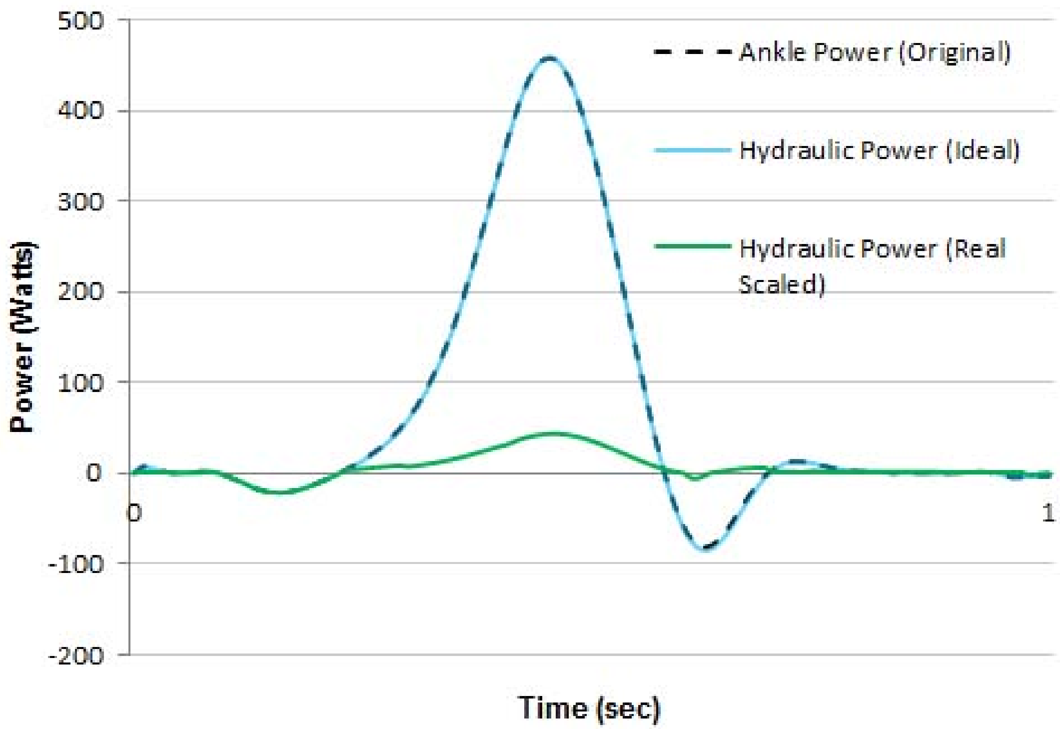

Figure 4.28: Power profile obtained for ideal and real conditions for 8.5° incline data from Lay et al., 2006.

Figure 4.28 indicates that, for incline walking, active positive work contribution dominates the elastic energy storage and return work of tendons. Therefore, being a passive system aimed to recycle the strain energy, there is very little energy to store and return, as indicated by the solid green curve.

b) 21° Incline

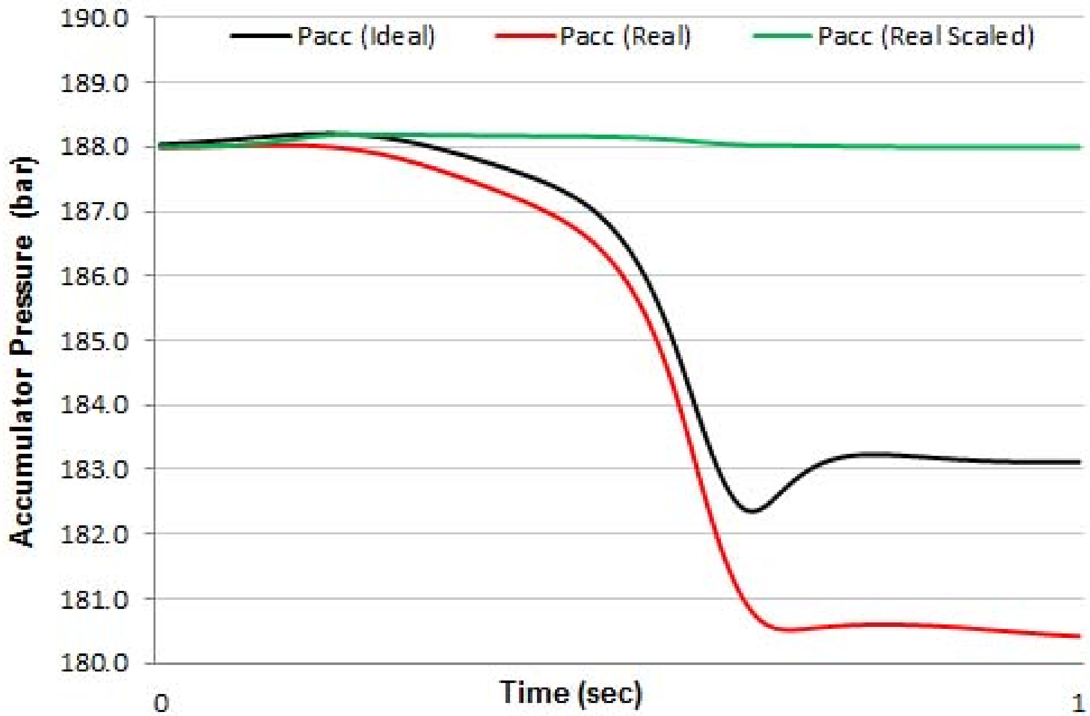

Figure 4.29: Pressure profile obtained for ideal and real conditions for 21° incline data from Lay et al., 2006.

During incline walking, the active positive work contribution dominates the elastic energy storage and return work of tendons. Therefore being a passive system aimed to recycle the strain energy, there is very little energy to store and return. A perfect control was assumed in the simulation and therefore, in order to produce similar levels of musculo-tendon work, the accumulator had to be drained (final pressure dropped lower than the initial pressure), as shown in Figure 4.29. For real conditions, the situation was worse, as the pressure dropped more in order to compensate for the losses. However, scaling the pressure profile for real conditions (solid green curve) indicates that, in order to prevent the accumulator to be completely drained over few cycles, there would be very little energy to store and return.

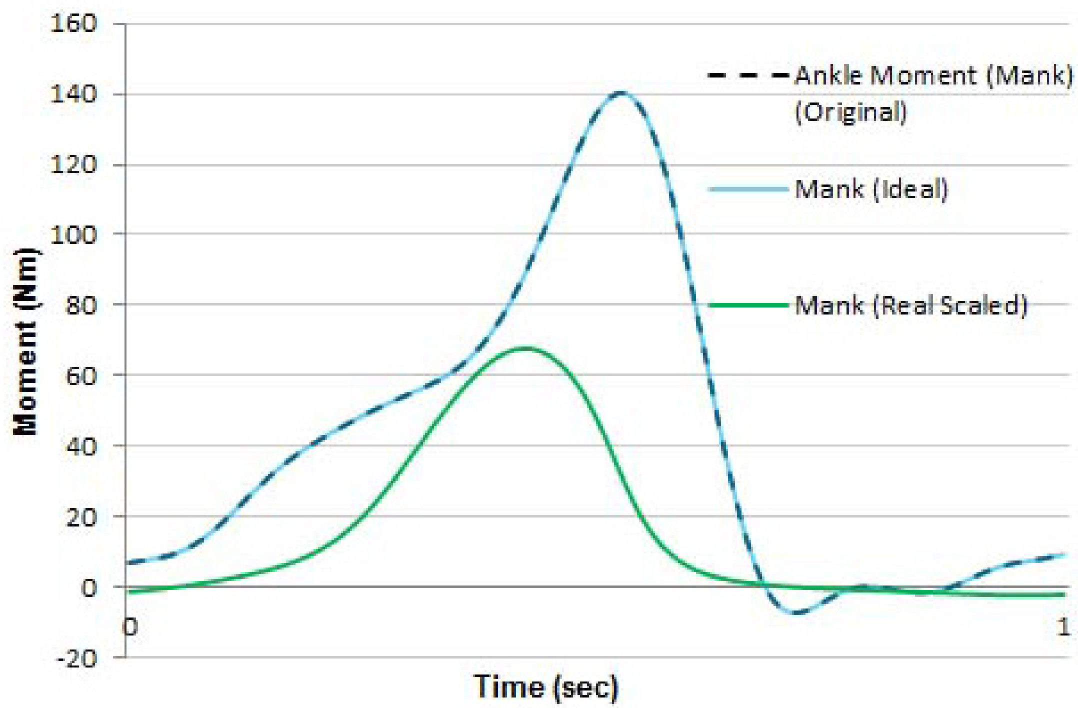

Figure 4.30: Torque profile obtained for ideal and real conditions for 21° incline data from Lay et al., 2006.

Figure 4.30 indicates that the torque obtained from simulation matches exactly with the in-vivo data used. However, this would cause the accumulator to be drained over few cycles, as discussed previously. The torque profile obtained by scaling the accumulator pressure (solid green curve) to prevent stalling the system represents a deviation from the normal ankle torque profile system for an 21° incline walking.

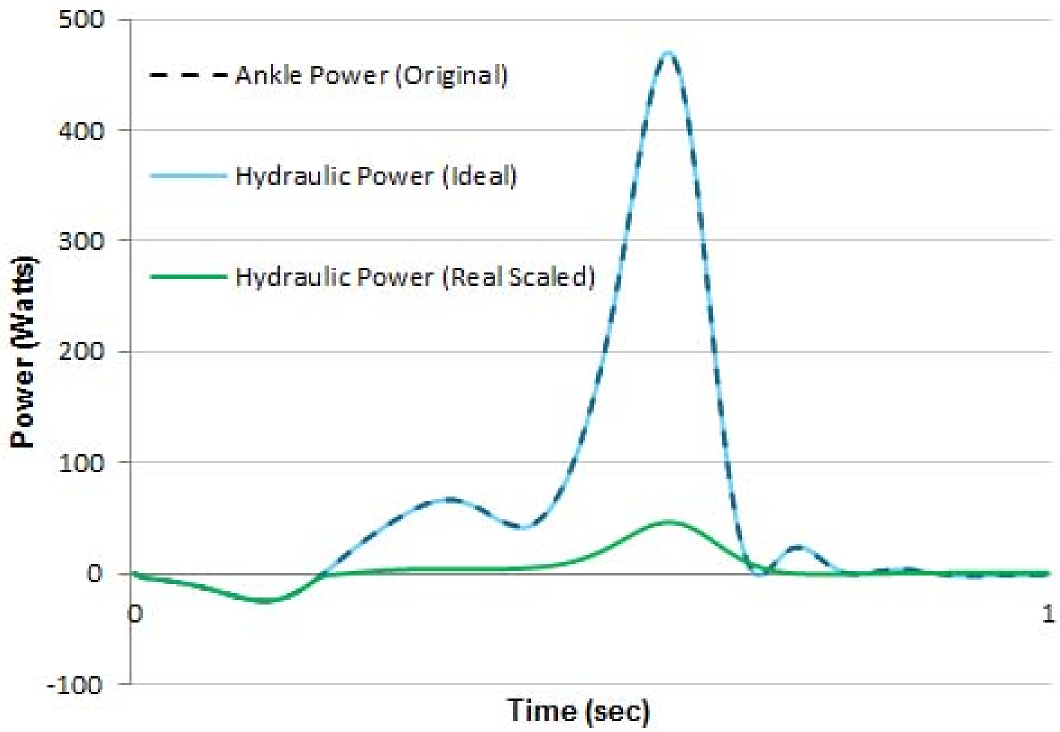

Figure 4.31: Power profile obtained for ideal and real conditions for 21° incline data from Lay et al., 2006.

Figure 4.31 indicates that, for incline walking, active positive work contribution dominates the elastic energy storage and return work of tendons. Therefore, being a passive system aimed to recycle the strain energy, there is very little energy to store and return, as indicated by the solid green curve.

4.5.4 SUMMARY

A summary of the peak power obtained from power profiles for real scaled conditions versus ideal conditions (Figure 4.16, Figure 4.19, Figure 4.22, Figure 4.25, Figure 4.28, and Figure 4.31), for the gait data tested is presented in Table 4.3 below along with values from Table 3.6, for a comparison of design II performance with design I.

Data Source	Walking Condition	Peak Power Required (Watts)	Peak Power Deliverd (Watts)	Peak Power Deliverd (Watts)	% Peak Power Delivered	
			Design I	Design II	Design I	Design II
University of Salford	Level	159	136	150	86	94
Lay et al., 2006	Level	200	137	195	69	98
	8.5° Decline	194	186	224	96	115
	21° Decline	111	116	117	105	106
	8.5° Incline	459	33	44	7	9
	21° Incline	395	12	44	3	11

Table 4.3: Comparison of performance of design I and design II.

4.6 Discussion

In this chapter a second novel design concept was explored, the aim being to overcome the weight problems of design I by reducing the torque load on the VDA/VDA-gearbox and consequently reducing the system's overall weight and size. Therefore, in this section, the performance of design II is compared with that of design I to establish whether the expected improvements in weight and efficiency were obtained. Finally, conclusions are drawn with regard to the feasibility of design II for the prosthesis application.

4.6.1 System Performance

From Table 4.3, it is clear that introducing the slider-crank spring mechanism to share the workload with the VDA clearly proved to be an advantage. For all the walking conditions tested, Design II delivered higher peak power than design I. For the two level walking datasets, an 8%, and 29% increase in peak power delivered was observed with design II (Table 4.3). For 8.5° decline walking, design II increased the peak power by 4% (to deliver 100% of the required power). For 21° decline walking, both designs delivered 100% peak-push off power, but the excess energy left in the accumulator was higher in design II than in design I. For incline walking, consistently improved performance of design II is observed. For 8.5° incline, it increased the peak push-off power by 2%, and for 21° inclined, it increased the peak push-off power by 8%, in comparison to design I.

While concept design I performed better than the commercially available and the prototype prostheses (as discussed in Section 3.10), design II clearly outperformed it. The reason for improved performance of design II was the reduction in losses compared with design I. This can be observed by comparing the pressure profiles of both designs, obtained for uncontrolled real conditions for each walking condition. For instance, for Salford's gait data for level walking (Figure 3.15), in design I the final pressure dropped over 1 bar, below the initial pressure. In design II however, Figure 4.14 indicates that the final pressure remained close to the initial pressure, indicating that losses were smaller, and hence less modulation was required by the control system in design II. This resulted in a lower reduction in push-off power in design II than design I. The same observation can be made for the level walking data from Lay et al, 2006, where the final pressure dropped approximately to 1 bar below the initial pressure in design I (Figure 3.18), whereas it remained close to the initial pressure in design II (Figure 4.17). Similar reductions in pressure losses over the gait cycle, when comparing design II to design I were seen in the results for sloped walking.

The pressure profiles confirm the initial hypothesis that led to the development of design II, i.e. sharing the workload on the actuator with an efficient spring mechanism might improve efficiency. In design II, the actuator was not used directly to drive the ankle (as opposed to design I), and a hydraulic cylinder was used in parallel to work as a major work provider, leaving the VDA to perform only the difference between the total work required and the work done by the spring. This has reduced the workload on the VDA, reducing its size and losses.

The loss models of the VDA were taken from experimental testing of an industrial VDA, and therefore, provide a conservative estimate of the losses with the VDA used in this design. Since the linear bearings are designed to have negligible friction, therefore the linear bearing was assumed frictionless. The losses in the cylinder were also neglected, which might be offset by the assumed conservative loss model for the VDA. These assumptions would closely approximate the performance of a physical prototype.

4.6.2 FEASIBILITY

For both the ideal as well as real conditions, Table 4.2 indicates that the VDA sizes are reduced in design II compared to design I. For the ideal conditions, an average VDA size of 50 cc/rev for the walking conditions tested in design I was reduced approximately by half in concept design II. Similar reductions in VDA size for design II for the real conditions is evident from Table 4.2, however, the gear ratios have been increased in design II. Therefore, in order to have an understanding of any benefits in terms of practical feasibility for design II, the following table presents a weight comparison of the optimum VDA and gearbox sizes obtained for the test data, with similar-sized commercially available VDAs (aluminium construction, for aerospace industry) and gearboxes (steel made for industrial applications) (see Appendix-D), which are capable of operating at or above 200 bar pressure, with an average maximum torque output of 60 Nm (this was found to be the average maximum torque load on the VDA for all walking conditions tested in design II).

		IDEAL CONDITIONS				REAL CONDITIONS						
Data Source	Terrain Type	Optimum VDA Sizes		Similar Commercially Available Sizes & Corresponding		Optimum VDA sizes	Similar Commercially Available VDA Size	Commercially Available VDA Weight	Optimum Gearbox Sizes	Similar Commercially Available Gearbox Size	Commercially Available Gearbox Weight	Total Weight (Real Case)
		VDA Size (cc/rev)	Gear Ratio	VDA Size (cc/rev)	VDA Weight (kg)	VDA Size (cc/rev)	VDA Size (cc/rev)	VDA Weight (kg)	Gear Ratio	Gear Ratio	Gearbox Weight (kg)	VDA + Gearbox Weight (kg)
Lay et al., 2006	**21° Incline**	42.5	1	39.33	***10.2***	2.3	1.803	1.8	20	20	1.1	***2.9***
Lay et al., 2006	**8.5° Incline**	42.5	1	39.33	***10.2***	2.8	3.15	1.7	21	20	1.1	***2.8***
Salford's Data	**Level**	19	1	18.85	***5.2***	0.98	1	1.1	20	20	1.1	***2.2***
Lay et al., 2006	**Level**	19.7	1	18.85	***5.2***	1.1	1	1.1	18	16	0.45	***1.55***
Lay et al., 2006	**8.5° Decline**	18.9	1	18.85	***5.2***	0.9	1	1.1	20	20	1.1	***2.2***
Lay et al., 2006	**21° Decline**	16.3	1	18.85	***5.2***	0.93	1.1	1.1	18	16	0.45	***1.55***

Table 4.4: A weight comparison of VDA and VDA/gearbox sizes obtained for ideal and real models for the test data with similar commercially available components for design II.

For ideal conditions, a reduction in VDA sizes in design II is evident from Table 4.2. However, a weight comparison of the reduced sizes in design II with similar sized commercially available aluminium-made VDAs (Table 4.4) indicates that, while the weights have also been reduced approximately by half, compared to design I, they are still very heavy as they reach a combined weight of 4.5 kg for the anatomical shank and foot. This suggests that a VDA-only mode in design II might be limited in practical feasibility, whereby the VDA-gearbox mode might be practically feasible.

Comparing the combined weight of the VDA-gearbox for all walking conditions (Table 4.4), it is evident that design II with VDA-gearbox configuration is promising, as the maximum combined weight is 2.9 kg (being conservative), which is well below the target weight of 4.5 kg for an anatomical limb. It is very reasonable to assume that there is scope to further reduce the weights of the combined VDA-gearbox to less than 2 kg, as the weight data presented in Table 4.4 was taken from industrial catalogues. Further, the curve (Figure 4.13), showing the accumulator pressure-displacement relationship, does not follow an inverted U-shaped profile, which means that any VDA-gearbox combination could be used from the point where the profile became almost flat, and a further reduced VDA size with a larger gear ratio could have been used depending on the combined weight of both components. With bespoke designs, using lighter materials, and further exploration of design trade-offs, the combined weight of the VDA-gearbox system in design II could be significantly reduced. The diameter (bore) of cylinder (*Dia*) used in the design was 1 cm, which is a realistic size and feasible to machine. The optimum position coordinates (x,y) of the VDA were found to be 3 cm and 10 cm, and hence, considering typical anatomical shank and foot dimensions, the mechanism is clearly compact enough to be incorporated in a prosthesis.

5. CONCLUSION

5.1 Summary

The overall aim of this work was to develop a prosthesis design that is efficient in the storage and release of energy to improve amputee gait biomechanics. Based on the conclusion of the literature review (Chapter 2), two novel designs were developed, and the results showed that the final design outperformed the commercially available passive prostheses (Barr et al., 1992 and Segal et al., 2006), as well as the only other novel passive controlled energy recycling prosthetic foot (Collins & Kuo, 2010).

To inform the work described in this thesis, a review of anatomically intact and amputee gait studies was undertaken in Chapter 2. In summary, human gait is an energy efficient task and requires only 255 kJ of metabolic energy to cover a distance of 1 km at comfortable walking speed. One of the key findings was that 60% of the positive work performed collectively by the hip, knee, and ankle for forward progression is contributed by the ankle joint (Sawicki et al., 2009). Ultrasound imaging revealed that most of the ankle work is attributed to the elastic energy storage and return in tendons crossing the ankle joint, which allows the muscles to remain nearly isometric (Sawicki et al., 2009). Therefore, a loss of the anatomical ankle joint and associated structures due to amputation adversely affects gait efficiency. The metabolic energy cost is increased by an average of 25% and 50% for transtibial and transfemoral amputees, respectively (Waters et al., 1976). This increased metabolic cost in amputees is at least partly a result of the inability of passive prostheses to store adequate amounts of energy and return the elastic energy at the right time (over the late part of the stance phase). Clinical studies show little difference in metabolic energy efficiency between wide ranges of passive commercially available prostheses, suggesting alternative designs are required.

To address this problem, a small number of actively powered prostheses have been designed and have shown apparently impressive results. For instance, a recently commercialized bionic prosthesis (Herr & Grabowski, 2012) is able to provide near normal ankle power, but analysis shows that the improvements are almost entirely attributable to the battery and it does not exploit the significant energy recycling opportunities during gait. Without the power source, it would functionally behave as a standard passive ESR prosthesis with similar problems of uncontrolled energy storage and return. A recent prototype, developed by Collins & Kuo, 2010, to store part of the eccentric work with controlled release of energy later in stance, highlighted the potential benefits of this general approach. However, although some aspects of its performance looked apparently impressive, the results were contradictory, raising significant questions about the study methods. In addition, the foot did not result in significant improvement in amputees' metabolic economy. Part of the reason for this was that it could only store load acceptance work, and the release of energy was delayed (Collins & Kuo, 2010). Further, their design is based on control of a mechanical spring at the ankle, making it very difficult to extend the design to take advantage of the substantial knee eccentric work available during level walking (Winter, 2004a).

These issues highlighted the need for an improved design that could harness all the eccentric work during gait, and release it with correct timing whilst providing continuous control of ankle torque. Inspired by regenerative braking systems, a first design concept using hydraulics was investigated (described in Chapter 3), to demonstrate the feasibility of using hydraulics for energy storage and return during gait and provide close to anatomically intact ankle push-off power, while keeping the size and weight constraints for a prosthesis under consideration. In summary, the key findings of the design showed that using a hydraulic accumulator as an energy storage medium was very effective, as it was shown to be able to store all of the available energy in a very compact volume (245 cc). It was noted that using an accumulator as a central energy storage component, allowed the potential for future designs to use it for energy storage from other joints, such as eccentric work at the knee. This would allow for controlled interchange of energy between major lower limb joints.

To drive the ankle, first a stand-alone variable displacement actuator (VDA) was investigated, which, under ideal conditions, was shown to produce the ankle torque and power profile required for level walking. However, the size and weight, and thus portability and feasibility of using it as a stand-alone component in the design, were a problem, when dimensions and masses of commercially available VDA were considered. Therefore, using a gearbox with the VDA was investigated, to reduce the size and mass of the VDA. The simulation results were very favourable, as it was shown that even with losses, the design outperformed the commercially available as well as other prototype prostheses, by providing 77% of peak push-off power required for level walking versus 7.5% and 24.7% for a conventional prosthesis (Barr et al., 1992) and ESR prostheses (Segal et al., 2006), respectively. For decline walking, it provided an average of 98% peak push-off power required. However, for incline walking with very little eccentric work available, as the design is completely passive, its performance remained poor. In addition, while the introduction of a gearbox reduced the size of the VDA compared to the stand-alone configuration, it nevertheless posed similar practical problems of portability.

The weight and size issues with the first design led to an investigation on how to reduce its size, while further improving the performance of the design. It was hypothesized that, instead of directly driving the ankle, using a hydraulic cylinder with a mechanical linkage to drive the ankle (acting as a spring), and using only the VDA to control the mechanical advantage of the cylinder, might be a more efficient approach. Therefore, another novel design concept was investigated in Chapter 4. In summary, the results supported the hypothesis. Compared to design I, design II performed better for all walking conditions. For level walking, it provided an average of 96% of required peak push-off power. Similarly, for decline walking, it provided 100% of the peak push-off power required. A small improvement was also seen in the performance for incline walking. With regard to incline walking and other conditions where there is insufficient energy at the ankle to harvest to allow full replication of the anatomical ankle, it would be possible to introduce an alternative way of putting energy into the system. One approach would be a separate hand pumping mechanism, which could be incorporated to charge the accumulator for providing power during incline walking.

In terms of portability, the optimum position of the actuator was found to be 10 cm from the ankle along the vertical, and 3 cm along the horizontal from the ankle. With the accumulator and oil tank to be made as an integral part of the shank, the mechanism is compact enough to be incorporated in a prosthesis. As far as weight and size of the gearbox and VDA is concerned, it was shown that these two parameters of both components were realistic to be used in a prosthesis.

During the write-up period of this thesis, Van Den Bogert et al., 2012, described a hydraulic system for controlled energy storage and release at the knee joint, similar to the approach used in this thesis. Their design comprised of a double acting rotary actuator and a hydraulic accumulator, controlled by two servo valves. This was only a simulation study focussing on control, and no efficiency data is presented. Considering the servo valves is a source of energy loss, we believe that their design is unlikely to be as efficient as that presented in this work. Nevertheless, this reinforces the view that using hydraulics to recycle energy during gait is a promising approach.

5.2 Novel Contributions

The major and novel contributions of this work can be summarised as follows:

1) Development of two novel designs based on hydraulics technology that were shown to be capable of efficiently storing and returning energy with continuous control of ankle torque.
2) First study to present a novel conceptual design based on hydraulics, shown to be practically realisable (Design II).
3) First study, which showed that a passive energy storing and return prosthesis with sophisticated control could equal the performance of an actively powered prosthesis over level ground and decline walking.

5.3 Limitations

The limitations with this work were:

a) The work undertaken was limited to virtual prototyping only. A physical prototype could not be developed due to funding and time constraints.
b) The limited range of gait data used as inputs to the design. This limited the generalizability of the results.
c) The limited information available on the relationships between component mass/size and function. While reasonable assumptions were made in the design process, a more detailed study would be required before proceeding to physical prototyping.

d) Another limitation was the manual optimisation approach adopted. This limited the optimisation to trade-offs between pairs of design variables. A formal comprehensive optimization approach would allow optimal design values to be identified.

5.4 Main Conclusions

A list of main conclusions that were drawn from this work is as follows:

1) It has been shown that hydraulic systems could be the basis for a new generation of advanced energy efficient prostheses.
2) The overall weight of the system could be reduced by inclusion of a compliant element to produce some of the ankle torque. Based on commercially available components, it was shown that using a compliant element reduced the overall weight from 5.2 kg to 2.2 kg.
3) The overall system weight of approximately 2.2 kg is based on off-the-shelf components. This could be reduced by using bespoke components based on advanced materials such as composites.
4) A design comprising a VDA with a compliant element, considerable improved the power and torque output at the ankle, compared to other commercially available and novel prostheses. It was shown that a natural ankle torque profile with a peak ankle push-off power of 98% and 100% for level and decline walking respectively could be achieved.

5.5 Future Work

The work described in this thesis is the beginning of an exciting area of prosthesis research. This is the first thesis that has demonstrated the potential to use hydraulics as a means of efficiently storing and returning ankle work over the gait cycle to improve amputee performance. However, further work is needed before the concept can be translated into a working physical design. A prioritised list of the recommendations to follow this work is as follows:

1) The first aspect is the need to test concept designs against a wider range of healthy gait data. For the completed work, level-walking data from only two sources was used, and slope-walking data came from a single publication. As was shown in Table 4.2, for different walking conditions, the optimum values of the VDA and gear ratio varied. Therefore, a more comprehensive and representative set of gait data would allow for a more informed choice.
2) The second aspect is the need to develop a control system, which could detect the gait phases and modulate the accumulator pressure in real time.
3) The third aspect is the need to further investigate the advantages gained from a more comprehensive optimisation of the design.
4) Finally, a detailed design specification is required to produce a working prototype system.

APPENDIX-A

Subjects performed ten walks at their self-selected speed whilst wearing standard shoes (ECCO Zen) along a 7m walkway. Data was collected using eight Qualisys Proreflex MCU240 cameras, sampling at 100 Hz, with bilateral force data gained from two Kistler (9861c) force platforms, sampling at 200 Hz. Markers were located on the calcaneus, first, second and fifth metatarsal, with clusters of four markers on the shank, thigh and pelvis. Anatomical reference frames were based on the Calibrated Anatomical System Technique (Cappozzo et al. 1995). The hip joint centre was calculated using the functional hip joint method (Leardini et al., 1999). Post-processing calculation of the kinematic and kinetic data was conducted using Visual3D software (C-Motion Inc., Rockville, MD, USA) where the 3-dimensional coordinates were interpolated, and low pass filtered using a Butterworth 4th order filter at 12 Hz. Analog data was filtered at 25 Hz. All lower extremity segments were modelled as rigid bodies. Anatomical frames were defined by landmarks positioned at the medial and lateral borders of the joint, from these right-handed segment co-ordinate systems were defined. Joint kinematics were calculated using an X–Y–Z Euler rotation sequence equivalent to the joint coordinate system (Grood & Suntay, 1983). Joint kinetic data were calculated using three-dimensional inverse dynamics, and the external joint moment data were normalized to body mass (Nm/kg), Jones R – personal communication.

APPENDIX-B

Differentials Block

```
function dA  =Differentials(A)%A is in-vivo ankle angle data
persistent Aprev; %Declaring variables that retains
                  %values between iterations
if isempty (Aprev)  %Initialize the persistent variable for
                    %1st iteration
    Aprev=A;        %First Value of ankle angle is persistant
    dA=0;           %First value of the change is zero
else
    dA=A-Aprev;
    Aprev=A;        %Save current value to use it as previous in next
                    %step
end
```

Gearbox Block

```
function [Tvda,dAvda] = fcn(dAgb, Mank, N, Tn)

dAvda=dAgb.*N;  %dAgb=Gearbox input shaft angular velocity*dt
                %dAvda=Gearbox output shaft angualr velocity*dt
                %N=gear ratio, Tn=Absolute maximum Torque (in-vivo
                %ankle torque)
Tfr=(6.913e-4.*N+0.02557).*Tn; %friction torque (set to zero for ideal
                               %conditions
if sign(Mank)~=sign(dAgb)    %VDA in pump mode, filling up accumulator
    absTtotal=(abs(Mank)-Tfr); %Absolute Total required torque
else                         %VDA in motor mode, accumulator emptying
    absTtotal=(abs(Mank)+Tfr); %Absolute Total torque
end
absMank=abs(Mank);
signs=Mank./abs(Mank);      %To get the actual signs of the
                            %Actuator/ankle moment
Ttotal=signs.*absTtotal;    %To convert the Absolute Total moment into
                            %Total moment with original signs
Tvda=Ttotal./N;             %Final torque input to the VDA that it
                            %needs to overcome, in order to produce the
                            %required ankle torque
```

VDA Block

```
function [dVF_real, X,VF] = fcn(Tvda,dAvda,Dmax, Pacc)
persistent VFprev ; %Declaring variables that retains
                    %values between iterations
w=dAvda./0.001; %VDA shaft input angular velocity for calculating
                %losses
X=(Tvda)./(Pacc.*Dmax);
%VDA LOSS MODEL
Cs=1.046e-8;    %Slip Coefficient
Patm=1;
meu=0.03797;    %Absolute viscosity
```

```
B=1.02e9;           %Bulk modulus
wmax=418.87901999979744;%maximum angular velocity at which the
                        %coefficients were determined. ~4000RPM
if sign(Tvda)~=sign(dAvda)%VDA in pump mode, accumulator filling up
    a=3.483;
    b=0;
    nq=-0.689;
    Vr=0;
    dVleak=0.001.*(Cs.*((Pacc./Patm).^nq).*(a+b.*(w./wmax)).*(Pacc).*Dma
    x./meu); %leakage losses, set to zero for ideal condditions
    dVcompress=0.001.*((Pacc).*(w).*Dmax./B).*(Vr+0.5.*(1+X));%GM2
    dVF_ideal=abs(Tvda).*abs(dAvda)./Pacc; %ideal qvda
 else   % VDA in motor mode, accumulator emptying,
   a=0.109;
   b=15.34;
   nq=-0.062;
   Vr=0.2;
   dVleak=0.001*(Cs.*((Pacc./Patm).^nq).*(a+b.*(w./wmax)).*(Pacc).*Dmax.
   /meu); %GM2
   dVcompress=0.001*((Pacc).*(w).*Dmax./B).*(Vr+0.5.*(1+X));%GM2
   dVF_ideal=-abs(Tvda).*abs(dAvda)./Pacc;
end
   dVF_real=dVF_ideal-abs(dVleak)-abs(dVcompress);

if isempty(VFprev)%initialize persistent variable for 1st iteration
    VF=1.0080747886E-04;%initial value of accumulator oil volume
    VFprev=VF;
else
    VF=VFprev+dVF_real;
    VFprev=VF;%save current value to use as previous in the next time
              %step
end
```

Accumulator Block

```
function Pacc  = Pressures(VF)
%Gas Charged Accumulator
Ppr=90e5;
VA=2.4509259475E-04; %Accumulator capacity
k=1.4;
Vpr=1e-13.*Ppr;
Pacc=(((VA-Vpr)./(VA-VF)).^k).*Ppr;

%Spring-Loaded Accumulator
%Pmax=200e5;
%Ppr=90e5;
%VA=5.99762E-05; %Accumulator size
%Pacc=Ppr+VF.*(Pmax-Ppr)./VA;
```

APPENDIX-C

Coefficients Block

```
function [C1, C2, C3, C4, C5, c, F1] = Coeff(A, Mank, x, y, Dia, Pacc)
a=cos(A);
b=sin(A);
F1=Pacc.*((pi().*((Dia).^2))./4);
c=Mank./F1;
C1=x+(a.^2).*c;
C2=(2.*y)+(4.*a.*b.*c);
C3=(4.*(b.^2).*c)-(2.*(a.^2).*c);
C4=(2.*y)-(4.*a.*b.*c);
C5=((a.^2).*c)-x;
```

Quartic Block

```
function Sol = Quartic (C1,C2,C3,C4,C5)
R=roots([C1 C2 C3 C4 C5]);
Sol = zeros(1,4);
n = 0;
thresh = 2*eps;
for k = 1:4
if ~isnan(R(k)) && abs(imag(R(k))) < thresh
n = n + 1;
Sol(n) = real(R(k));
end
end
```

Mechanics Block

```
function [Mact,l,B,d]  = Mechanics(Sol,x,y,A,c,F1)
t=Sol(:, 2, :);
B=2.*(atan(t));
d=c.*cos(A+B);
l=sqrt((x-d.*cos(A)).^2+(y-d.*sin(A)).^2);
Mact=(F1.*(l)).*tan(A+B);
```

Differentials Block

```
function [dA,dB,dl] =Differentials(l,B,A)
persistent Aprev Bprev lprev ; %Declaring variables that retains
                                          %values between iterations
%For Ankle%
if isempty (Aprev)  %Initialize the persistent variable for 1st
iteration
    Aprev=A;        %First Value of ankle angle is persistent
    dA=0;           %First value of the change is zero
else
    dA=A-Aprev;
    Aprev=A;        %Save current value to use it as previous in next
step
end
```

```
%FOR ACTUATOR%
if isempty (Bprev)  %Initialize the persistent variable for 1st
iteration
    Bprev=B;        %First Value of Beta
    dB=0;           %First value of the change is zero
else
    dB=B-Bprev;
    Bprev=B;    %Save current value to use it as previous in next time
step
end

%For Cylinder%
if isempty(lprev)
    lprev=l;
    dl=0;
else
    dl=l-lprev;
    lprev=l;
end
```

Gearbox Block

```
function [Tvda,dBvda] = fcn(dBgb, Mact, N, Tn)
dBvda=dBgb.*N;
Tfr=(0.0006913.*N+0.02557).*Tn;
if sign(Mact)==sign(dBgb)   %VDA in pump mode
 absTtotal=(abs(Mact)-Tfr);
else                         %VDA in motor mode, accumulator emptying
 absTtotal=(abs(Mact)+Tfr); %Absolute Total torque with gearlosses
included
end

signs=Mact./abs(Mact);      %To get the actual signs of the
                            %Actuator/ankle moment
Ttotal=signs.*absTtotal;    %To convert the Absolute Total moment into
                            %Total moment with original signs
Tvda=Ttotal./N;
```

VDA & Cylinder Block

```
function [dVF_real, X,VF_real] =VDA_CYL(Tvda, dBvda,Dmax, Pacc, dl,Dia)
persistent VFprev ; %Declaring variables that retains
                    %values between iterations
w=dBvda./0.001; %VDA shaft inputangular velocity,
                %for calculating losses
X=(Tvda)./(Pacc.*Dmax); %Use for calculating losses
%VDA LOSS MODEL
Cs=1.046e-8;
Patm=1;
meu=0.03797;
B=1.02e9;
wmax=418.87901999979744
if sign(Tvda)==sign(dBvda)%VDA in pump mode, accumulator filling up
    a=3.483;
```

```
    b=0;
    nq=-0.689;
    Vr=0;
dVleak=0.001.*(Cs.*((Pacc./Patm).^nq).*(a+b.*(w./wmax)).*(Pacc.*Dmax./m
eu));
dVcompress=0.001.*((Pacc.*w.*Dmax./B).*(Vr+0.5.*(1+X)));
dVvda_ideal=abs(Tvda).*abs(dBvda)./Pacc;
else% VDA in motor mode, accumualator emptying, positive work
a=1.109;
b=15.34;
nq=-0.062;
Vr=0.2;
dVleak=0.001*(Cs.*((Pacc./Patm).^nq).*(a+b.*(w./wmax)).*(Pacc.*Dmax./me
u));
dVcompress=0.001*((Pacc.*w.*Dmax./B).*(Vr+0.5.*(1+X)));
    dVvda_ideal=-abs(Tvda).*abs(dBvda)./Pacc;
end
    dVvda_real=dVvda_ideal-abs(dVleak)-abs(dVcompress);

%For Cylinder%
dVcyl= -((pi().*((Dia).^2))./4).*(dl);

%FOR Accumulator
dVF_ideal=dVvda_ideal+dVcyl;
dVF_real=dVvda_real+dVcyl;

if isempty(VFprev)
    VF_real=1.0080747886E-04; %initial value of accumulator oil volume
    VFprev=VF_real;
else
    VF_real=VFprev+dVF_real;
    VFprev=VF_real;
end
```

Accumulator Block

```
function Pacc  = Pressures(VF)
%Gas Charged Accumulator
Ppr=90e5;
VA=2.4509259475E-04; %Accumulator capacity
k=1.4;
Vpr=1e-13.*Ppr;
Pacc=(((VA-Vpr)./(VA-VF)).^k).*Ppr;

%Spring-Loaded Accumulator
%Pmax=200e5;
%Ppr=90e5;
%VA=5.99762E-05; %Accumulator size
%Pacc=Ppr+VF.*(Pmax-Ppr)./VA;
```

APPENDIX-D

Gearbox Manufacturer: Neugart GmbH (http://www.neugart.de/index.php/gb/).
Gearbox Models: PLN-70, PLFN-64, PLE-60, PLE-40

VDA Manufacturer: Vickers (Eaton Hydraulics group, USA)
(https://www.google.co.uk/url?sa=f&rct=j&url=http://www.eaton.com/ecm/groups/public/@pub/@eaton/@aero/documents/content/ct_195869.pdf&q=&esrc=s&ei=2ZdLUe3AKIaO0AXHvoGQAg&usg=AFQjCNGeCvE9OE9KxKRXIv3VRTby5O00yw).
Refer to Page 23 for the specifications of the VDA models.

REFERENCES

Al-Kharusi, S. a. M. (2004). The design and mechanics of an efficient hydraulically driven legged robot.

Alaranta, H., Lempinen, V. M., Haavisto, E., Pohjolainen, T. & Hurri, H. (1994). Subjective benefits of energy storing prostheses. Prosthetics and Orthotics International, 18(2)**,** 92-97.

Au, S., Berniker, M. & Herr, H. (2008). Powered ankle-foot prosthesis to assist level-ground and stair-descent gaits. Neural Networks, 21(4)**,** 654-666.

Au, S. K., Herr, H., Weber, J. & Martinez-Villalpando, E. C. (2007). Powered ankle-foot prosthesis for the improvement of amputee ambulation. In: Engineering in Medicine and Biology Society, 2007. EMBS 2007. 29th Annual International Conference of the IEEE. 3020-3026.

Au, S. K., Weber, J. & Herr, H. (2009). Powered ankle-foot prosthesis improves walking metabolic economy. IEEE Transactions on Robotics, 25(1)**,** 51-66.

Baker, H. (2012). Why we walk the way we do? In: Lecture Series, University of Salford, UK.

Barr, A. E., Siegel, K. L., Danoff, J. V., Mcgarvey, C. L., 3rd, Tomasko, A., Sable, I. & Stanhope, S. J. (1992). Biomechanical comparison of the energy-storing capabilities of SACH and Carbon Copy II prosthetic feet during the stance phase of gait in a person with below-knee amputation. Physical Therapy, 72(5)**,** 344-354.

Barth, D., Schumacher, L. & Thomas, S. (1992). Gait analysis and energy cost of below-knee amputees wearing six different prosthetic feet. JPO: Journal of Prosthetics and Orthotics, 4(2)**,** 63.

Bellman, R. D., Holgate, M. A. & Sugar, T. G. (2008). SPARKy 3: Design of an active robotic ankle prosthesis with two actuated degrees of freedom using regenerative kinetics. In: Proceedings of the 2nd Biennial IEEE/RAS-EMBS International Conference on Biomedical Robotics and Biomechatronics, BioRob 2008. 511-516.

Brockway, J. (1987). Derivation of formulae used to calculate energy expenditure in man. Human Nutrition Clinical Nutrition, 41(6), 463-471.

Buckley, J. G., Spence, W. D. & Solomonidis, S. E. (1997). Energy cost of walking: Comparison of "intelligent prosthesis" with conventional mechanism. Archives of Physical Medicine and Rehabilitation, 78(3), 330-333.

Casillas, J. M., Dulieu, V., Cohen, M., Marcer, I. & Didier, J. P. (1995). Bioenergetic comparison of a new energy-storing foot and SACH foot in traumatic below-knee vascular amputations. Archives of Physical Medicine and Rehabilitation, 76(1), 39-44.

Cavagna, G. A. & Margaria, R. (1966). Mechanics of walking. Journal of Applied Physiology, 21(1), 271-278.

Cavagna, G. A., Saibene, F. P. & Margaria, R. (1963). External work in walking. Journal of Applied Physiology, 18, 1-9.

Colborne, G. R., Naumann, S., Longmuir, P. E. & Berbrayer, D. (1992). Analysis of mechanical and metabolic factors in the gait of congenital below knee amputees. A comparison of the SACH and Seattle feet. American Journal of Physical Medicine & Rehabilitation, 71(5), 272-278.

Collins, S. H. & Kuo, A. D. (2010). Recycling energy to restore impaired ankle function during human walking. PLoS One [Online], 5(2), e9307. Available from: http://www.ncbi.nlm.nih.gov/pubmed/20174659.

Cundiff, J. S. (2010). Fluid power circuits and controls: fundamentals and applications. CRC Press.

Daerden, F. & Lefeber, D. (2001). The concept and design of pleated pneumatic artificial muscles. International Journal of Fluid Power, 2(3), 41-50.

Dahlen, M. (2003). Investigation on storage technologies for intermittent renewable energies: Evaluation and recommended R&D strategy. Storage Technology Report: Ni-Batteries.

Eng, J. J. & Winter, D. A. (1995). Kinetic analysis of the lower limbs during walking: What information can be gained from a three-dimensional model? Journal of Biomechanics, 28(6), 753-758.

Farris, D. J. & Sawicki, G. S. (2012). The mechanics and energetics of human walking and running: A joint level perspective. Journal of the Royal Society Interface, 9(66), 110-118.

Fukunaga, T., Kubo, K., Kawakami, Y., Fukashiro, S., Kanehisa, H. & Maganaris, C. N. (2001). In vivo behaviour of human muscle tendon during walking. Proceedings of the Royal Society of London. Series B: Biological Sciences, 268(1464), 229-233.

Gailey, R. S., Wenger, M. A., Raya, M., Kirk, N., Erbs, K., Spyropoulos, P. & Nash, M. S. (1994). Energy expenditure of transtibial amputees during ambulation at self-selected pace. Prosthetics and Orthotics International, 18(2), 84-91.

Ganguli, S., Datta, S. R., Chatterjee, B. B. & Roy, B. N. (1974). Metabolic cost of walking at different speeds with patellar tendon-bearing prosthesis. Journal of Applied Physiology, 36(4), 440-443.

Gard, S. A. & Childress, D. S. (1997). The effect of pelvic list on the vertical displacement of the trunk during normal walking. Gait & Posture, 5(3), 233-238.

Gard, S. A. & Childress, D. S. (1999). The influence of stance-phase knee flexion on the vertical displacement of the trunk during normal walking. Archives of Physical Medicine and Rehabilitation, 80(1), 26-32.

Geil, M. D. (2000) Energy storage and return in dynamic elastic response prostheticfeet. Pediatric Gait, 2000. A new Millennium in Clinical Care and Motion Analysis Technology. Georgia Inst. of Technol., Atlanta, GA

Genin, J., Bastien, G., Franck, B., Detrembleur, C. & Willems, P. (2008a). Effect of speed on the energy cost of walking in unilateral traumatic lower limb amputees. European Journal of Applied Physiology, 103(6)**,** 655-663.

Genin, J. J., Bastien, G. J., Franck, B., Detrembleur, C. & Willems, P. A. (2008b). Effect of speed on the energy cost of walking in unilateral traumatic lower limb amputees. European Journal of Applied Physiology, 103(6)**,** 655-663.

Gitter, A., Czerniecki, J. M. & Degroot, D. M. (1991). Biomechanical analysis of the influence of prosthetic feet on below-knee amputee walking. American Journal of Physical Medicine & Rehabilitation, 70(3)**,** 142-148.

Gordon, K. E., Ferris, D. P. & Kuo, A. D. (2009). Metabolic and mechanical energy costs of reducing vertical center of mass movement during gait. Archives of Physical Medicine and Rehabilitation, 90(1)**,** 136-144.

Grabowski, A., Farley, C. T. & Kram, R. (2005). Independent metabolic costs of supporting body weight and accelerating body mass during walking. Journal of Applied Physiology, 98(2)**,** 579-583.

Grabowski, A. M. & Herr, H. M. (2009). Leg exoskeleton reduces the metabolic cost of human hopping. Journal of Applied Physiology, 107(3)**,** 670-678.

Grandall, D. R. (2010). The Performance and Efficiency of Hydraulic Pumps and Motors. Univeristy Of Minnesota.

Grood, E. S. & Suntay, W. J. (1983). A joint coordinate system for the clinical description of three-dimensional motions: Application to the knee. Journal of Biomechanical Engineering, 105(2)**,** 136-44.

Hadjipaschalis, I., Poullikkas, A. & Efthimiou, V. (2009). Overview of current and future energy storage technologies for electric power applications. Renewable and Sustainable Energy Reviews, 13(6-7), 1513-1522.

Hafner, B., Sanders, J., Czerniecki, J. & Fergason, J. (2002). Energy storage and return prostheses: Does patient perception correlate with biomechanical analysis? Clinical Biomechanics, 17(5), 325-344.

Herr, H. M. & Grabowski, A. M. (2012). Bionic ankle–foot prosthesis normalizes walking gait for persons with leg amputation. Proceedings of the Royal Society B: Biological Sciences, 279(1728), 457-464.

Hitt, J. K., Beliman, R., Holgate, M., Sugar, T. Q. & Hollander, K. W. (2008). The SPARKy (Spring Ankle with Regenerative Kinetics) project: Design and analysis of a robotic transtibial prosthesis with regenerative kinetics. In: ASME Conference Proceedings. ASME, 1587-1596.

Hitt, J. K., Bellman, R., Holgate, M., Sugar, T. G. & Hollander, K. W. (2007). The SPARKy (Spring Ankle With Regenerative Kinetics) project: Design and analysis of a robotic transtibial prosthesis with regenerative kinetics. ASME Conference Proceedings, 2007(4806X), 1587-1596.

Hollander, K. W., Ilg, R., Sugar, T. G. & Herring, D. (2006). An efficient robotic tendon for gait assistance. Journal of Biomechanical Engineering, 128(5), 788-791.

Houdijk, H., Pollmann, E., Groenewold, M., Wiggerts, H. & Polomski, W. (2009). The energy cost for the step-to-step transition in amputee walking. Gait & Posture, 30(1), 35-40.

Ishikawa, M., Komi, P. V., Grey, M. J., Lepola, V. & Bruggemann, G. P. (2005). Muscle-tendon interaction and elastic energy usage in human walking. Journal of Applied Physiology, 99(2), 603-608.

Kemmetmüller, W., Fuchshumer, F. & Kugi, A. (2010). Nonlinear pressure control of self-supplied variable displacement axial piston pumps. Control Engineering Practice, 18(1), 84-93.

Kenneth Jr, W. (1995) Advanced Thermodynamics for Engineers. McGraw-Hill, New York.

Kerrigan, D. C., Riley, P. O., Lelas, J. L. & Croce, U. D. (2001). Quantification of pelvic rotation as a determinant of gait. Archives of Physical Medicine and Rehabilitation, 82(2), 217-220.

Kirtley, C. (2006). Clinical gait analysis: Theory and practice. Churchill Livingstone.

Klute, G., Czerniecki, J. & Hannaford, B. (2000). Muscle-like pneumatic actuators for below-knee prostheses. In: Proceedings of the 7th International Conference on New Actuators, Breman, Germany. 289–292.

Klute, G. K., Czerniecki, J. M. & Hannaford, B. (2002). Artificial muscles: Actuators for biorobotic systems. The International Journal of Robotics Research, 21(4), 295-309.

Kuo, A. D., Donelan, J. M. & Ruina, A. (2005). Energetic consequences of walking like an inverted pendulum: Step-to-step transitions. Exercise and Sport Sciences Reviews, 33(2), 88-97.

Lay, A. N., Hass, C. J. & Gregor, R. J. (2006). The effects of sloped surfaces on locomotion: a kinematic and kinetic analysis. Journal of Biomechanics, 39(9), 1621-8.

Leardini, A., Cappozzo, A., Catani, F., Toksvig-Larsen, S., Petitto, A., Sforza, V., Cassanelli, G. & Giannini, S. (1999). Validation of a functional method for the estimation of hip joint centre location. Journal of Biomechanics, 32(1), 99-103.

Lehmann, J. F., Price, R., Boswell-Bessette, S., Dralle, A., Questad, K. & Delateur, B. J. (1993). Comprehensive analysis of energy storing prosthetic feet: Flex Foot and Seattle Foot versus standard SACH foot. Archives of Physical Medicine and Rehabilitation, 74(11), 1225-1231.

Li, Q., Young, M., Naing, V. & Donelan, J. M. (2010). Walking speed estimation using a shank-mounted inertial measurement unit. Journal of Biomechanics, 43(8), 1640-1643.

Lichtwark, G. A. & Wilson, A. (2006). Interactions between the human Gastrocnemius muscle and the Achilles tendon during incline, level and decline locomotion. Journal of Experimental Biology, 209(21), 4379-4388.

Mackay, D. (2008). Sustainable Energy-without the hot air. UIT Cambridge.

Malatesta, D., Simar, D., Dauvilliers, Y., Candau, R., Borrani, F., Prefaut, C. & Caillaud, C. (2003). Energy cost of walking and gait instability in healthy 65- and 80-yr-olds. Journal of Applied Physiology, 95(6), 2248-2256.

Massaad, F., Lejeune, T. M. & Detrembleur, C. (2007). The up and down bobbing of human walking: a compromise between muscle work and efficiency. The Journal of Physiology, 582(2), 789-799.

Mccandlish, D. & Dorey, R. (1984). The mathematical modelling of hydrostatic pumps and motors. Proceedings of the Institution of Mechanical Engineers, Part B: Journal of Engineering Manufacture, 198(3), 165-174.

Mccann, D. J. & Adams, W. C. (2002). A dimensional paradigm for identifying the size-independent cost of walking. Medicine and Science in Sports and Exercise, 34(6), 1009-1017.

Menard, M. R. & Murray, D. D. (1989). Subjective and objective analysis of an energy-storing prosthetic foot. JPO: Journal of Prosthetics and Orthotics, 1(4), 220.

Minetti, A. E., Moia, C., Roi, G. S., Susta, D. & Ferretti, G. (2002). Energy cost of walking and running at extreme uphill and downhill slopes. Journal of Applied Physiology, 93(3), 1039-1046.

Mochon, S. & Mcmahon, T. A. (1980a). Ballistic walking. Journal of Biomechanics, 13(1), 49-57.

Mochon, S. & Mcmahon, T. A. (1980b). Ballistic walking: An improved model. Mathematical Biosciences, 52(3-4), 241-260.

Neptune, R. R., Kautz, S. A. & Zajac, F. E. (2001). Contributions of the individual ankle plantar flexors to support, forward progression and swing initiation during walking. Journal of Biomechanics, 34(11), 1387-1398.

Nielsen, D., Shurr, D., Golden, J. & Meier, K. (1988). Comparison of energy cost and gait efficiency during ambulation in below-knee amputees using different prosthetic feet. The Iowa Orthopaedic Journal, 8, 95.

Orendurff, M. S., Segal, A. D., Klute, G. K., Mcdowell, M. L., Pecoraro, J. A. & Czerniecki, J. M. (2006). Gait efficiency using the C-Leg. Journal of Rehabilitation Research & Development, 43(2), 239-246.

Ortega, J. D. & Farley, C. T. (2005). Minimizing center of mass vertical movement increases metabolic cost in walking. Journal of Applied Physiology, 99(6), 2099-2107.

Paysant, J., Beyaert, C., Datie, A. M., Martinet, N. & Andre, J. M. (2006). Influence of terrain on metabolic and temporal gait characteristics of unilateral transtibial amputees. Journal of Rehabilitation Research and Development, 43(2), 153-160.

Perry, J. (1992). Gait analysis: normal and pathological function. SLACK incorporated.

Postema, K., Hermens, H. J., De Vries, J., Koopman, H. F. & Eisma, W. H. (1997). Energy storage and release of prosthetic feet. Part 2: Subjective ratings of 2 energy storing and 2 conventional feet, user choice of foot and deciding factor. Prosthetics and Orthotics International, 21(1), 28-34.

Pratt, G. A. & Williamson, M. M. (1995). Series elastic actuators. In: Intelligent Robots and Systems 95. 'Human Robot Interaction and Cooperative Robots', Proceedings. 1995 IEEE/RSJ International Conference on. 399-406.

Racic, V., Pavic, A. & Brownjohn, J. M. W. (2009). Experimental identification and analytical modelling of human walking forces: Literature review. Journal of Sound and Vibration, 326(1-2), 1-49.

Ralston, H. J. (1958). Energy-speed relation and optimal speed during level walking. European Journal of Applied Physiology and Occupational Physiology, 17(4), 277-283.

Rose, J. & Gamble, J. G. (2006). Human walking. Philadelphia: Lippincott Williams & Wilkins.

Rydberg, K.-E. (2009). Energy efficient hydraulic hybrid drives.

Saibene, F. & Minetti, A. (2003). Biomechanical and physiological aspects of legged locomotion in humans. European Journal of Applied Physiology, 88(4-5), 297-316.

Saunders, J. B., Inman, V. T. & Eberhart, H. D. (1953). The major determinants in normal and pathological gait. The Journal of Bone and Joint Surgery. American Volume, 35-A(3), 543-548.

Sawicki, G. S., Lewis, C. L. & Ferris, D. P. (2009). It pays to have a spring in your step. Exercise and Sport Sciences Reviews, 37(3), 130-138.

Schmalz, T., Blumentritt, S. & Jarasch, R. (2002). Energy expenditure and biomechanical characteristics of lower limb amputee gait: The influence of prosthetic alignment and different prosthetic components. Gait & Posture, 16(3), 255-263.

Segal, A. D., Orendurff, M. S., Klute, G. K., Mcdowell, M. L., Pecoraro, J. A., Shofer, J. & Czerniecki, J. M. (2006). Kinematic and kinetic comparisons of transfemoral amputee gait using C-LEG and MAUCH SNS prosthetic knees. Journal of Rehabilitation Research & Development, 43(7), 857-869.

Segal, A. D., Zelik, K. E., Klute, G. K., Morgenroth, D. C., Hahn, M. E., Orendurff, M. S., Adamczyk, P. G., Collins, S. H., Kuo, A. D. & Czerniecki, J. M. (2012). The effects of a controlled energy storage and return prototype prosthetic foot on transtibial amputee ambulation. Human Movement Science, 31(4), 918-931.

Silverman, A. K. & Neptune, R. R. (2012). Muscle and prosthesis contributions to amputee walking mechanics: A modeling study. Journal of Biomechanics, 45(13), 2271-2278.

Skinner, H. B. & Effeney, D. J. (1985). Gait analysis in amputees. American Journal of Physical Medicine & Rehabilitation, 64(2), 82-89.

Starholm, I. M., Gjovaag, T. & Mengshoel, A. M. (2010). Energy expenditure of transfemoral amputees walking on a horizontal and tilted treadmill simulating different outdoor walking conditions. Prosthetics and Orthotics International, 34(2), 184-194.

Stepien, J. M., Cavenett, S., Taylor, L. & Crotty, M. (2007). Activity levels among lower-limb amputees: Self-report versus step activity monitor. Archives of Physical Medicine and Rehabilitation, 88(7), 896-900.

Sup, F., Bohara, A. & Goldfarb, M. (2007). Design and control of a powered knee and ankle prosthesis. In: Robotics and Automation, 2007 IEEE International Conference on. 4134-4139.

Sup, F., Bohara, A. & Goldfarb, M. (2008). Design and Control of a Powered Transfemoral Prosthesis. The International Journal of Robotics Research, 27(2), 263-273.

Sup, F., Varol, H., Mitchell, J., Withrow, T. & Goldfarb, M. (2009) Self-contained powered knee and ankle prosthesis: Initial evaluation on a transfemoral amputee. Rehabilitation Robotics, 2009. ICORR 2009. IEEE International Conference on

Torburn, L., Perry, J., Ayyappa, E. & Shanfield, S. L. (1990). Below-knee amputee gait with dynamic elastic response prosthetic feet: A pilot study. Journal of Rehabilitation Research and Development, 27(4), 369-384.

Torburn, L., Powers, C. M., Guiterrez, R. & Perry, J. (1995). Energy expenditure during ambulation in dysvascular and traumatic below-knee amputees: a comparison of five prosthetic feet. Journal of Rehabilitation Research and Development, 32(2), 111-119.

Van Den Bogert, A. J., Samorezov, S., Davis, B. L. & Smith, W. A. (2012). Modeling and optimal control of an energy-storing prosthetic knee. Journal of Biomechical Engineering, 134(5), 051007.

Versluys, R., Desomer, A., Lenaerts, G., Beyl, P., Van Damme, M., Vanderborght, B., Vanderniepen, I., Van Der Perre, G. & Lefeber, D. (2008a) From conventional prosthetic feet to bionic feet: A review study. Biomedical Robotics and Biomechatronics, 2008. BioRob 2008. 2nd IEEE RAS & EMBS International Conference on. Scottsdale, AZ.

Versluys, R., Desomer, A., Lenaerts, G., Van Damme, M., Beyl, P., Van Der Perre, G., Peeraer, L. & Lefeber, D. (2008b). A pneumatically powered below-knee prosthesis: Design specifications and first experiments with an amputee. In: Biomedical Robotics and Biomechatronics, 2008. BioRob 2008. 2nd IEEE RAS & EMBS International Conference on. 372-377.

Versluys, R., Lenaerts, G., Van Damme, M., Jonkers, I., Desomer, A., Vanderborght, B., Peeraer, L., Van Der Perre, G. & Lefeber, D. (2009). Successful preliminary walking experiments on a transtibial amputee fitted with a powered prosthesis. Prosthetics and Orthotics International, 33(4), 368-377.

Waters, R. L. & Mulroy, S. (1999). The energy expenditure of normal and pathologic gait. Gait & Posture, 9(3), 207-231.

Waters, R. L., Perry, J., Antonelli, D. & Hislop, H. (1976). Energy cost of walking of amputees: The influence of level of amputation. The Journal of Bone and Joint Surgery. American Volume, 58(1), 42-46.

Whittle, M. W. (2003). Gait analysis: An introduction.

Willer, B. (2003). Investigaiton on storage technologies for intermittent renewable energies: Evaluation and recommended R&D strategy. Storage Technology Report: Supercaps.

Winter, D. (1983). Energy generation and absorption at the ankle and knee during fast, natural, and slow cadences. Clinical Orthopaedics and Related Research, (175), 147.

Winter, D. (2004a). Biomechanics and Motor Control of Human Movement. Wiley.

Winter, D. A. (1991). Biomechanics and motor control of human gait: Normal, elderly and pathological.

Winter, D. A. (2004b). Biomechanics and motor control of human movement. 3 ed. New York, Chichester: Wiley.

Winter, D. A. & Sienko, S. E. (1988). Biomechanics of below-knee amputee gait. Journal of Biomechanics, 21(5), 361-367.

Zmitrewicz, R. J., Neptune, R. R. & Sasaki, K. (2007). Mechanical energetic contributions from individual muscles and elastic prosthetic feet during symmetric unilateral transtibial amputee walking: A theoretical study. Journal of Biomechanics, 40(8), 1824-1831.